On-site Pure Hydrogen Production in a Catalytic Membrane Reactor by Ethanol Steam Reforming

Doctoral Thesis

Ali Hedayati

POLYTECHNIC UNIVERSITY OF CATALONIA
ECOLE DES MINES DE NANTES
Barcelona, 2016

Universitat Politècnica de Catalunya BarcelonaTECH
Institut de Tècniques Energètiques

On-site Pure Hydrogen Production in a Catalytic Membrane Reactor by Ethanol Steam Reforming

Doctoral Thesis

Ali Hedayati

Supervised by:

Dr. Jordi Llorca Piqué

Dr. Olivier Le Corre

Dr. Bruno Lacarrière

SELECT+ Erasmus Mundus Joint Doctoral Program

Acknowledgments

Abstract

As an alternative to fossil fuels, hydrogen is considered as a clean energy carrier that can be converted to electricity by fuel cell with high efficiency. Usually, to be economically feasible, hydrogen needs to be liquefied, compressed, or adsorbed in metallic hydrides in large scale prior to delivery. This requires very high pressure or very low temperature, which make a very high risk during transfer and storage. Hence, it is highly beneficial to produce and consume pure hydrogen at the same place/time. The use of renewable biofuels such as bio-ethanol as a source of hydrogen is highly beneficial due to the higher H/C ratio, lower toxicity, and higher safety of storage that distinguish ethanol over other substrates. Among the reforming processes, steam reforming of ethanol delivers the highest amount of hydrogen per mole of converted ethanol. Noble metal-based catalysts are well known for very high reactivity in terms of ethanol conversion and hydrogen selectivity together with nearly zero carbon deposition over the surface of the catalyst. Ethanol steam reforming (ESR) over noble metal-based catalysts can be considered as an efficient and reliable method for hydrogen production. The application of membrane reactors (MR) – in which production and separation of hydrogen (pure hydrogen production) occurs in the same reactor vessel – is highly beneficial to omit costly and complicated unit processes for hydrogen purification. Besides, by removal of one of the products (hydrogen) via permeation through the membrane, equilibrium limitations are overcome even at unbeneficial operating conditions, leading to higher production of hydrogen and higher efficiency of the process. In case of a palladium-based membrane, highly pure hydrogen is obtained, suitable for feeding a low-temperature fuel cell online.

In this work, in-situ production of pure hydrogen via catalytic ethanol steam reforming (ESR) in a membrane reactor (MR) was investigated. A mixture of pure ethanol and distilled was used as the fuel. ESR experiments were carried out over Pd-Rh/CeO$_2$ catalyst in a Pd-Ag membrane reactor – named as the fuel reformer – at variety of operating conditions regarding the operating temperature, pressure, fuel flow rate, and the molar ratio of water-ethanol (S/C ratio). The performance of the catalytic membrane reactor (CMR) was studied in terms of ethanol conversion, pure hydrogen production rate, hydrogen yield, and hydrogen recovery.

Thermodynamic evaluation of the CMR was presented as a complement to the comprehensive investigation of the overall performance of the fuel reformer. Exergy analysis was performed based on the experimental results aiming not only to understand the thermodynamic performance of the fuel reformer, but also to introduce the application of the exergy analysis in CMRs studies. Exergy analysis provided important information on the effect of operating conditions and thermodynamic losses, resulted in understanding of the best operating conditions. The exergy efficiency of the CMR was evaluated considering both an insulated reactor (without heat loss), and a non-insulated reactor (with heat loss).

The simulation of the dynamics of hydrogen production (permeation) was performed as the last step to study the applicability of the fuel reformer. The simulation presented in this work is similar to the hydrogen flow rate adjustments needed to set the electrical load of a fuel cell, if fed online by the studied pure hydrogen generating system. A static model for the catalytic zone was derived from the Arrhenius law to model the production rate of the ESR species (CO, CO_2, CH_4, H_2O, and H_2). The permeation zone (membrane) was modeled based on the Sieverts' law as the physical definition of hydrogen permeation through the membrane, and a block box model as a function of the fuel flow rate and the reactor pressure. Finally, a dynamic model was proposed under ideal gas law assumptions to simulate the dynamics of pure hydrogen production rate in the case of the fuel flow rate or the operational pressure set point adjustment (transient state) at isothermal conditions.

Abstract

Com a alternativa als combustibles fòssils, l'hidrogen es considera un vector energètic net que es pot convertir a electricitat amb una gran eficiència en una pila de combustible. Normalment, per ser econòmicament atractiu, cal liquar, comprimir o adsorbir en metalls l'hidrogen a gran escala per a transportar-lo. Això requereix pressions molt altes o temperatures molt baixes, cosa que suposa riscos en el seu transport i emmagatzematge. Per aquest motiu resulta molt interessant el produir i consumir l'hidrogen al mateix lloc i en el mateix moment. L'ús de biocombustibles renovables com el bioetanol com a font d'hidrogen és molt avantatjós donada la seva relació H/C elevada, baixa toxicitat i elevada seguretat en l'emmagatzematge, aspectes difícils de trobar en altres substrats. D'entre els processos de reformació, la reformació amb vapor d'aigua d'etanol origina la màxima quantitat d'hidrogen respecte l'etanol convertit. Els catalitzadors que contenen metalls nobles mostren una alta activitat en la conversió d'etanol i alta selectivitat a hidrogen al temps que eviten la deposició de carboni a la seva superfície. Així, la reformació catalítica d'etanol (ESR) fent ús de catalitzadors que contenen metalls nobles es pot considerar un mètode eficient i robust per a produir hidrogen. L'ús de reactors de membrana (MR) en els que la producció i separació d'hidrogen té lloc en el mateix reactor resulta especialment útil a l'hora de simplificar i abaratir la purificació de l'hidrogen que es produeix. A més, mitjançant la separació d'un dels productes de la reacció a través de la membrana, l'hidrogen, es superen els límits termodinàmics i es pot treballar en condicions més suaus de reacció, el que comporta una producció més alta d'hidrogen i una millor eficiència del procés. En el cas d'utilitzar membranes basades en pal·ladi s'obté un corrent d'hidrogen ultrapur capaç d'alimentar directament una pila de combustible de baixa temperatura.

En aquest treball s'investiga la producció in situ d'hidrogen pur per reformació catalítica d'etanol amb vapor d'aigua (ESR) en un reactor de membrana (MR). El combustible utilitzat ha estat una mescla d'etanol pur i aigua i els experiments s'han dut a terme amb un catalitzador Pd-Rh/CeO$_2$ i una membrana Pd-Ag (reformador) sota diferents condicions d'operació de temperatura, pressió, cabal de combustible i relació molar d'aigua-etanol (relació S/C). El comportament del reactor catalític de membrana (CMR) s'ha avaluat en termes de conversió d'etanol, producció d'hidrogen pur, rendiment d'hidrogen i recuperació d'hidrogen.

La investigació exhaustiva del comportament del CMR s'ha complementat amb un estudi termodinàmic. S'ha dut a terme una anàlisi detallada de l'exergia en base als resultats experimentals amb la intenció, no només d'entendre el comportament del reformador, sinó també com a eina en l'estudi, per primer cop, de reactors catalítics de membrana. L'anàlisi exergètica ha donat lloc a informació innovadora sobre les condicions de treball del CMR i les pèrdues termodinàmiques del sistema, cosa que permet entendre quines són les millors condicions d'operació. L'anàlisi exergètica s'ha dut a terme considerant un reactor aïllat (sense pèrdues de calor) i un reactor no aïllat (amb pèrdues de calor).

Per últim, s'ha modelat i simulat la dinàmica en la producció d'hidrogen (permeació) com a darrer pas en l'estudi de l'aplicabilitat del reformador. La simulació realitzada permet ajustar l'alimentació d'hidrogen pur d'una pila de combustible necessària per a garantir el subministrament elèctric en una aplicació. S'ha construït un model estàtic per a la zona catalítica del CMR a partir de la llei d'Arrhenius per a modelitzar la producció de les espècies de la ESR (CO, CO_2, CH_4, H_2O i H_2). La zona de permeació del CMR (membrana) s'ha modelitzat, bé amb la llei de Sieverts' en base al fenomen físic de transport d'hidrogen a través de la membrana, o bé amb un model de "caixa negre" tenint en compte la producció d'hidrogen i la pressió. El model dinàmic s'ha realitzat assumint gasos ideals per a simular la dinàmica en la producció d'hidrogen pur quan hi ha canvis en l'alimentació de combustible o canvis en la pressió del CMR en condicions isotermals.

Table of contents

List of figures

List of tables

Personal reference

- **Journal publications**

  o Ali Hedayati, Olivier Le Corre, Bruno Lacarrière, Jordi Llorca, Dynamic Simulation of Pure Hydrogen Production via Bio-ethanol Steam Reforming in a Catalytic Membrane Reactor, ENERGY, October 2015, *Revised manuscript submitted*.

  o Ali Hedayati, Olivier Le Corre, Bruno Lacarrière, Jordi Llorca, Experimental and Exergetic Evaluation of Bioethanol Catalytic Steam Reforming in a Membrane Reactor, Catalysis Today, Feb. 2016, DOI: 10.1016/j.cattod.2016.01.058.

  o Ali Hedayati, Olivier Le Corre, Bruno Lacarrière, Jordi Llorca, Exergetic Study of Catalytic Steam Reforming of Bio-ethanol over Pd-Rh/CeO_2 with Hydrogen Purification in a Membrane Reactor, International Journal of Hydrogen Energy; 40, 3574-3581, 2015

- **Book sections**

  o Jordi Llorca and Ali Hedayati, Alcohols and Bio-alcohols Steam and Autothermal Reforming in a Membrane Reactor, In: Angelo Basile, Francesco Dalena (Editors), Alcohols and Bioalcohols: Characteristics, Production and Uses, Nova Science Publishers, pp.181-204, New York, 2015

- **Conference contributions**

  o Ali Hedayati, Olivier Le Corre, Bruno Lacarrière, Jordi Llorca, Dynamic Modeling of Pure Hydrogen Production via Bio-ethanol Steam Reforming in a Membrane Reactor, 28th International Conference on Efficiency, Cost, Optimization, Simulation, and Environmental Impact of Energy Systems **ECOS2015**, Pau, France, June 2015.

  o Ali Hedayati, Olivier Le Corre, Bruno Lacarrière, Jordi Llorca, Experimental and Exergetic evaluation of Bio-ethanol Catalytic Steam Reforming in a Membrane Reactor, 12th International Conference on Catalysis in Membrane Reactors (**ICCMR12**), Szczecin, Poland, June 2015.

  o Ali Hedayati, Olivier Le Corre, Bruno Lacarrière, Jordi Llorca, Experimental and Modeling study of Catalytic Steam Reforming of Bio-ethanol over Pd-Rh/CeO_2 in a Membrane Reactor, 7th International Exergy, Energy and Environment Symposium (**IEEES7**), Valenciennes, France, April 2015.

  o Ali Hedayati, Olivier Le Corre, Bruno Lacarrière, Jordi Llorca, Exergy and Energy Evaluation of Bio-ethanol Steam Reforming in a Catalytic Membrane Reactor, 7th International Exergy, Energy and Environment Symposium (**IEEES7**), Valenciennes, France, April 2015.

  o Ali Hedayati, Olivier Le Corre, Bruno Lacarrière, Jordi Llorca, Exergetic Study of Catalytic Steam Reforming of Bio-ethanol over Pd-Rh/CeO_2 with Hydrogen Purification in a Membrane Reactor, European Hydrogen Energy Conference **EHEC2014**, March 2014, Seville, Spain.

Chapter 1

Introduction and general overview

Abstract

In this chapter, a general overview of the environmental concerns of the world energy demand and power production is given. The importance of clean energy production and the solutions for on-site energy supply especially in the case of the buildings are discussed briefly. Finally, the objectives and scope of this thesis together with the outlines are presented.

1.1 Background and general overview

It is proven that the increasing rate of energy consumption and high dependency of energy production on fossil fuels has caused obvious negative environmental consequences of climate change. According to the intergovernmental panel on climate control (IPCC), growing concentration of greenhouse gases in the atmosphere - mostly by burning of fossil fuels for power generation processes - is the main reason of climate change and global warming [5]. Svante Arrhenius was one of the first who mentioned global warming probability due to the increasing concentration of CO_2 in the atmosphere [6]. He suggested that the mean temperature of the earth would probably increase due to the emission of carbon dioxide originating from human activities. Now the atmospheric concentrations of CO_2 have increased from natural mean value of 280 ppm to 379 ppm in 2005 and it is estimated to exceed 400 ppm by 2030 [7]. It is expected that the worldwide energy consumption will be increasing rapidly so that the yearly CO_2 emissions from energy production sectors will reach 33.8 Gt in 2020 and 42.4 Gt in 2035 [8]. According to the IPCC, a 50–85% reduction in total CO_2 emission by 2050 is mandated to limit the anticipated rise in global temperature to within 2°C [9].

Besides, energy conversion is a key factor for the development of human society so that living without energy supply – mainly electricity – is not possible in the modern world. Thus, as development continues with an aim to eradicate poverty and enhance quality of life, energy consumption by all the sectors of the society is unavoidable [10,11]. A rapid shift towards efficient and cost effective sources of energy is obviously required. These facts have forced human to start serious movements towards clean energy production and energy saving strategies.

Among different sectors of the society, it is indicated that in the modern world more than 40% of the total produced energy is demanded by buildings, mainly in the form of electricity [12]. Consequently, a big share of emission of greenhouse gases can be attributed to the buildings so that according to the reference scenario 2013 by European Union, 11% of total CO_2 emission belongs to only residential buildings [1]. European electricity demand is estimated to increase from 3081 TWh in 2012 to 3250 TWh in 2020 [13]. The CO_2 emission by sector is given in Fig. 1.1. CO_2 emission from buildings originates from on-site energy generation and burning fuels for heat in buildings or cooking in homes. CO_2 emission from electricity use in buildings is included in the Power generation/District heating sector.
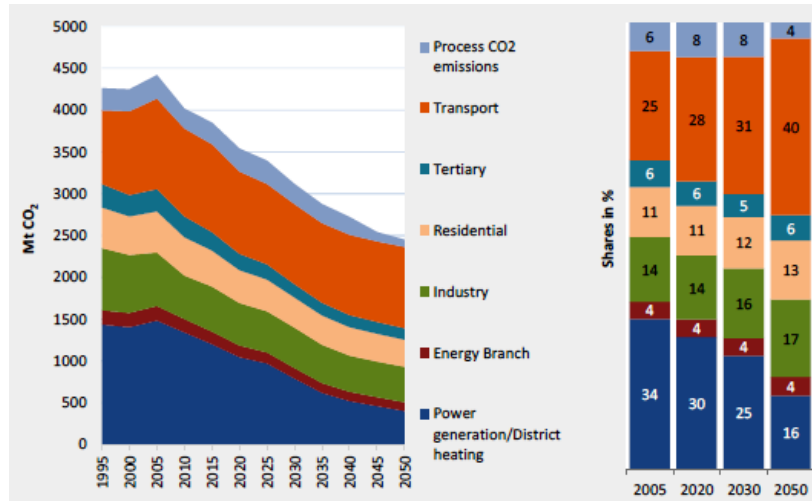
Fig. 1.1 CO_2 emission by sector in EU [1]

As determined by EU, to meet the electricity requirements together with clean energy production targets, the share of renewable resources in power generation should be 35, 43, and 50% in 2020, 2030, and 2050, respectively. Particularly in the electricity generation sector, the share of renewable electricity must reach 45% in 2030 and 53% in 2050. The net electricity production by the type of fuel for EU is given in Fig. 1.2.
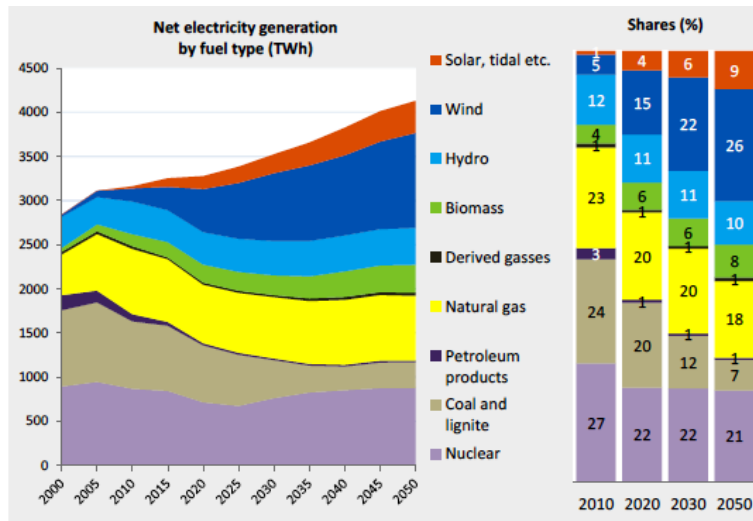
Fig. 1.2 Electricity generation by fuel type in EU [1]

Renewable energy resources are now considered as the fastest and most feasible solution to achieve the targets of clean electricity production. Nevertheless, one of the most important challenges is the dependency of availability and utilization of renewable sources on the geographical and local conditions and infrastructures. Besides, inevitable CO_2 emission and most importantly, transmission of produced electricity to the end users remain among the challenges to be encountered. In this regard, on-site electricity production to lower the dependency of different sectors of the society on gridded power sources has been

investigated recently. Hence, new solutions such as small scale on-site energy generation units in buildings may open a new era to harness available clean energy sources efficiently at the place/time where needed.

The concept of Zero Energy Building (ZEB) has recently received significant attention as a realistic solution to electricity and power generation for the building sector applications independent from gridded power. Although Zero Energy Buildings (ZEB) concept does not have a commonly agreed and clear definition, it is in general referred to a building which is able to provide itself with the required energy demand; in any form needed (i.e. electricity, heating, cooling, lighting. etc) [14,15]. A sub-definition of ZEB is the theory of Net Zero Energy Building (NZEB) denoting a ZEB, which is connected to the grid. In this case, the building is capable of supplying the grid (when the building produces energy more than it needs) with the same amount of energy that it has obtained from the grid (when the energy produced by the building is lesser than the requirements). According to Marszal [14] and Sartori [15], the quantity of energy taken out from the grid, is equal to the quantity which is sent back to the grid by the building, considering normally a duration of one year. Moreover, if a building total energy production over a specific period exceeds its needs and requirements, so that the excess energy is given to the grid, it is defined as a Positive Energy Building.

Currently, serious worldwide attempts are under way by the researchers and policy makers for development and commercialization of ZEBs. EU policies indicate that buildings should be nearly Net Zero Energy Building by 2020 [12] and also the US Department of Energy (DOE) has the strategy of achieving commercial ZEBs by 2025 [16]. In view of the explanations of ZEBs, the idea of on-site production of clean energy is a key factor for ZEBs to develop. Although renewable sources seem the first option, as mentioned before, issues such as economical and feasibility aspects of solar and wind energy for small scale (home scale) applications, and the dependency of these resources upon geographical and local climate conditions must be taken into account.

Among different methods and technologies tested for small scale on-site electricity production – mainly to be used in the buildings and light transportation sector -, fuel cells technology has shown proven potentials for different tasks and can be applied in sub-MW size at any condition independent from local factors. Being compatible with modern energy carriers such as hydrogen, fuel cells are considered as the energy convertors of the future power generation systems [17]. In a fuel cell, chemical energy of a fuel (mainly hydrogen) is converted into electricity via a chemical reaction of positively charged hydrogen ions with a source of oxygen, which is air. The products of such a conversion are electricity, water, and heat. To summarize, the advantages of fuel cells can be listed as:

- Reduced harmful emissions: in the case of utilizing pure hydrogen as fuel, the emission (of the fuel cell stack) is supposed as zero (excluding the emissions for the

H$_2$ production). This is considered as the most important advantage of fuel cell technology over the heat engines and conventional power cycles.

- High efficiency: up to 60% efficiency has been reached, and in the case of high temperature fuel cells, considerable amount of heat can be recovered.
- Modularity: the power output of the fuel cell can be adjusted easily by adding/removal of the stacks.
- Prompt load flowing: thanks to the instant nature of the electrochemical reactions, the dynamic behavior of fuel cell in responding to the load change is reliable.
- No noise pollution: fuel cells are static apparatuses and due to absence of mechanical moving parts, no noise pollution is caused.
- Fuel flexibility: not only the pure hydrogen, but also some carbonaceous fuels such as light alcohols are directly used in the fuel cells as the source of hydrogen.

Pure hydrogen is used as the main fuel for fuel cells to produce electrical power (plus lots of recoverable heat from high temperature operating types) via electrochemical reactions. While the combustion of hydrogen produces very clean energy, its conversion to electricity and heat by means of fuel cells is known as the highest efficient energy producing process [3]. The high efficiency of the fuel cells is attributed to the single-step energy conversion pathway during which chemical energy is converted to electrical energy [17]. This is comparable to the complicated conventional power generation cycles where chemical energy is converted to thermal energy, then to the mechanical energy and finally to the electrical energy considering the thermodynamic losses occurring in each process.

Apart from pure hydrogen, several research works has been focused on direct application of methanol, ethanol, and ethylene glycol mainly for prevention of pure hydrogen production units. A comprehensive review on the fuel cells has been published by Sharaf and Orhan [17]. The case of Direct Ethanol Fuel Cells (DEFC) is briefly discussed due to the similarities between this concept and the concept of this PhD work. The necessity of pure hydrogen production can be a matter of question while some liquid fuels can be directly used in fuel cells. The idea of DEFC was first developed and investigated in 1995 when ethanol steam reforming in a Molten Carbonate Fuel Cell (MOFC) was simulated and studied [18]. DEFCs are one type of the Direct Alcohol Fuel Cells (DAFSc) in which a type of alcohol – mainly methanol or ethanol – is used directly in the electrochemical process [19]. DEFCs operate at very high temperatures with efficiency between 20% and 40%, however, the development and technology approval of this kind of fuel cell stays at early stages [17].

Some positive points such as ease of transport and delivery of ethanol, and higher energy density of ethanol compared to hydrogen, cause DEFSc to compete in efficiency and price with Proton Exchange Membrane Fuel Cells (PEMFCs, as the most commercial type of fuel cells for car and building applications). However, some challenges are hindering the commercialization of DEFSc. Very high sensitivity to carbon monoxide, low performance

in C-C bond breakage due to low temperature (considered as the main feedback), acetic acid formation and inability of the oxidation of this specie, and permeation of ethanol through the membrane are the most important challenges to be conquer for the optimization and further development of DEFCs [20]. According to Leone et al. [21], DEFCs operating at 700°C and higher still suffer from carbon deposition. Additional water in the feed may hinder carbon formation to some extent, but on the other hand lowers the current density of the fuel cell. As the open literature presents, there is not a lot of study performed on the development and investigation of DEFCs, although since 2007 the amount of research work has increased notably. A comprehensive literature review on DEFCs was presented in the work by Kamarudin et al. [19].

According to the discussion above, the application of DEFCs is not technically approved and has a long way to be optimized and developed to enter the market and compete the commercial and well-developed types of fuel cells – mainly PEMFCs.

Although fuel cell technology is among the cleanest techniques to produce energy, the main challenge remains unresolved. How to produce and deliver pure hydrogen in a sustainable, safe, applicable, and efficient way? Conversion technologies for pure hydrogen production and most importantly the saving and transportation of pure hydrogen are still a concern. To be economically feasible and comparable, hydrogen needs to be liquefied or compressed (high risk of high pressure), or adsorbed in metallic hydrides in large scale prior to the transfer (very low temperature or huge masses of metallic hydrides). Hence, it can be concluded that it is highly beneficial to produce and consume pure hydrogen at the same place/time.

Hydrogen can be obtained by different techniques such as electrolysis of water, catalytic reforming of alcohols, catalytic conversion of methane, photochemical splitting of water, and biological conversion of waste biomass. To reach the cleanest way, it is inevitable to convert a renewable source to hydrogen.

Ethanol itself as a beverage has been in used for thousands of years and has been produced via fermentation of natural resources. However, this especial organic chemical has been in use broadly for various applications such as a solvent, an antifreezing agent, disinfecting agent, and most importantly as a fuel. Ethanol is a hydrogen rich fuel with hydrogen to carbon ratio of 3. Besides, there are ethanol distribution infrastructures in many countries. Ethanol is not considered as a toxic liquid, is safe to reserve at ambient temperature and pressure, not explosive, and its special molecular structure makes it easier for C-C breakage in reforming processes.

Bioethanol is referred to the ethanol produced via biological conversion of biomass (fermentation or enzymatic catalysts) [22] and is also applied for the alcoholic liquid products obtained by the mentioned fermentation process. The molar alcohol to water ratio of such products is between 1:7 and 1:12. If ethanol is considered as a fuel, further distillation for water removal is necessary which means highly energy consuming and

costly processes. Instead, the mixture of water and ethanol in the form of bioethanol directly can be used as a feedstock for reforming processes. This leads to significant reduction in global energy consumption and the costs of the process by omitting the additional alcohol purification unit operations [23]. Depending on the availability of the biomass, the source of hydrogen differs from region to region through the world. For example, sugar cane is used in Brazil and grains like corn are used in US. In 2012, Brazil and US as the largest ethanol producers, produced around 86% of ethanol used globally [24]. In Europe, the leaders of bio-ethanol production are Germany, Spain, France and Sweden, mostly from beet and wheat [25]. The price of the edible plants as a source of fuel ethanol has increased recently resulting in a conflict between using them as a source of fuel or a source of food. Besides, the increasing trend of the universal need of food has resulted in recent researches in the use of non-edible natural resources such as grasses and straw to produce bioethanol, although the bioethanol production process from these kind of resources is more complicated due to the complex molecular structures [22].

Noble metal-based catalysts are well known for very high reactivity in terms of ethanol conversion and hydrogen selectivity together with nearly zero carbon deposition over the surface of the catalyst [22,26,27]. Among noble metals, Rh, Pt, Pd, Ru, and Ir have been in the center of attention during last 10 years [28]. Ethanol steam reforming (ESR) over noble metal-based catalysts can be considered as an efficient and reliable method for hydrogen production. The application of membrane reactors (MR) – in which production and separation of hydrogen (pure hydrogen production) occur in the same reactor vessel – is highly beneficial to omit costly and complicated unit processes for hydrogen purification. Besides, by removal of one of the products (hydrogen) via permeation through the membrane, equilibrium limitations are overcome even at unbeneficial operating conditions, leading to higher production of hydrogen and higher efficiency of the reforming system [2]. In the case of a palladium-based membrane, fuel cell grade hydrogen can be obtained, so that a fuel cell can be fed online as pure hydrogen is generated (permeated).

1.2 The objectives of the PhD work

The main objective of this thesis is to perform a comprehensive investigation on a pure hydrogen generating system – named as the reformer – in which ethanol steam reforming is performed over noble metal-based catalysts in a membrane reactor for on-site production of fuel cell grade hydrogen. The specific scopes are:

- To perform ethanol steam reforming (ESR) over Pd-Rh/CeO$_2$ in a membrane reactor (MR) containing Pd-Ag membranes to observe the performance of the MR in the ESR atmosphere at several different operating conditions aiming to introduce the best operating conditions in terms of hydrogen production and recovery
  - Experimental study of the performance of a Pd-Rh catalyst in ethanol steam reforming (ESR) atmosphere at different operating conditions regarding temperature, pressure, flow rate of the ethanol-water mixture (fuel), and

different molar ratios between ethanol and water (S/C ratio), in terms of ethanol conversion, hydrogen and byproduct selectivity, the permeation rate of hydrogen through the membrane, hydrogen yield and hydrogen recovery.

o Comparison between the CMR (presented in this thesis) and the Staged Membrane Reactor configuration (SMR) [2,3] reported in the literature to emphasize the enhancements and benefits of the CMR.

- To perform a thermodynamic analysis on the performance of the reformer at different operating conditions in terms of energy and exergy efficiency to understand the most favorable operating conditions based on the exergy efficiency, and to obtain detailed information on the sources of thermodynamic losses and to introduce the possible ways to optimize the reforming system thermodynamically.
  o Exergy evaluation of the reformer based on the experimental results.
  o Investigation of the sources of exergy loss and exergy destruction.
  o Analysis of the heat losses and potential resources of recoverable exergy to give relevant solutions to increase the exergy efficiency of the reformer aiming to optimization of its thermal performance.
  o Comparison between the CMR (presented in this thesis) and the Staged Membrane Reactor configuration (SMR) [2,3] in terms of exergy evaluation factors based on the experimental results.

- To model and simulate the reformer presented in this thesis at steady and transient states regarding the production rate of ESR products and the permeation rate of pure hydrogen aiming to model a system capable of regulating the pure hydrogen production rate according to the modifications needed to adjust the electrical load of a fuel cell, when fed online.
  o Simulation of the production rate of different species – especially hydrogen – as the main products of the ESR process in the catalytic membrane reactor (CMR) at tested operating conditions.
  o Simulation of pure hydrogen production both based on the Sieverts' Law and a black box model, as an essential step for dynamic modeling of the reformer.
  o Simulation of the dynamic performance of the reformer in terms of pure hydrogen production rate and its variations in the case of pressure or fuel flow rate set point modifications

1.3 Outline of the thesis

In the second chapter, an introduction to hydrogen energy is given followed by a comprehensive literature survey on the production of hydrogen via catalytic reforming of

ethanol. Moreover, the state of the art is given regarding the catalytic steam reforming of ethanol in membrane reactors.

In the third chapter, the experimental results of the ethanol steam reforming (ESR) over the Pd-Rh/CeO$_2$ in a membrane reactor (MR) containing Pd-Ag membranes are given. The experimental results include the selectivity of the ESR products (H$_2$, CO, CO$_2$, and CH$_4$), hydrogen permeation rate (pure hydrogen production rate), hydrogen yield, and hydrogen recovery. The effect of the operating conditions (pressure, temperature, fuel flow rate, and the composition of the fuel, i.e. the molar ratio of water to ethanol) on the mentioned evaluation factors are discussed in details. Finally, a comparison between the reforming system presented in this thesis (CMR) and the Staged Membrane Reactor (SMR) configuration reported in the literature [2,3] is given.

Chapter 4 is devoted to the comprehensive thermodynamic analysis of the CMR based on thermal and exergy efficiency using the experimental results. Exergy factors such as exergy destruction, unused exergy, and exergy efficiency are discussed and the results are presented via several figures and tables. The sources of exergy loss and the possible ways of the exergy recovery and optimization of the reformer in terms of the exergy efficiency are given. The advantages of the exergy analysis over the traditional thermodynamic analysis (based on thermal efficiency) are stated. This chapter also includes the thermodynamic analysis of the Staged Membrane Reactor (SMR) base on the experimental results reported in the literature for this configuration in ESR environment at similar operating conditions. A comparison between the CMR and the SMR also is presented.

The results of the modeling and simulation of the reformer (the CMR) are presented in chapter 5. The methodology to develop the static models and dynamic simulation is discussed. Static models to calculate the molar production rate of ESR products, together with the calculation of the permeation rate of hydrogen through the membrane are given. Arrhenius' law based formulation is used to model the molar production rate of ESR products. In the case of the pure hydrogen production rate, two models, i.e. a black box model and a model based on the Sieverts' law are presented. The dynamic simulation model of the hydrogen permeation rate (transient state) is developed based on ideal gas law assumptions by using a first order function solved by Ordinary Differential Equation (O.D.E) solver.

Two appendixes are given in this thesis. The first appendix (appendix A) is devoted to the analysis of the errors and uncertainty of the experimental measurements and exergy analysis. Appendix A is presented to support the data given via tables and figures and to demonstrate the range of the validity based on the maximum errors.

The second appendix (appendix B) is devoted to the full results of the modeling of the molar flow rate of the ESR species (H_2, CO, CO_2, CH_4, H_2O) in the CMR. The formulation of the models and the parity plots are presented and are supported by tables of the fitting parameters for the species.

An introduction to the hydrogen production via catalytic reforming processes, and the membrane reactors, together with a comprehensive literature review on the hydrogen production over common catalysts in the membrane reactors are given in the next chapter.

Chapter 2

Hydrogen production and membrane reactors

Abstract

The previous chapter provided a general overview and a short history of the world energy demand and probable solutions for clean energy production, together with the objectives and scope of this thesis. In this chapter, an introduction to the hydrogen production is given. A short history about using hydrogen as an energy carrier together with the current considerations of hydrogen as a renewable source of energy is presented. The introduction and definition of a membrane reactor (MR) is followed by the review of the production of hydrogen via catalytic steam reforming of ethanol in membrane reactors (MRs). The state of the art on the production of hydrogen in catalytic membrane reactors (CMRs) via steam reforming of ethanol over noble metal based catalysts is presented.

2.1 Hydrogen

The first ideas of using hydrogen as a source of energy appeared and revived around two centuries ago, when for the first time the French writer Jules Verne talked about the future when humankind will heat himself using water splitted into hydrogen and oxygen [29,30]. In the 20th century, the idea of hydrogen energy was brought to the scientific and engineering level and developed rapidly by many research groups worldwide and finally in 1974 The Clean Energy Research Institute of Miami University (USA) established the International Association for Hydrogen Energy (IAHE). Soon after, the IAHE started to publish the International Journal of Hydrogen Energy (IJHE), which is one of the most well-known references of the scientific research literature on hydrogen-related research works.

Concerning the attempts to achieve the clean energy production targets, hydrogen as an energy carrier can serve the energy production sector with the necessary requirements. In short, the advantages of hydrogen as energy carrier over other energy sources are [31]:

- If hydrogen is combusted with air, heat is released and pure water is produced as the only product; hydrogen is the only carbon-free fuel available for combustion engines.
- It is produced via conversion of biofuels – for example bioalcohols – as promising replacements to the fossil fuels.
- It is used in centralized or remote applications with reduced impact of energy production.
- Thanks to commercially available fuel cells, hydrogen is the main fuel of fuel cells, as electricity producer devices with numerous advantages.
- In the future, on-site hydrogen production can be possible (transportation infrastructure not needed).

However, there are challenges and obstacles to be overcome for the utilization of hydrogen as a reliable energy carrier for comprehensive applications in the society. Although a lot of researches have been done recently to investigate the techniques and methods of production of hydrogen, no authoritative position compared to other clean energy resources is seen yet in the energy policy frameworks [32]. The European energy policy framework does not ignore hydrogen energy systems as carbonless sources of energy. But on the other hand, it has been sufficed to mention the importance of regulations and infrastructures development for hydrogen applications in the energy sector [33]. This can be attributed to some issues. First, hydrogen and fuel cells are in the early stage of entering the market commercially. Second, requirements of special infrastructures for distribution of hydrogen makes it complicated to utilize hydrogen and fuel cells. In conclusion, more supportive policies are

needed to push hydrogen technology and systems toward an existing option for the energy sector.

Regarding the attempts for introducing the hydrogen energy systems, the concept of hydrogen economy has recently defined. Hydrogen economy in general aims to serve the human with hydrogen for its energy demand, considering the point that hydrogen is an energy carrier, not a source of energy [34]. The same challenges facing the production of hydrogen will face to the hydrogen economy. There is no point in investments on hydrogen infrastructures for distribution and refueling, if there is no market for hydrogen. Again, the high cost of fuel cells and hydrogen production from renewable resources adds another challenge to the future of hydrogen economy. Nevertheless, according to McDowall and Eames [35] there are 4 major drivers of a hydrogen economy: climate change, energy security, local air quality, and competitiveness.

In the light of EU energy policies and by knowing the fact of taxation exemption of hydrogen energy, the effort to introduce hydrogen as a competitive and reliable energy carrier must be continued [32]. The key factor to success in hydrogen technology development is to receive the governmental supports via energy policies set mainly by the two main powers i.e. EU and U.S.A. The economic, technological and institutional challenges of introduction of hydrogen in the energy systems in Europe are addressed by The European Hydrogen Energy Roadmap, known as HyWays [36]. The HyWays aims to open an eye and give ideas on how to receive the political support and overcome the barriers that hydrogen energy encounters. According to HyWays, 80% of the light duty vehicles and city buses should be supplied by clean hydrogen by 2050. Consequently, several initiatives such as 'Fuel Cells and Hydrogen Joint Technology Initiative' and 'Hydrogen and Fuel Cell Program Plan' were started in Europe and U.S.A, respectively [34].

2.2 Hydrogen Production

As previously stated, the production of hydrogen is dependent on the technological advancements, policymaking, and even the price of fossil fuels as the main sources of energy. Apart from this, according to Ros et al. [37] at least 75% of the produced hydrogen will be used in the transportation sector. Until 2030, the main hydrogen production technologies are anticipated to be methane steam reforming and electrolysis of water, both accompanied with carbon capture and sequestration (CCS) processes. But figures for 2050 perspective show that the hydrogen production would be mainly dependent on natural gas reforming and biomass conversion [38]. Again, the hydrogen production is claimed to be supported by CCS techniques. In this regard, and having in mind that CCS technology is not approved for the large scale and worldwide scale applications, the concept of CO_2-free hydrogen production rises. Although renewable energy sources such as solar and wind can be utilized for production of electricity needed for electrolysis of water [37], the challenge

of renewable resources still exist. Electrolysis of water will require huge amount of electricity, which makes it unavoidable to be supplied by a clean electricity source, and on the other hand, natural gas reforming will result in enormous amount of CO_2 production that needs to be supported by CCS.

In general, the so-called renewable hydrogen can be produced by electrolysis or thermolysis of water (as long as the required electricity is supplied by wind or solar power plants), thermochemical and biological conversion of biomass, and photolysis of water [39]. However, all these technologies are in the development and research stage and need to access renewably produced electricity.

2.2.1 Catalytic conversion of ethanol

Hydrogen is directly produced from ethanol by three main catalytic conversion routes i.e. steam reforming (ESR), partial oxidation (POX), and autothermal reforming (ATR). The main difference between the three ways refers to the converting coreactants used in each process. The pros and cons of each process are briefly discussed.

The highest amount of hydrogen is obtained by steam reforming of ethanol so that theoretically (complete conversion of coreactants to carbon dioxide and hydrogen) 6 moles of hydrogen is formed per one mole of ethanol in the feed. Ethanol can catalytically be converted to hydrogen and carbon dioxide in the presence of steam via the following reactions [24]:

$$C_2H_5OH \rightarrow H_2 + CO + CH_4 \hspace{4cm} 2.1$$

$$CO + H_2O \leftrightarrows H_2 + CO_2 \hspace{4cm} 2.2$$

$$CH_4 + 2H_2O \leftrightarrows 4H_2 + CO_2 \hspace{4cm} 2.3$$

$$CH_3CH_2OH + 3H_2O \leftrightarrow 2CO_2 + 6H_2 \hspace{3cm} 2.4$$
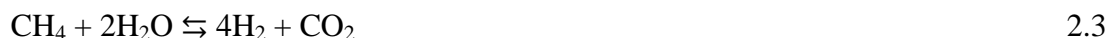
$(\Delta H^0{}_{298\ K} = 173.3\ \text{kJ/mol})$

Equation 2.4 represents the overall ESR reaction. The mechanism is presented by reactions 2.1 to 2.3 that accounts for ethanol decomposition, water gas shift (WGS) reaction, and methane steam reforming (MSR), respectively. As reported in the literature, other chemical species such as ethylene, acetaldehyde, and dimethyl ketone can be formed during catalytic reactions depending on the catalysts used [40–42]. The stoichiometric molar steam to ethanol ratio (S/E) is 3; however, higher amounts can be used. The bioethanol produced by fermentation of biomass has S/E ratio of 7-12 that can directly be used for the ESR process.

The main drawback of ESR is the endothermicity. In one hand high energy input is needed for running the reaction and evaporating the liquid fuel, and on the other hand, the

hydrogen formation is limited by thermodynamic equilibrium due to the nature of the reactions. The thermodynamic equilibrium limit can be overcome at S/E ratios higher than 20, leading to 5.5 mole hydrogen per mole of ethanol at 773-873 K [22].

At any rate, much higher energy input is needed at high S/E ratios for evaporation of water. Another disadvantage of this process is the formation of CO, which can poison the electrocatalysts of the PEMFCs and makes it inevitable to purify the produced hydrogen prior to feed the fuel cell. Water gas shift reaction promotion is one of the most investigated methods for CO removal together with preferential oxidation of CO.

In partial oxidation of ethanol (POX), ethanol is reacting with oxygen for production of hydrogen and carbon dioxide. Thus, the disadvantages of ESR are overcome but the hydrogen yield drops to three moles of hydrogen per mol ethanol (eq. 2.5).

$$CH_3CH_2OH + \frac{3}{2}O_2 \rightarrow 2CO_2 + 3H_2 \hspace{3cm} 2.5$$

$(\Delta H^0_{298 K} = -552 \text{ kJ/mol})$

The advantages of POX process over ESR can be summarized as [22]:

- POX is a self-sustaining process and no external heating is required. Consequently, not only the energy consumption is decreased, but also the process plan is simplified and more compact.
- There is no equilibrium limitation resulting in operating at temperatures as low as 473 K.
- The chemical reactions are faster and the reactor scale needed for POX process is smaller than the one needed for ESR.

Apart from this, oxygen is a gaseous coreactant that does not need evaporation, and the presence of oxygen hinders the carbonaceous species to be formed and the lifetime of the catalyst is extended.

The drawbacks of the POX lie on the nature of oxidizing process in presence of oxygen because the total oxidation (combustion) of ethanol and hydrogen is thermodynamically favored. Both reactions (combustion of ethanol and hydrogen) are highly exothermic and competing with the partial oxidation of ethanol. This may cause low hydrogen selectivity. Besides, the mixture of ethanol and oxygen at high temperature in gas phase raises the risk of explosion.

ATR reaction is a combination of ESR and POX so that the reforming process is performed in presence of water steam and oxygen aiming to utilize the heat released by POX for ESR. For this reason, the concentration of oxygen and steam must be adjusted to be near the stoichiometric values to take the advantage of a thermally neutral process. Also by correctly

adjustment of oxygen content in the fuel, the disadvantages of POX can also be avoided and the process can be operated at lower temperatures rather than ESR. The presence of water steam can decrease the risk of explosion and the competitiveness of combustion reactions.

The disadvantage of ATR is the complexity of the process and the difficulty of adjustments for a steady state operation.

In general, the energy demand per mole of hydrogen produced during reforming processes follows the trend of ESR $\geq$ ATR > POX. The highest hydrogen yield belongs to the ESR, despite being endothermic. As a result, major share of research has been devoted to the investigation and technological maturity of ESR.

2.2.2 Side products of reforming processes

The main reaction pathway of ethanol reforming starts with the decomposition of ethanol to two important intermediates i.e. acetaldehyde and ethylene according to the following reactions:

$$CH_3CH_2OH \rightarrow CH_3CHO + H_2 \qquad\qquad 2.6$$

$$CH_3CH_2OH \rightarrow C_2H_4 + H_2 \qquad\qquad 2.7$$

The presence of these two species has been reported by some researchers [43,44]. Ethylene and acetaldehyde are formed prior to formation of carbon oxides. Ethylene plays an important role in coke formation, which is one the most important factors leading to catalyst deactivation. On the other hand, acetaldehyde further promotes the formation of hydrogen. Both intermediates undergo steam reforming resulting in the formation of carbon oxides, hydrogen, methane and ethane [22,44]. Lu et al. [44] reported the observation of ethane formation that could be a result of ethylene hydrogenation:

$$C_2H_4 + H_2 \rightarrow C_2H_6 \qquad\qquad 2.8$$

$(\Delta H^0{}_{298\,K} = 14\ kJ/mole)$
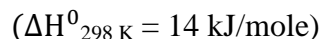
The reactions in presence of water are endothermic (except WGS) and lead to more hydrogen production. Methane generation mechanisms are exothermic and are favored at low temperatures leading to less hydrogen production.
The formation of coke in reforming processes is common [45]. Coke formation is a result of several complex reactions. In this regard, the formation of ethylene has an important role of the deposition of carbon on the surface of the catalyst:

$$C_2H_4 \rightarrow polymeric\ chains \rightarrow 2C + 2H_2 \qquad\qquad 2.9$$

According to the open literature, numerous catalysts have been investigated for the ESR process and, among them noble metals have shown superior catalytic reactivity in terms of higher hydrogen production (higher ethanol conversion) and robustness of the performance (durability) at different operating conditions [46,47]. Further, the formation of undesired chemical species is almost zero when noble metal-based catalysts are used for ESR process. This is considered as one of the main advantages of noble metals over other catalysts that may compensate to some extent the relatively higher price of these catalysts compared to conventional ones.

2.3 Ethanol steam reforming in the literature

A catalyst must maintain special properties to be appropriate for the ESR process. The most important characteristics of catalysts can be named as ability to dissociate the C-C band preferably at low temperature, high reactivity toward CO conversion, and durability under catalytic reaction conditions [22]. Before 2007, Rh and Ni were the most commonly tested catalysts for hydrogen production via ESR [46,48]. After 2007, Co and other noble metals such as Pd, Pt, and Ir, and bimetallic active phases attracted a lot of attention due to enhanced reactivity and robustness in the ESR environment. The catalytic activity depends both on the selection of the relevant support and the preparation method. Thanks to special characteristics that favor ethanol dehydrogenation but inhibit dehydration, supports such as MgO, ZnO, CeO_2, La_2O_3, promoted Al_2O_3, and promoted ZrO_2 were introduced as suitable supports for Ni and Ru in terms of hydrogen production and long-term stability [28]. Additionally, the development of bimetallic catalysts results in higher hydrogen production and catalyst stability. The promoted ethanol conversion and hydrogen selectivity in the case of the development of bimetallic catalysts have been reported by several researchers [49–53]. Investigations on the performance and applicability of the catalysts for ethanol steam reforming can be divided into two groups: catalysts without noble metals, and catalysts containing noble metals.

2.3.1   Ethanol Steam Reforming over catalysts without noble metals

Cobalt and nickel are among the most tested catalysts for ESR process. Cobalt is a cheap catalyst able to convert ethanol at temperatures as low as 623 K so that WGS reaction is enhanced and CO concentration is kept low. Besides, methane is not formed as an intermediate, leading to higher hydrogen yield. Co supported on Al_2O_3 and SiO_2 was tested by Batista et al. [54] and complete conversion and selectivity of 65% were shown at 673 K. The concentration of CO in the gaseous mixture dropped to 800 ppm in the case of Co/Al_2O_3 with 18% Cobalt. The authors reported that the produced CO reacted with water (water gas shift reaction) or with hydrogen (methanation), which resulted in higher conversion over Co catalyst. Co/Al_2O_3 showed superior activity in terms of CO removal. Lucredio et al. [55] tested cobalt catalysts supported on Al_2O_3 and SiO_2 in the ESR

environment. The catalysts were prepared using a Co precursor dissolved in methanol. The Co/SiO_2 showed the highest selectivity towards hydrogen. The carbon formation over the catalyst surface after the reaction was characterized by means of Raman spectroscopy. The Raman results of the samples after the catalytic tests showed that the type of carbon formed was affected by the particle size. Co-based catalysts over several supports such as ZnO, MgO, Al_2O_3, SiO_2-TiO_2, V_2O_5, La_2O_3, CeO_2, and Sm_2O_3 were prepared by Llorca et al. [56,57] and tested at 573-723 K in the ESR environment. The best catalytic activity was shown by Co/ZnO so that at 100% ethanol conversion, selectivity up to 73.8% to H_2 and 24.2% to CO_2 was obtained. After the reaction, Co particles were covered by disorder carbon. Carbon deposition was found on the surface of the ZnO support as well. In another study by the same authors [58], they prepared Co catalysts by coating the micromonolithic support with Co_3O_4-ZnO. They reported more than 73% volume of hydrogen in the gaseous product at 773 K and S/C=3. Cobalt supported on CeO_2 has shown superior activity and hydrogen yield compared to other commercial supports of similar particle size at 673-773 K [59–61]. The greater performance of Co/CeO_2 nanocubes is attributed to improved metal dispersion, increased reducibility, and higher oxygen mobility [59]. Li et al. [62] studied the synergic effect of ZrO_2 and CeO_2 (to suppress the methanation of the ZrO_2) on ethanol conversion promotion. The $Co/CeZrO_2$ showed higher activity than Co/ZrO_2 so that ethanol conversion of 100% and hydrogen yield of 82% (4.9 mol H_2/mol ethanol) at 723 K was reached.

Co/Mg/Al hydrocalcite catalysts over ceramic honeycombs were tested by Espinal et al. [63] for ESR and it was reported that the hydrocalcite with a Co:Mg:Al molar ratio of 1:2:1 showed the best catalytic performance with very small coke formation. Dominguez et al. [64] used cobalt talc doped with iron for ESR process and reported that at 673 K and 2 bar, 1.04 l_N H_2 per ml of ethanol is obtained at steam to carbon ratio of 3 (S/C=3). In another study, Espinal et al. [65] studied the effect of the addition of potassium to catalytic regarding the activity and stability of Co/Mg/Al hydrocalcite catalysts for ESR process. Very low carbon deposition together with presence of oxidized cobalt as an active species was observed. As mentioned by Llorca [66], cobalt catalyst doped over K^+ was tested successfully for bio-ethanol conversion during 300 hours without carbon formation, which is an advancement in ethanol conversion over cobalt-based catalyst. Dominguez et al. [40] tested a catalytic membrane reactor consisting of cobalt talc ($Co_3[Si_2O_5]_2(OH)_2$) supported on cordierite. The experiments were performed in a Pd-Ag metallic membrane to separate hydrogen from produced gases. The test was done in two ways. First, honeycomb catalysts were placed in series, and second, the membrane was covered by small pieces of the catalyst and a superior reactivity in terms of pure hydrogen production was reported.

Nickel-based catalysts are used due to their known and approved high capability of C-C bond cleavage [67]. Ni is normally supported on alumina for better endurance in the reaction conditions but still having the disadvantage of being prone to carbon deposition

[22]. Consequently, other elements are added to Ni-based catalysts as a promoter to the catalytic activity. Supports such as MgO, SiO_2, CeO_2, Al_2O_3, Al_2O_3 – La_2O_3, and ZrO_2 have been tested and in all cases improved activity, durability and resistance against coke formation has been reported [68–72]. Ni/Al_2O_3 catalyst mixed with CeO_2 was tested by Laosiripojana and Assabusrungrat [73]. The results showed that while the selectivity of the catalyst toward hydrogen was lower compared to pure Ni/Al_2O_3, the resistance against carbon formation was considerably higher. Chen et al. [74] used perovskite-type oxides $La_{1-x}Ca_xFe_{0.7}Ni_{0.3}O_3$ as an improved catalyst for ESR process capable to resist against carbon deposition. They found it promising to regulate the redox ability of the perovskite-type oxides for carbon deposition prevention. Many other additives such as copper, lanthanide, molybdenum, calcium, and magnesium in combination with nickel have been investigated and reported in the literature [22,75–78]. Adding elements such as La and Mg decreased the formation of C_2H_4 and increased the activity of the catalyst and the selectivity towards hydrogen [79,80]. Hernandez et al. [81] added W to Al_2O_3 to stabilize the Ni-based catalyst. The surface area of the catalyst decreased and the pore volume of the mesoporous materials increased. Hydrogen selectivity of around 70% was reached at 823 K on alumina with Ni-W. Complete conversion and selectivity of 70% over $NiAl_2O_4$ spinels was reported by Barroso et al [82]. $Ni/MgAl_2O_4$ was doped with Ce and in this case the selectivity was slightly improved and increased to 74% at 923 K after 10 h [83]. Biswas and Kunzru studied the adding of Cu and Ca to Ni supported on CeO_2-ZrO_2 and reported an enhancement in catalyst activity and promotion of the WGSR [84]. Ca was the best dopant in terms of hydrogen production. ZrO_2 played the role of stabilizer in Ni-based catalysts. The high activity was ascribed to the high dispersion of Ni and intimate contact between the metals, which resulted in carbon formation prevention on the catalyst surface [85]. Souza et al [86] studies Co, Mo, and Zn prepared in Ni-based hydrotalcite catalyst at 673-873 K and concluded that lower reaction temperatures favored the dehydration and dehydrogenation of ethanol, while synthesis gas was produced mainly at higher temperatures . Co-, Mo- and unmodified samples presented higher selectivity towards H_2 and CO at higher temperatures, while samples modified with Co, Mo and Zn showed higher activity at intermediate temperatures [86].

2.3.2 Ethanol Steam Reforming over noble metal-based catalysts

As discussed before, one of the major problems of catalytic steam reforming of ethanol is carbon deposition on the catalyst leading to the severe deactivation. It is proven that noble metals not only are able to highly convert ethanol due to their significant reactivity, but also hinder carbon from deposition on the active sites [47,87]. This distinctive property has attracted the attention of a lot of research groups toward noble metals for ESR application so that according to Llorca et al. [22] nearly 40% of the published works talked about Rh-based catalysts and other 30% corresponds to the evaluation of Pt-based ones.

According to the literature, CeO_2, ZrO_2, and Al_2O_3 are among the most used supports for the noble metals. The catalytic activity of Pt supported by Al_2O_3, ZrO_2, and Al_2O_3-ZrO_2 was investigated by Domok et al. [88] in terms of the performance of catalyst in conversion of ethanol and CO. Ciambelli et al. [89] also tested Pt/CeO_2 catalyst for ESR at 573K and reported total conversion of ethanol and very low production of CO. CeO_2-supported Pt/Ni catalyst for conversion of biomass derived ethanol was synthetized and tested by Palma et al. [90]. The study was done at 523-873 K and very high selectivity of catalyst was reported leading to very low coke formation even at stoichiometric ratio of ethanol/water. The catalyst selectivity improved by increasing the amount of water in the feeding fuel.

Goula et al. [91] used commercial Pd/γ-Al_2O_3 for production of hydrogen rich gas via ESR and they obtained hydrogen selectivity up to 95% at 873 K. Complete ethanol conversion reached at even low temperature and the selectivity hydrogen and CO_2 decreased with S/C ratio. The same catalyst was tested by Auprêtre et al. [92] and hydrogen selectivity of 55% was reached at 973 K and atmospheric pressure under stoichiometric reaction conditions (S/C$\approx$1.5). Chen et al. [93] studied Pd/ZnO-Al_2O_3 at 723 K and concluded that acetaldehyde and hydrogen were the main product of ESR reactions and coke formation was not hindered by Pd promotion. Ethanol conversion of 65% together with hydrogen selectivity of 65% were reached, which are considerably lower compared to similar reported studies. Other authors mentioned that Pd/CeO_2-Y_2O_3 stabilized by ZrO_2 showed good initial activity but significant deactivation was observed [94]. Complete ethanol conversion was reached at 873 K where hydrogen selectivity was 67-74%. Ru/Pd/Ag supported on CeO_2/YSZ was used for ESR experiments and the Ru-based one showed the superior activity. Positive effect of CeO_2 on preventing the carbon deposition plus metal selectivity of catalyst to syngas was mentioned as the main reason of the good performance of the mentioned catalyst. Scott et al. [52] found that the bimetallic catalyst 0.5%Rh-0.5%Pd is able to break the C-C bond of ethanol at 400 K. This catalyst showed maximum ethanol conversion (nearly complete) and hydrogen selectivity (64%) at 773 K. Pd/HZSM-5 catalyst with 5%wt Pd and prepared by wet impregnation method was tested by Lie et al. [95]. The best performance was reached at 973 K and S/C=9.2, where the hydrogen selectivity was 58.1-84.3%. Frusteri et al. [96] reported the selectivity of 70% for Pd/MgO. The selectivity towards CO_2 decreased drastically because of catalyst deactivation, which consequently increased the selectivity towards CO. Acetaldehyde, and ethylene were both detected (15% and 6%, respectively). The study of the temperature effect on the performance of Pd-Ru/Nb_2O_5-TiO_2 in terms of hydrogen production in the ESR environment showed the maximum performance at 573 K [97]. The presence of H_2, CO_2, CH_4, CO, C_2H_4, C_2H_6, C_2H_4O and $(C_2H_5)_2O$ was reported at 300-723 K.

More investigations on Rh can be found in the literature compared to Pt or Pd. For ethanol steam reforming reactions, Rh-based catalysts are very active and well known for the high selectivity towards hydrogen. Hydrogen selectivity of 73.5% at 873 K over Rh/Al_2O_3

catalyst was reported by Auprêtre et al. [92]. The activity of Ni-based catalyst was compared to Ru-based one and it was reported that although Ni-based catalyst gave higher hydrogen yield, its selectivity towards CO_2 was lower. In the case of $Ce_xZr_{1-x}O_2$ mixed oxide-supported 1 wt.%Rh catalysts, the best performance in terms of the highest hydrogen yield and the lowest coke deposition belonged to the $Rh/Ce_{0.5}Zr_{0.5}O_2$ at 873 K [98]. At all operating conditions (temperature and S/C ratio); the ethanol steam reforming yielded a large amount of methane, which reduced the hydrogen production. The formation of methane was ascribed to the CO hydrogenation. Roh et al. [99] focused on a support prepared by a co-precipitation method having composition of $Ce_{0.8}Zr_{0.2}O_2$. The best performance in terms of hydrogen yield was reported at 723 K in the case of a $2\%Rh/Ce_{0.8}Zr_{0.2}O_2$ catalyst, prepared via impregnation without pre-calcination of support. The high activity of this catalyst (100% ethanol conversion and 4.3 mol hydrogen per mol ethanol at 723 K) was ascribed to the strong interaction between Rh and $Ce_{0.8}Zr_{0.2}O_2$ and the high oxygen transfer rate favoring reforming of acetaldehyde instead of methane production. Rh-based catalysts were prepared by co-precipitation of aqueous solutions of Ce and Zr (and/or Pr and Y) nitrate and tested at 723 K and pressure up to 15 bar in the ESR environment [100]. According to the reaction pathway of ESR over Ru, the selectivity towards methane reaches an equilibrium leading to high selectivity at higher pressures. Huang et al. [101] studied CeO_2-supported catalysts for low temperature (573 K) ethanol steam reforming using a multi-channel reactor. The addition of Co to Rh/CeO_2 results in decreased catalytic selectivity towards CO and CH_4. Catalyst deactivation was seen probably due to catalyst sintering, metal oxidation and coke deposition during ESR. Wu and Kawi [102] studied Ru-based catalysts based on several supports at 923-1073 K. Ru/Y_2O_3 produced the highest hydrogen rate via ethanol steam reforming due to the synergic effect of electron-accepting Y_2O_3 electron donating Rh. Thanks to the strong ability of Y_2O_3, the hydrogen of ethanol was oxidized to produce gaseous hydrogen and reduced the hydrogen from water. In general, the order of reactivity was Rh/Y_2O_3 > Rh/ CeO_2 > Rh/La_2O_3 > Rh/Al_2O_3. For the first time a novel iron promoted Rh-based catalyst $(Rh–Fe/Ca–Al_2O_3)$ was prepared by Chen et al. [103] to produce a CO free hydrogen rich gas via ethanol steam reforming at low temperature (623-673 K). The iron oxides in the vicinity of Rh sites reduce the CO adsorption on Rh sites resulting in high hydrogen selectivity of 66% at 623 K. Iron oxide promoted the WGSR via which CO is converted to CO_2. In another study, it was shown that addition of Ni to $Rh-Y_2O_3-Al_2O_3$ wildly improved the catalytic reactivity correlated to increase in the methane steam reforming activity [104].

Rh supported on CeO_2 was tested by Da Silva et al. [105]. They used both low and high surface area ceria and concluded that despite the deactivation of the catalysts, no carbon formed on the catalyst. $Rh/CeO_2/Al_2O_3$ catalyst at temperature range of 673-873 K was tested by Peela et al. [106] for ESR and they found that when ceria was added to 2% Rh/Al_2O_3, the catalytic activity was improved. The test was done using two configurations of packed bed reactor and microchannel reactor. It was shown that although the hydrogen

yield of microchannel reactor was slightly higher, the overall reactivity stayed the same for both configurations. The coke formation decreased by 3.5 times. Wanat et al. studied Rh and Rh-Ce catalyst in water gas shift and steam reforming of ethanol reactors [107]. More than 99% conversion and methane selectivity of less than 1% were obtained with Rh–Ce catalyst at 1073 K. Very high hydrogen selectivity (98%) was obtained by coupling the steam reforming reactor with combustion Pt-based catalyst (Pt-Ce). Rh and Rh-Co catalysts supported on ZrO_2, Al_2O_3, MgO, and Mg-Al showed high catalytic activity and carbon formation was lower specially on the bimetallic noble metal catalysts [108,109].

Gucciardi et al [110] used Rh/Al_2O_3 for both bio-ethanol and DME steam reforming at atmospheric pressure and temperature range of 823-923 K. They studied the catalytic activity and stated that the catalyst was less prone to coking in case of DME. Rh and Co-based catalysts supported on MgO, Al_2O_3, and Mg-Al oxides were evaluated for the ESR by Moura et al. [108]. In terms of the hydrogen yield, ethane selectivity, and specific surface area during the reaction, Mg-Al supported Rh and Co catalysts were introduced as the best ones. Lopez et al. [2] evaluated the performance of $Pd-Rh/CeO_2$ for ESR by using a membrane reactor for online hydrogen purification. The effect of different operational conditions was studied and the best performance was obtained at 923 K and pressure of 9-11 bar. The same catalyst was tested by Divins et al. [41]. The microchannels of the silicon micromonolith were coated with $Pt-Rh/CeO_2$ and were tested for ESR process at 873 K using bio-ethanol with S/C of 2. Up to 3.8 moles hydrogen per one mole of ethanol was obtained and a significant improvement in the reactivity was cited compared to the conventional cordierite monoliths. In another work by Cobo et al. [111] Pt-Rh bimetallic catalyst supported on La_2O_3 was selected for ESR process. Temperature of 873 K together with the S/C of 7 was chosen for the experiments. 99% of the ethanol was converted and small carbon deposition was detected that was attributed to the formation of $Rh-Pt-Rh_2O_3$ sites. Cavallaro [112] used Rh/Al_2O_3 catalyst for ESR at 323-923 K and reported that at 923 K no carbon deposition was detected and the reactivity of the catalyst was maintained for several hours. Complete ethanol conversion was reached at S/C ratio of 4.2. A range of noble metals including Rh, Pd and Pt was evaluated by J.P. Breen et al. [113] for ESR process at 673-1023 K. They used CeO_2, ZrO_2, and Al_2O_3 as the supports and concluded that Rh and Pt, when supported on CeO_2/ZrO_2 showed the best activity of 100% ethanol conversion at around 923 K. Co, Ni, Rh, Rh-Co or Rh-Ni supported on mixed Zr-Ce oxides for redox characteristic enhancement were tested by Sarria et al. [114]. They mentioned that the stability of cobalt catalyst together with resistance against carbon formation was remarkably improved by addition of small amount of Rh. The enhanced activity of Ni/CeZr catalyst for ESR process was reported thanks to the addition of Rh. D.K. Liguras et al. [115] comprehensively studied the active metallic phases of Rh, Ru, Pt and Pd over different supports of Al_2O_3, MgO and TiO_2 for ESR process at 873-1123 K. They reported that Ru/Al_2O_3 was able to fully convert ethanol with a hydrogen selectivity of 95%.

Idriss et al. [87] showed that Rhodium in presence of Platinum or palladium is able to completely convert ethanol to gaseous species. Besides, they reported very stable activity with no sign of carbon deposition after three weeks of operation for ESR process. The reported results clearly represent the advantages of noble metal-based catalysts and the possibility of overcoming the major challenges of ESR process i.e. coke formation, and catalytic durability. The robustness of noble metals under the operational conditions can be considered as compensation to the high price of these materials.

Regarding the application of ceria, still, better results belong to the combination of Rh and Pd supported on ceria. It has been proved that high oxygen storage capacity (OSC) together with the properties such as easy reducibility via facile $Ce^{III} \leftrightarrow Ce^{IV}$ equilibrium, makes ceria a very durable material at high temperatures and very active during reducing/oxidizing processes [116].

2.4 Catalytic Membrane Reactors (CMRs)

The reaction temperature is an important operational parameter when conducting alcohol and bio-alcohol reforming reactions. High temperatures are necessary for bond cleavage, but moderate temperatures are preferred for the WGS equilibrium to favor the formation of hydrogen and CO_2 at the expense of CO and water, thus maximizing the production of H_2 and avoiding the requirement of bulky WGS units at the reactor outlet. For that reason, the use of catalytic membrane reactors (CMRs), where the generation and separation of hydrogen take place simultaneously (extractor membrane), appears as a very attractive approach to strongly simplify alcohol reformers. In addition, the shift effect that occurs in CMRs results in even higher hydrogen yields because the presence of a membrane selective to the hydrogen permits attaining very high conversion values in comparison with the traditional reactors operating under the same conditions [27]. In fact, the continuous removal of one of the reaction products, the hydrogen, promotes the reaction conversion beyond the equilibrium values. With respect to a classical configuration consisting of a reactor unit in series with a separation unit, CMRs represent a modern configuration in which an integrated reaction/separation unit has many potential advantages: reduced capital costs, improved yields and selectivities and drastically reduced downstream separation costs [117,118]. In addition, the reject gas from the membrane can be used as a fuel source for a catalytic combustor to provide a self-sustainable operation [119,120].

If hydrogen is intended to feed a low-temperature fuel cell based on proton exchange membranes (PEMFC), it needs to be purified in addition to WGS by means of further processes like pressure swing adsoprtion (PSA), CO preferential oxidation (COPrOx) or membrane separation. In this context, membrane reactor technology plays an important role as an advanced solution to conventional systems based on in series reactors, offering the opportunity of combining the reforming process for producing hydrogen and its separation in the same device (Fig. 2.1).
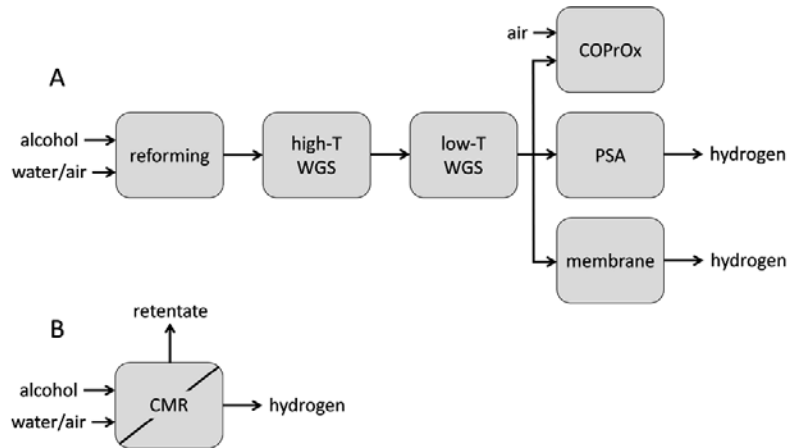
Fig. 2.1 Scheme of alcohol reforming using a catalytic membrane reactor for generating hydrogen (B) compared to a conventional system based on in-series reactors (A).
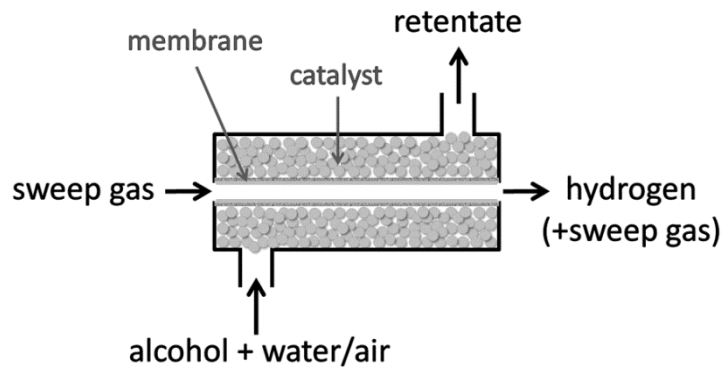
Fig. 2.2 Scheme of a catalytic membrane reactor

Retentate refers to the reaction side of the membrane. Hydrogen permeates through the membrane, a process that is usually assisted by a sweep gas. Among CMRs, palladium-based membrane reactors fulfill the requirements to obtain an ultra pure hydrogen stream (full hydrogen perm-selectivity) suitable for low-temperature fuel cell feeding (Fig. 2.2). The hydrogen permeation through dense Pd-based membranes follows the transport mechanism called solution-diffussion [121]. It involves five different activated steps [122]: dissociation of molecular hydrogen from the reformate at the gas-metal interface, adsorption of atomic hydrogen on the membrane surface, dissolution through the membrane, recombination of atomic hydrogen at the permeate side of the gas-metal interface to form hydrogen molecules, and desorption of molecular hydrogen. Each of this steps may control the permeation of hydrogen through the membrane depending on temperature, pressure, reformate composition, and membrane thickness [117]. The hydrogen flux permeating through the membrane, J_{H2}, can be expressed as:

$$J_{H2}=P_{H2}(p^n_{H2,r}-p^n_{H2,perm})/\delta \qquad\qquad 2.10$$

P_{H2} is the hydrogen permeability, $p_{H2,r}$ and $p_{H2,perm}$ are the hydrogen partial pressures in the retentate and permeate sides of the membrane, respectively, and δ is the membrane thickness. The thiner the membrane the higher the hydrogen flux. However, to ensure mechanical resistance and strenght of the membrane, thicknesses greater than 5 μm are commonly required. Assuming that the solid-state diffusion of hydrogen is rate-determining, and that hydrogen atoms form an ideal solution in the metal, the hydrogen pressure exponent (n) is equal to 0.5, which corresponds to the Sieverts' law:

$$J_{H2}=P_{H2}(p^{0.5}_{H2,r}-p^{0.5}_{H2,perm})/\delta \qquad\qquad 2.11$$

Then, a relatively large difference in the partial pressure of hydrogen between the reaction and separation sides is necessary for promoting hydrogen separation. Deviations from the Sieverts' law (n>0.5) may be attributed to the accumulation of impurities on the membrane surface or pinholes or microcracks in the membranes, or it may be attributed to mass-transport resistance. On the other hand, the hydrogen permeability dependence on the temperature can be expressed by a classical Arrhenius equation. Therefore, when the Sieverts' law is valid, the hydrogen flux can be expressed as:

$$J_{H2}=P^{0}_{H2}[(exp(-E_a/RT)](p^{0.5}_{H2,r}-p^{0.5}_{H2,perm})/\delta \qquad\qquad 2.12$$

which is known as the Richardson's equation. P^{0}_{H2} is the pre-exponential factor and E_a the apparent activation energy. The hydrogen permeation through the membrane is very sensitive to E_a.

As stated by Al-Mufachi et al. [123] , a variety of commercial dense metal membranes such as vanadium (V), niobium (Nb) and tantalum (Ta) have been studied to have the highest hydrogen permeability. The major drawback of such metals is their tendency to form stable oxide layers under ambient conditions. Palladium-based membranes are favorable in this regard (Pd) showing relatively high hydrogen permeability and are the suitable alternatives as a dense metal membrane.

Pd-based membrane is able to dissociate molecular hydrogen into monatomic form ready for fast diffusion through its lattice. Besides, in 1866, Thomas Graham discovered that Pd is capable of absorbing approximately 600 times its own volume in hydrogen whilst maintaining its physical properties and structural integrity [123]. Commercial applications of Pd-based permeators for producing very pure hydrogen have been studied for more than fifty years (i.e. in the fuel cycle of nuclear reactors). In fact, palladium membranes are among the oldest membranes studied for gas permeation and separation applications and are still the membranes with the highest hydrogen permeability and selectivity [124]. They are receiving renewed attention because of the prospect of the hydrogen economy. PEMFC require high-purity hydrogen for operation, with less than ca. 20 ppm of CO. The most critical issue for practical applications of Pd membranes in CMRs for hydrogen production is the chemical stability of the metal membranes (poisoning effects of the reaction mixture

on hydrogen permeation, carbon deposition on the membrane, etc.). The poisoning through exposure to hydrogen sulphide affects negatively Pd membranes, which can be destroyed irreversibly. This may be particularly important for reforming reaction of bio-alcohols, where H_2S traps may be necessary. The presence of CO in the reformate can cause the decrease of the hydrogen permeation at low temperature because CO molecules adsorb on Pd and displace adsorbed hydrogen, blocking the hydrogen adsorption sites (competitive adsorption). Water also blocks hydrogen permeability through the adsorption of oxygen atoms that form on the Pd surface during recombinative desorption of adsorbed water molecules. Coke affects negatively the hydrogen permeation by covering the membrane surface and lowering the hydrogen permeating flux. In addition, carbon atoms penetrate into the Pd lattice causing membrane failure owing to the concomitant expansion of the Pd lattice.

For a better chemical stability (poisoning) and physical stability (mechanical stress, hydrogen embrittlement), membrane reactors do not use pure Pd but various different types of Pd alloyed with other metals such as silver, copper, nickel, iron and platinum. Most Pd alloy membranes studied are of binary components, with a few of multicomponents. Pd-Ag (23 wt% Ag) and Pd-Cu (38-42 wt% Cu) alloy membranes are nowadays widely employed in CMRs for hydrogen production. The Pd-Ag is a plastic alloy with a specific hydrogen permeability of P_{H2}=3.4 $nm^3 \cdot mm \cdot m^{-2} \cdot h^{-1}$ $MPa^{-0.5}$ at 873 K [125]. The permeation rate of hydrogen through the membrane is a function of the membrane properties, and also the driving force, which is given by the difference of the square root of the hydrogen partial pressure on each sides of the membrane (Sieverts' law). The hydrogen permeation via a dense Pd-based membrane follows the mechanism of solution-diffusion transport. The membrane thickness plays an important role in the permeation rate, but on the other hand the mechanical strenght of the membrane must be taken into account. Membranes are generally deposited onto porous supports such as SiO_2, Al_2O_3, B_2O_3 and porous stainless steel (PSS), the later being advantageous because it has mechanical durability, a thermal expansion coefficient close to that of Pd, and ease of gas sealing. Unfortunately, PSS alloys the Pd at high temperatures, leading to lowering of the hydrogen permeability. This is usually solved by using an intermediate inert layer.

Pd membranes have been prepared by a variety of methods such as cold-rolling, evaporation, sputtering, spray pyrolysis, chemical vapor deposition, electroplating, and electroless plating [126]. During the rolling, a dense film without any pinholes and cracks can be maintained to the level of the appropriate thickness because the film is mechanically formed from the corresponding dense metal lump [127]. In the other methods a thin film is formed by rebuilding metal atoms and clusters, so that a considerable effort is required to avoid pinholes. Via cold-rolling and diffusion welding, robust Pd-based thin wall tubes less than 0.05 mm wall thickness have been systematically produced and their complete hydrogen selectivity and durability have been demonstrated in long term tests of CMRs

[128]. Today, numerous catalytic membrane reactors designs are available containing a bundle of Pd-based tubes or fingers [26,125]. These devices are capable for producing high hydrogen throughputs and can be used in compact reforming systems.

Pd alloy membranes have been used in catalytic membrane reactors mainly for WGS and steam reforming reactions of methane and methanol [117], but their use in the steam reforming of ethanol and higher alcohols is relatively new [129]. The main aim of the researchers involved in this field is oriented to emphasize the role of the membrane by analyzing the performances of the reaction system in terms of alcohol conversion, hydrogen yield and hydrogen recovery, that is, the amount of hydrogen collected in the permeate side vs. the total hydrogen produced during the reaction.

2.4.1 Ethanol steam reforming in CMRs

A large piece of work on ethanol steam reforming (ESR) with Pd-Ag membranes (wall thickness of 50 μm) using sweep gas has been carried out by Basile's group at the University of Calabria, Italy. Gallucci et al. [130] studied ethanol steam reforming over Ru/Al$_2$O$_3$ catalyst in three different Pd-Ag membrane reactors. The highest conversion attained at 723 K was about 50% in counter-current mode, which was significantly higher than that attained in a traditional reactor. However, in the CMR coke deposition occurred to a large extent with consequent deactivation of the catalyst. Basile et al. [131] used the same catalyst for performing ESR in a dense Pd-Ag CMR by varying the water:ethanol molar ratio between 3:1 and 9:1 at 573-673 K and 1.3 bar in counter current mode. Hydrogen recovery values of 22% were reached as well as ethanol conversion higher than 99% with a 56% hydrogen yield, which represented a significant improvement over the performance obtained with conventional catalytic reactors according to the shift effect [132]. Over the same catalyst, Tosti et al. [133] at ENEA (Italy) reached hydrogen yields as high as 80% working at 723 K and 2 bar using a dense thin wall Pd-Ag tube. The same device was used by the same authors [134] for studying Pt- and Ni-based catalysts, which showed a poor performance in terms of hydrogen yield with respect to the Ru-based catalyst (Ru>Ni>Pt at low feed, while for higher feed flow ratios the sequence was Ru>Ni=Pt).

Tosti et al. [135] also obtained kinetic expressions and modeled the CMR operation with the Ru-, Ni- and Pt-based catalysts in order to optimize the membrane reformer by assessing the ratio between the reaction and permeation kinetics. The membrane tube was divided into finite volume elements where the mass balances for both lumen and shell sides are carried out. The model was validated via experiments using three different kinds of catalyst, i.e. Ru, Pt and Ni-based. The effect of pressure was studied by Tosti et al. [136] in a Pd-Ag tube of 150 mm wall thickness in the range 1-8 bar. A Ru-based catalyst was used and water/ethanol mixtures of molar ratio 10/1 and flow rates of 5, 10 and 15 g h^{-1} was fed. At 723 K and 4 bar and under a feed flow rate of 5 g h^{-1}, maximum values of hydrogen yield (5.5) and hydrogen recovery values close to 100% were measured. At lower

temperatures and pressures the hydrogen yield declined. Lulianelli et al. [137] studied the additon of oxygen to the ESR environment in a Pd-Ag membrane reactor. The Ru/Al$_2$O$_3$ catalyst was studied at 673 K, S/C=5.5, GHSV=2000 h^{-1} and by using a sweep gas into the permeate side of the reactor, being the maximum hydrogen recovery (ca. 30%) achieved at O/C=1.2. It was claimed that oxygen addition can prevent ethylene and ethane formation caused by dehydration of ethanol as well as carbon deposition [137]. A combined methane and ethanol steam reforming was carried out over a Pt/Al$_2$O$_3$ catalyst at 1-5 bar in a multi-membrane module (Pd-Ag, 150 μm), where pure H$_2$ was recovered in the shell side by vacuum pumping [138]. The authors nicely showed that ethanol concentration could be avoided by the combined steam reforming of diluted ethanol (bio-ethanol) and methane, that is, the excess of water in the bio-ethanol is used to perform the methane reforming. At 5 bar, hydrogen yields up to 70% were obtained with a water:ethanol:methane molar ratio of 14:1:1.

ESR over Co/Al$_2$O$_3$ catalyst was conducted by Lulianelli and Basile [139] and Iulianelli et al. [140]. Several operational parameters such as temperature, pressure, sweep gas flow (SF) and load were evaluated and hydrogen yield and recovery values as high as 60% and 95%, respectively, were reached at 673 K, 3 bar, and SF=25.2 mL·min^{-1} (countercurrent flow). Experiments were performed in two types of reactor, i.e. a traditional reactor (TR) and a membrane reactor (MR). 95% ethanol conversion was reached by the MR in both co-current and counter-current flow configurations, while only 84% was reached in the TR. The hydrogen selectivity was 67% and 64% in the case of MR and TR, respectively. [139]. The effect of the reaction pressure and the sweep factor on the reaction system was studied by means of the counter-current sweep gas flow configuration [140]. The same catalyst was tested at 673 K in a porous stainless steel (PSS) supported Pd membrane reactor (25 μm Pd layer deposited onto a stainless steel tubular macroporous support) with the aim of investigating the influence of the membrane characteristics as well as of the reaction pressure from 3 to 8 bar [141]. 100% ethanol conversion was reached at 673 K and 8 bar. Hydrogen recovery of more than 50% with a purity around 65% was obtained. Co/Al$_2$O$_3$ and Ni/ZrO$_2$ catalysts were used in a Pd/PSS membrane reactor at 673 K and 8-12 bar for simulating bio-ethanol steam reforming by using a mixture of water-ethanol-acetic acid-glycerol with 1:13:0.18:0.04 molar ratio [142]. About 94% of ethanol conversion was obtained at 12 bar over the Co/Al$_2$O$_3$ catalyst, with 40% hydrogen yield and 40% hydrogen recovery.

Papadias et al. [143] at Argonne National Laboratory, USA, explored the benefits of high-pressure ESR for the production of hydrogen needed to refuel the high-pressure tanks of PEMFC vehicles. The experiments were conducted at 7-70 bar, 873-1023 K, and S/C=3-12 in a Pd-Ag (30 μm) CMR loaded with Rh/La$_2$O$_3$-Al$_2$O$_3$ catalyst. As expected from thermodynamics, higher pressures showed inhibition of the hydrogen yield in favor of methane. Domínguez et al. from the Technical University of Catalonia, Spain, studied the

ESR in a CMR over cobalt talc at 598-673 K and 5-15 bar [40]. In addition to an improvement of the hydrogen yield with respect to a fluidized bed reactor (FBR), the CMR showed a rapid response to changes in the ethanol-water mixture load; a constant hydrogen flow was obtained after 2 s following variations of the ethanol-water load of ±10%. The experiments of Papadias et al. [143] and Domínguez et al. [40] were performed without sweep gas, therefore, pure hydrogen was obtained in the permeate side of the membrane, ready to feed a PEMFC. López et al. [2] studied the ESR using a Pd-Rh/CeO_2 catalyst over cordierite monoliths in-series in a CMR. Reaction yields of 3.1 mol hydrogen generated per mol ethanol in feed and total yields of 1.4 mol H_2 permeated per mol ethanol in feed were measured, with maximum hydrogen recuperation of 70% (no sweep gas). This CMR was directly connected to a PEMFC and several control algorithms were developed to study suitable strategies for obtaining fast response from the CMR following variations in the hydrogen demand from the fuel cell [3].

Iulianelli et al. [144] studied bioethanol steam reforming over A 7.5 wt.% Ni/CeO_2 catalyst in a thin layer Pd-based (8 μm thin Pd-layer deposited onto a porous Al_2O_3 support) membrane reactor at 673 K. The study focused on the effect of feed composition and reaction pressure (2-3 bar) on the performance of the membrane reactor in terms of hydrogen permeation rate, permeated hydrogen purity, and ethanol conversion. The best performance of the membrane reactor was reached the highest pressure (3 bar). Almost complete ethanol conversion and a hydrogen yield of 67% was reached. The evaluation of the effect of presence of bioethanol impurities such as glycerol ($C_3H_8O_3$) and acetic acid (CH_3COOH) showed that these species could positively contribute to more hydrogen production via attending the steam reforming reactions, specially in presence of excess steam (high steam to carbon ratio) [144]. For the first time, self-heated carbon nanotubes (CNT) as membranes were fabricated and used in steam reforming of ethanol by Janas et al [145]. The surface of CNT was used as both the support of a Ni catalyst to perform the ESR reaction, and the source of heat to run the ESR reactions. The main advantages of such a configuration are more uniform temperature distribution (heterogeneous product distribution due to the temperature gradients is prevented), and light and portable setups. The temperature of 723 K was reached where 25% of hydrogen was detected in the effluent stream. Murmura et al. [146] performed ethanol steam reforming over Pt/Ni-CeO_2 catalyst in a Pd-based membrane reactor (4-5 μm palladium layer, deposited by electroless plating on the outside of a porous alumina tube). The experiments were performed at 613-753 K, 6-10 bar, steam to carbon ratio of 1.5 (stoichiometric conditions), and using a nitrogen sweep gas flow rate of 0.5 $l_N min^{-1}$ at the permeate side. At complete ethanol conversion, 4.5 mol hydrogen per mol EtOH in the feed was obtained at 753 K. The hydrogen recovery of 100% was reported in the case of using the sweep gas at the permeate side [146]. Rh/La_2O_3-SiO_2 and Rh/CeO_2 catalysts were studied in a self-supported Pd-Ag membrane reactor for ethanol steam reforming [147]. The reaction experiments were performed in a traditional reactor and a membrane reactor using different sweep gas flow rates to feed the

reactor with the mixture of ethanol and water (the reactant mixture was 2.5% ethanol, 7.5% water, and 90% nitrogen). The only products of the ESR reactions were CO, CO_2, CH_4, and H_2 and complete ethanol conversion was kept in all cases. The reactions were favored in the case of the membrane reactor without coke formation. The best results were obtained at at S/C ratio of 10. Hydrogen recovery of 70% was reached where 2.8 mol hydrogen was produced per mol converted ethanol.

Although most of the ESR work in CMR has been done with Pd-Ag metallic membranes, there are also some examples of ESR in different types of membrane reactors with the scope of reducing the cost. Yu et al. from the Korea Research Institute of Chemical Technology used Pt-impregnated Knudsen membranes to carry out simultaneously the ESR reaction and WGS [148]. The ethanol reforming-membrane reactor showed ethanol conversion improvement up to ca. 15% in comparison with a conventional reactor, with an improvement of hydrogen yield up to 10.5%. A similar experiment was performed with a CMR loaded with Pt/TiO_2 catalyst, which showed hydrogen recovery values of 78-87% in the temperature range 573-873 K [149]. Oyama's group at the Virginia Polytechnic Institute & State University, US, employed silica-alumina composite membranes with moderate hydrogen permeance as well as Pd and Pd-Cu (2 μm) composite membranes over Al_2O_3 for ESR over Na-Co/ZnO catalyst [150–152]. Ethanol conversion and hydrogen production enhancement were measured to be ca. 20% in the Pd-Cu CMR. High-effective hydrogen production from ethanol and water was reported in a tubular dense mixed-conducting oxygen permeable membrane reactor, in which the water splitting takes place at the tube side of the membrane and the oxidative steam reforming of ethanol occurs at the shell side simultaneously [153]. Yttria stabilized zirconia hollow fibers were used as substrate for the deposition of a Pd-Ag membrane on the outer shell of the hollow fiber and for deposition of $NiO/MgO-CeO_2$ catalyst inside the hollow fiber to develop a catalytic hollow fiber membrane reactor for conducting ESR [154,155]. At 583 K, the hydrogen produced in the catalytic hollow fiber membrane reactor was twofold higher than that in the catalytic hollow fiber reactor without Pd-Ag membrane.

2.4.2 Effect of co-existence of ESR products on the permeation behavior of Pd-Ag membrane

As stated before, the influence of reforming products such as CO, CO_2, H_2O, and CH_4 on the hydrogen permeability of the Pd-based membranes (hydrogen inhibition) is considered as a drawback. Several works have been devoted to the investigation of the permeation behavior of the Pd-based membranes in the WGS and MSR environment [156–164]. Catalano et al. [157] stated that CH_4 and N_2 acted as inert gases in terms of hydrogen inhibition, although in their permeation tests the hydrogen flux drastically decreased when a mixture of hydrogen and N_2 and/or CH_4 was used. This was ascribed to the hydrogen partial pressure decrease in the case of binary or ternary mixtures. Several permeation tests were performed by Gallucci et al. [159] at 523-723 K and 2-3.5 bar using a palladium

membrane to evaluate the influence of the presence of gases such as CO, N_2, CO_2, and Ar. The remarkable and quick influence of CO on the hydrogen permeation was reported, specially at low concentrations of CO. In the case of the rest of the gases, only the dilution effect was seen, by which the hydrogen flux was decreased but only due to the lower partial pressure of hydrogen (no membrane surface effect) [159]. The same results was reported by Li et al. [161] where a notable decrease in hydrogen permeation was observed at low concentrations of CO. Addition of steam to low concentrations of CO showed a stronger hydrogen inhibition.

Several authors mentioned the evident negative effect of presence of CO on the hydrogen permeance behavior of Pd-based membranes due to the covalent interaction of carbon monoxide with the membrane surface [160,165,166]. Peters et al. [163] studied a Pd-Ag membrane reactor in WGS reaction environment at 673 K and reported the significant effect of CO on the hydrogen permeation rate through the membrane. Amandusson et al. [156] tested a 25 μm thick Pd membrane in presence of hydrogen, CO, and O_2 at low temperatures of 373-523 K. They found out that both CO and O_2 influenced the membrane permeation performance. The available hydrogen dissociation sites were blocked by CO, and O_2 reacted with the present hydrogen to form water. The authors reported that at lower temperatures, CO dominated the effect of the formed water and blocked the permeation sites of the Pd membrane surface, resulting in less hydrogen permeation rate. Coroneo et al. [158] developed a CFD model to compute the permeation rate of hydrogen through a Pd-Ag membrane in binary and ternary gas mixtures at 647-773 K and P=1-7 bar. The separation performance of the membrane was evaluated in presence of N_2, CO, and CH_4 and at constant temperature and partial pressure of hydrogen. The negative effect of CO on the permeation flow rate of hydrogen was seen.

Mejdell et al. [167] investigated CO inhibition at 573-623 K on a very thin Pd-Ag membrane (3 μm) before and after an air treatment done at 573 K. The hydrogen flux declined drastically by 60% when the membrane was exposed to 1 mol% CO before the air treatment, while after the air treatment the same effect (CO inhibition) was 15 %. The enhanced performance of the membrane after the air treatment was attributed to the changes in CO and H_2 heats of adsorption due to the surface segregation of Pd or Ag [167]. As presented in the literature, CO has the dominant effect on the hydrogen permeation decrease by poisoning the permeation sites of the Pd metallic membranes.

Sanz et al. [168] carried out permeation tests using a Pd membrane reactor at 623-723 K and trans membrane pressure difference of 2.5 bar. The tests were done in the atmosphere of pure H_2/N_2, and mixed with CO or/and CO_2. In all cases, a decrease in the hydrogen permeance was observed. However, the selectivity towards hydrogen was kept in all the cases. The results of the permeation tests at 623 K done by Sanz et al. [168] are given in Fig. 2.3. P_{H2ret} and P_{H2perm} represent the partial pressure of hydrogen at the retentate side and the permeate side, respectively.
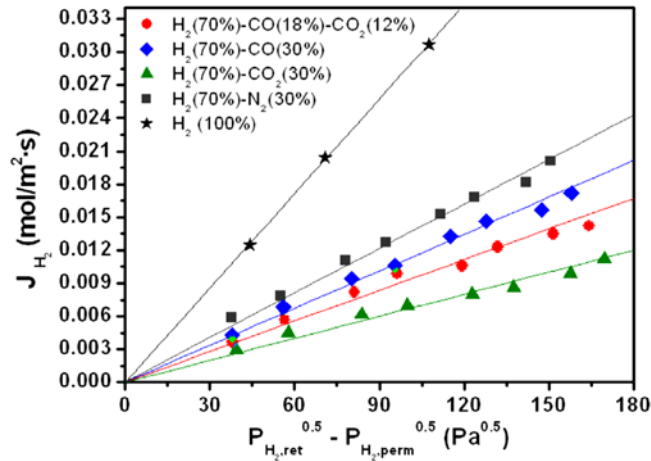
Fig. 2.3 Effect of gas mixtures on the permeation performance of the Pd membrane at 623 K. Figure taken from the work by Sanz et al. [168].

As can be seen, the strongest effect belonged to the H_2/CO_2 mixture so that at hydrogen partial pressure of 2 bar ($P^{0.5}_{H2.ret} - P^{0.5}_{H2.perm} = 120$), the hydrogen flux is 4.5 times lower than in the case of pure hydrogen. Moreover, it is shown that the influence of the lower concentration of CO is more noticeable. Taking into account the dominant effect of the presence of CO in the reactor [156], this figure gives an example of the negative effect of the co-existence of the ESR products, specially CO and CO_2, on the permeation Performance of a Pd-based membrane.

Water also can poison the surface of the membrane and block the hydrogen permeation sites. The influence of water vapor on the permeability of a 2.5 μm Pd_{80}-Ag_{20} membrane was studied by Catalano et al. [169] at 473 to 723 K. Binary mixtures of hydrogen-nitrogen and hydrogen-water vapor were used at trans membrane pressure of up to 3 bar. Although nitrogen is considered as an inert agent, the experiments of hydrogen-nitrogen mixture at different temperatures proved a non-negligible concentration polarization. However, at the same operating conditions and hydrogen partial pressure, the hydrogen flux in the case of hydrogen-water vapor was considerably lower in comparison with the hydrogen-nitrogen mixture. The influence of the water vapor increased at higher temperatures and higher water vapor concentrations. However, the permeation decrease was reversible thanks to the competitive H_2-H_2O adsorption on the Pd-Ag surface [169]. According to Barreiro et al. [170], the permeation tests of a Pd-based membrane at 593-723 K and hydrogen partial pressure of 1.5 bar showed that hydrogen flux reduced in presence of water, while CO_2 had no influence on the permeation rate of hydrogen. Gielens et al. [171] tested very thin Pd and Pg-Ag (1 and 0.5 μm) membranes in presence of water and carbon dioxide at 623, 673 and 723 K. The hydrogen permeation flux was measured for periods of more than 80 h during and after the addition of CO_2 or H_2O. They reported a very large hydrogen flux decrease of 70 and 69% for H_2O and CO_2, respectively, at 623 K. After stopping the steam addition, the hydrogen flux was recovered. However, in the case of CO_2, the hydrogen flux

got stable at a lower rate compared to the pure hydrogen stream. The authors claimed that in the WGS environment, the hydrogen inhibition effect of CO (the product of the reaction of H_2O and CO_2) is not noticeable in front of the significant effect of carbon deposition on the surface of the membrane [171].

Hou et al. [172] reported that the hydrogen inhibition effect of CO, CO_2, and H_2O in the case of a Pd-Ag membrane could be classified as $H_2O>CO>>CO_2$. The order of influence corresponded to the competitive adsorption capability of the gases on the Pd-Ag membrane surface. At temperatures higher than 673 K, the hydrogen inhibition was not noticeable. In the study by Unemoto et al. [164] the comparison between CO, CO_2, and H_2O showed that at T<600 K, CO had the strongest influence on the hydrogen permeability of the Pd membrane. They suggested that at T>873 K, the effect of co-existence of other species for a membrane with a thickness higher than 10 μm was negligible. On the contrary, Patrascu and Sheintuch [173] concluded that the effect of very small amount of CO on hydrogen permeation inhibition could be notable even in presence of H_2O, and especially in the steam reforming environment.

Overall, the published open literature offers no robust model/analysis on the effect of the different species on the performance of the membrane in the real atmosphere of methane steam reforming and water gas shift reactions. The competitive adsorption of CO and H_2O on the surface of the metallic Pd membrane, the effect of reverse reactions of WGS and MSR, and the effect of operating at high pressure and temperature do not give a consistent idea of the hydrogen inhibition of the ESR products in the real atmosphere of the steam reforming of ethanol over noble metals. Moreover, there is not a consistent conclusion on the effect of H_2O on the permeability or active surface area of the membrane. It is not totally agreed if CO_2 and CH_4 are considered as inert gases, as the decomposition of these two species, or the reactions with water via WGS and MSR, respectively, can lead to a more complicated situation regarding the influence on the hydrogen permeation. According to the review given by Cornaglia et al. [174], it can be understood that the hydrogen inhibition phenomenon caused by the ESR products; specially in presence of H_2O, is a very complicated issue. Specific considerations in each case in terms of the properties of the membrane, operating conditions, and the composition of the fuel fed into the reactor (S/C ratio) may be a relevant solution.

In this chapter an introduction to the membrane reactors and a literature review on the ethanol steam reforming in the membrane reactors over noble metal based catalyst were given. While many interesting studies have been performed recently on the application of membrane reactors in pure hydrogen production, this area requires further research and development to introduce efficient, robust, and applicable pure hydrogen-producing systems. The next chapter is devoted to the experimental investigation of the ethanol steam reforming reaction over Pd-Rh/CeO_2 in a Pd-Ag membrane reactor at different operating

conditions to study the effect of catalyst reactivity, hydrogen selectivity, fuel conversion, and pure hydrogen permeation rate through the Pd-Ag membrane.

Chapter 3

Experimental results of ethanol steam reforming over Pd-Rh/CeO$_2$ in the Pd-Ag membrane reactor

Abstract

A comprehensive introduction and literature review on hydrogen, membrane reactors, and common catalysts for hydrogen production via catalytic steam reforming of ethanol was given in previous chapter. As the first step, ethanol steam reforming (ESR) experiments over Pd-Rh/CeO$_2$ catalyst were performed in a catalytic membrane reactor (CMR) at different temperatures and pressures, using a mixture of ethanol and water at various S/C ratios. The reactor was filled by the catalyst so that the membranes were fully covered to achieve the maximum amount of hydrogen production and permeation. Hydrogen yield of 0.6 at 12 bar and 923 K was reached at S/C=3 and hydrogen recovery was 92%. 0.9 L$_N$ hydrogen/ml EtOH equal to 3.5 mole of pure hydrogen per mole of inlet EtOH was obtained at 12 bar. The prototype was established so that pure hydrogen was obtained as it was generated, thanks to the high selectivity of the Pd-Ag membranes towards hydrogen. Hydrogen was obtained at the purity of 99.999%, suitable for direct online use for low temperature fuel cells [3]. The experimental results were compared to a staged membrane reactor (SMR) [2,3] configuration in which the same experimental conditions were applied and the same catalyst was used.

3.1 Materials and methods

3.1.1   Catalyst preparation

Honeycomb monoliths were used as catalysts to perform the ESR reaction. Monoliths are well known for the mechanical and thermal strength and stability in harsh chemical reaction conditions [175]. Besides, ceramic monoliths are known as reliable and useful supports for catalytic reactions, thanks to their very high surface to volume ratio [176]. Several works have been reported recently, using monoliths as a support for the catalytic conversion of bioethanol in membrane reactors [2,41,175,177,178]. A ceramic monolith is shown in Fig. 3.1.
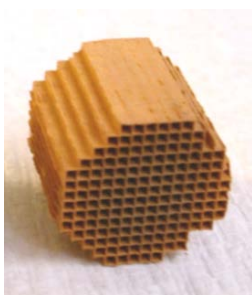
Fig. 3.1 Ceramic monolith [41]

To prepare the catalyst required for this work, the honeycomb monoliths (cordierite) were crushed into small pieces. The crushed monoliths were sieved to be larger than 1 mm (1-5 mm) not to block the outlet of the reactor. Then, sieved pieces were soaked with a saturated solution of cerium salt of $Ce(NO_3)_2.6H_2O$ (Fluka) in distilled water. For this purpose, the monolith pieces were sunk in the homogenous solution of $Ce(NO_3)_3$ in water so that the surface of porous crushed monoliths was coated. The process was followed by a two-step calcination process i.e. 1 hour at 393 K and 2 hours at 773 K to obtain a homogenous CeO_2 layer. After coating with ceria, a mixture of 0.5% Pd-0.5% Rh was prepared to be added using aqueous solutions of $PdCl_2$ and $RhCl_3$ (Sigma-Aldrich). The composition was selected because of the proven catalytic reactivity of 0.5% Pd-0.5% Rh in ESR environment in terms of ethanol conversion and hydrogen selectivity [87]. The solution was impregnated on the ceria-coated catalysts during five successive wetness impregnations and drying, for certain homogeneity and settlement of noble metals solution onto the surface of the CeO_2 particles. After each wetness impregnation, the catalysts were dried at 353 K for 1 hour. Finally, the catalyst was dried and calcined at 393 K for 1 hour and at 673 K for 2 hours, respectively. To reduce the coated noble metal oxides back to the metallic phase, the catalysts were reduced at 623 K using the stream of 5% H_2 in N_2 for 3 hours prior to the reactions. The prepared catalyst is shown in Fig. 3.2. The analysis by electron microscopy revealed a homogenous distribution of catalyst aggregate of about 0.2-0.5 μm.

Fig. 3.2 Prepared catalyst (left hand side) and its microscopic picture (SEM) (right hand side)

3.1.2 Experimental setup

The laboratory setup used for the ESR experiments (fuel reformer) consisted essentially of a fuel tank, a liquid pump, a catalytic membrane reactor, a pressure transducer, and a condenser. A schematic plan of the fuel reformer system is shown in Fig. 3.3.
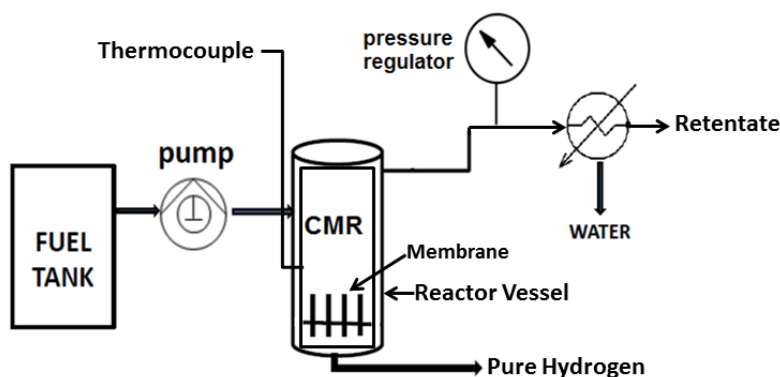
Fig. 3.3 Scheme of the fuel reformer

The reactor was 10 in. tall and 1 in. in diameter. There were four Pd-Ag membrane tubes highly selective to hydrogen inside the reactor; each one 3 in. tall and 1/8 in. diameter in order to separate hydrogen. The membrane tubes consisted of Pd-Ag (30 μm layer) supported on porous stainless steel (PSS) provided by REB Research & Consulting, MI, USA [179], accounting for 30.4 cm^2 total active membrane area. To perform the experiments, the reactor was filled with 25 grams of the catalysts (monolith plus Pd-Rh/CeO$_2$ catalyst, containing ≈0.341 gr of Pd+Rh) so that the metallic membranes were fully covered. Fig. 3.4 presents a scheme of the Catalytic Membrane Reactor (CMR) filled with the catalyst.
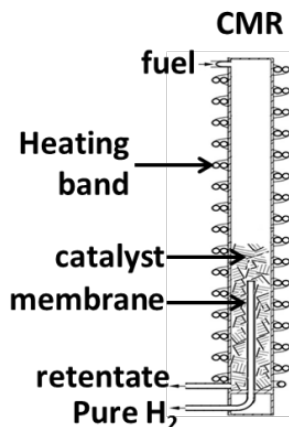
Fig. 3.4 Scheme of the reactor with the catalyst

The reactor itself included the evaporator tubes stick to the same heating plate used to keep the reactor at the desired temperature. The heating plate is placed between the reactor and the evaporator tubes. The CMR module is shown in Fig. 3.5.
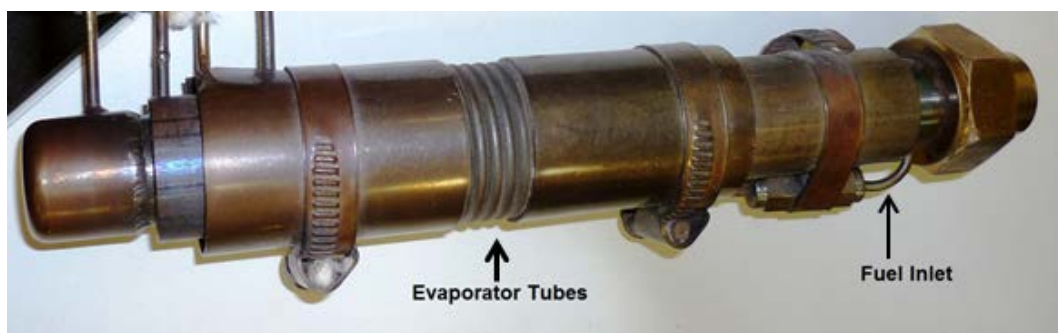
Fig. 3.5 CMR module

The obvious advantages of this setup are:

1. Using a single heating source for evaporation of the liquid fuel and heating the reactor.
2. Significant volume decrement by using a single heating plate for heating and use of the membranes inside the reactor for hydrogen purification.
3. Possibility of using a liquid pump to maintain the desired pressure.

The heating plate was controlled by an electronic controller (Fuji PXR4), provided the temperature measurement registered by a K-type thermocouple which was in close contact with the reactor wall. The reactor was sandwiched between a 22 mm of glass wool aiming to thermal insulation. A HPLC pump (Knauer) was used to pump the water-ethanol mixture (fuel) and to keep the pressure. The retentate pressure was adjusted by a backpressure regulator (Swagelok) which was regulated by means of a computer program. No pressure

regulation was implemented on the permeate side (pure hydrogen outlet), so the permeate side pressure was kept automatically at ambient pressure. Besides, no sweep gas was used and pure hydrogen was obtained at atmospheric pressure. At the retentate side, a condenser with a liquid level indicator was placed so that all the gases were air-cooled and the steam was condensed by transferring heat to the environment (air). The composition of the outlet gases (retentate) was analyzed using an online Gas Chromatograph (Agilent 3000A MicroGC using MS 5 Å, PlotU and Stabilwax columns). The flow rate of pure hydrogen was directly measured by a mass flow meter (Bronkhorst F-111B) in ml/min.

The assembled experimental setup used in this work is shown in Fig. 3.6.
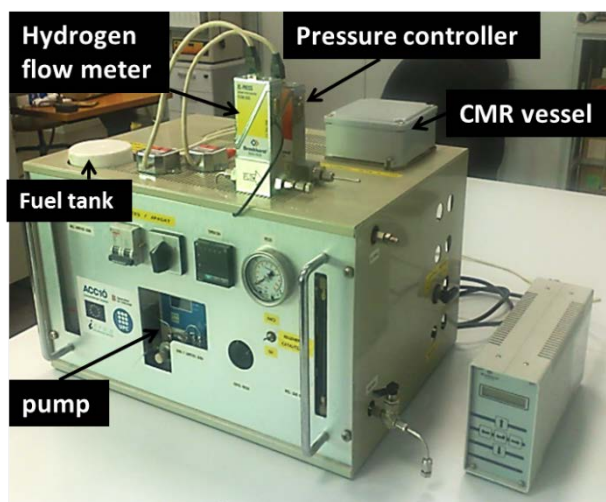
Fig. 3.6 Experimental setup

The Gas Chromatograph (GS) showed an error of ±3% absolute in the total measured composition of the retentate gas. The mass flow meter of pure hydrogen fluctuated within ±2 ml/min, equal to ca. 0.11×10^{-5} mol/s. This is attributed to the small variations of the pressure inside the reactor, as the pressure valve acts on the outlet retentate stream (causing a pressure fluctuation of ±0.05 bar). The errors of the measurements apparatus are considered in the uncertainty analysis presented in Appendix A.

For all the experiments, a solution of ethanol and distilled water – according to the different steam to carbon ratios – was used as the fuel to feed the reactor. The operational conditions of the ESR experiments are summarized in Table 3.1.

Variable	Temperature (K)	Pressure (bar)	Fuel flow rate (μl/min)	S/C (steam to carbon ratio)
Variation range	873 – 923	1 – 12	50 – 100	1.6, 2, 3
Intervals size	50	2	50	-

Table 3.1 Operating conditions

Pressures higher than 12 bar and temperatures higher than 923 K were not tested because of the experimental setup limitations.

Prior to the experiments, and during the successive intervals, the pump was checked for its calibration. The calibration curve of the pump is given in Fig. 3.7.
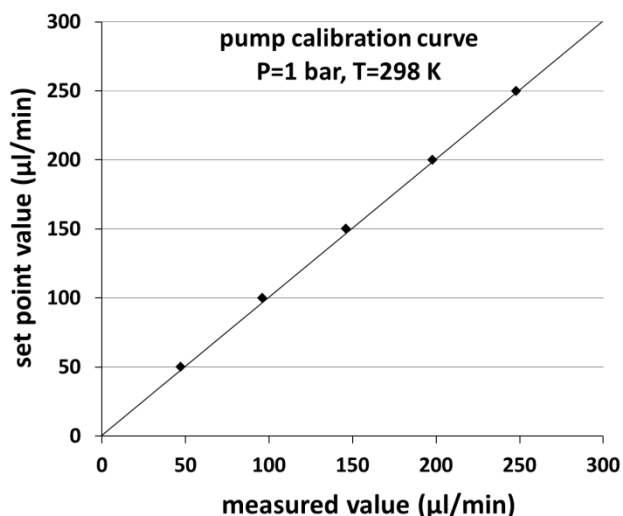
Fig. 3.7 The calibration curve of the pump

The deviation of the real flow rate provided by the pump from the set point value (error) was more noticeable at lower flow rates. The error of the pump for flow rates of 50, 100, 150, and 200 μl/min was 6, 4, 3, and 1%, respectively. This error is considered in the uncertainty analysis presented in Appendix A.

At the beginning of each experiment, the selectivity of gases at atmospheric pressure and the desired temperature (873 or 923 K) are checked by monitoring the activity of the catalyst and the calibration of the gas chromatograph using the fuel flow rate of 100 μl/min.

To check the performance of the membrane, at the end of some experimental periods (nearly every 3 months), an experiment with known values (temperature, S/C ratio, and fuel

flow rate) was run at high pressure (8-12 bar) and the purity and the flow rate of the pure hydrogen stream was compared with the previous data.

3.1.3   Pd-Ag Membrane characteristics

The characterization of the Pd-based membranes in terms of hydrogen permeability is done via permeation tests in the pure hydrogen environment, or in the presence of other gases such as N_2, CO, CO_2, and CH_4, at different conditions [131,137,143,180–182]. The aim of such experiments is mainly to verify the infinite permeation selectivity of the hydrogen with respect to other gases, and to prove that the membrane and the hydrogen permeation behavior follow the Sieverts' law (eq. 2.10) [131]. Papadias et al. [143] in Argonne National Laboratory, IL, USA, used the same membrane as used in this work, with the same characteristics and synthetized by the same manufacturer (REB Research & Consulting, MI, USA). They performed permeation tests in the 100% pure hydrogen environment at 473-923 K, keeping the permeate side at ambient pressure (no sweep gas). The temperature of the reactor environment and the membrane surface was set by means of a furnace, and the flow rate of hydrogen at the permeate side was measured. The measured permeation rate (calculated flux across the membrane) as a function of temperature and pressure is shown in Fig. 3.8 [143]. 'A_0' is the pre-exponential factor in the formulation of the Sieverts' law.
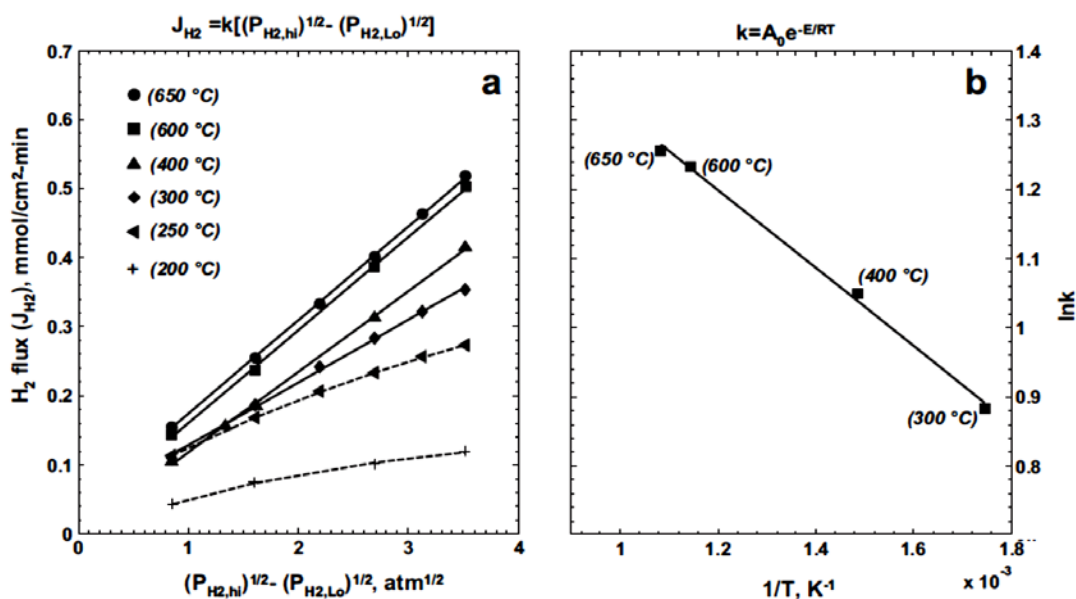
Fig. 3.8 Dependence of hydrogen transport through the Pd-alloy membrane on pressure and temperature. Figure taken from the work by Papadias et al. [143].

The increase of hydrogen flux by temperature is not sharp at high temperatures so that the flux of hydrogen at 873 and 923 K (600 and 650°C, respectively) is very similar. As stated by Papadias et al. [143], the hydrogen flux is limited by the rate of dissociation of the hydrogen molecule to hydrogen atoms on the surface of the metallic membrane.

Differently, at temperatures higher than 573 K, the dissociation rate is limited by the diffusion of the hydrogen atoms through the palladium layer, where the hydrogen flux follows the Sievert's law. Based on Fig. 3.8 and considering a membrane area of 30.4 cm^2, the hydrogen permeation rate at 923 K (650˚C) and different pressures is obtained, as presented in Table 3.2.

Partial pressure of hydrogen (atm)	20	12	7.2	3.4
$P_{H2,r}^{0.5} - P_{H2,perm}^{0.5}$ (atm$^{0.5}$)	3.5	2.5	1.7	0.9
Hydrogen flux (mol/s)	2.6×10^{-4}	1.9×10^{-4}	1.4×10^{-4}	8.1×10^{-5}

Table 3.2 The hydrogen flux at T=923 K for a membrane area of 30.4 cm^2

The maximum and minimum pressures at which the permeation test in pure hydrogen environment was performed are 20 and 3.4 bar [143]. The maximum pressure at which the ESR reaction in the CMR were performed in this work is 12 bar, and finally the maximum partial pressure of hydrogen reached in this work was around 7.2 bar (in the ESR environment in the CMR). The values presented in Table 3.2 are the highest hydrogen permeation rates possible through the studied membrane at mentioned temperature and pressure.

3.1.4   Comparison between two reactor configurations

In addition to the evaluation of the CMR configuration, a comparison to the previously studied reactor configuration named as the Stage Membrane Reactor (SMR) [2,3] is given. In the CMR configuration, the membrane was fully covered by the catalyst, therefore, the ESR reaction and the hydrogen permeation occurred simultaneously in the CMR. In the case of the SMR, the catalytic zone was separated from the permeation zone, which was the membrane, so that firstly the ESR reaction were complete and came to equilibrium, then the gaseous products passed along the membrane letting the hydrogen to permeate through the membrane. The two different configurations are shown in Fig. 3.9.
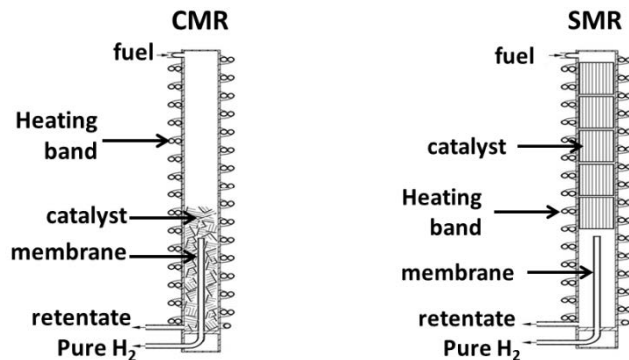
Fig. 3.9 Scheme of the configurations of the reactors: Catalytic Membrane Reactor (CMR), and Stage Membrane Reactor (SMR)

The main difference between the two reactor configurations lies in the fact that in the CMR, the steam reforming reactions are pushed towards the product side (hydrogen generating side, see eq. 2.2 and 2.3) as the hydrogen is permeated through the membrane and exits the reactor atmosphere. This is due to the availability of the catalyst as it sandwiches the membrane so that hydrogen is produced as it is leaving the catalytic zone. Hence, the reactions are promoted beyond the equilibrium limitations to produce more hydrogen (the shift effect) and the partial pressure of hydrogen – as the driving force for hydrogen permeation – is kept high around the membrane. In the SMR, the partial pressure of hydrogen inside the reactor decreases along the membrane as more hydrogen is permeated and its molar fraction declines [3]. The ESR experiments in the SMR configuration were performed only at S/C ratio of 1.6 [2].

3.1.5   Experimental data analysis

The system is tested under different operational conditions and it is evaluated in terms of the conversion of ethanol, hydrogen yield (Y_{H_2}), and hydrogen recovery (R_{H_2}). However, the pure hydrogen production rate is considered as the main point of evaluation of the CMR. The mentioned terms are defined as:

$$Y_{H_2} = \frac{F_{H2.perm}}{6 \times F_{EtOH}} \qquad \text{Hydrogen yield} \qquad\qquad 3.1$$

$$R_{H_2} = \frac{F_{H2.perm}}{F_{H2.total}} \qquad \text{Hydrogen recovery} \qquad\qquad 3.2$$

Where $F_{H2 \cdot perm}$, F_{EtOH}, and $F_{H2 \cdot total}$ are pure hydrogen permeation rate, ethanol flow rate, and total hydrogen production rate, respectively, in mol/s. Total hydrogen production included the permeated hydrogen and the hydrogen content of the retentate gas. Hydrogen yield can reach up to 1 at complete conversion of ethanol and hydrogen recovery of 1 (100% recovery of produced hydrogen as pure hydrogen permeated through the membrane) since theoretically 6 moles of hydrogen are formed per mol of ethanol in the feed. In reality, the

hydrogen yield of 1 is not accessible due to the limitations of the recovery of all the hydrogen produced via ESR. In the literature, the definition of the hydrogen yield may be different so that total hydrogen production is considered instead of permeated hydrogen in the numerator of the equation 3.1. In this work, only the permeated part of hydrogen is considered to focus on the pure hydrogen production capability of the CMR.

The pure hydrogen efficiency is a measure of the reactor performance to compare the CMR and SMR configurations and is defined as:

$$\eta_{H_2} = \frac{F_{H2.perm}}{F_{H2.in}} \qquad \text{Pure hydrogen efficiency} \qquad\qquad 3.3$$

The inlet hydrogen flow rate ($F_{H2.in}$) is the sum of hydrogen fed to the reactor i.e. one mole of hydrogen per one mole of water and three moles of hydrogen per one mole of ethanol.

3.2 Results and discussion

3.2.1 Performance of the CMR

Based on the experimental observations and in agreement with the reported results in the literature [2,87], the only species detected in the retentate stream by the GC are CH_4, CO_2, CO, and H_2. No ethanol was detected in the retentate stream, proving complete conversion of ethanol. Prior to the experiments at high pressure, the performance of the CMR was checked at atmospheric pressure in terms of the selectivity of the ESR products. The selectivity of gases at 873 and 923 K and S/C=1.6, 2, and 3 is given in Fig. 3.10.
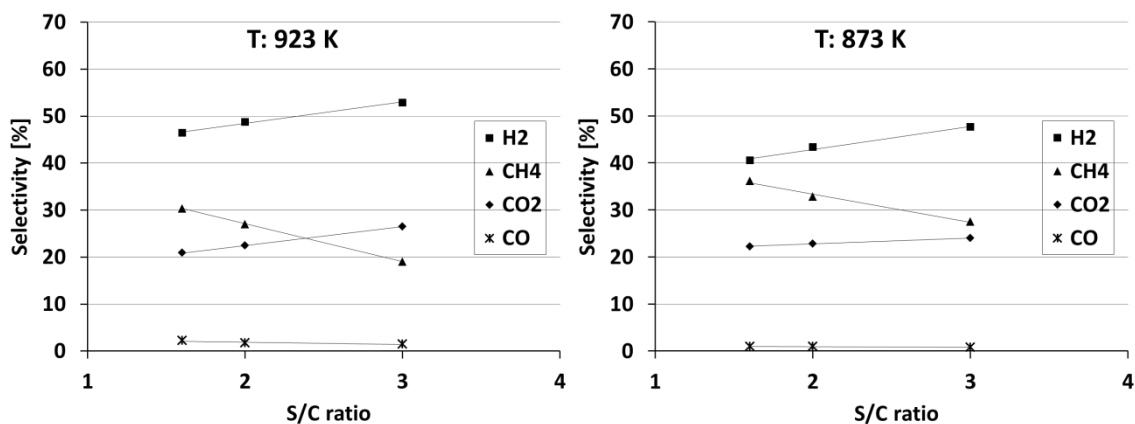
Fig. 3.10 Selectivity of the ESR products at atmospheric pressure

The selectivity of hydrogen increases with S/C, while the methane selectivity decreased. This is attributed to the availability of excess water at higher S/C ratio, which promoted the methane steam reforming (MSR) reaction. The increasing trend of CO_2 proves the reaction promotion at higher S/C ratio. Very small amount of CO was detected, which is considered as an advantage of the CMR configuration specially at 923 K where the temperature is not

in favor of the WGS reaction. The slightly higher selectivity of CO at 923 K is attributed to the exothermic nature of the WGS reaction.

Temperature plays a key role in hydrogen selectivity permeation through the membrane. On one hand, hydrogen permeation through the membrane is a temperature activated phenomena and on the other hand, the progress of methane steam reforming (MSR) as the dominant hydrogen producing reaction is favored naturally with temperature as it is an endothermic chemical reaction (eq. 2.3). Moles of methane in the retentate gas stream (unconverted methane) per mole of converted ethanol are presented in Fig. 3.11. The lines show the general declining trend of the presented results over pressure.
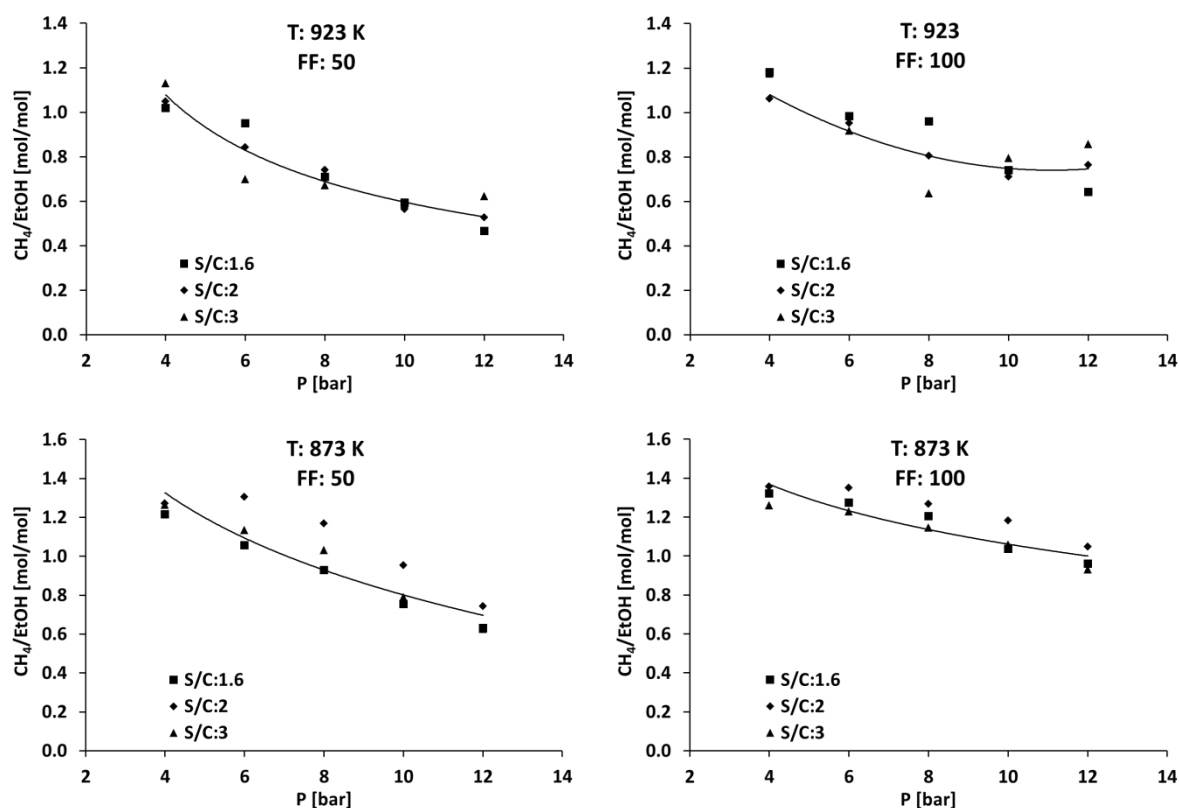
Fig. 3.11 Moles of methane produced in the CMR per mol of ethanol in the feed

Traces of methanation are seen when $\frac{\text{mole CH}_4}{\text{mole EtOH}} > 1$ keeping in mind that one mole of methane is generated per one mole of converted ethanol. This phenomenon was caused by operating at high pressure where the MSR reaction (eq. 2.3) was pushed backward according to Le Chatelier's Principle. This phenomenon is more visible at 873 K, which proves the effect of temperature on the MSR reaction. Besides, hydrogen permeation rate is lower at 873 K resulting in less promotion of the ESR reaction. The unconverted methane is clearly higher at 873 K due to the dependency of the MSR reaction on temperature.

Another visible feature in Fig. 3.11 is less methane conversion at FF=100 µl/min, which can be a result of the shorter residence time of the reactants in the CMR at higher fuel flow rate together with less pure hydrogen permeation per mole of ethanol, which means less promotion in the ESR reaction. As methane conversion increases with pressure, more hydrogen is generated and permeated. As expected, there is a direct link between the conversion rate of methane and the production rate of hydrogen. Total produced moles of hydrogen (Total) together with the permeated moles of hydrogen through the membrane (Pure) per mole of ethanol in the feed are presented in Fig. 3.12.
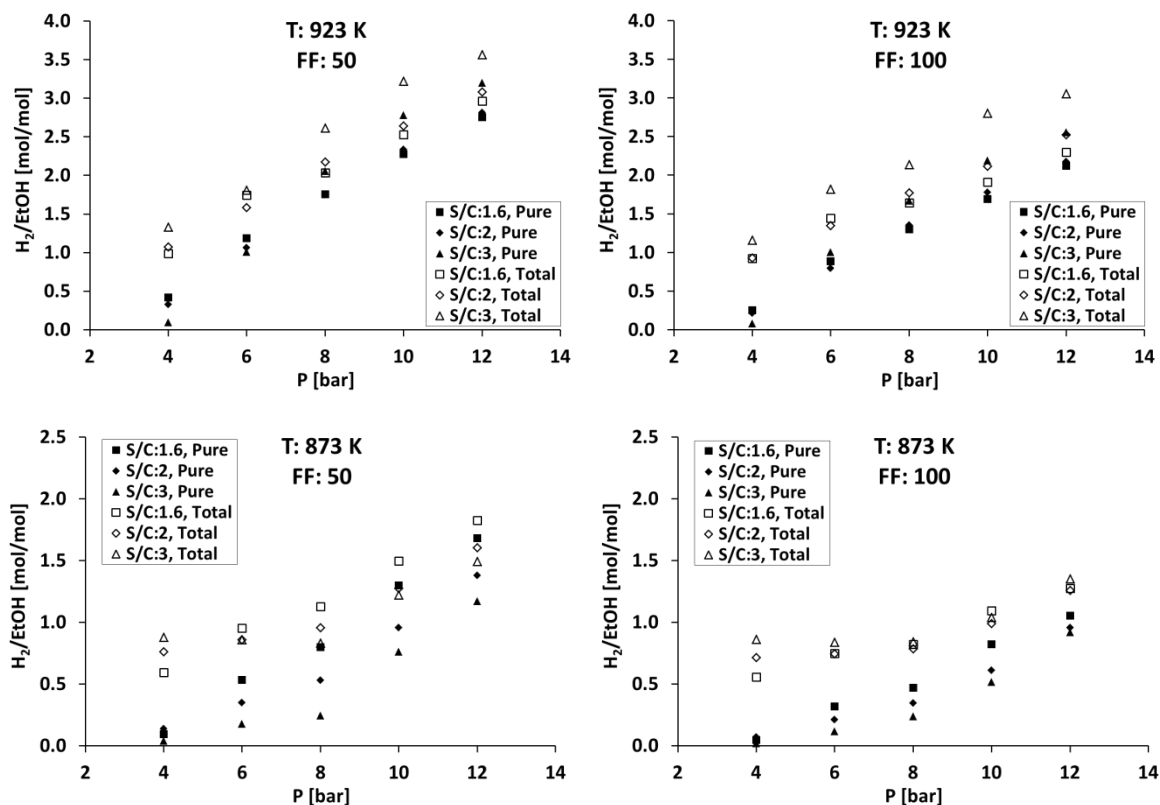
Fig. 3.12 Total and permeated moles of hydrogen per mol of ethanol in the feed

Total hydrogen production increases with S/C ratio because on one hand the molar flow rate of ethanol is lower at higher S/C ratio (at constant fuel flow rate), and on the other hand more methane is converted in presence of excess steam at higher S/C ratio (see Fig. 3.11) specially at 923 K. At higher pressures, hydrogen permeation is improved because of higher partial pressure of hydrogen around the membrane (Sieverts' law). Therefore, MSR and WGS reactions are promoted, as the catalyst is available around the membrane to compensate for the removed product (permeated hydrogen). This is an evident result of the shift effect in the CMR configuration leading to the promotion of the reforming reactions. In the light of the shift effect, it is obvious that as more methane is converted, more hydrogen is produced and therefore is permeated as pure hydrogen. In other words, the

special configuration of the CMR results in overcoming the negative effect of pressure on the reforming reaction.

Temperatures lower than 873 K were not tested because the permeation of hydrogen was very small.

In the case of carbon monoxide, a similar trend to methane is observed. However, the molar production rates of CO are very low, proving two advantages. First, the promotion of the WGS reaction, which means nearly complete conversion of CO, and second, very low production rate of CO, which is considered an enhancement in reforming processes. The molar production rate of CO per mol of ethanol in the feed is shown in Fig. 3.13.
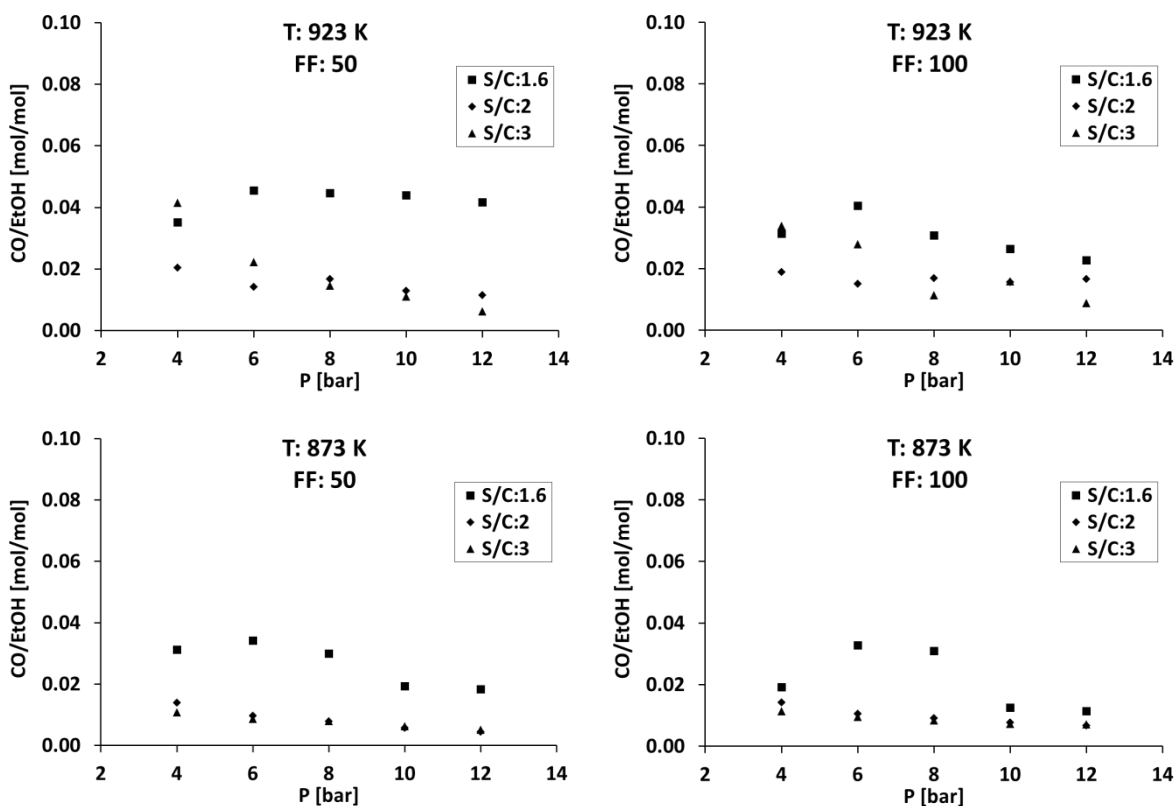
Fig. 3.13 Molar production rate of CO per mol of ethanol in the feed

The slightly higher CO selectivity at S/C ratio of 1.6 is attributed to the operating at stoichiometric conditions, where there is no excess water. At these conditions, the operating pressure plays an important role where higher hydrogen permeation results in the promotion of ESR reaction. The effects of temperature and the fuel flow rate are not noticeable.

3.2.2 Pure hydrogen production

As stated before, temperature and pressure (as the driving force of hydrogen permeation) are the determining factors in the rate of hydrogen production. Pure hydrogen production rate at all operating conditions is given in Fig. 3.14.
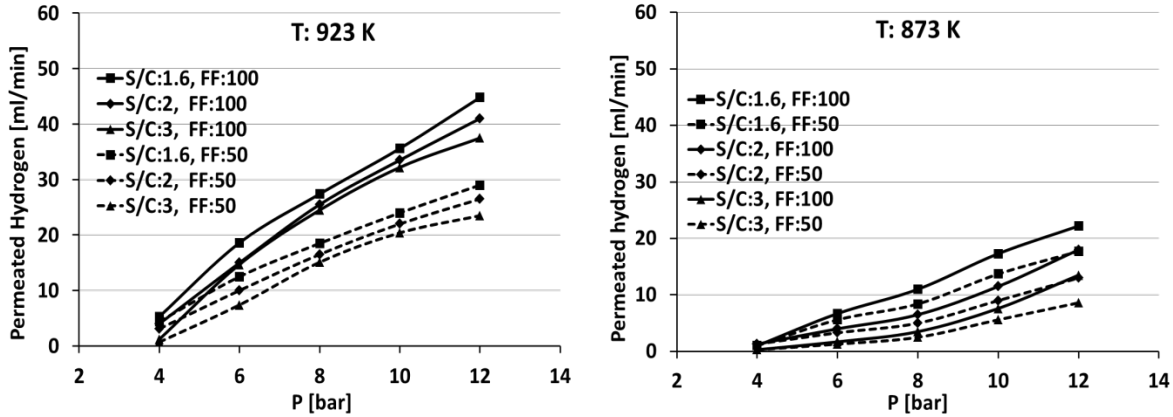
Fig. 3.14 Hydrogen permeation rate at different operating conditions

The total production of hydrogen is at least doubled as the temperature increases by 50 K from 873 K to 923 K, at the same S/C ratio, fuel flow rate, and pressure. At higher pressures, the gap between the two flow rates is widened because of higher rates of hydrogen permeation through the membrane. It is proved that the catalyst around the membrane is able to compensate for the permeating hydrogen by simultaneous hydrogen production. Therefore, in the case of availability of more fuel, relatively more hydrogen is permeated.

The effect of the fuel flow rate on production of pure hydrogen is obvious. The higher the fuel flow rate, the higher the amount of fuel available for production of hydrogen in the reactor. At FF=100 μl/min, the pure hydrogen permeation rate is not exactly doubled compared to the one at FF=50 μl/min since not all the converted hydrogen can permeate through the membrane while the inlet ethanol is doubled. As shown in Fig. 3.12, the number of moles of permeated hydrogen per mol of inlet ethanol is higher at lower fuel flow rate.

The pure hydrogen flow rate declines with S/C ratio because less ethanol as the source of hydrogen is fed into the CMR at higher S/C ratios. Besides, the excess water results in a lower hydrogen partial pressure inside the reactor. One of the important observations is the approximately linear pure hydrogen production with pressure specially at 923 K. The reformer operates linearly with the pressure in terms of hydrogen permeation, leading to higher hydrogen recovery and hydrogen yield at higher pressure and the same temperature and fuel flow rate. This feature directly results in very high efficiency of the reformer when operating at high pressure. The linear behavior of pure hydrogen permeation with operating

pressure makes it possible to consider the pressure as one of the controlling factors of pure hydrogen flow rate if a fuel cell is intended to be fed by the reformer. This behavior was not observed in the SMR configuration. A comparison between the CMR and the SMR will be given later in this work.

The values obtained during ESR experiments are lower than the ones presented in Table 3.2 at the same partial pressure of hydrogen inside the reactor. Hydrogen flux of 1.95×10^{-5} mol/s was reached for the CMR at hydrogen partial pressure of 7.2 bar (reactor pressure of 12 bar at 923 K), while according to Table 3.2, a hydrogen flux of 1.4×10^{-4} mol/s is expected. This can be clearly attributed to the influence of the coexistence of the species such as CO and H_2O, which affected the permeation performance of the membrane, resulting in lower hydrogen permeation rate. The observed behavior proved the assumption of the poisoning effects of CO and H_2O, as discussed in chapter 2.

3.2.3 Hydrogen yield

Hydrogen yield is one of the important indicators of the performance of the CMRs. According to eq. 3.1, hydrogen yield can reach up to 1, if 6 moles of hydrogen are obtained per one mole of inlet ethanol at ideal conditions, which means the total conversion of ethanol and water to CO_2 and H_2. The hydrogen yield at 873 and 923 K are presented in Fig. 3.15.
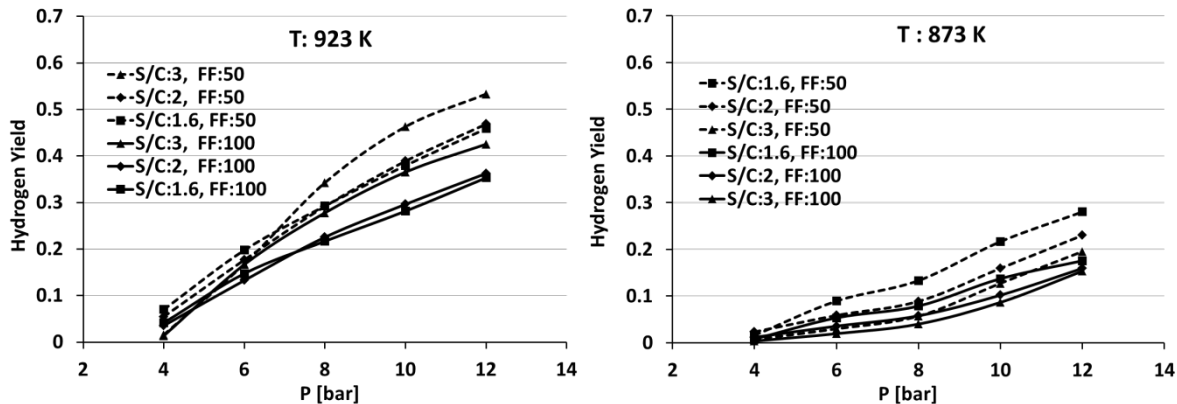
Fig. 3.15 Hydrogen yield

According to the definition of hydrogen yield, it is expected to reach higher values at higher S/C ratios because of the lower concentration of ethanol in the inlet fuel. Hydrogen yield at 923 K reaches up to 0.6. Naturally at 873 K, lower hydrogen yield is reached. At 873 K, the water gas shift (WGS) reaction is dominant because it is favored at lower temperatures. At a lower S/C ratio, more ethanol is fed into the system and more CO is formed and used in the WGS reaction. Accordingly, more hydrogen is produced at lower S/C ratio. On the contrary, at 923 K, the MSR reaction is favored. In presence of higher amount of water (at

higher S/C), more hydrogen was produced. Therefore, hydrogen yield increases and decreases with S/C ratio at 923 and 873 K, respectively.

However, the influence of the S/C ratio on hydrogen yield is not straightforward; on one hand the reforming process is promoted at high S/C ratio and on the other hand, the excess water results in lower hydrogen partial pressure and lower hydrogen permeation (eq. 3.1).

3.2.4 Hydrogen recovery

At complete conversion of ethanol, hydrogen recovery is an indicator of the ability of the reformer to produce pure hydrogen. This refers to both the reforming reactions and the membrane performance. The higher value of hydrogen recovery is an evidence of the shift effect on the progress of the reforming reactions to leave less unconverted CO and CH_4 in the reactor. The hydrogen recovery as a function of pressure is presented in Fig. 3.16.
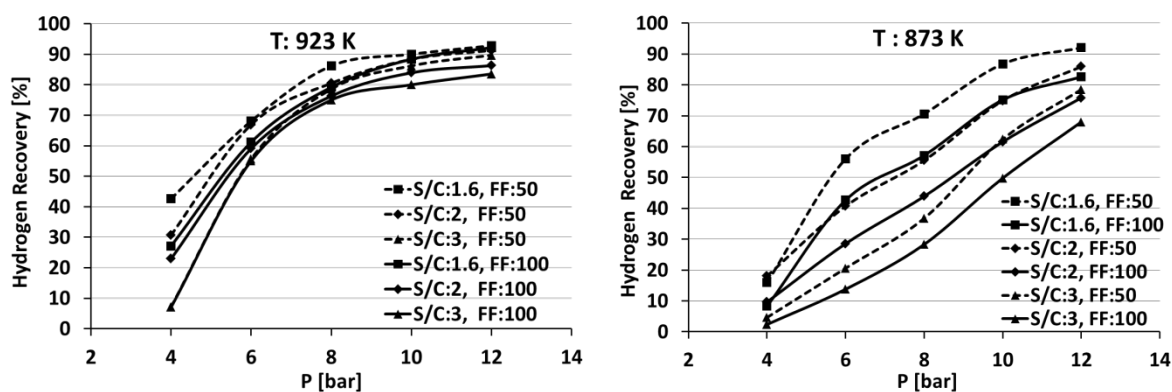
Fig. 3.16 Hydrogen recovery

Contributing to the shift effect to push the reforming reactions to the product side, very high hydrogen recovery of up to 95% is a representative of the ability of the CMR to recover and deliver a large portion of pure hydrogen. Almost all the produced hydrogen at high pressure is permeated through the membrane. As expected, hydrogen recovery is favored at lower S/C values since the partial pressure of hydrogen in the reactor is higher (less excess water); hence, the permeation through the membrane is improved according to the Sieverts' law. In addition, at a lower fuel flow rate the contact time increases and the permeation of hydrogen is favored. On average, for every 2 bar increase in pressure, the pure hydrogen production increases by 0.5 mol/mol ethanol in the feed (see Fig. 3.14). Accordingly, the fraction of hydrogen in the retentate side decreases with pressure, which is attributed to the fact that more hydrogen is permeated (recovered) through the membrane. Pure hydrogen production rate and hydrogen fraction in the retentate side as a function of pressure are illustrated in Fig. 3.17.

66
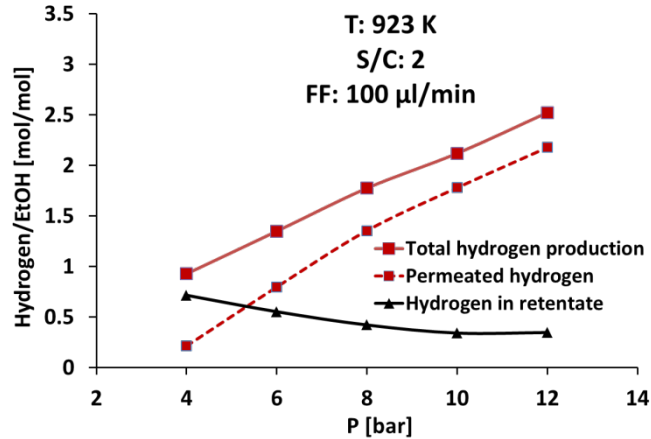
Fig. 3.17 Hydrogen content in the retentate side and total hydrogen production as a function of pressure at 923 K

As shown in Fig. 3.17, the difference between the total hydrogen production and permeated hydrogen per mol ethanol in the feed decreases with pressure. Having the definition of hydrogen recovery in mind (eq. 3.2), the behavior of the CMR regarding the hydrogen recovery at 923 K (Fig. 3.16) can be described. The hydrogen content of the retentate stream is almost unchanged with pressure at P>8 bar, indicating that the membrane reaches its limitations regarding the permeation of the produced hydrogen, although the total and pure hydrogen production rates increases.

At 873 K, however a different behavior is seen. This can be a result of the notable effect of temperature on the ESR performance.
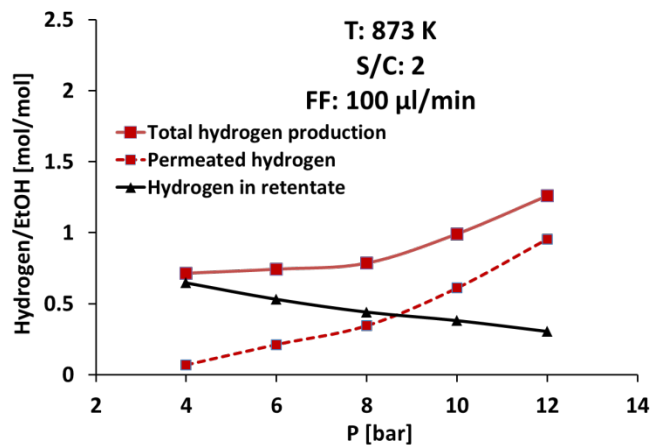
Fig. 3.18 Hydrogen fraction in the retentate side and total hydrogen production as a function of pressure at 873 K

As can be seen in Fig. 3.18, the trend of reduction in the fraction of hydrogen in the retentate side with pressure is linear. Besides, total hydrogen production increases exponentially with pressure, which is an indicator of the role of pressure in the production

of hydrogen at low temperatures. This can again be described considering the shift effect, which pushes the reactions to the product side at high pressures as hydrogen is extracted.

3.3 Comparison between the CMR and the SMR configurations

3.3.1 Overall performance of the CMR and SMR

In this section, a comparison between the two configurations is given based on the experimental results. The superior performance of the CMR was observed regarding the pure hydrogen production, hydrogen yield and hydrogen recovery. The pure hydrogen production rate at different operating conditions is presented in Fig. 3.19. The ESR experiments for the SMR configuration were performed only at S/C ratio of 1.6.
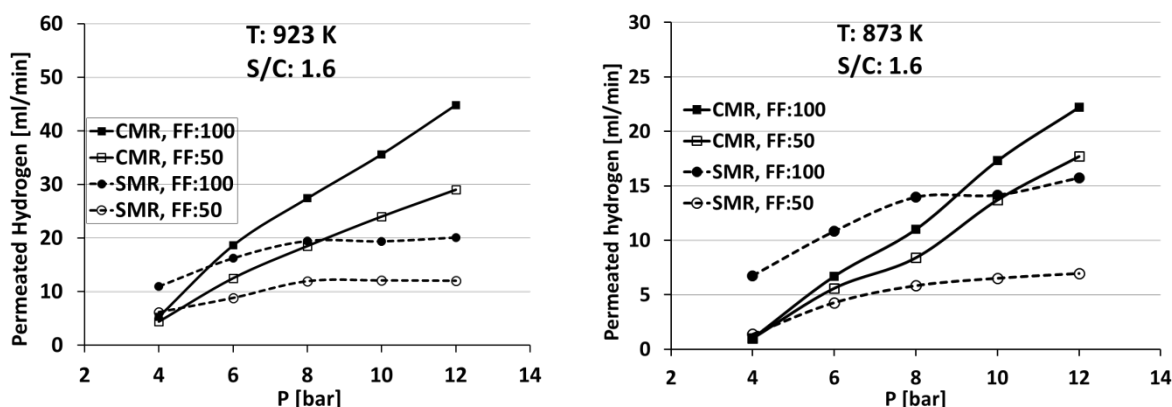
Fig. 3.19 Comparison of pure hydrogen production in the CMR and SMR at S/C=1.6

The difference between the two configurations is visible especially at 923 K. In the case of the CMR, hydrogen production is promoted with pressure while in the case of the SMR, the increase in hydrogen production rate is not notable at P>8 bar. This is attributed to the enhancement in ESR reaction promotion as an evident result of the shift effect, thanks to the existence of the catalyst as it sandwiched the membrane in the CMR. The catalyst compensates for the permeated hydrogen by simultaneous production of hydrogen. Hence, the partial pressure of hydrogen is kept high around the membrane. At 873 K and FF=100 μl/min, however the performance of the CMR was not better than the SMR. It can be a reason of the longer catalytic zone of the SMR where the ERS reactions may progress more because of the longer residence time. At 873 K, where the temperature is not high enough for the MSR reaction to complete, the residence time during which the reactants are in contact with the catalyst might play an important role. Higher hydrogen permeation rate in the case of the SMR at 873 K and FF=100 μl/min proves the idea of the effect of the residence time.

The hydrogen yield showed a trend similar to the pure hydrogen production.
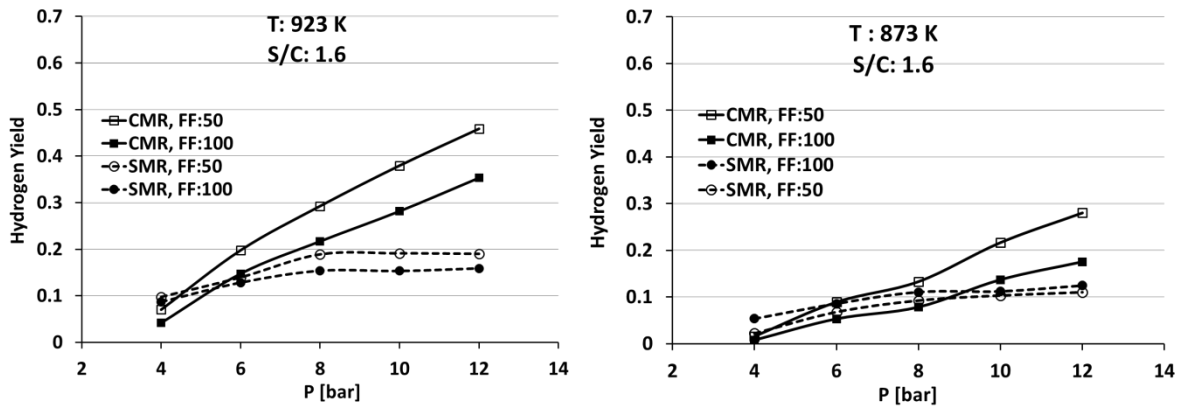
Fig. 3.20 Comparison of hydrogen yield in the CMR and SMR

Superior performance of the CMR is presented in Fig. 3.20 where the hydrogen yield reaches up to 0.55. Despite unfavorable conditions (high pressure), the positive effect of high pressure is evident in the case of the CMR due to its special configuration. In the case of the SMR, although the hydrogen production rate increased slightly with pressure, the influence of pressure on the ESR reaction hindered the hydrogen yield to increase by pushing the MSR reaction back towards the reactant side (reverse reactions). The effect of the pressure on the performance of the CMR and SMR is given in the next section.

A comparison between the hydrogen recovery of the CMR and SMR is illustrated in Fig. 3.21.
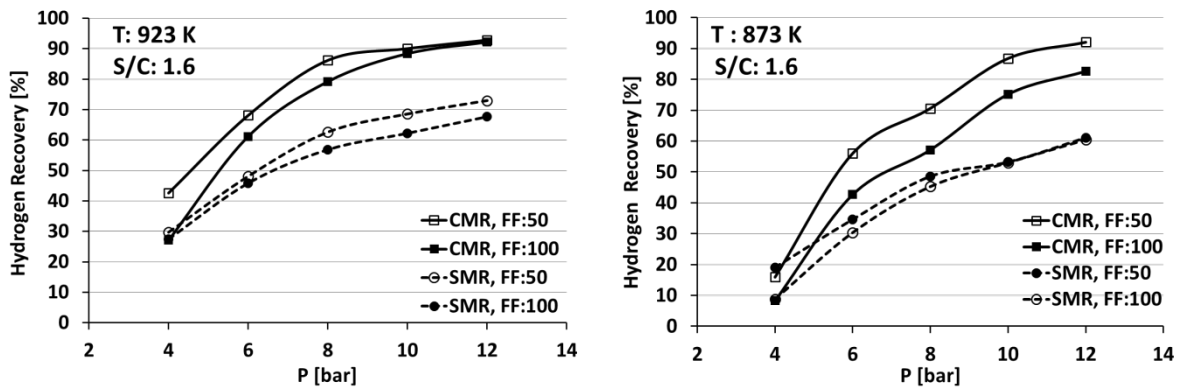
Fig. 3.21 Comparison of hydrogen recovery in the CMR and SMR

Hydrogen recovery at the highest reaches 70% at 923 K in the case of the SMR. Hydrogen recovery is independent from the operating temperature, instead, it is a measure of the ability of the configuration to recover the produced hydrogen (via ESR) as pure hydrogen permeated through the membrane. The determining factor in the case of the SMR is the reactor pressure, while in the case of the CMR, the recovery of hydrogen reaches a threshold (a maximum possible value). Hydrogen recovery of the SMR configuration

increases by pressure, which is not atributed to the higher pure hydrogen production rate (see Fig. 3.19), but to the less total hydrogen production rate (see eq. 3.2).

3.3.2 The effect of pressure

As stated before, pressure had a positive effect on the performance of the CMR, while at the pressures higher than 8 bar, the performance of the SMR did not improve. One of the enhanced performances of CMR compared to the SMR is presented in Fig. 3.22.
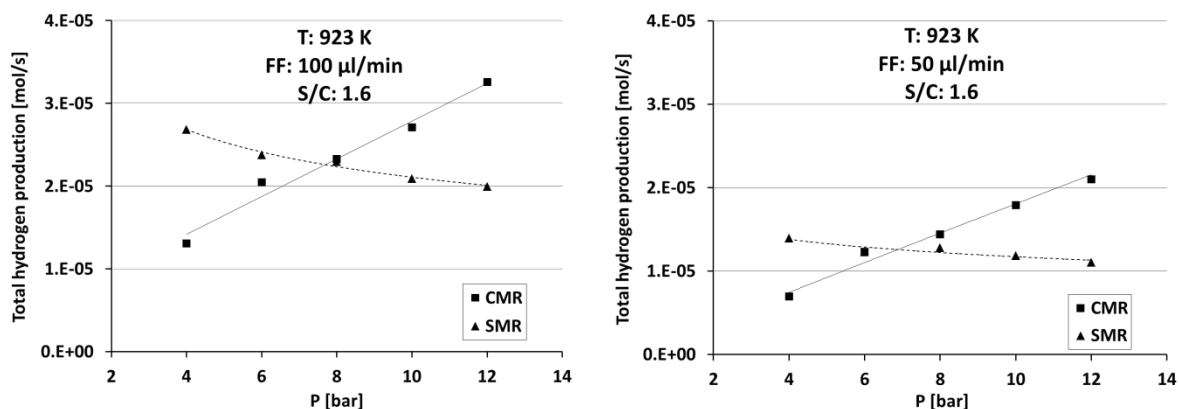
Fig. 3.22 Total hydrogen production (permeated + retentate) with pressure

Contrary to the SMR, in the CMR the total hydrogen production rate increases with pressure. In the SMR configuration, when the ESR products leave the catalytic zone, the reforming reactions have already reached the equilibrium at the corresponding operating temperature and pressure. The influence of the pressure on the reforming reactions, specially the methane steam reforming reaction (see eq. 2.3), is obvious in the case of the SMR, as the hydrogen production rate declines with pressure. In the SMR, the produced gases pass over the membrane and as hydrogen is permeated, its partial pressure declines simultaneously along the membrane, resulting in a decreasing permeation rate along the membrane. A simulated example of the pressure reduction along the membrane is shown in Fig. 3.23 [3].
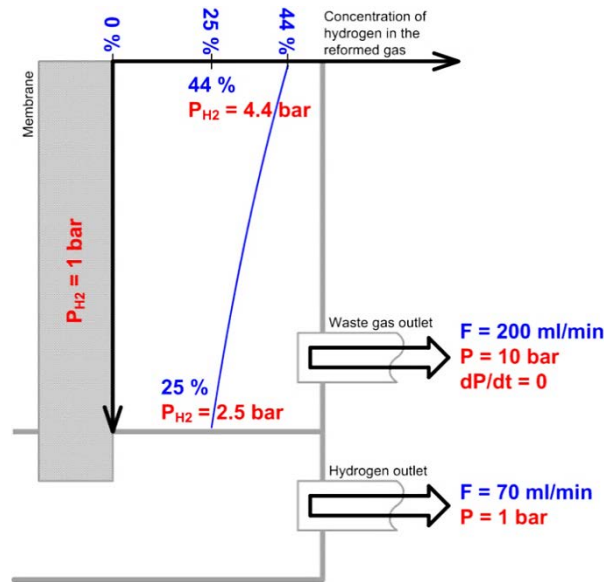
Fig. 3.23 Partial pressure of hydrogen along the membrane in the SMR configuration at 10 bar and 923 K. Figure taken from the work by Koch et al. [3].

P_{H2} represents the partial pressure of hydrogen inside the reactor at the membrane wall. The partial pressure of hydrogen at the permeate side was one bar (no sweep gas used).

In the CMR, the dynamics is different. Up until the retentate gas exits the reactor, the reforming reactions are in progress considering the shift effect. In the CMR, the higher the pressure, the higher the hydrogen permeation rate, and the higher the production rate of hydrogen. In fact, the thermodynamic equilibrium limits are conquered owing to the shift effect and the brilliant activity of the catalyst to convert largely the fuel to CO_2 and H_2. It is assumed that the partial pressure of hydrogen is kept high along the membrane because of simultaneous and continuous hydrogen production.

The selectivity of the retentate gas (outlet gas) at the same experimental conditions also proves the superior performance of the CMR. The molar flow rates of CO and CH_4 as a function of pressure for both configurations are shown in Fig. 3.24.
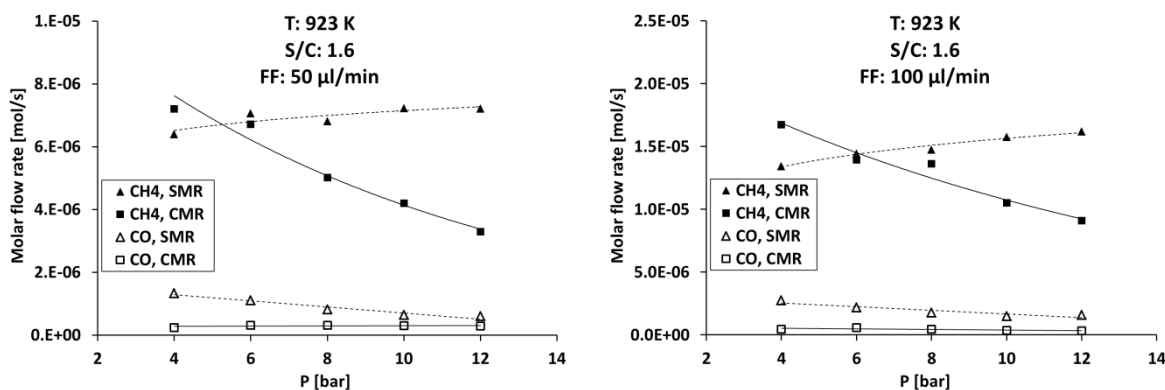
Fig. 3.24 Molar flow rate of CH_4 and CO at the reactor exit for CMR and SR configurations

Very low concentration of CO in the retentate together with declining molar production of methane clearly proves the critical role of pressure in the CMR for ESR reaction promotion. This is an indicative of the water gas shift (WGS) and methane steam reforming (MSR) reactions promotion in the CMR configuration leading to higher hydrogen production as discussed before. In the SMR, methane formation is promoted at higher pressures as expected from thermodynamics (reverse MSR reaction). The hydrogen production rate decreases with pressure (Le Chatelier's principle). CO concentration was kept almost constant and very low in the CMR during the process.

The flow rate of the retentate gas in CMR experiments is less than the one of the SMR at the same experimental conditions. At pressures higher than 8 bar the CMR retentate flow rate is almost half of the one of the SMR. The retentate flow rate at T=923 K and S/C=1.6 is given in Fig. 3.25.
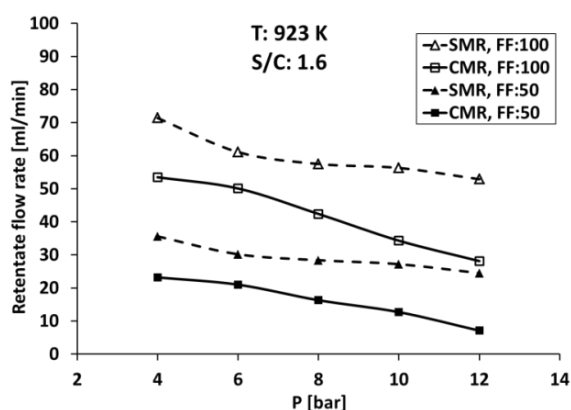
Fig. 3.25 Retentate flow rate

At complete conversion of ethanol and constant S/C ratio, the flow rate of the retentate gas can be directly interpreted as an indicator of the performance of the membrane reactor in terms of ESR reaction promotion, which is in agreement with previous discussions. The

comparison of CMR and SMR in terms of the pure hydrogen production rate per mole of ethanol in the feed is given in Fig. 3.26.
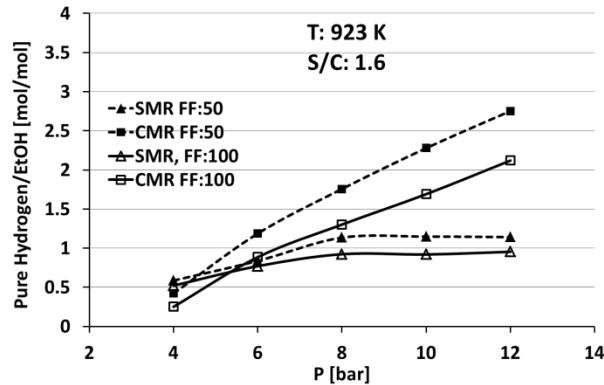
Fig. 3.26 Pure hydrogen production rate per mole of ethanol in the feed

Considering higher production rate of hydrogen, which directly means higher conversion of CO and CH_4, the CMR configuration proves a superior performance. Therefore, not only the challenge of negative effect of pressure on the ESR reaction and pure hydrogen production is overcome, but also pressure turns to play an important positive role in the enhancement of the CMR performance towards higher hydrogen generation and recovery.

3.3.3 Pure hydrogen efficiency

Pure hydrogen efficiency is presented in Fig. 3.27. The inlet hydrogen is the sum of hydrogen fed to the reactor (i.e. 1 mole of hydrogen per mole of water and 3 moles of hydrogen per mole of ethanol).
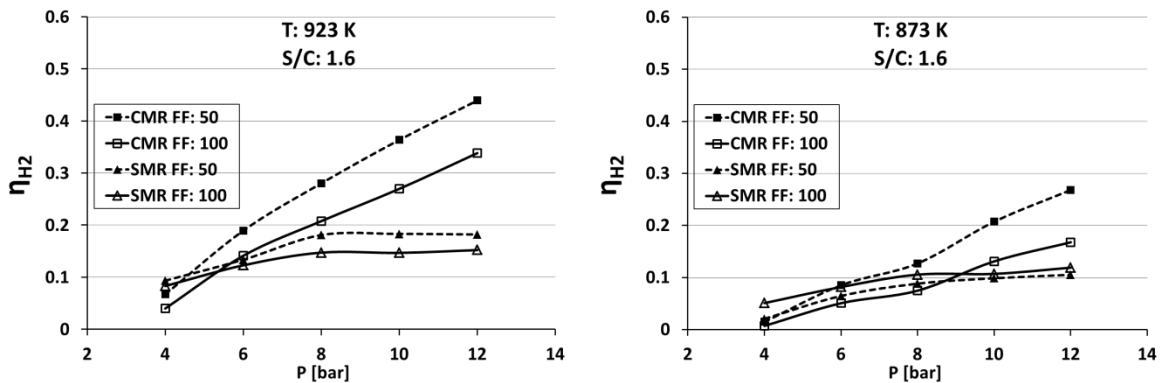
Fig. 3.27 Pure hydrogen production efficiency at stoichiometric conditions

Pure hydrogen efficiency at S/C=1.6, where the fuel mixture is almost at stoichiometric ratio considering the molar ratio of water and ethanol (water/EtOH: 1/3.2) is a true measure of the performance of the SMR and CMR configurations.

3.4 Conclusion

ESR experiments over Pd-Rh/CeO$_2$ were performed in a CMR containing Pd-Ag separation membranes using ethanol and water mixtures at different S/C ratios. The effect of operating conditions, specially temperature and pressure, was discussed. The performance of the CMR was studied in terms of pure hydrogen production, hydrogen yield, and hydrogen recovery. The shift effect resulted in very high hydrogen production and the equilibrium limitations at high pressure were conquered. The influence of the coexistence of species such as CO and CH$_4$ was shown based on the experimental results of the permeation tests in the atmosphere of pure hydrogen and ethanol steam reforming. A comparison between the CMR and the SMR clearly revealed the superior performance of the CMR. Many observed features in the case of SMR were not seen in the CMR so that pure hydrogen production rate and methane conversion were promoted at high pressure.

To conclude, some of the highlights of the experimental work can be listed as:

- Complete ethanol conversion at all the operating conditions.
- Hydrogen yield of 0.55 at 923 K, 12 bar, and S/C=3 in the CMR (0.2 in the SMR).
- Hydrogen recovery reaches up to 95% at 923 K, 12 bar, and S/C=3 in CMR (70% in SMR).
- 0.9 L$_N$ Hydrogen/ml EtOH at 12 bar, and 923 K.
- More than 3 moles of pure hydrogen per mole of inlet EtOH.
- ESR reaction promotion beyond the equilibrium limitations at high pressure.
- Positive effect of pressure on the performance of the CMR despite unfavorable thermodynamic conditions at high pressure.

The next chapter presents the results of the thermodynamic analysis of the reforming system mainly in terms of thermal and exergy efficiency based on the experimental results given in this chapter. Both CMR and SMR configurations are discussed and compared in detail as a complement to the experimental study, to provide a detailed overview of the discussed reforming system.

Chapter 4

Thermodynamic analysis of the CMR and SMR systems

Abstract

The experimental results of the ESR reaction in the CMR and the effect of various operating conditions on the hydrogen selectivity and pure hydrogen production rate were given in previous chapter. Aiming to understand the thermodynamic performance of the reformer, the energy and exergy analysis are given in this chapter. Thermodynamic evaluation is presented as a supplement to the comprehensive investigation of the performance. The experimental results presented in the previous chapter (selectivity of ESR products and the pure hydrogen production rate at all the presented operating conditions) were used to perform the exergy analysis. The exergy efficiency and exergy destruction of the CMR were evaluated based on inlet and outlet streams. The exergy efficiency of the reformer was evaluated considering both an insulated reactor (without heat loss), and a non-insulated reactor (with heat loss). The significant effect of pressure and temperature on the exergy efficiency was observed. Exergy efficiency up to 50% was reached in the case of an insulated reactor at 12 bar and 923 K. It was concluded that the highest rate of exergy destruction occurred via heat losses. The study showed that the exergy content of the retentate gas especially at lower pressures could provide the reactor with a notable fraction of its required heat at steady state conditions. This notably increased the exergy efficiency of the reformer. In the case of recovery of the retentate gas and insulation of the reactor, exergy efficiency placed between 70-90%. It was concluded that operating at the highest pressure, the lowest S/C ratio, and at 923 K gives the best exergy efficiency. Thermal efficiency of the reformer was between 60-90% for an insulated reactor and decreased to between 40-60% when the heat loss was considered. The exergy analysis proved superior performance of the CMR.

4.1 Exergy analysis

Regarding the thermodynamic investigations of the ESR process, the studies reported in the literature are mainly focused on energy efficiency (ratio of energy output to energy input), but not on exergy analysis. Exergy analysis is a powerful tool to investigate the imperfections of single components of an energy system to obtain a better understanding of the local irreversibility by means of a more detailed picture of the process.

The term exergy is defined as the maximum work that can be obtained theoretically from a system interacting with the source environment to equilibrium [183]. Exergy differs from energy in the way that energy is conserved, but exergy can be dissipated. Exergy is defined based on both the first and second laws of thermodynamics stating that it is not possible to fully utilize the thermal energy [184]. In other words, exergy is the ability of available energy to convert into other forms of energy.

Taking into account the second law of thermodynamics, exergy is derived from the entropy, free energy (Helmholtz energy), and free enthalpy (Gibbs free enthalpy). Therefore, exergy is a function of the thermodynamic state of the substance and the reference environment [184]. In the light of exergy definition, it can be understood that the main difference between energy (thermal) efficiency and exergy efficiency lies in the consideration of the thermodynamic state of every single component, which results in an exact understanding of the available amount of work, together with the unavoidable irreversibility during a process. Exergy analysis makes it possible to study the effect of thermodynamic factors on the performance of an energy system to decide on the most favorable operational conditions in terms of process efficiency and energy usage [185,186].

According to the open literature, there are a few reported studies on exergy efficiency evaluation for hydrogen production. Kalinci et al. [187] studied the production of hydrogen via a gasification-boiler system based on experimental data taken from the literature using different types of biomass. They found the maximum exergy efficiency to be about 12%. An exergy analysis of the biological hydrogen production from biomass was done by Modarresi et al. [188] based on experimental results. They reported exergy efficiencies of 36-45%, depending on the process configuration. For reforming processes, Simpson et al. [189] modelled the methane steam reforming process and both irreversible chemical reactions and heat losses were identified as the main source of exergy destruction, whereas exhaust gases contained large amounts of chemical exergy. Casas-Ledón et al. [186] studied hydrogen production from ESR based on the first and second laws of thermodynamics. They evaluated the exergy efficiency of the system experimentally at different operational conditions (pressure, temperature, and S/C ratio) considering the unused and destructed exergy during the ESR process. They concluded that the exergy efficiency of the ESR system was a function of temperature and S/C ratio, while no effect of pressure on exergy efficiency was observed. A comprehensive exergy analysis of the

different types of ethanol reforming processes (ESR, POX and ATR) based on a model in Aspen Plus was performed by Khila et al. [185]. The same formulation as Casas-Ledón et al. [186] was used by Khila et al. and they used Aspen Plus software to calculate the exergy of the inlet and outlet streams at selected operational conditions, according to hydrogen production per mole of inlet ethanol. An exergy efficiency of 70% was claimed for the ESR process, considering total hydrogen production via ESR as the main product. In another study, Tippawan et al [190] employed the first and second law of thermodynamics to evaluate energy and exergy performance of a modelled ethanol reforming system in connection with a solid oxide fuel cell (SOFC) with a similar formulation as Casas-Ledón et al. [186] and Khila et al [185]. They studied ESR, partial oxidation (POX), and autothermal reforming (ATR) processes as the reforming sections for hydrogen production, and the best efficiency of the system (reforming+SOFC) was stated equal to 60% when ESR was used as the reformer unit.

In this chapter, the application of exergy analysis in the evaluation of the ethanol steam reforming (ESR) process in the CMR and SMR configurations is presented. The molar flow rates of the pure hydrogen stream and all the ESR products (CO, H_2, CH_4, and CO_2 in the retentate stream) obtained via experiments were used for calculation of the exergy rate of different streams. Exergy evaluation was used to study the effect of the operating conditions on the performance of the system and to understand the thermodynamic losses, to decide on the best operating conditions in terms of both pure hydrogen production and the exergy efficiency.

4.2 Materials and methods

The traditional method of process performance evaluation is based on the first law of thermodynamics, which considers the lower heating value (LHV) of the inlet and outlet streams, and the amount of work or heat provided to run the process. Thermal efficiency of the reformer system is defined as [120,185]:

$$\eta_{Thermal} = \frac{\dot{m}_{retentate} \times LHV_{retentate} + \dot{m}_{pure\ hydrogen} \times LHV_{hydrogen}}{\dot{m}_{EtOH} \times LHV_{EtOH} + \dot{w}_{pump} + \dot{Q}} \qquad 4.1$$

$\dot{W}_{pump}$ is the work of the pump. The work of the pump is neglected in this work. $\dot{Q}$ represents the rate of heat losses and the required energy to run the ESR in the CMR. Heat losses account for the heat released to the environment through the reactor wall, products cooling down, and water condensation. All the products (the retentate gas stream and condensed water) are cooled down by transferring heat to the environment via the pipes and the condenser wall.

Reactor wall temperature (in contact with air) was measured by means of a K-type thermocouple to calculate the heat loss at different operating temperatures (873 and 923 K). The heating band is the heat source for the evaporation of the fuel and heating up to

reaction temperature, ESR reaction, and to maintain the temperature at the set point. The reactor vessel is a cylindrical stainless steel of 1 mm thickness in which the heart reactor is sandwiched between a 22 mm thick layer of glass wool (thermal conductivity K=0.04 W/m·K). The catalytic zone is a stainless steel cylinder with the height of 67 mm and periphery of 280 mm, accounting for 0.019 m^2 area. The axial temperature gradients are neglected in this work and it is assumed that the catalyst bed and the membrane are kept at the set point reaction temperature (873 or 923 K). The cross sectional scheme of the reactor vessel is shown in Fig. 4.1.
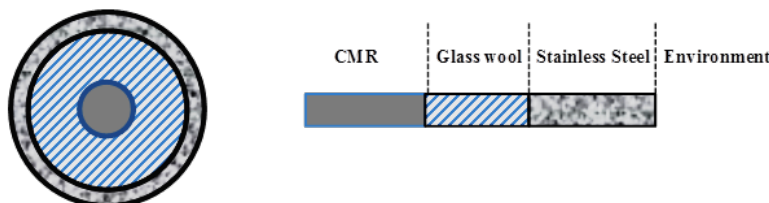
Fig. 4.1 Cross sectional scheme of the reactor vessel

The temperature of the reactor vessel wall was measured while the process was ongoing at steady state conditions at 873 and 923 K. Assuming the reactor vessel as a tube, the heat loss through the reactor wall ($Q_{loss}^{reactor}$) is calculated:

$$Q_{loss}^{reactor} = \frac{2\pi LK(T_r - T_w)}{Ln\left(\frac{r_o}{r_i}\right)}$$

4.2

'L' is the length of the catalytic zone of the reactor, i.e. where the membrane is fully covered by the catalyst (67 mm), and 'K' stands for the thermal conductivity of the glass wool (0.04 W/m·K). 'T_r' and 'T_w' are the temperature of the reactor (reaction set point) and the reactor vessel wall, respectively. The inside radius (only the heart reactor without insulation) and outside radius of the reactor vessel (reactor and the insulation) are indicated by r_i (0.0127 m) and r_o (0.0347 m), correspondingly. The thermal resistance of the stainless steel layer is neglected due of its high thermal conductivity and the small thickness. The values of T_w and the corresponding heat loss at 873 and 923 K are given in Table 4.1.

Reactor Temperature T_r (K)	873	923
Wall Temperature T_w (K)	378	393
Heat loss rate $Q_{loss}^{reactor}$ (W)	10	12

Table 4.1 Wall temperature and the heat loss rate at 873 and 923 K

The required heat for the evaporation and heating up the reactants (ethanol and water mixture) was calculated according to the fuel flow rate and S/C ratio of each experiment using the enthalpy change occurring during the heating process. The heat required for the

reforming reactions (ESR) was also calculated based on the progress of each of the chemical reactions involved in the ESR (eq. 2.1-2.3) using the retentate composition, i.e. the molar flow rate of CH_4 and CO. Ethanol decomposition is the only reaction via which CO and CH_4 are formed and then react with water to form CO_2 and H_2. According to eq. 2.1, at complete conversion of ethanol (which was reached in this work), one mole of CO and one mole of CH_4 are produced per each converted mole of ethanol. The molar flow rate of CO and CH_4 are then a measure of the promotion of WGS and MSR reactions, respectively. It is supposed that coke formation is zero, so that all the products of the ESR are obtained in the gas phase at the outlets of the reactor (pure hydrogen and retentate streams, see Fig. 3.4).

It is assumed that the reactants enter the system at reference conditions and products are released to the same environment. In this work, the reference conditions are defined as $T_0 = 298$ K and $P_0 = 1$ bar. The scheme of the reforming in the case of exergy evaluation is shown in Fig. 4.2.
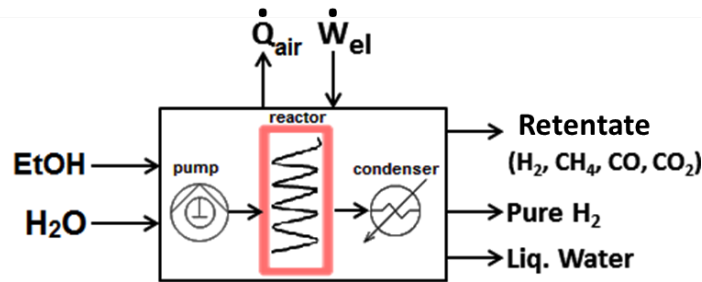
Fig. 4.2 Scheme of the reformer system

$\dot{Q}_{air}$ represents the heat loss rate released to the reference environment (hydrogen and retentate gases cooled from the reactor temperature down to ambient temperature with the concomitant condensation of water, plus the heat loss via the reactor wall). In fact, this heat (in the form of exergy) is a part of the inlet exergy stream ($\dot{W}_{el}$), which is released to the environment as unused exergy. $\dot{W}_{el}$ represents the electrical input of the system used by the heating band to provide the reactor with required heating. The required exergy is limited to the exergy that is lost via heat losses (reactor wall + products cooling process) and the required exergy to run the CMR (fuel evaporation and heating up to reaction temperature plus the required exergy for the chemical reactions); which is equal to $\dot{W}_{el}$. In this study, $\dot{W}_{el}$ is replaced by the rate of required heat for the ESR process plus the value of $\dot{Q}_{air}$ (heat loss rate).

As shown in Fig. 4.2, the reformer consists of two energy-consuming parts, i.e. the pump and the reactor. The condenser is energy neutral since the condensation occurs via physical water condensing traps (air-cooled). Although there are metallic membrane tubes inside the reactor for separation of hydrogen from the other gases, the permeation of hydrogen is a physical phenomenon. The efficiency of hydrogen separation depends upon its partial

pressure inside the reactor and outside the membrane (Sieverts' law). Nevertheless, this phenomenon is considered as energy neutral because the pressure needed is supplied by the pump.

Exergy efficiency is calculated based on exergy destruction and unused exergy, as a function of the exergy rate of the inlet and outlet streams. This formulation has been repetitively used by different researchers [120,185,186,191]. Exergy destruction rate is defined as:

$$EX_{destruction} = EX_{in} - EX_{out} \qquad\qquad 4.3$$

Where EX_{in} and EX_{out} are the exergy rates of the inlet and outlet streams. Therefore, EX_{in} represents the exergy rate of inlet fuel, i.e. ethanol (with its specific exergy ex_{fuel}), plus the required exergy rate for the ESR process including heat losses ($EX_{\dot{W}_{el}} = \dot{W}_{el}$), and EX_{out} denotes the exergy rate of pure hydrogen stream ($ex_{H2.perm}$), plus the retentate gases exiting the reactor ($ex_{retentate}$):

$$EX_{in} = F_{EtOH}ex_{fuel} + \dot{W}_{el} \qquad\qquad 4.4$$

$$EX_{out} = F_{H2.perm}ex_{H2.perm} + F_{retentate}\,ex_{retentate} \qquad\qquad 4.5$$

The condensed water is considered to have zero exergy value. The rate of unused exergy is calculated as:

$$EX_{unused} = EX_{destruction} - EX_{retentate} \qquad\qquad 4.6$$

Where $EX_{retentate}$ is the exergy rate of the retentate gas. The exergy of the pure hydrogen stream is considered as useful part of exergy. Accordingly, the fraction of hydrogen in the retentate gas (not permeated) is not taken into account as the main product. Finally, the exergy efficiency of the ESR process is given by eq. 4.7:

$$\eta_{ex} = 1 - \frac{EX_{unused}}{EX_{in}} \qquad\qquad 4.7$$

The specific exergy content of each species (ex) in each stream consists of physical exergy ($ex_{physical}$), chemical exergy ($ex_{chemical}$), and mixing exergy (ex_{mixing}):

$$ex = ex_{physical} + ex_{chemical} + ex_{mixing} \qquad\qquad 4.8$$

Physical exergy ($ex_{physical}$) is the maximum obtainable work produced when a stream is brought from the actual conditions (T, P) to the reference conditions (P_0, T_0) and is defined as [18,30] :

$$ex_{physical} = h - h_0 - T_0(s - s_0) \qquad\qquad 4.9$$

h and s are the specific enthalpy and specific entropy of the substance at actual (reaction) conditions, and h_0 and s_0 are the specific enthalpy and specific entropy of the substance at reference conditions, respectively. The dependency of the physical exergy on enthalpy and entropy highlights two features. First, exergy is a function of the state of the matter, and second, each matter is considered independently in a stream. Both features result in a more precise idea on the performance of a thermal system. To calculate the values of enthalpy and entropy, NASA polynomials (Chemkin polynomial coefficients) for temperatures below 1000 K are applied according to the database of the Department of Mechanical Engineering of The University of California, Berkeley [4].

$$\frac{H}{RT} = a_1 + a_2 \frac{T}{2} + a_3 \frac{T^2}{3} + a_4 \frac{T^3}{4} + a_5 \frac{T^4}{5} + \frac{a_6}{T} \qquad 4.10$$

$$\frac{S}{R} = a_1 Ln(T) + a_2 T + a_3 \frac{T^2}{2} + a_4 \frac{T^3}{3} + a_5 \frac{T^4}{4} + a_7 \qquad 4.11$$

The polynomial coefficients of the species present in the inlet and outlet streams are given in Table 4.2.

Component	a_1	a_2	a_3	a_4	a_5	a_6	a_7
H_2	2.344	0.00798	-1.95E-05	2.02E-08	-7.38E-12	-9.18E+02	6.83E-01
CH_4	5.1499	-0.013671	4.92E-05	-4.85E-08	1.67E-11	-1.02E+04	-4.64E+00
CO	3.58E+00	-6.10E-04	1.02E-06	9.07E-10	-9.04E-13	-1.43E+04	3.51E+00
CO_2	2.36E+00	8.98E-03	-7.12E-06	2.46E-09	-1.44E-13	-4.84E+04	9.90E+00
H_2O	3.386842	3.47E-03	-6.35E-06	6.97E-09	-2.51E-12	-3.02E+04	2.590233
C_2H_5OH	4.23E-01	2.93E-02	-1.74E-05	5.34E-09	-6.75E-13	-2.96E+04	2.34E+01

Table 4.2 NASA Polynomials [4]

Chemical exergy originates from the difference between the chemical potentials when a substance is changed at reference conditions to the chemical equilibrium state with the concentrations of components. In this work, the chemical exergy of each specie was calculated using the standard chemical exergy table given by Bejan model II [183]. Chemical exergy occasionally is reported as a sum of two terms, i.e. the standard chemical exergy plus a logarithmic term as a function of the fraction of each substance in a mixture [186,190]:

$$ex_{chemical} = x_i \varepsilon_i + RT_0 x_i Ln x_i \qquad 4.12$$

Where x_i is the fraction of any species in the mixture of gases, ε_i is the standard chemical exergy of the species, and R is the universal gas constant. The physical properties together

with standard chemical exergy for the chemical species are presented in Table 4.3 according to the Bejan model II [183].

Component	Density (kg/m^3)	Molar Weight (g/mol)	Standard chemical exergy (J/mol)
H$_2$	0.0813	2.016	236100
CH$_4$	0.648	16.04	831650
CO	1.13	28.01	275100
CO$_2$	1.775	44.01	19870
Water	1000	18.02	900
Ethanol	783	46.07	1357700

Table 4.3 Physical properties and standard chemical exergy of species

The second term in eq. 4.12 ($RT_0x_iLnx_i$), as is always negative, can be ascribed to the exergy of mixing. Exergy of mixing is the entropy generated when pure substances are mixed and is given by eq. 4.13 [184]:

$$ex_{mixing} = x_iRT_0Lnx_i \qquad\qquad 4.13$$

However, the value of mixing exergy is normally negligible in front of standard chemical exergy [192]. A comprehensive discussion on various types of exergy calculation is given by Sato [184] and Hinderink et al. [192]. Similar definitions have been reported in some studies, which are based on the entropy difference between the mixture of substances and the pure components (which exist in the mixture) individually [185,192]. In this work, all three types of exergy were considered for each species in the inlet and outlet streams. The molar flow rate of reactants and products obtained during the experimental work were used to calculate the exergy rate of each stream.

4.3 Results and Discussion

4.3.1 Thermodynamic analysis of the CMR

The optimization of the reforming system not only depends on the improvement of pure hydrogen permeation rate, but also on the thermodynamic efficiencies. Thermodynamic evaluation provides a better understanding of the effect of the operating conditions on the performance of the reformer. Pure hydrogen production gets higher naturally with the fuel flow rate, as discussed earlier. This is in agreement with the thermal efficiency, but not with exergy efficiency, due to the criteria based on which the thermal and exergy efficiencies are defined (eq. 4.1 and 4.7, respectively). Thermal and exergy efficiency at FF=50 and 100

μl/min are presented versus pure hydrogen permeation rate in Fig. 4.3, respectively. As more methane is produced at higher fuel flow rate, thermal efficiency is higher. Nevertheless, as less hydrogen is produced per mol of converted ethanol at higher fuel flow rate (see Fig. 3.12), the exergy efficiency decreases with fuel flow rate.
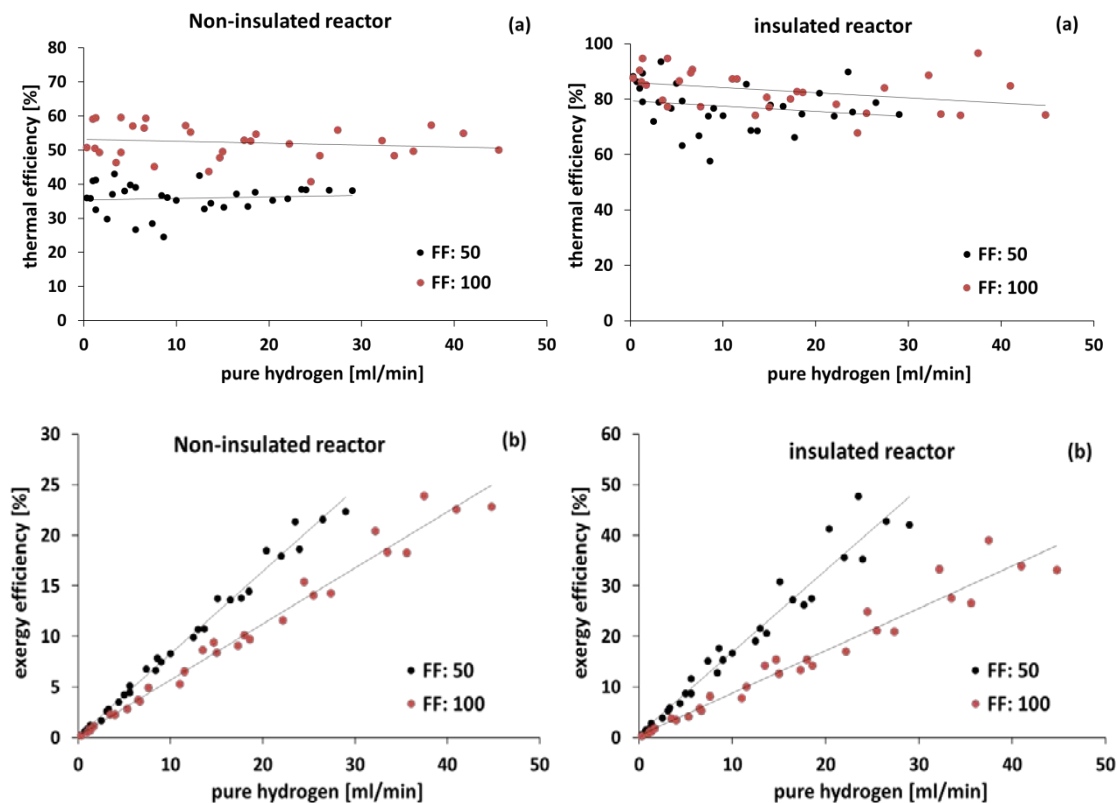
Fig. 4.3 Thermal efficiency (a) and exergy efficiency (b) versus pure hydrogen permeation rate

Apart from the fuel flow rate, the operating temperature and pressure are the key factors in high production rate of pure hydrogen, as discussed in the experimental chapter (chapter 3). As shown in Fig. 4.3a, almost the same magnitude of thermal efficiency is obtained at different pure hydrogen production rates, which corresponds to the different operating conditions. Obviously, the performance of the reformer cannot be explained precisely by means of thermal efficiency, bearing in mind that pure hydrogen is the product of this reforming system.

In the case of exergy efficiency, the effect of operating conditions, especially pressure, is clearly explained. The effect of pressure as the driving force for hydrogen permeation can be found out remembering that production rate of hydrogen increases with pressure. As seen in Fig. 4.3b, in the case of the CMR, the exergy efficiency linearly increases with pure hydrogen production, which means the operating pressure. It can be concluded that the effect of operating conditions can be explained better by means of exergy evaluation. Fig.

4.3b states that the improvement of the reformer depends on decreasing the irreversibility and losses of the reforming system at higher production rates of pure hydrogen. Accordingly, it is essential to study the effect of temperature, pressure, fuel flow rate, and S/C ratio on the exergy efficiency, together with the source of thermodynamic losses of the reformer.

An optimum operational pressure can be encountered considering two opposite effects. On one hand pressure favors hydrogen permeation through the membrane (Sieverts' law), but on the other hand higher pressures result in a lower overall production of hydrogen (Le Chatelier's principle), resulting in a lower hydrogen partial pressure inside the reactor. Consequently, large amounts of reject gas from the membrane are usually present under realistic operation, which can then be combusted to provide self-sustainable operation [193]. Despite of such a hypothesis, it was proven that not only the hydrogen production rate increased with pressure, but also the flow rate of the retentate gas and especially the methane content in the retentate stream significantly declined at higher pressure, thanks to the brilliant performance of the CMR to promote the MSR reaction.

- **Effect of operational conditions**

Pressure has a strong effect on exergy efficiency. As seen in Fig. 4.4, the best exergy efficiency is obtained at 12 bar, whatever the temperature.
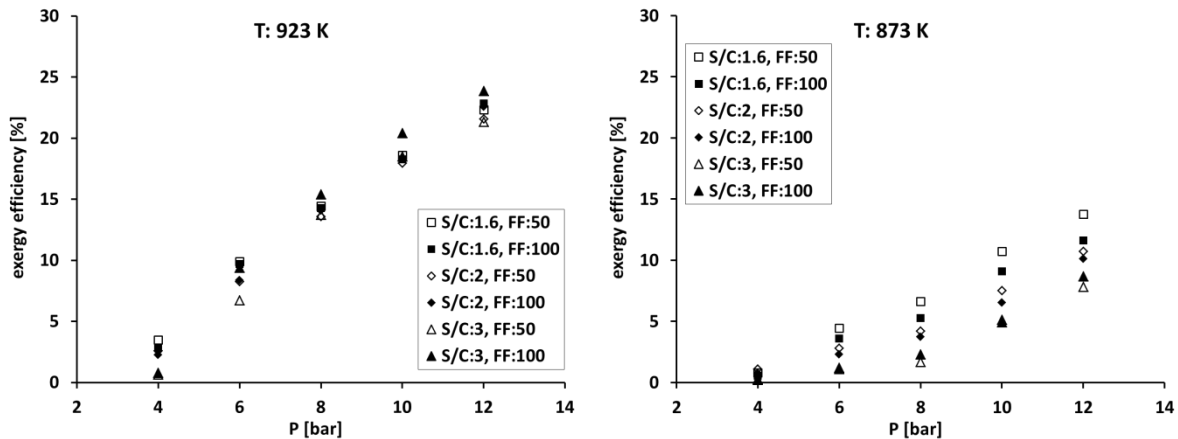
Fig. 4.4 Effect of pressure on exergy efficiency at 873 and 923 K

Following the pure hydrogen permeation rate (Fig. 3.14), the highest exergy efficiency is reached at the highest pressure, which is in agreement with hydrogen production and hydrogen yield. At 873 K the system is not efficient, even at high pressure. This is ascribed to the important role of methane steam reforming (MSR) reaction, which in one hand produces the highest number of moles of hydrogen, and on the other hand is counted as destructed exergy in the retentate stream. This clearly demonstrates the importance of high temperature and pressure to reform methane and run the system efficiently. At high

temperature and pressure, methane is reformed and at the same time, the higher hydrogen permeation rate results in higher conversion of methane (the shift effect). The effect of the fuel flow rate on the exergy efficiency is not noticeable.

The steam to carbon ratio (S/C) shows different effects on the exergy efficiency at FF=100 μl/min. A presented in Fig. 4.5, the exergy efficiency increases slightly with S/C ratio at 923 K while an opposite effect is seen at 873 K.
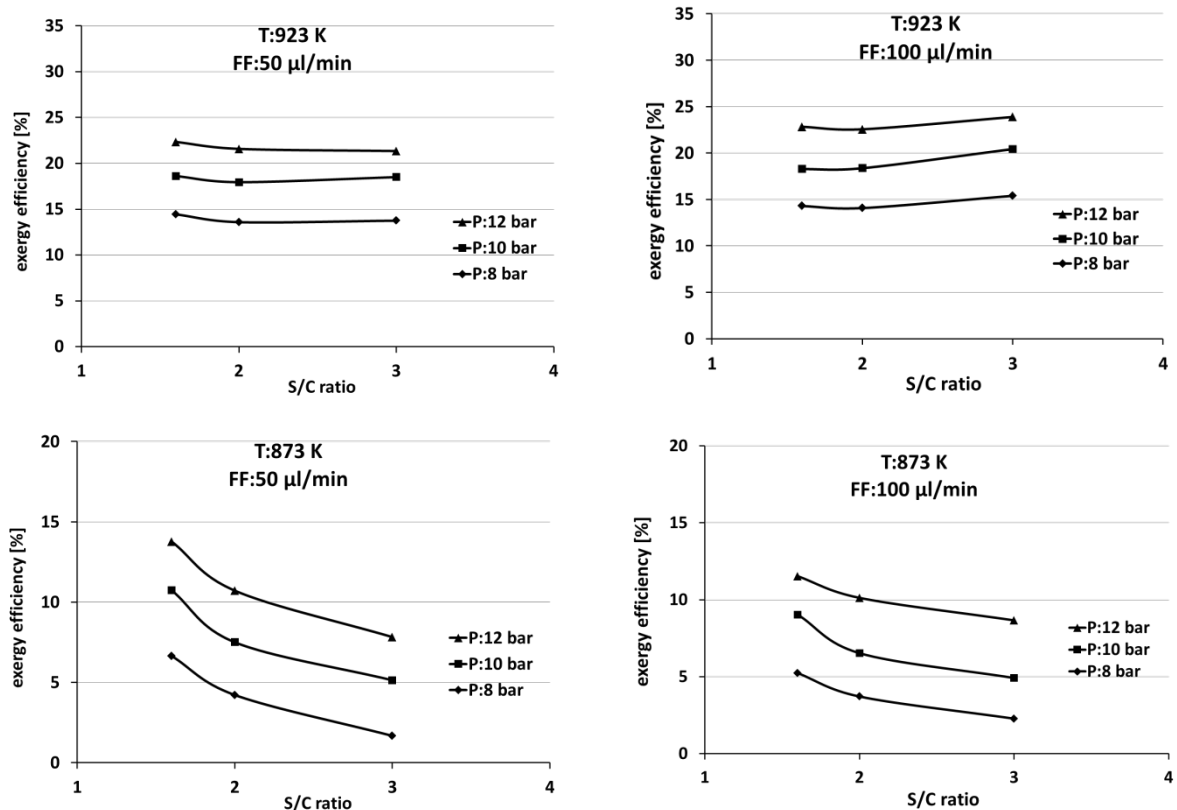
Fig. 4.5 Effect of S/C ratio on exergy efficiency

The exergy efficiency increases slightly with the S/C ratio at 923 K, while an opposite effect is seen at 873 K. This is explained considering the molar production rate of pure hydrogen per mol ethanol in the feed. At complete conversion of ethanol, the extent of the methane steam reforming reaction determines the hydrogen production rate and therefore the value and the trend of exergy efficiency as a function of the S/C ratio. At 923 K, the MSR reaction is promoted and more hydrogen is produced, more of water is available (higher S/C). At 873 K, the dilution effect of excess water is dominant, so that the exergy efficiency declines with S/C ratio.

Comparatively lower values of the exergy efficiency are obtained in this work compared to the ones reported in the literature [185,186,190] because only the exergy content of the pure

hydrogen stream (not the total hydrogen produced) is considered as the evaluation base, i.e. the product of the reformer.

Thermal efficiency of the reformer is presented in Fig. 4.6.
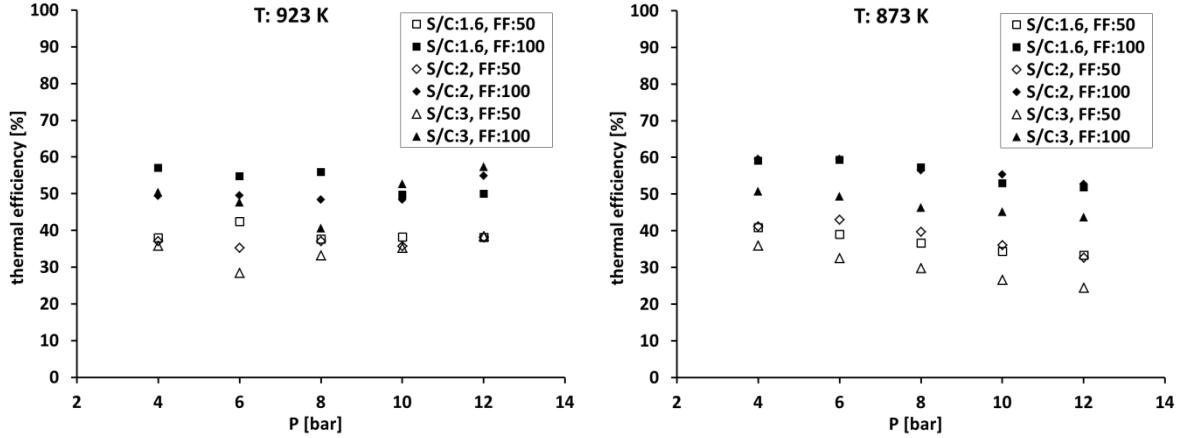
Fig. 4.6 Thermal efficiency of the CMR

Thermal efficiency of the CMR stays in the range of 30-60 %, whatever the temperature. The effect of S/C is not notable, instead, only the fuel flow rate shows a noticeable effect on the thermal efficiency. In this case, thermal efficiency increases with the fuel flow rate. Based on the definition of the thermal efficiency (eq. 4.1), it is understood that higher thermal efficiency is reached as more methane is present in the retentate gas stream. It is worthy to mention that in this case, at high pressure where more methane is converted to hydrogen, the thermal efficiency declines since the lower heating value (LHV) of hydrogen (244 kJ/mol) is lower than methane (802 kJ/mol). At high pressure, more hydrogen and less methane are produced. This effect is clearer at 873 K where the effect of pressure is significant in MSR promotion as discussed before.

The results of the thermal efficiency are contrary to the ones of the exergy efficiency, where higher exergy efficiency was obtained at higher pressure. If only pure hydrogen is considered as the product of the reformer in the definition of the thermal efficiency, the effect of the pressure can be explained better [194,195]. In this case, eq. 4.1 is written as:

$$\eta_{Thermal}^{H2} = \frac{\dot{m}_{pure\ hydrogen} \times LHV_{hydrogen}}{\dot{m}_{EtOH} \times LHV_{EtOH} + \dot{w}_{pump} + \dot{Q}}$$

4.14

Where $\eta_{Thermal}^{H2}$ represents the thermal efficiency if only pure hydrogen is considered as the product of the reformer. This thermal efficiency versus the pure hydrogen production rate is illustrated in Fig. 4.7.
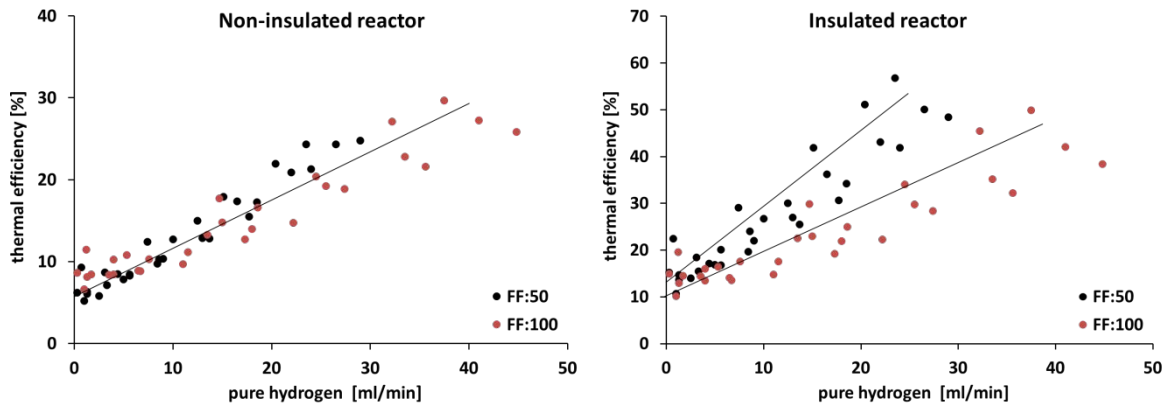
Fig. 4.7 Thermal efficiency (only pure hydrogen) versus pure hydrogen permeation rate

A comparison between Fig. 4.7 and Fig. 4.3 reveals that with a new consideration in the formulation of the thermal efficiency, the effect of pressure, which means the dependency of the thermal efficiency on the pure hydrogen production rate, can be explained. However, the effect of fuel flow rate cannot be described even by a more precise definition of the thermal efficiency. As presented in Fig. 4.8, when new definition of the thermal efficiency is considered, the thermal efficiency is lower compared to Fig. 4.6.
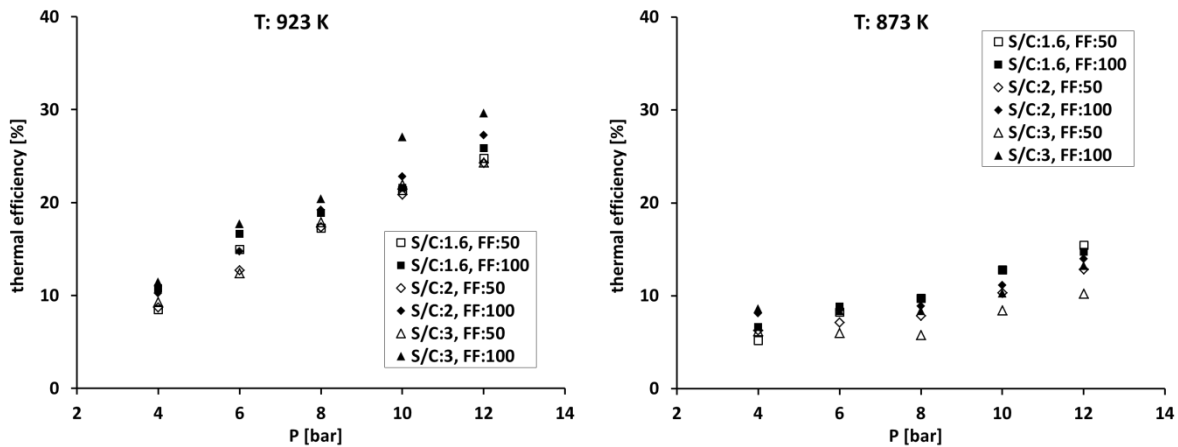
Fig. 4.8 Thermal efficiency of the CMR when only pure hydrogen is considered

As seen, the new definition of the thermal efficiency turns it to a function of pressure similar to what had been seen before in the case of the exergy efficiency. Still, considering only the pure hydrogen stream as the product of the CMR is not a relevant and complete definition, as the retentate stream, which contains mostly unconverted methane and unpermeated hydrogen, is not taken into account. The only possibility to correctly consider only pure hydrogen is the retentate gas recovery option, which is discussed in detail in the following section.

- **Efficiency improvement**

Analysis of the exergy content of each inlet/outlet stream leads to obtain a better understanding of the performance of the system and the feasibility to recover or decrease the exhaust or destructed exergy. Heat loss constitutes a big share of exergy destruction, accounting for 50% of the outlet exergy flow on average at FF=50 µl/min. Another notable source of exergy loss is the retentate gas, which contains CH_4, CO, and not permeated H_2 especially at lower pressures. The comparison between the inlet and outlet exergy flows and the share of each component in the related stream calculated at 923 K and 12 bar (where the system best performance is achieved) under different fuel flow rates and S/C ratios is given in Fig. 4.9.
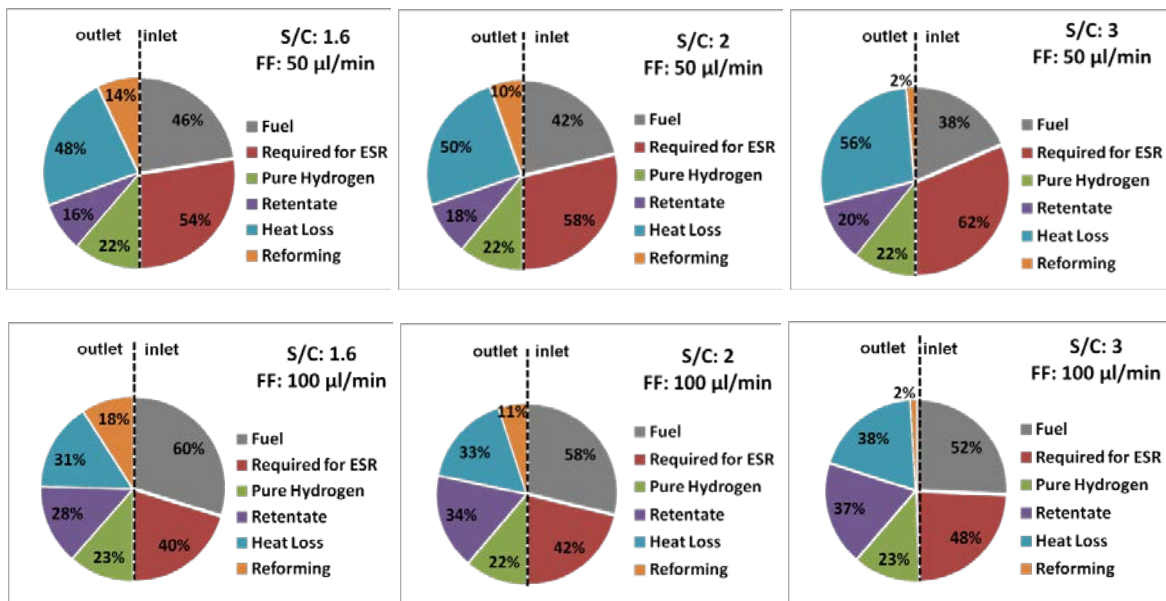
Fig. 4.9 Exergy flows and the share of the different components in the inlet and outlet streams at 923 K and 12 bar

The inlet stream consists of the exergy of the fuel and the required exergy for the CMR, which is the same as $\dot{W}_{el}$ in eq. 4.4 (see also Fig. 4.2). At the outlet, the exergy of retentate (non-condensable products), pure hydrogen, and heat losses, are presented. Exergy of reforming represents the exergy destruction due to the irreversible chemical reforming reactions (the exergy of the condensing water is negligible). Exergy required for ESR means the exergy rate needed for fuel evaporation and heating up to reaction temperature plus the required exergy for the chemical reactions. The exergy content of the retentate stream originates mainly from the presence of unconverted CH_4 and not permeated H_2. As shown, heat loss and retentate gas are the major sources of exergy loss. Therefore, the exergy efficiency of the reforming system can be improved by insulation of the reactor and recovery of the retentate gas exergy. The exergy losses due to the reforming reactions are inevitable. The sum of the exergy rates of the heat loss and the retentate gas stream

increases with S/C ratio, which shows the essential role of the reactor insulation and exergy recovery of the retentate gas at higher S/C ratio for process optimization.

- **Retentate gas recovery**

The exergy rate of the retentate stream declines with pressure since more methane and carbon monoxide are converted via the steam reforming reactions (MSR and WGS reactions, respectively), leading to more hydrogen production. The ratio of the retentate and pure hydrogen exergy rates over the inlet exergy rate is given in Fig. 4.10.
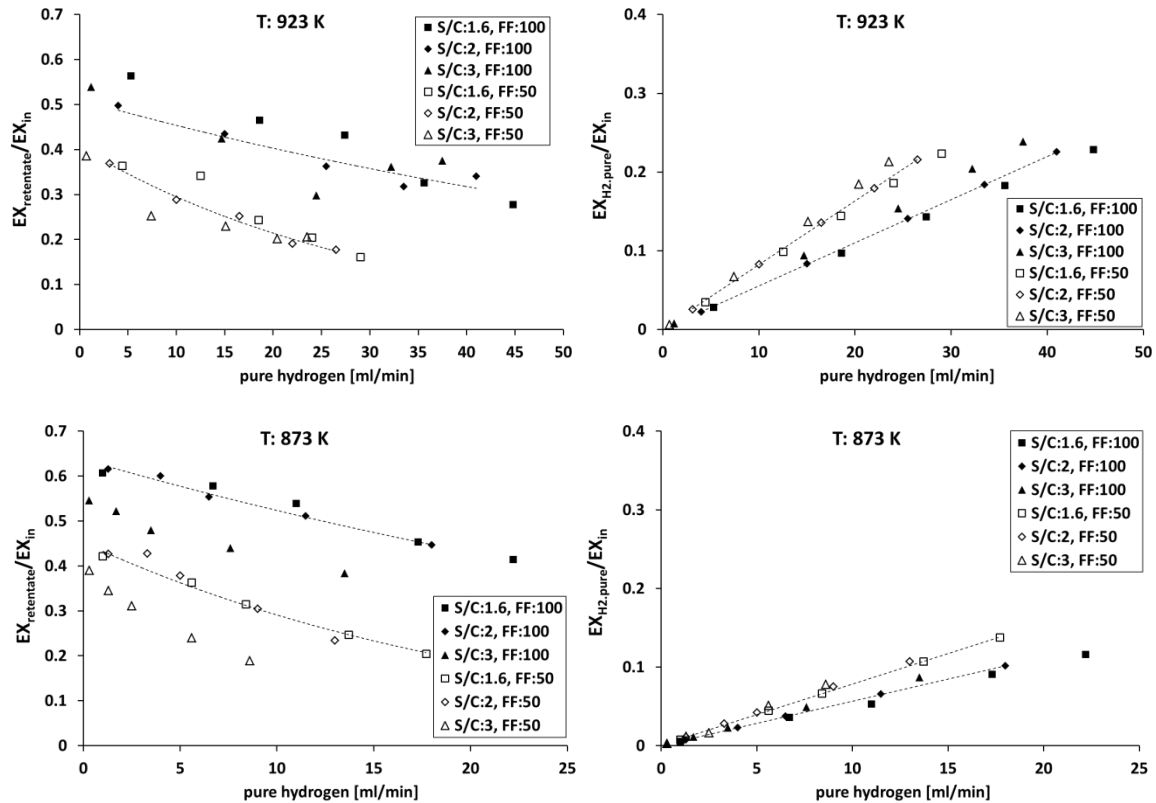
Fig. 4.10 $EX_{retentate}/EX_{in}$ and $EX_{H2.pure}/EX_{in}$ vs the pure hydrogen production rate

As presented, the retentate stream contains a notable fraction of the inlet exergy rate. At high production rate of hydrogen, the recovery of the retentate gas exergy can result in higher exergy efficiency.

The combustion of the retentate gas is a clear source of energy to provide the required heat for the ESR reactor, which accounts for evaporation and heating up the reactants, the ESR reaction, and heat losses. In Fig. 4.11, the ratios of the exergy rate of the retentate gas ($EX_{retentate}$) and the required exergy rate for the ESR reactor over the inlet exergy rate (EX_{in}) at 923 K are shown.
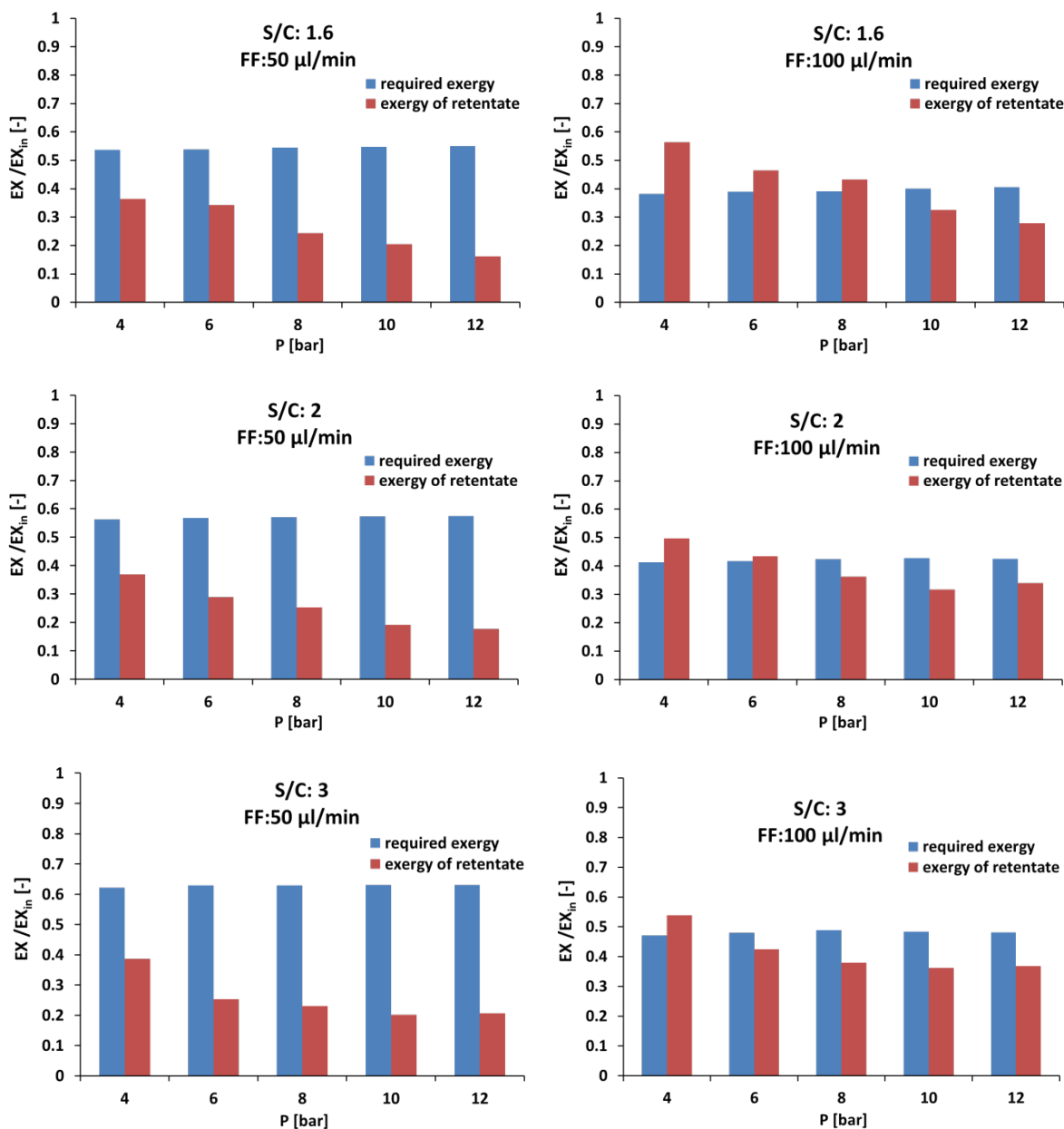
Fig. 4.11 Exergy rate of the retentate gas and required exergy rate over the exergy rate of the inlet vs. pressure at T = 923 K

The exergy rate of the retentate gas is high enough to provide the reactor with a notable fraction (at FF=50 μl/min) or almost all (at FF=100 μl/min) of its required exergy at steady state conditions. The exergy rate of the retentate gas is significantly higher at FF=100 μl/min due to the high molar production rate of methane. Higher hydrogen yield and molar production rate of hydrogen per mol ethanol in the feed are reached (see Fig. 3.11 and Fig. 3.12) at 923 K and FF=50 μl/min due to higher methane conversion.

At 873 K and FF=100 μl/min, the exergy rate of the retentate gas is enough to cover the whole exergy demand of the CMR almost at all operating conditions. As presented in

Fig. 4.12, the exergy rate of the retentate gas at 873 K and FF=50 μl/min is higher than the ones at 923 K, which is attributed to the lower methane conversion and hydrogen production rate at 873 K.
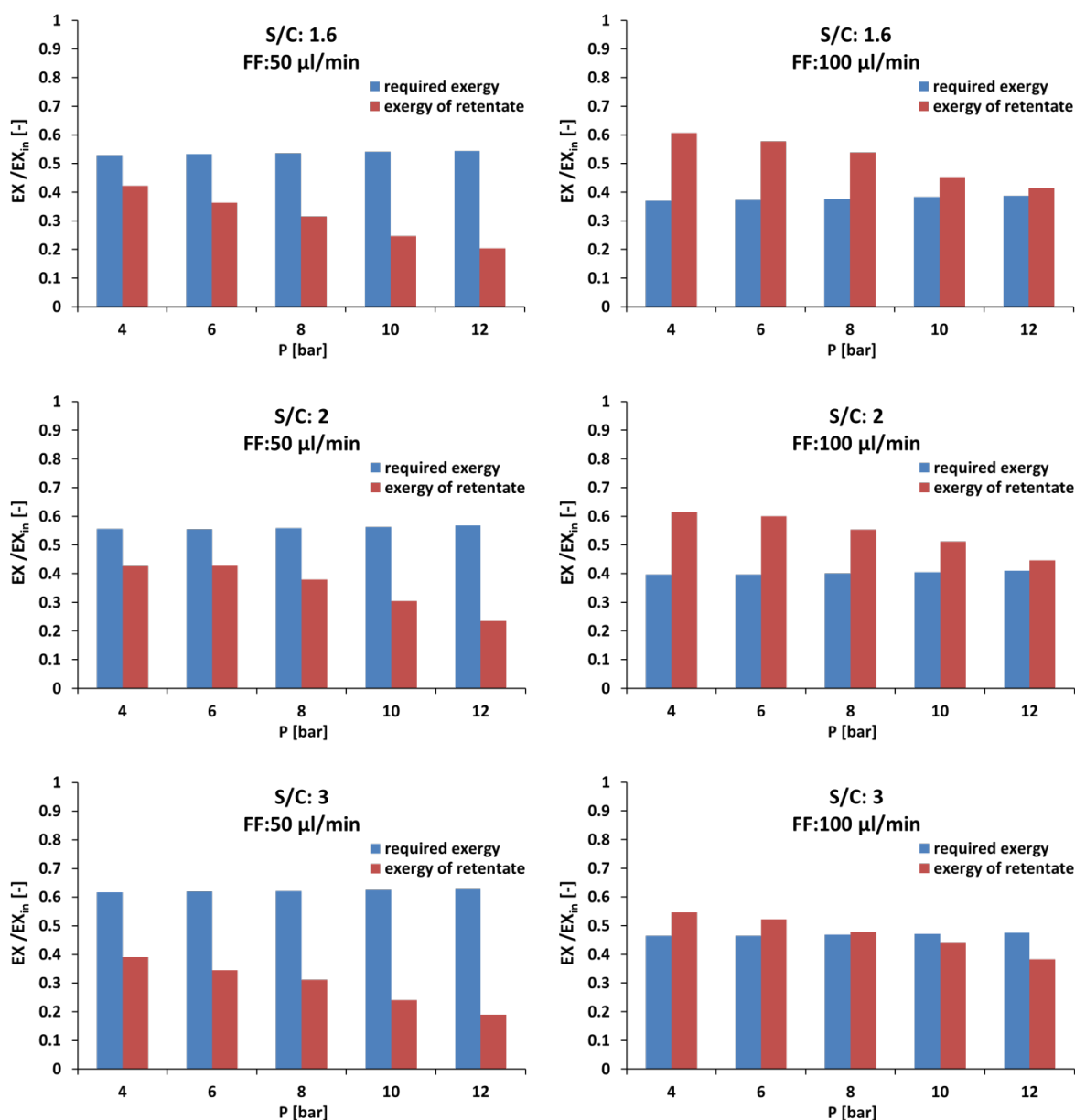
Fig. 4.12 Exergy rate of the retentate gas and required exergy rate over the exergy rate of the inlet vs. pressure at T = 873 K

As discussed in the previous chapter, the flow rate of the retentate stream decreases with pressure so that at 12 bar, the lowest flow rate of retentate is obtained, which directly corresponds to the lowest molar flow rate of unconverted methane and the highest molar flow rate of hydrogen. Therefore, the lowest exergy rate of the retentate is at 12 bar (Fig. 4.11 and Fig. 4.12). At lower pressure, the increase in the exergy efficiency (absolute

value) is higher due to the higher exergy rate of the retentate stream. The scheme of the reforming system in the case of the retentate gas exergy recovery is shown in Fig. 4.13.
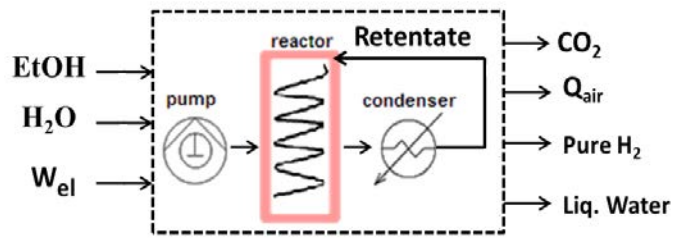
Fig. 4.13 Scheme of the reformer system

The values of exergy efficiency in the case of utilization of the retentate gas at 923 K is presented in Fig. 4.14.
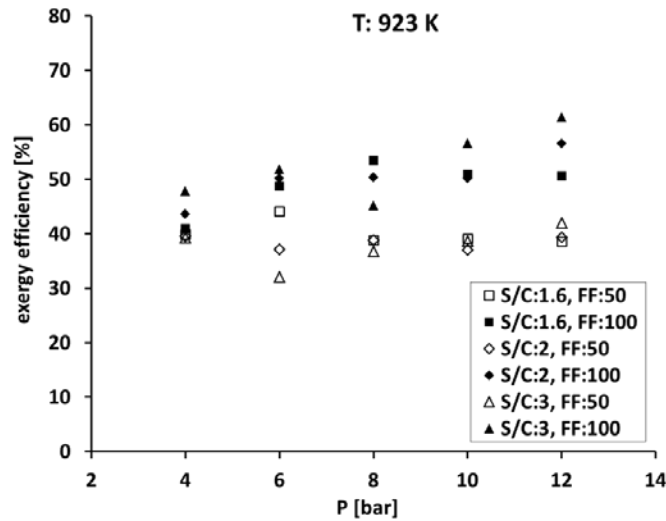
Fig. 4.14 Comparison of exergy efficiency in case of retentate gas utilization at 923 K

At 923 K and FF=50 μl/min, the exergy rate of the retentate gas is lower than the required rate of exergy (Fig. 4.11). Therefore, the exergy of the retentate gas can be recovered to compensate partially for the required exergy rate and the heat losses. At 873 K and FF=100 μl/min (except at S/C=3 and P=12), the exergy rate of the retentate stream is higher than the required exergy rate (Fig. 4.12) due to the high production rate of methane. Hence, the exergy rate of the retentate stream is partially recovered, and the rest is lost (exergy loss). The comparison between the values of exergy efficiency in the case of utilization of the retentate gas at 873 K is presented in Fig. 4.15.
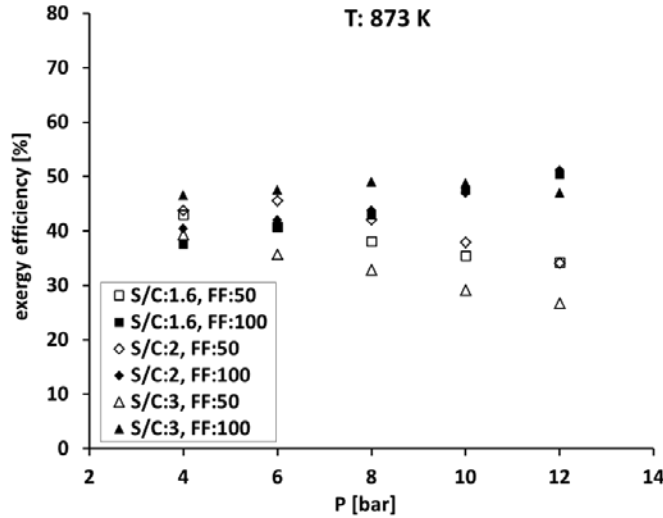
Fig. 4.15 Comparison of exergy efficiency in case of retentate gas utilization at 873 K

Exergy efficiency is not a function of pressure when the exergy of the retentate gas stream is recovered. This is attributed to the combination effect of many factors such as the exergy rates of pure hydrogen and the retentate stream, and the required exergy rate at each operating conditions. The higher the pressure, the higher the exergy rate of the pure hydrogen stream (higher hydrogen permeation rate) and the lower the exergy rate of the retentate stream (lower molar flow rate of methane, carbon monoxide, and unpermeated hydrogen). Besides, the required exergy rate for the ESR reaction increases with pressure.

Thermal efficiency in the case of retentate gas recovery is presented in Fig. 4.16. In this case, the energy flux of the retentate stream can compensate partially for the energy requirements of the CMR (ESR reaction and heat loss).
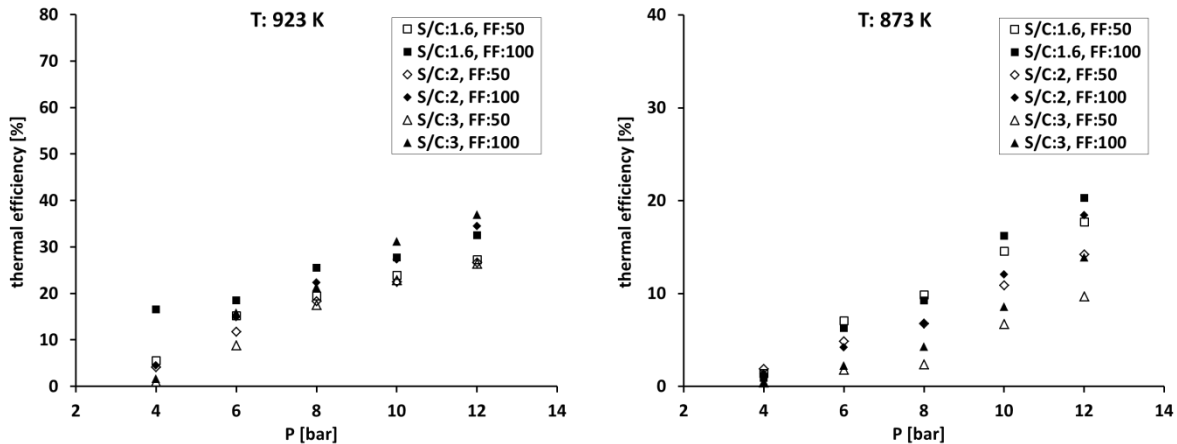
Fig. 4.16 Thermal efficiency of the CMR in the case of retentate gas recovery (only pure hydrogen is the product of the reformer)

Compared to Fig. 4.8, a higher thermal efficiency is obtained. Consideration of pure hydrogen as the product of the CMR is relevant in the case of retentate gas recovery since it is assumed that the retentate gas is fully converted to CO_2 and H_2O during the combustion to provide the CMR partially with its energy requirements. The increasing rate of the thermal efficiency with pressure is due to the higher hydrogen production at higher pressure.

- **Insulation of the CMR**

In the case of an insulated reactor, the exergy efficiency is remarkably improved. The scheme of the insulated reactor where the heat losses are minimized is shown in Fig. 4.17.
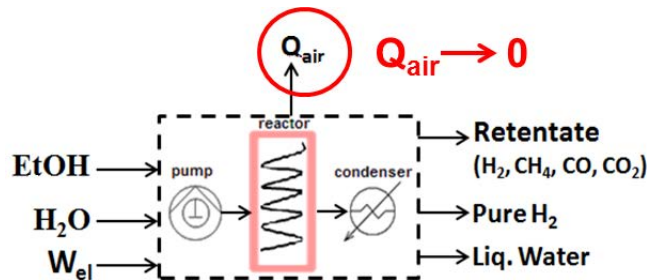
Fig. 4.17 Scheme of an insulated reactor

If the reactor is insulated, the energy demand of the reformer is limited to the heat needed to run the CMR at a given temperature. This heat is used for fuel evaporation and heating up to reaction temperature, and the ESR reaction. The exergy efficiency of the insulated reactor is presented in Fig. 4.18.
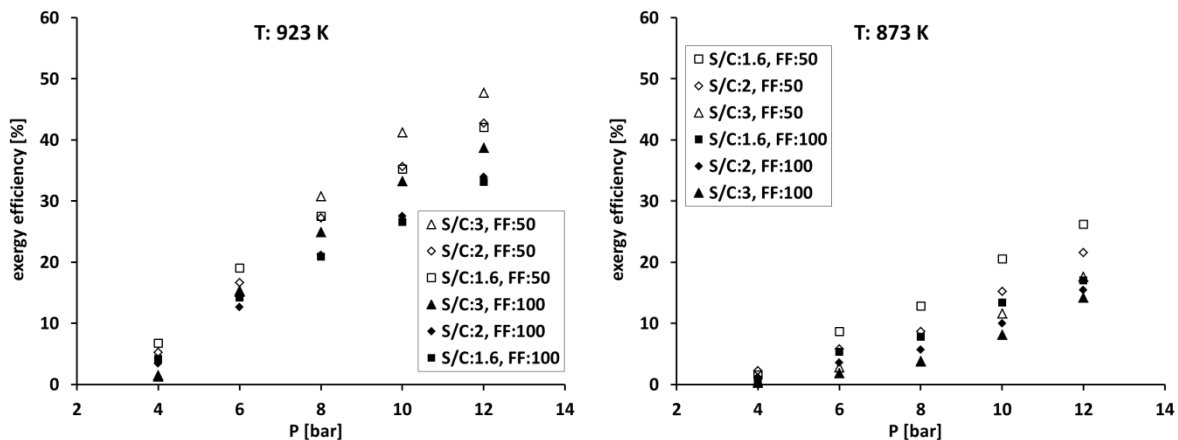
Fig. 4.18 Exergy efficiency of the insulated reactor

At pressures higher than 8 bar, and especially at 923 K the exergy efficiency is highly improved. In the case of the insulated reactor, the effect of the fuel flow rate is more obvious (see Fig. 4.4), which is attributed to the dominant effect of heat losses when the

96

reactor is not insulated. Exergy efficiency is higher at FF=50 μl/min because the pure hydrogen production rate does not double when the fuel flow rate (molar flow rate of ethanol) does (FF=100 μl/min). The dependency of exergy efficiency on S/C ratio is clearer in an insulated reactor due to the dominant value of ethanol exergy in the inlet stream. The concentration of ethanol in the feed is lower at higher S/C ratio.

Following the trend of exergy efficiency, unused exergy is an obvious function of temperature and pressure when an insulated reactor is considered. The reason lies in the rate of pure hydrogen production and the presence of methane as the major component of the retentate. Methane production per mole of inlet ethanol decreases by 50% as pressure increases from 4 bar to 12 bar at S/C = 1.6 (see Fig. 3.11). At higher pressure, as less methane appears in the retentate stream, the exergy content of retentate is greatly decreased. The rate of unused exergy over the rate of inlet exergy (EX_{in}) at different operating conditions is given in Fig. 4.19.
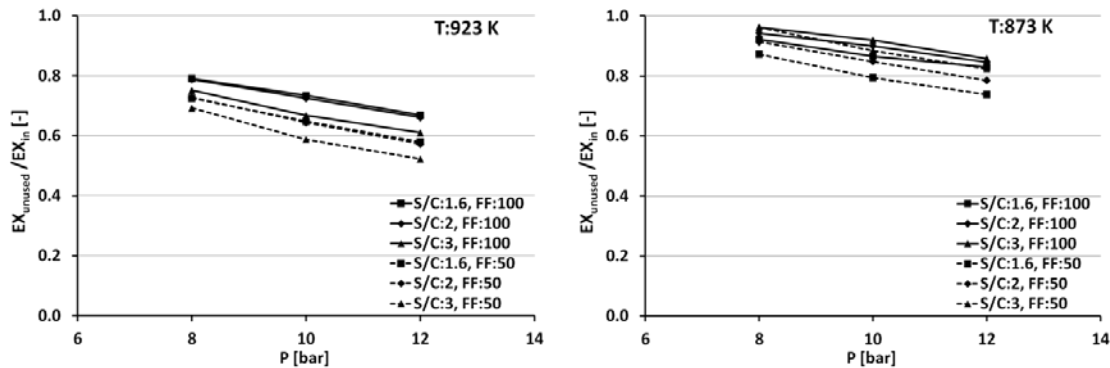
Fig. 4.19 Unused exergy rate over inlet exergy rate for the insulated reactor

At P < 8 bar, hydrogen permeation rate is very low, resulting in huge amounts of reformed gases leaving the reactor as retentate stream. Hence, a huge share of inlet exergy is lost in the form of unused exergy.

As shown in Fig. 4.20, thermal efficiency of the reformer in the case of insulation of the reactor is placed between 70-95%.
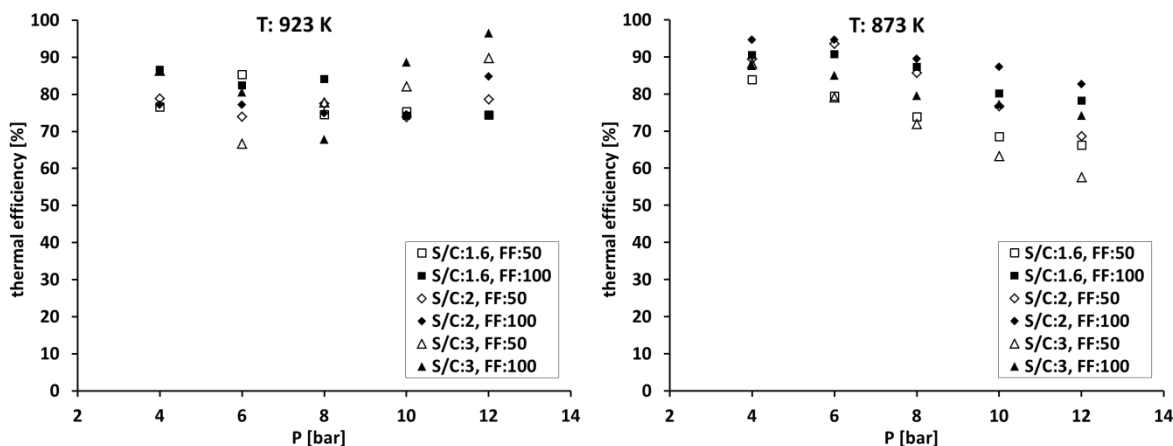
Fig. 4.20 Thermal efficiency of the reformer in the case of an insulated reactor

Compared to Fig. 4.6, the effect of S/C ratio on the thermal efficiency is stronger at 923 K, which is attributed again to the dominant value of the LHV of the ethanol in the feed. The molar flow rate of ethanol is doubled as S/C decreases from 3 to 1.6.

At 873 K, a different behavior is seen. The effect of S/C ratio is not notable at 873 K due to the effect of temperature on the MSR reaction, which is not favored at 873 K. Therefore, the presence of more methane in the reactor (at higher S/C ratio) does not promote the hydrogen production and the pure hydrogen production rate. Besides, the declining trend of the thermal efficiency over pressure at 873 K is attributed to the essential role of pressure in MSR reaction promotion and hydrogen permeation at low temperature, as discussed in the previous chapter. As more hydrogen is permeated, the methane content of the retentate gas decreases notably resulting in lower total LHV of the retentate gas stream.

Exergy efficiency discloses inevitable irreversibility even when the reactor is insulated, while according to the thermal efficiency, the CMR reaches its best operating conditions at 923 K and high pressure. According to the thermal efficiency, the CMR reaches an ideal performance and the values of 80-100%, while the exergy analysis shows that exergy efficiency of the system cannot exceed 45%. A remarkable difference between the exergy and thermal efficiency is the different interpretation of the pressure. Exergy efficiency reveals how the pressure can improve the efficiency of the reformer, while thermal efficiency is not a suitable tool to discuss on the effect of pressure by considering all the components and streams of the reformer, unless in the case of retentate recovery.

By utilization of the retentate gas in an insulated reactor, the exergy efficiency is increased drastically and is placed between 60-90 %, which is a high value, bearing in mind that permeated pure hydrogen is considered as the only product of the reforming system. This result is expected since in one hand, exergy destruction decreases and, on the other hand, the energy requirement of the system is met partially or totally by utilization of the retentate gas.

Based on the exergy evaluation, the best operating conditions are the most intense conditions, i.e. the highest pressure and temperature, and the lowest S/C ratio at which carbon deposition is probable. As presented in Fig. 4.11 and Fig. 4.12, lower fuel flow rate is more beneficial. Again it should be mentioned that if higher rate of pure hydrogen is needed (probably by a fuel cell fed online), the higher fuel flow rate is needed. However, it is obvious that the difference between exergy efficiencies at two fuel flow rates at the same pressure, temperature, and S/C ratio, is not negligible.

4.3.2 Thermodynamic analysis of the Stage Membrane Reactor (SMR)

Based on the definition of the exergy efficiency introduced in this work, the exergy efficiency of the SMR is low even at high temperature and low fuel flow rate. The exergy efficiency of the SMR as a function of pressure is shown in Fig. 4.21. The ESR experiments in the SMR were performed at S/C ratio of 1.6 [2,3].
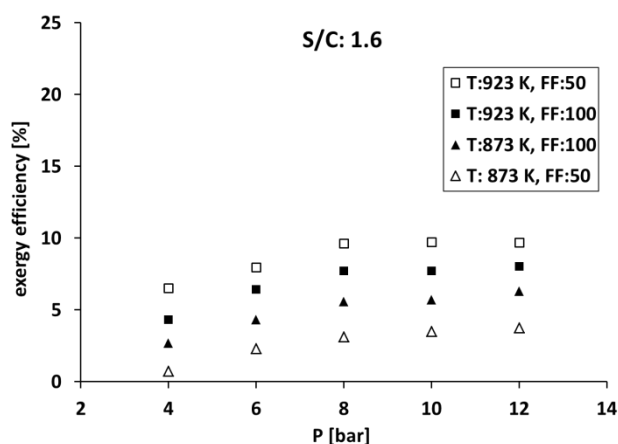
Fig. 4.21 Exergy efficiency of the SMR vs. pressure

The low values of the SMR exergy efficiency is attributed to two factors. Firstly, relatively low production rate of pure hydrogen per mole of ethanol in the feed (see Fig. 3.12). Secondly, high molar production rate of methane per mole of ethanol in the feed builds a very high rate of unused exergy. The moles of methane and pure hydrogen produced per mole of ethanol are presented in Fig. 4.22.
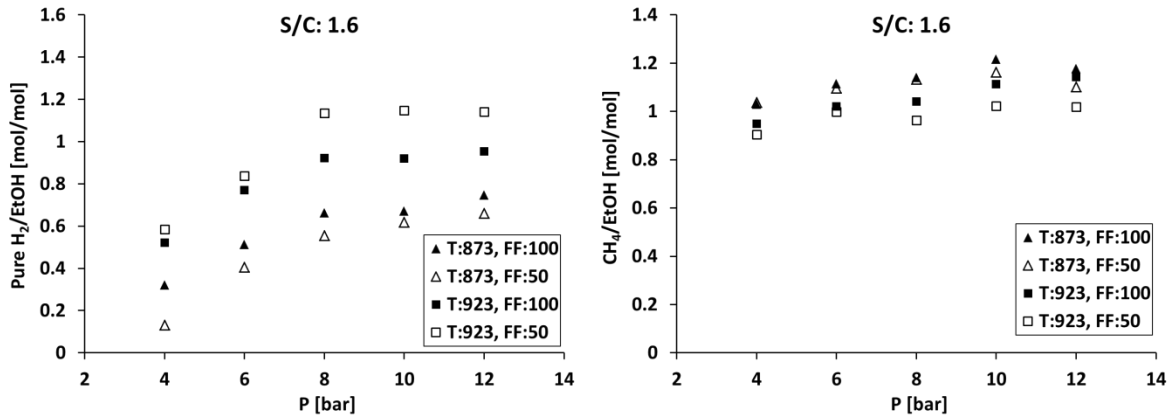
Fig. 4.22 The molar production rate of pure hydrogen and methane per mol ethanol in the feed for the SMR

As can be seen, the molar production rate of pure hydrogen does not improve with pressure at P>8 bar due to the limitations of the SMR as discussed in the previous chapter. Following the same trend as the pure hydrogen production rate, exergy efficiency of the SMR does not increase with pressure. Meanwhile, molar production rate of methane increases with pressure because of the unfavorable operating conditions at high pressure, where the MSR reaction is pushed toward the reactants side (methanation). The exergy efficiency increases slightly with temperature because of higher pure hydrogen production rate.

Thermal efficiency of the SMR is shown in Fig. 4.23.
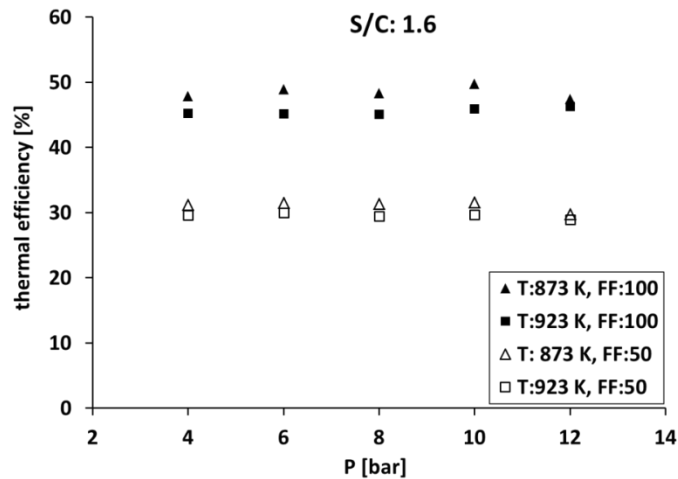
Fig. 4.23 Thermal efficiency of the SMR

The effect of operating pressure and temperature on the thermal efficiency of the SMR is not notable. Instead, the fuel flow rate is the determining factor. This is attributed to the higher production rate of hydrogen and retentate at higher fuel flow rate.

- **Efficiency improvement**

Analysis of the exergy content of the inlet and outlet streams is done similar to the case of the CMR to understand the important factors via which the efficiency of the SMR can be improved. As shown in Fig. 4.24, a large amount of exergy is lost by heat losses and the retentate gas stream.
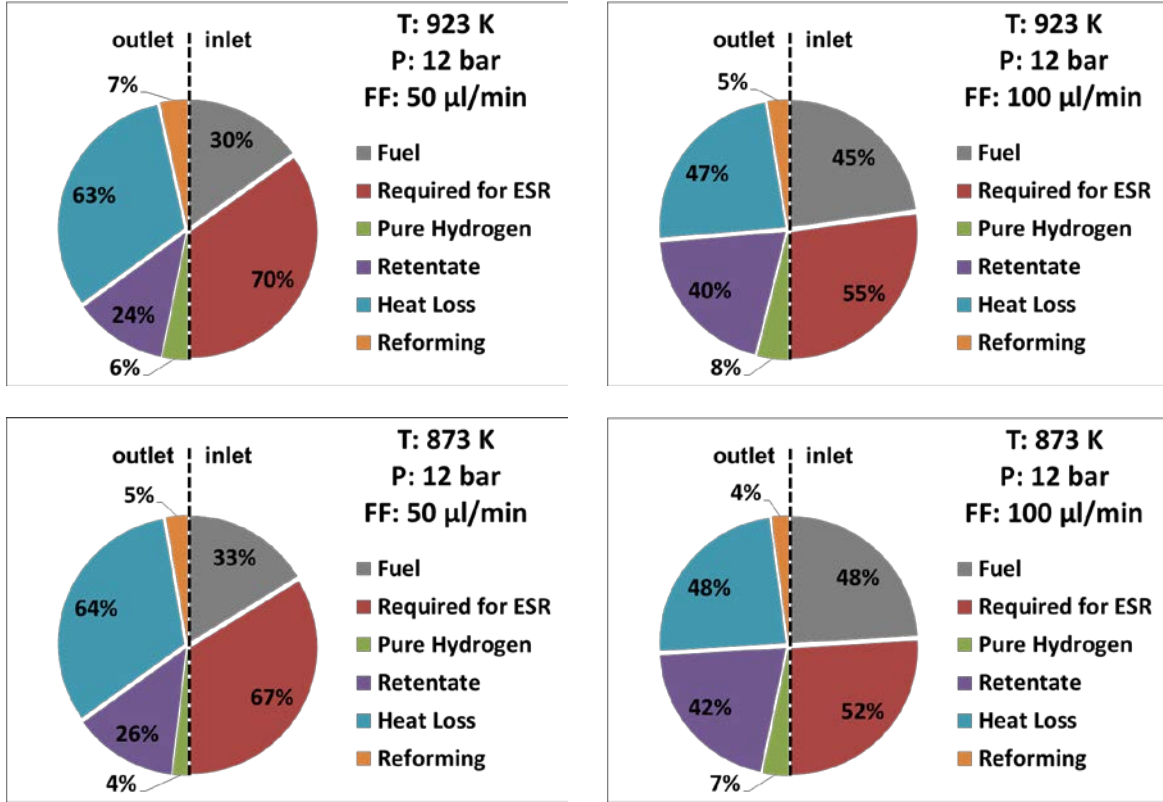
Fig. 4.24 Exergy flows and the share of the different components in the inlet and outlet streams at 12 bar

More than 80% of the outlet exergy rate belongs to the heat loss and the retentate exergy content. In the case of the SMR, the recovery of the retentate gas and the insulation of the reactor are the essential factors for optimization of the reforming system. It should be mentioned that due to the configuration of the SMR in which the catalytic zone and the permeation zone (membrane) are separated, the heat loss area is twice of the case of the CMR. Therefore, the heat loss rate is two times higher, resulting in the high rate of heat loss via the reactor vessel. The exergy rate of the retentate stream of the SMR does not change with pressure due to its configuration where the ESR reaction is not promoted by pressure. The retentate gas exergy rate over the inlet exergy rate versus pure hydrogen production rate is given in Fig. 4.25.
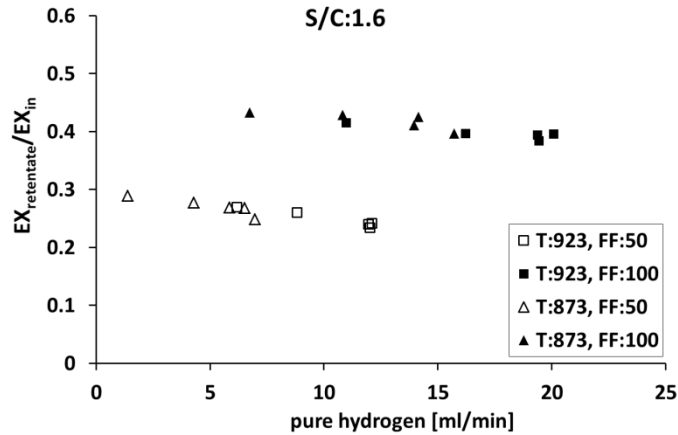
Fig. 4.25 $EX_{retentate}/EX_{in}$ vs pure hydrogen production rate

It is clear that the exergy efficiency improvement in the case of the retentate gas recovery is not a function of pressure. However, the exergy rate of the retentate can compensate for the required exergy rate of the SMR largely at FF=100 μl/min, as presented in Fig. 4.26.
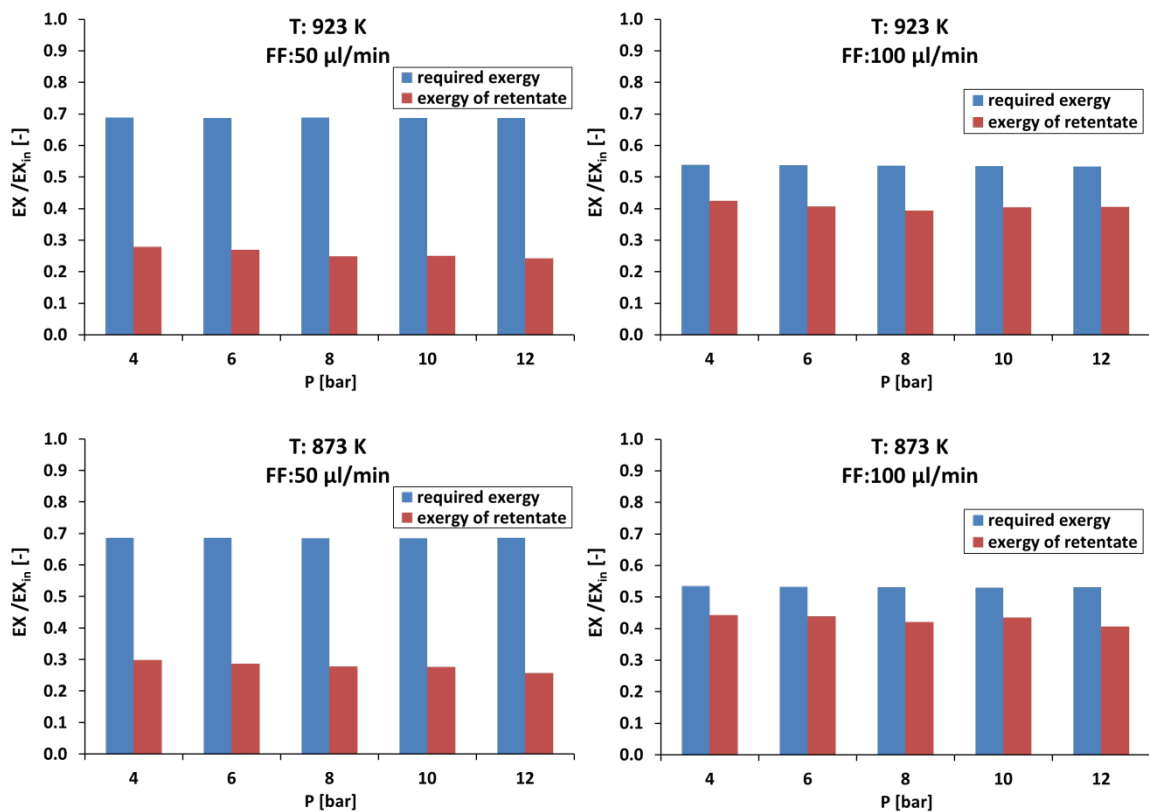
Fig. 4.26 Exergy rate of the retentate gas and required exergy rate over the exergy rate of the inlet vs. pressure

The exergy efficiency of the SMR in the case of the retentate gas recovery is presented in Fig. 4.27.
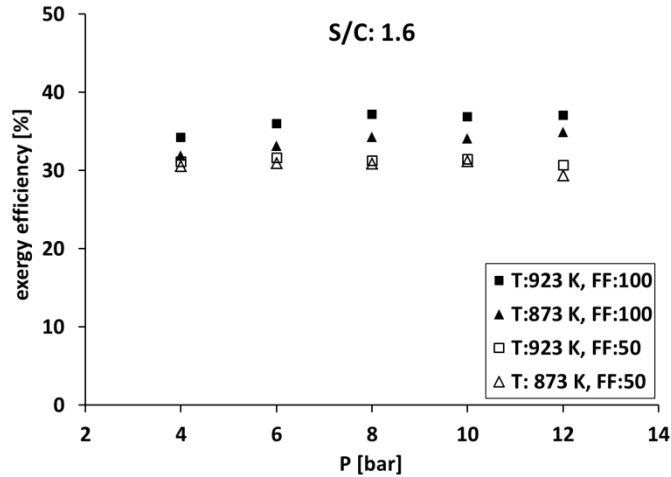
Fig. 4.27 Exergy efficiency of the SMR in the case of retentate gas recovery

Compared to the values of the exergy efficiency presented in Fig. 4.21, the retentate gas recovery notably improves the exergy efficiency of the SMR but, as expected, the exergy efficiency does not improve with pressure.

Regarding the thermal efficiency, different results are obtained. Taking into the definition of the thermal efficiency, by recovery of the retentate gas, the LHV of the products is limited to the pure hydrogen stream. Although the recovery of the retentate gas covers partially the energy demand of the SMR, the LHV of the product side is much lower when the retentate gas (which is mostly unconverted methane) is not taken into account (is recovered). The thermal efficiency of the SMR vs pressure is given in Fig. 4.28.
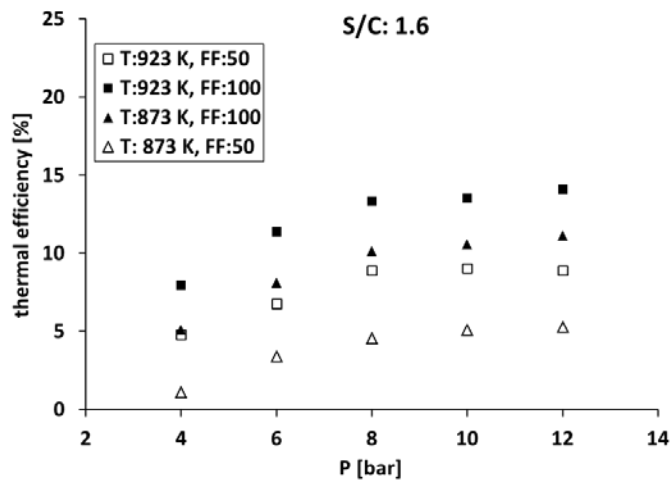
Fig. 4.28 Thermal efficiency of the SMR in the case of retentate gas recovery

As can be seen, the values of thermal efficiency are lower than the ones presented in Fig. 4.23. Besides, in the case of retentate gas recovery, thermal efficiency is a function of pressure following the same trend as pure hydrogen production (see Fig. 4.22).

As presented in Fig. 4.25, the largest share of the exergy loss belongs to the heat losses. Exergy and thermal efficiencies of the SMR are improved in the case of insulation of the reactor, as shown in Fig. 4.29. However, according to the thermal efficiency, the system functions ideally when the reactor is insulated.
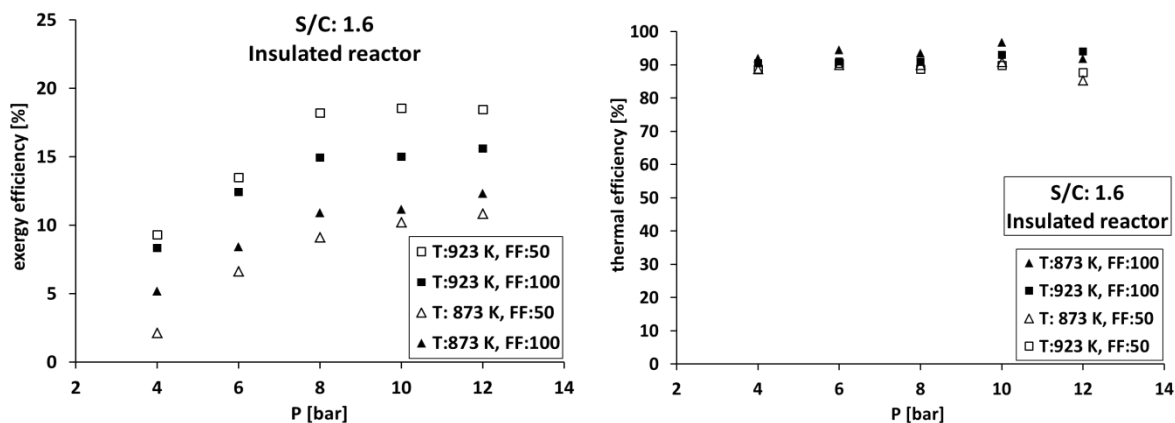
Fig. 4.29 Exergy and thermal efficiency of the SMR in the case of an insulated reactor

Exergy efficiency of the SMR is significantly improved if the reactor is insulated and the retentate gas is recovered at the same time. The SMR reaches its optimum operating conditions in this case, as exergy efficiency is placed between 60-70% at FF=100 μl/min, and 80-90% at FF=50 μl/min.

4.3.3   Comparison between the CMR and SMR configurations

The CMR configuration showed a superior performance in terms of thermodynamic analysis, which is attributed to several advantages of the CMR over the SMR. First of all, the heat loss area of the SMR is larger because of separated catalytic and permeation zones. Moreover, the hydrogen production rate and hydrogen recovery are much higher in the case of the CMR, as discussed in the previous chapter. The lower flow rate of the retentate gas and lower methane production (as a result of MSR reaction promotion) results in lower rate of unused exergy in the CMR. The rate of unused exergy over the inlet exergy rate at S/C ratio of 1.6 is given in Fig. 4.30.
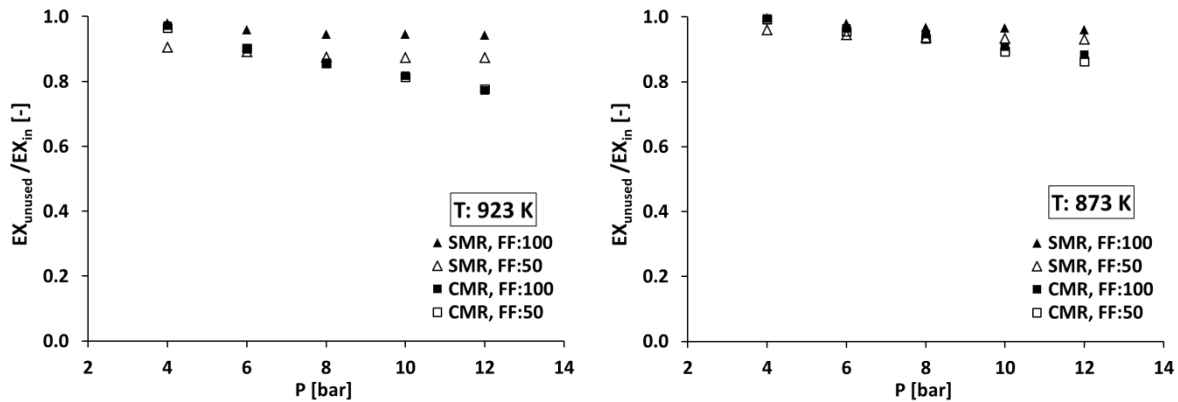
Fig. 4.30 Unused exergy rate over the inlet exergy rate at S/C=1.6

The configuration of the CMR makes it possible to produce and recover more hydrogen with pressure, while it is not possible in the SMR. The so-called pressure effect is the fundamental of the significant differences between the CMR and SMR regarding the thermodynamic analysis.

Exergy efficiency of the CMR at 923 K is higher because of higher hydrogen production rate and lower methane content in the retentate stream (considered as unused exergy). This value is comparable to the SMR where exergy efficiency reaches 10% at the highest. Besides, the effect of temperature on the exergy efficiency is not notable in the case of the SMR. Accordingly, it can be concluded that operating at lower temperature can be beneficial in the case of the SMR, while in the case of the CMR at higher temperature better exergy efficiency in reached.

Thermal efficiency of the CMR is higher than the SMR, which is attributed to the lower heat loss rate in the case of the CMR, while methane production rate is higher in the SMR. The share of heat losses and retentate gas stream in the unused exergy rate of the SMR is higher than the ones of the CMR at the same operating conditions (S/C ratio, pressure, temperature, and fuel flow rate) because of higher methane production and heat loss rates in the case of the SMR. The efficiency of the CMR is improved better by retentate gas recovery compared to the SMR, again attributed to the dominant high rate of heat losses. Regarding the thermal efficiency, the performance of the CMR is enhanced when the retentate gas is recovered.

Reactor insulation to minimize the heat losses as the largest source of the exergy loss results in higher exergy efficiency and a better improvement in the case of the CMR, while the efficiency of the SMR is not improved notably since a large share of exergy is lost as unconverted methane and unpermeated hydrogen. The rate of unused exergy over the inlet exergy for insulated CMR and SMR is presented in Fig. 4.31.
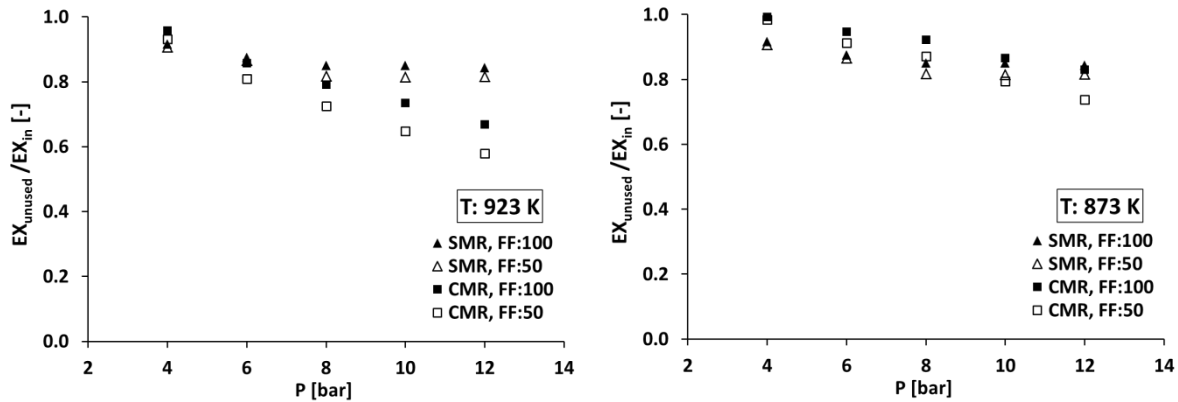
Fig. 4.31 Unused exergy rate over the inlet exergy rate for an insulated reactor at S/C=1.6

As a result of the pressure effect, at P>8 bar, the rate of unused exergy in the CMR decreases significantly with pressure, following the increasing trend of the pure hydrogen production rate. This behavior is not seen in the case of the SMR, where at higher pressure almost no change is seen in the rate of unused exergy.

In the case of reactor insulation, thermal efficiency of the SMR is drastically improved, taking into account that the largest source of exergy loss (heat loss) is blocked and large amount of methane in the retentate gas stream is considered as the product of the system. Thermal efficiency of the SMR is higher than the CMR in this case.

If the reactors are insulated and the retentate gas is recovered, the exergy and thermal efficiency of both systems are significantly improved, resulting in nearly perfect systems in terms of the thermodynamic losses minimization. The exergy efficiency of the insulated CMR and SMR in the case of retentate gas recovery is given in Fig. 4.32.
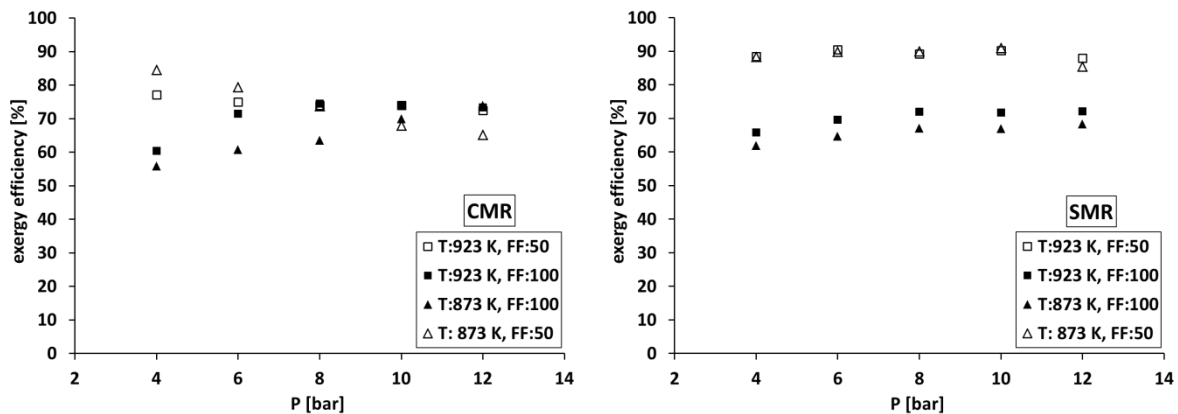
Fig. 4.32 Exergy efficiency of the insulated CMR and SMR in the case of retentate gas recovery

The presented values are the highest possible obtainable exergy efficiency of the studied CMR and SMR configurations. Pressure does not influence the exergy efficiency of the

SMR, but in the case of the CMR, two different behavior is seen. At FF=50, the exergy efficiency declines with pressure, which can be a result of higher exergy rate required for the ESR reaction at recovery of the retentate gas when the reactor in insulated. However, at FF=100, the hydrogen production rate is high enough to improve the exergy efficiency. It is seen that, generally, exergy efficiency of the SMR is higher than CMR, but it must be taken into acount that the exergy efficiency is taken into account together with the rate of pure hydrogen production, methane conversion, and hydrogen yield and recovery. Accordingly, at high pressure, the performance of the CMR is advantageous in terms of pure hydrogen production, low unused exergy rate, and high exergy efficiency.

4.4 Conclusion

Exergy analysis of the CMR and SMR configuration was performed in terms of exergy and thermal efficiency based on the experimental results at various operating conditions. It was concluded that exergy analysis is a relevant criteria for evaluating the reforming system. The advantages of exergy evaluation over thermal efficiency study was stated according to the explanation of the effects of operating conditions on both pure hydrogen production rate, and total efficiency of the CMR.

An exergy analysis was performed based on the experimental results aiming not only to evaluate the performance of the CMR system, but also to introduce the application of the exergy analysis in CMRs studies. Exergy analysis provided important information on the effect of operating conditions and thermodynamic losses, resulted in understanding of the best operating conditions. Both insulated and non-insulated reactor systems were evaluated in terms of exergy destruction, exergy efficiency, and thermal efficiency.

The effects of pressure and temperature were dominant and the study showed that the system reached around 50% exergy efficiency at 923 K and 12 bar in an insulated reactor. Unused exergy decreased with pressure since the MSR reaction is promoted at high pressures in CMR as more hydrogen is permeated due to the availability of the catalyst around the membrane and the shift effect. The exergy content of the retentate gas could compensate the energy requirements of the reactor to improve the exergy efficiency significantly. The highest exergy destruction occurred via heat losses and the retentate stream. In the case of recovery of the retentate gas and insulation of the reactor, exergy efficiency of the CMR placed between 60-90%. It was concluded that operating at the highest pressure, the lowest S/C ratio and at 923 K gives the best exergy efficiency for the CMR. Although operating at higher fuel flow rate is more beneficial regarding the production rate of pure hydrogen, the exergy efficiency is slightly lower.

The thermal efficiency of the CMR was also evaluated based on the LHV of ethanol and the products and was compared to the exergy efficiency. While thermal efficiency offered

an ideal performance at high pressure and temperature, exergy efficiency disclosed inevitable irreversibilities even in the case of an insulated reactor.

The thermodynamic analysis of the SMR showed different results so that the exergy and thermal efficiency were lower compared to the CMR. This was attributed to lower hydrogen production, more methane flow rate in the retentate stream (lower methane conversion in the case of the SMR), and very large heat loss area (high heat loss rate) of the SMR. The exergy rate of the retentate stream in the case of the SMR was higher than the CMR due to the low methane conversion in the SMR.

At least 80% of the inlet exergy was lost by heat losses and the retentate stream in the SMR. The insulation of the SMR resulted in a significant increase in the thermal efficiency, but not exergy efficiency because of low methane conversion and hydrogen recovery (high rate of unused exergy).

Superior performance of the CMR was proved thermodynamically. Taking into account the pure hydrogen production rate and exergy efficiency at the same time, the CMR showed an overall enhanced performance. In the case of the recovery of the retentate gas in an insulated reactor, the exergy efficiency of the SMR was slightly higher than the CMR, however, much higher hydrogen yield and recovery was reached in the case of the CMR.

As the area of the membrane science and pure hydrogen production in membrane reactors is growing, exergy evaluation of the CMR systems – as the first essential step for system analysis via exergo-economical optimization – can open a new chapter in this science to approach larger scale applications.

The next chapter is devoted to the modeling and dynamic simulation of the reforming system specially at transient state where the operating pressure or fuel flow rate is adjusted. The dynamic simulation can be considered as modeling the response of the reforming system to a fuel cell – when fed online – in terms of pure hydrogen production rate modification.

Chapter 5

Modeling and dynamic simulation of the reforming system

Abstract

In chapters 3 and 4, the results of the experimental and thermodynamic analysis of the reformer were discussed. In this chapter, the simulation of the dynamics of hydrogen production (permeation) is presented as the last step to study the applicability of such a system in connection with a real end user, which can be a fuel cell. The simulation presented in this chapter is similar to the hydrogen flow rate adjustments needed to set the electrical load of a fuel cell, when fed online by the reformer. Ethanol steam reforming experiments were performed at 923 K, 6-10 bar, and fuel flow rates of 50 to 200 µl/min using a mixture of ethanol and distilled water with steam to carbon ratio of 3. Dynamic experiments were carried out to observe the behavior of the CMR in terms of the pure hydrogen production rate in the case of operating pressure or fuel flow rate adjustments. A static model for the catalytic zone was derived from the Arrhenius law as a function of operating conditions to simulate the total molar production rates of ESR products. The pure hydrogen production rate at steady state conditions was simulated by means of two static models named as model 1 and model 2. Model 1 represented the simulation based on the Sieverts' law, which is known as the physical definition of hydrogen permeation through the membrane via which the robustness of the simulation was proved. Model 2 represented a black box model as a function of total hydrogen production via ESR, and the reactor pressure. Finally, a dynamic model was proposed under the ideal gas law assumptions to simulate the dynamics of pure hydrogen production rate in transient state at isothermal conditions. Both pressure and fuel flow rate change steps simulations fitted the experimental values very well. However, the simulation of the dynamics of the fuel flow rate change was more essential, as the system responds much faster to such an adjustment. The dynamic simulation proved a successful essential step needed to simulate an "Ethanol to Electricity" system.

5.1 Dynamic simulation of the CMRs

A large piece of work on ESR in CMRs using different catalysts and reactor configurations can be found in the literature [196]. Generally, ESR in membrane reactors has been simulated based on the experimental results, aiming to mathematical modeling and kinetic studies. The reported models have been derived from conventional power-law, at different operating conditions (temperature, pressure, and S/C ratio) mainly to model the reaction rates, ethanol conversion, and the selectivity of reforming products [90,133,143,197–200].

Some modeling studies followed by experimental validations have been devoted to the design and optimization of the water gas shift (WGS) reaction in CMRs containing Pd composite membranes (mostly Pd-Ag). These studies aimed to produce pure hydrogen and monitoring the effect of temperature, catalyst loading, steam to carbon ratio S/C, and permeate side pressure on the performance of the CMRs [201–203]. Dong et al. [204] studied hydrogen production via WGSR in a membrane reactor with a tubular ZSM-5/silicalite bilayer membrane. They optimized the process by means of modeling so that they could reach high CO conversion (>95%) and H_2 recovery (>90%) for WGS in the zeolite membrane reactor. A three-dimensional numerical model was developed by Chein et al. [205] to simulate hydrogen production from coal-derived syngas via the WGS reaction in membrane reactors at 1173 K. High temperature was chosen to simulate the typical temperature of the syngas at the exit of a gasifier. The negative effect of CO_2 content on the hydrogen permeation rate was observed. In addition to WGS reaction, methane steam reforming (MSR) reaction have been investigated by performing experiments and development of models [173,206,207]. In this regard, the adverse effects of the presence of different species such as CH_4, CO, and H_2O on the permeation rate of membrane have been studied. WGS reaction and MSR are the two determining reactions when ESR is performed over Pd-Rh/CeO_2 catalyst used also in the present work.

If a fuel cell is fed online by a pure hydrogen generating system (reformer), the dynamics of the pure hydrogen supply must be fitted to the load variations (dynamic behavior) of the fuel cell. Considering the dynamic energy demand of an end user – for example a building – a reformer must be able to realize and track the dynamic electrical output of the fuel cell in charge of electricity supply of the end user. Adjustment of the flow rate of pure hydrogen provided by a reformer is a crucial phase to respond promptly and aptly to the electrical load modifications of a fuel cell, aiming to optimize the whole system (reformer + fuel cell) performance. Although some studies are reported in the literature regarding the dynamic performance of the fuel cells, works devoted to the investigations of the dynamic performance of the online fuel reformers – corresponding to the load variation of the fuel cells – are not sufficiently reported [208].

Garcia et al. [209] developed a dynamic model for a three module reformer made up of ethanol dehydrogenation, acetaldehyde steam reforming, and water gas shift units for

feeding hydrogen to a fuel cell. They simulated the dynamic response of the reforming unit in terms of the selectivity of the products of the ESR reaction rate to the changes in concentration of the feed (ethanol + water). The same authors in another study [210] focused on the controllability and the dynamic simulation of the same system as they reported in [209] by acting on the feed concentration at isothermal conditions. A dynamic numerical model for the methane fuel processor of a PEMFC was developed by Funke et al. [211] aiming at optimizing the reaction conditions and heat integration especially during start up, shut down, and load change. The effect of two constructions (the reactor and the evaporator with and without thermal coupling) on the temperature profile, reaction rates, and methane conversion was investigated. Hydrogen yield was higher when the reactor and the evaporator were not thermally coupled. John and Schroer [212] presented a dynamic model of a methane steam reformer for a residential fuel cell system. The dynamic model covered the full operating range including the startup and shut down, and described the dynamics of the hydrogen yield and thermal behavior of the reformer when the flow rate of water or natural gas changed. The thermal system was affected by increasing the flow rate of the water. Higher hydrogen yield and lower methane concentration at the outlet were reported at higher temperature, i.e. lower concentration of inlet water. A dynamic model for an interconnected reformer and PEMFC stack was developed by Stamps and Gatzke [213] with emphasis on the influence of various design and operating parameters on system performance. Operating at higher temperature resulted in higher system performance.

A dynamic modeling study of a catalytic steam reformer by Kvamsdal et al. [214] showed that the steam or gas (CO, CO_2, H_2, and CH_4) supply interruption affects the reactor wall temperature, which can directly lead to material failure or coke formation. Lin et al. [215] modeled the dynamics of an experimental multi-stages methane reformer in charge of providing hydrogen to a PEMFC to design a control system to provide the responsiveness of the fuel reformer to the alterations in the hydrogen demand. The response of the fuel reformer to changes in the process variables such as CH_4 feed flow rate, H_2O/CH_4 feed ratio, O_2/CH_4 feed ratio and the reformer inlet temperature was studied. Tsourapas et al. [216] presented a dynamic model based on thermodynamics and energy balance for a JP5 fuel reformer in connection with a membrane separator (SEP) and a PEM fuel cell to investigate the effects of the operating set point of SEP on the overall system efficiency. They concluded that the open loop response of the system is shown to be satisfactory in terms of the response time and hydrogen production. It was shown that there is a trade-off between the SEP efficiency and the overall efficiency of the system.

In another work by Koch et al. [3], a dynamic model of an ethanol steam reformer (as the fuel reformer for pure hydrogen production to feed a PEMFC) was developed to implement an adaptive and predictive control. The static behavior of the reformer system was described by means of several maps developed in Matlab. Further, the dynamics of the fuel reformer (SMR) in connection with a PEMFC by acting upon reactor pressure and feed flow rate (ethanol + water) was studied. They proposed an efficient controller that reduced

the response time of the reformer by a factor of 7 down to 8 s in terms of following the dynamic of a fuel cell load by acting simultaneously on the fuel flow rate and pressure. However, such advanced controllers require internal models and simulations for further development.

The purpose of this chapter is to present a simple approach mainly based on physical laws (adapted Arrhenius model, mass balance, ideal gas law, and Sieverts' law) or numerical fitting (black box model). Such models can be applied for the development of controllers, which is out of the scope of this thesis. A dynamic model of a reforming system (the CMR) is given to simulate the dynamics of the pure hydrogen production rate at unsteady state conditions (between two steady state points) under fuel flow rate and pressure set-up steps. The model considers the kinetics of the catalytic reforming reactions regarding the molar production of ESR products, especially hydrogen inside the reactor at unsteady operating conditions. Additionally, application of the CMR makes it possible to investigate the effect of the byproducts of the ESR (CO, CO_2, H_2O, and CH_4) on the performance of a real case Pd-Ag membrane based on the observed reaction kinetics (concentration of the ESR products). The latter is an important factor in monitoring and simulation of the performance of the membrane in ESR environment so that many works have been reported on the investigation of the effect of the gaseous byproducts on the permeation behavior of the membranes.

In this chapter, a static model is developed to calculate the molar production rate of the ESR products (CO, CO_2, CH_4, H_2, and H_2O) in the CMR. Two different models were developed based on the experimental results to predict the pure hydrogen production rate at steady state conditions. The models are named as model 1 (Sieverts' law) and model 2 (a black box model). Several critical factors such as the partial pressure of hydrogen, the activation energy of the hydrogen permeation process, and most importantly, the effect of co-presence of the ESR products on the permeation activity of the membrane were only taken into account by means of the Sieverts' law, which reinforced and supported the aim of the simulation of the CMR. The aim of developing the black box model (model 2) was to investigate a numerical model not based on the physical rules and definitions (Sieverts' law) that is normally applied for calculation of hydrogen permeation rate. However, the two important factors in hydrogen permeation rate, i.e. fuel flow rate and pressure, were taken into account.

Finally, the alteration of the pure hydrogen production rate (transient state) during the fuel flow rate and pressure changes at isothermal conditions are simulated. The application of the model is in the design and control of a hydrogen producing system capable of online feeding a fuel cell with the possibility of instant adjustments of the pure hydrogen stream, following the changes in the fuel cell electric load.

5.2 Materials and methods

5.2.1   General and specific models

The reformer was simulated to develop models to predict the molar production rate of ESR products (CO, CO_2, CH_4, H_2, and H_2O) and the rate of pure hydrogen permeation through the membrane. As the first step, several steady state models as functions of the operating conditions (temperature, pressure, S/C ratio, and the fuel flow rate) were developed. All the experimental points (regarding all the experimental results at all operating conditions) were considered at this step, so, the models are called the General Models.

For the modeling task, the CMR was divided into two sections, i.e. the catalytic zone, and the permeation zone (the membrane) as shown in the Fig. 5.1. The ESR reaction was supposed to occur in the catalytic zone, resulting in total production of the retentate gas plus the permeated hydrogen. The permeation zone (the membrane) stands for the pure hydrogen-generating step for which the dynamic model was developed. The outputs of the catalytic zone model were used as the input of the static models of the permeation zone (i.e. the membrane).
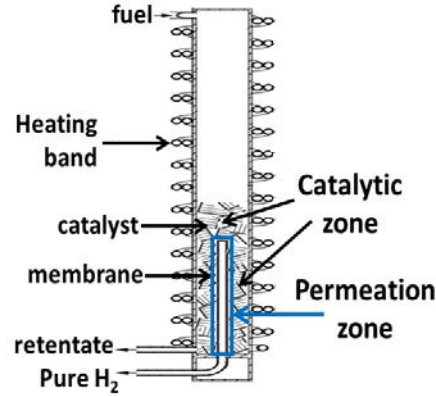
Fig. 5.1 The catalytic zone and the permeation zone of the CMR

The steady state models of the catalytic zone were derived based on the Arrhenius law in the form of:

$$\dot{n}_{specie} = \alpha \times F \times P^{\beta} \times SC^{\theta} \times exp(\frac{\gamma \times P + \omega \times SC + \lambda}{RT}) \qquad 5.1$$

$$\dot{n}_{specie} = \alpha \times F \times P^{\beta} \times SC^{\theta} \times exp(\frac{\gamma \times P^{\omega} \times SC^{\lambda} + \varepsilon}{RT}) \qquad 5.2$$

$$\dot{n}_{specie} = \alpha \times F \times (\beta \times P + \theta \times SC + \gamma) \times exp(\frac{\omega \times P + \lambda \times SC + \varepsilon}{RT}) \qquad 5.3$$

$\dot{n}_{specie}$ [mol/s] is the molar production rate of each species (the subscript *specie*) present in the CMR as the products of ESR. 'α', 'β', 'θ', 'γ', 'ω', 'λ', and 'ε', are the fitting

parameters of the equations. In the formulation of the molar production rate of the ESR products ($\dot{n}_{specie}$), temperature [K] is noted as 'T', pressure [Pa] as 'P', steam to carbon ratio as 'SC', and the fuel flow rate [m^3/s] as 'F'.

Accordingly, the fitting parameters were given the values of "0" or "1" to form the various final models. Eight models out of the several tested ones showed interesting results in terms of fitting the experimental (measured via experiments) values. The mentioned models are given in Table 5.1.

Model	Equation on which the model is based	parameters	$\dot{n}_{specie}$
1	5.1	$\beta=1, \theta=0, \gamma=0$	$\alpha \times F \times P \times \exp(\dfrac{\omega \times SC + \lambda}{RT})$
2	5.1	$\theta=0, \lambda=0$	$\alpha \times F \times P^{\beta} \times \exp(\dfrac{\omega \times SC + \lambda}{RT})$
3	5.1	$\beta=0, \theta=1, \omega=0$	$\alpha \times F \times SC^{\theta} \times \exp(\dfrac{\gamma \times P + \lambda}{RT})$
4	5.1	$\beta=1, \theta=1$	$\alpha \times F \times P \times SC \times \exp(\dfrac{\gamma \times P + \omega \times SC + \lambda}{RT})$
5	5.2	$\beta=1, \theta=0, \omega=0$ $\varepsilon=0$	$\alpha \times F \times P \times \exp(\dfrac{\gamma \times SC^{\lambda}}{RT})$
6	5.2	$\theta=0, \omega=0, \varepsilon=0$	$\alpha \times F \times P^{\beta} \times \exp(\dfrac{\gamma \times SC^{\lambda}}{RT})$
7	5.2	$\beta=1, \theta=0, \omega=0$	$\alpha \times F \times P \times \exp(\dfrac{\gamma \times SC^{\lambda} + \varepsilon}{RT})$
8	5.2	$\theta=0, \omega=0$	$\alpha \times F \times P^{\beta} \times \exp(\dfrac{\gamma \times SC^{\lambda} + \varepsilon}{RT})$

Table 5.1 General models for calculation of the molar flow rate of the ESR products

Apart from the general models, which include all the experimental points (presented in Table 3.1), specific models were developed at specific temperatures, i.e. at 873 K or 923 K, mainly to improve the accuracy of the modeling results. This is a crucial step for the isothermal dynamic simulation of the reformer, which will be discussed in the next section. Indeed, a specific model is a general model, which has been developed only at 873 K or 923 K, hence, one parameter (temperature T) has been omitted in the data fitting, resulting in more precise modeled results (better fitting to the experimental data). The specific models are given in Table 5.2.

Model	$\dot{n}_{specie}$
1	$\alpha \times F \times P \times \exp(\dfrac{\omega \times SC}{RT})$
2	$\alpha \times F \times P^{\beta} \times \exp(\dfrac{\omega \times SC}{RT})$
3	$\alpha \times F \times SC^{\theta} \times \exp(\dfrac{\gamma \times P}{RT})$
4	$\alpha \times F \times SC^{\theta} \times \exp(\dfrac{\gamma \times P^{\omega}}{RT})$
5	$\alpha \times F^{\beta} \times SC^{\theta} \times \exp(\dfrac{\gamma \times P^{\omega} + \varepsilon}{RT})$

Table 5.2 The specific models

As presented in Table 5.2, the models are functions of fuel flow rate, pressure, and steam to carbon ratio.

The same methodology was used to calculate the permeation rate of hydrogen through the membrane pure hydrogen production rate (pure hydrogen production rate in the permeation zone). Several models were developed as functions of the molar production rate of hydrogen inside the reactor ($\dot{n}_{H2}$) that was obtained by the steady state model of the catalytic zone, and the operating pressure and temperature. Contributing to the partial pressure of hydrogen inside the reactor, pressure and the rate of hydrogen production are the determining factors in the rate of hydrogen permeation through the membrane. The general form of the hydrogen permeation model is:

$$J_{H2} = a \times \dot{n}_{H2}^{b} \times P^{c} \times T^{d} + e \qquad\qquad 5.4$$

Where J_{H2} is the rate of hydrogen permeation [mol/s] through the membrane (permeation zone). 'a', 'b', 'c', 'd', and 'e' are the fitting parameters.

The models based on which the calculated values of the hydrogen permeation rate fitted the experimental ones are given in Table 5.3.

Model	Parameters	J_{H2}
1	c=d=0	$a \times \dot{n}_{H2}^{b} + e$
2	d=0	$a \times \dot{n}_{H2}^{b} \times P^{c} + e$
3	b=1, e=0	$a \times \dot{n}_{H2} \times P^{c} \times T^{d}$
4	e=0	$a \times \dot{n}_{H2}^{b} \times P^{c} \times T^{d}$
5	-	$a \times \dot{n}_{H2}^{b} \times P^{c} \times T^{d} + e$

Table 5.3 Models for calculation of the hydrogen permeation rate

5.2.2 Dynamic simulation

The dynamic behavior of the membrane in terms of hydrogen permeation rate at transient conditions was simulated. Transient conditions were applied by acting on the fuel flow rate or operating pressure.

For this purpose, a specific steady state model was used to calculate the total hydrogen production rate in the reactor. In order to monitor the dynamic performance of the reformer, pure hydrogen production (permeation through Pd-Ag membranes) was measured during dynamic tests. Then two different models were developed based on the experimental results to calculate the pure hydrogen production rate at steady state conditions. The models were named as model 1 and model 2, referred to the Sieverts' law and black box models, respectively. The Model 2 presented in Table 5.3 was used as the black box model.

- **Dynamic experiments**

Using the same experimental setup presented before, several dynamic tests were performed to measure the rate of hydrogen permeation through the membrane at transient conditions. During the dynamic experiments, the fuel flow rate and the operating pressure of the reactor were altered. While giving time to the system to reach the next steady state point in terms of pure hydrogen flow rate, the variation of the hydrogen permeation rate over time was recorded. Therefore, the reformer can be assumed to have two different controlling parts at isothermal conditions: the fuel flow rate controller, and the pressure controller. A schematic plan of the fuel reformer system is shown in Fig. 5.2 to illustrate the fuel flow rate and pressure control subdivisions of the reformer.
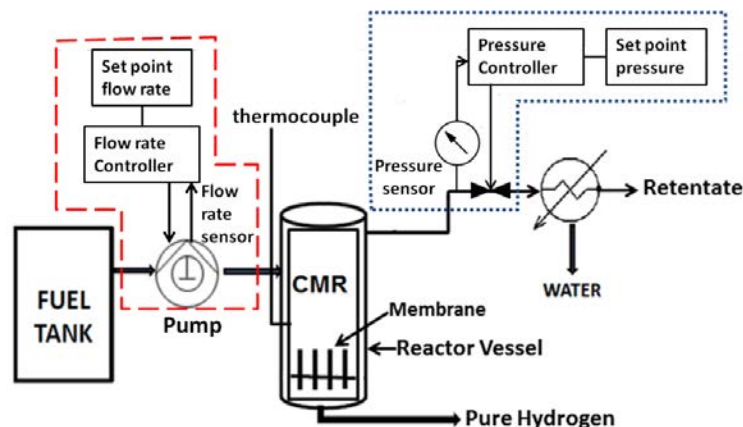
Fig. 5.2 Scheme of the Reformer.

The red dashed line and blue dotted line represent the fuel flow rate and pressure controlling systems, respectively. The operating conditions of the dynamic experiments under steady conditions are summarized in Table 5.4. The experiments were performed at isothermal conditions.

Temperature $T^{set\ point}$	K	923
Pressure $P^{setpoint}$	bar	6-10
Fuel flow rate $F^{set\ point}$	µl/min	50-200
Steam to carbon ratio SC		3

Table 5.4 Experimental conditions for the dynamic experiments

The S/C ratio is presented as "SC" in this section. At 923 K, the ESR over 0.5% Pd-0.5% Rh/CeO$_2$ catalyst is optimized in terms of hydrogen selectivity, hydrogen recovery, and ethanol conversion [2,41,87]. At SC ratio of 3, the highest value of hydrogen recovery was obtained during the experimental work that is attributed to the availability of water for the reforming reactions. On the other hand, coke formation is absent.

A controlling computer program was used to apply the set pressure or fuel flow rate changes and to record the hydrogen permeation rate every 0.5 second measured by a mass flow meter. As mentioned before, two types of dynamic tests were performed in this study: pressure change and flow rate change. In the case of pressure change dynamic tests, both increasing and decreasing steps were considered. As presented in Fig. 5.3, the pressures range of 7-10 bar was selected because at these pressures the fuel reformer was more stable.
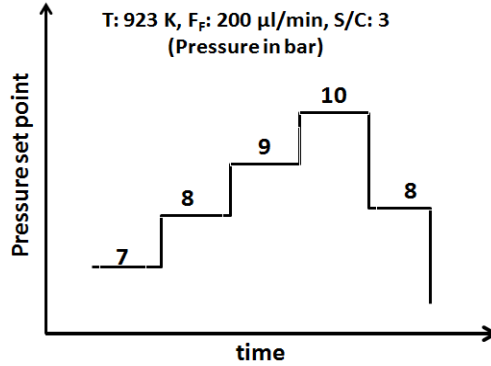
Fig. 5.3 Scheme of the pressure change for the dynamic tests.

Dynamic tests regarding the response of the system to the fuel flow rate changes were performed through two schemes, i.e. intervals of 50 μl/min, and intervals of 25 μl/min, both between 50 and 100 μl/min, as shown in Fig. 5.4.
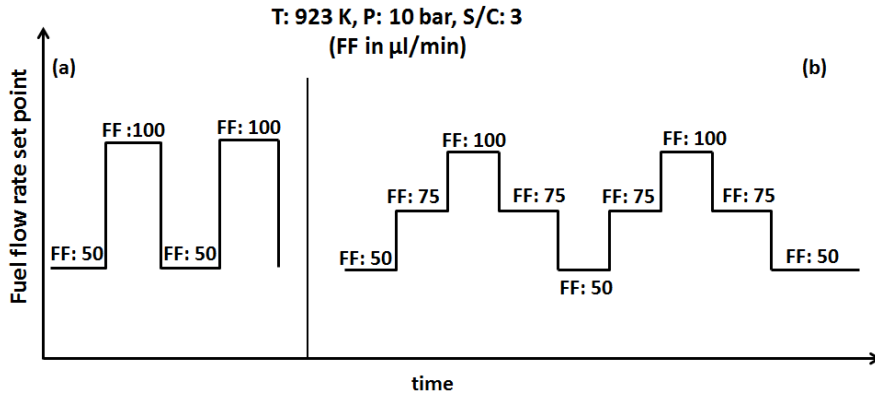
Fig. 5.4 Scheme of the fuel flow rate change for the dynamic tests. a) Steps of 50 μl/min, b) steps of 25 μl/min

It is assumed that the fuel (ethanol+water) is in its gas phase at the entrance of the volume of the CMR and the ideal gas law is applied.

5.2.3   CMR isothermal simulation

- **Steady state model of the catalytic zone**

The Model 5 presented in Table 5.2 for the catalytic zone was used to calculate the total molar production rate of species present in the catalytic zone of the CMR, i.e. CO, CO_2, CH_4, H_2, and H_2O as the products of the catalytic conversion of ethanol (around the membrane). At constant steam to carbon ratio and $\omega=1$:

$$\dot{n}_{specie} = \alpha_{specie} \times F^{\beta_{specie}} \times \exp(\frac{-(\gamma_{specie} \times P + \varepsilon_{specie})}{RT}) \qquad 5.5$$

F [m³/s] and P [Pa] represent the fuel (ethanol + water) flow rate and the reactor pressure, respectively. The molar production rate of the ESR products were used to calculate the partial pressure of hydrogen ($P_{H2,r}$ in eq. 5.6) around the membare surface (right before the permeation zone).

- **Steady state models of the permeation zone**

The hydrogen permeation rate through the membrane at steady state was modeled via two different pathways. The first model, named as "model 1", was derived from the Sieverts' law via which the hydrogen permeation phenomenon through the membrane is explained based on the mass transfer and surface reactions principals. As stated by the Sieverts' law, hydrogen permeation is a temperature activated phenomena driven by the difference between the partial pressure of hydrogen at two sides, i.e. the retentate side (inside the reactor, around the membrane) and the permeate side (right after the membrane) [2,40]:

$$J_{H2}^{model\ 1} = \frac{Q_0}{\delta} e^{\frac{-E_a}{RT}} \left(\sqrt{P_{H2,r}} - \sqrt{P_{H2,perm}} \right)$$ 5.6

Where $J_{H2}^{model\ 1}$ is the pure hydrogen production rate obtained via the Sieverts' law (model 1). 'δ' is the thickness of the membrane and Q_0 is the pre-exponential factor. E_a, R, and T are the activation energy, the universal gas constant, and temperature, respectively. $P_{H2,r}$ and $P_{H2,perm}$ are the partial pressure of hydrogen at the retentate and permeate sides, respectively. The partial pressure of hydrogen inside the reactor was calculated based on the hydrogen fraction in the gas phase assuming that the only present species in the catalytic bed (and around the membrane) are CO, CO_2, CH_4, H_2 and H_2O. Therefore:

$$P_{H2,r} = P \times y_{H2,r}$$ 5.7

Where P and $y_{H2,r}$ represent the reactor pressure and the fraction of hydrogen in the catalyst bed, respectively. The activation energy (E_a) and the pre-exponential factor (Q_0) are calculated by means of permeation experiments during which pure hydrogen at known temperature and pressure is purged and the permeation rate of hydrogen through the membrane is measured (atmospheric pressure at the permeate side) [201–203,205–207].

As discussed in chapter 2, the published open literature offers no robust model or pattern on the effect of different species on the performance of the membrane in the real atmosphere of methane steam reforming and water gas shift reactions. It was concluded that to understand the influence of co-existence of the ESR products on the permeation performance of the membrane, special models must be developed regarding specific operational conditions of the ESR environment.

Accordingly, a model was developed for hydrogen permeation through the Pd-Ag membrane; specifically for the ESR environment at the operating conditions presented in this work. It is assumed that the concentrations of CO and H_2O affect the permeation

performance of the membrane, differently at different operating conditions. The static model of the catalytic zone (based on the Arrhenius law) was used to fit the molar flow rate of the species present in the retentate gas, i.e. CO, CO_2, CH_4, H_2, and H_2O (to calculate the partial pressure of hydrogen at the retentate side).

Regarding eq. 5.6, the activation energy (E_a) was taken from the work by Papadias et al. [143] as they used the same membrane module as the one used in this work, with the same characteristics and synthetized by the same manufacturer (REB Research & Consulting [179]). Therefore, the term $\dfrac{e^{\frac{-E_a}{RT}}}{\delta}$ in eq. 5.6 was directly calculated, which is equal to 54.9 [m^{-1}]. Then, the term 'Q_0' was obtained firstly from the experimental results ($Q_0^{measure}$), and then modeled (Q_0^{model}) by means of a static model as a function of the reactor pressure (P) and fuel flow rate (F):

$$Q_0^{measure} = \frac{J_{H2} \times \delta}{e^{\frac{-E_a}{RT}} \times (\sqrt{P_{H2,r}} - \sqrt{P_{H2,perm}})} \qquad 5.8$$

$$Q_0^{model} = k_1 \times F \times exp(k_2 \times P) \qquad 5.9$$

Where 'k_i' is the fitting parameter. $P_{H2,r}$ in eq. 5.8 is obtained via eq. 5.7 by using the modeled values of the molar production rate of ESR products to calculate the hydrogen fraction in the catalytic zone. In fact, this factor (Q_0^{model}) was used to fit the results of the Sieverts' law based model to the experimental ones.

The second model, named as "model 2", is a black box model, which was introduced as Model 2 in Table 5.3. This model is a function of the reactor pressure and the molar production rate of hydrogen ($\dot{n}_{H2}$) obtained by the steady state model developed for the catalytic zone (Model 5 presented in Table 5.2):

$$J_{H2}^{model\ 2} = a \times \dot{n}_{H2}{}^{b} \times P^c + e \qquad 5.10$$

$J_{H2}^{model\ 2}$ [mol/s] is the pure hydrogen production rate obtained via the black box model.

Accordingly, the hydrogen permeation rate at steady state conditions was modeled by means of model 1 and model 2, to be used in the simulation of the dynamics of hydrogen permeation rate at transient conditions, i.e. between two steady state points.

- **Isothermal dynamic simulation of the permeation zone**

Prior to the dynamic simulation of the permeation zone, the reactor pressure was modeled in the case of pressure set point adjustment during which the pressure valve of the reforming systems acts on the retentate gas flow rate to adjust to a higher or lower pressure. The ideal gas law in the form of $PV = \dfrac{mRT}{M_W}$ was used to model the pressure of the reactor.

P, V, T, and M_W are reactor pressure, the volume of the reactor, reactor temperature, and the molar mass of the fuel mixture, respectively. 'm' is the accumulated mass of the fuel added to the reactor volume. It was assumed that the accumulation rate of the pumped fuel into the constant volume of the reactor at constant temperature, results in pressure rise as the pressure valve acts on the outlet of the system to block the retentate stream when pressure increase is required. Conversely, the pressure valve lets the retentate gas be released to decrease the reactor pressure, so that the inlet mass flow rate of the fuel gets lower than the outlet mass flow rate. Regardless of the action of the pressure valve on the retentate gas stream, hydrogen constantly permeates through the membrane. Therefore, the added mass to the reactor volume is the difference between the fuel flow rate, and the retentate gas flow rate plus hydrogen permeation rate, so that:

$$\frac{dm}{dt} = \dot{m}_{fuel} - \dot{m}_r - \dot{m}_{H2.perm} \qquad 5.11$$

Where $\dot{m}_{fuel}$ and $\dot{m}_{H2.perm}$ represent the fuel flow rate and hydrogen permeation rate, respectively, both in [kg/s]. Then, the ideal gas law is written as:

$$\frac{dP}{dt} = \left(\frac{RT}{VM_W}\right) \times \frac{dm}{dt} \qquad 5.12$$

Where $\frac{dm}{dt}$ is the rate of the accumulation of the mass in the reactor volume. In this work, the CMR is a packed bed reactor running at isothermal conditions, with negligible axial mixing. The temperature and concentration difference is neglected, so that the models are considered as ideal plug flow pseudo-homogenous ones [217].

To develop the dynamic model of the permeate zone, a first order function was used:

$$\frac{J_{H2}^D}{F} = \frac{J_{H2}^{model\ 1,2}}{1+\tau s} \qquad 5.13$$

J_{H2}^D is the pure hydrogen production rate obtained by the dynamic model. The superscript "D" stands for the dynamic model. $J_{H2}^{model\ 1,2}$ represents the hydrogen permeation rate calculated via model 1 or 2, considering every single operating point as steady state. The time constant is presented as τ. The measured dynamic of fuel flow rate was faster than the sampling time (<1 second). Therefore, the fuel flow rate is always equal to its set point value:

$$F = F^{set\ point} \qquad 5.14$$

Finally, equation 5.13 is written as:

$$\frac{J_{H2}^D}{F^{set\ point}} = \frac{J_{H2}^{model\ 1,2}}{1+\tau s} \qquad 5.15$$

Where $F^{set\ point}$ is the fuel flow rate set point (see Fig. 5.4).

The simulation was performed by means of Ordinary Differential Equation (O.D.E) solver.

The dynamic simulation of the reforming system was performed in Matlab Simulink. The Simulink simulator used to model the reactor pressure and pure hydrogen flow rate is shown in Fig. 5.5.
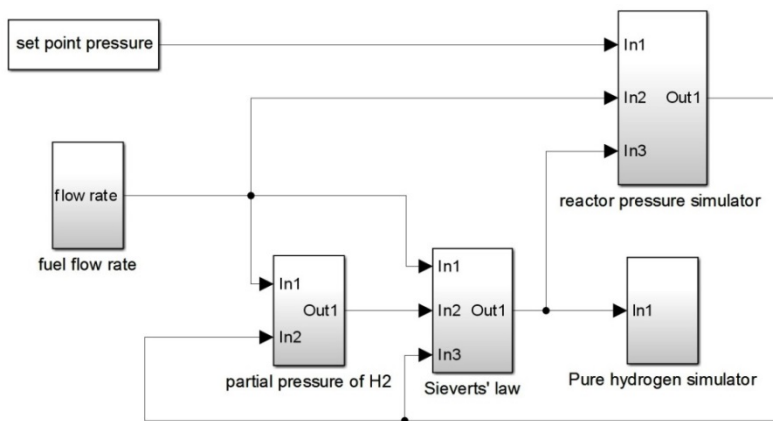
Fig. 5.5 Simulink model to simulate the reactor pressure and the pure hydrogen production rate

The simulated pressure is used as an input for the calculation of the partial pressure of hydrogen and the production rate of pure hydrogen via the Sieverts' law. The set point pressure value is needed since a PID controller is used to set the pressure and act on the pressure valve.

5.3 Results and discussion

Least Square Method (LSM) was applied to obtain all the fitting parameters regarding the steady state models. The time constant was estimated from a set of trials and errors. The time constant is a function of operating conditions (pressure or fuel flow rate). This is attributed to the dependency of the time constant on the function of the CMR during pressure or fuel flow rate change cycles. The response of the system to the fuel flow rate adjustments was faster due to instant modification made by the pump and instant increase in the inlet flow rate of the fuel into the reactor. In the case of pressure change steps, the CMR needed to be given time to increase the reactor pressure gradually as the fuel is added to the reactor constant volume.

5.3.1   Steady state models of the permeation zone

The products of ESR (CO, CO_2, CH_4, H_2, and H_2O) and the pure hydrogen permeation rate was modeled at four different fuel flow rates, i.e. 50, 100, 150, 200 µl/min and three different pressures (6, 8, and 10 bar). As mentioned before, the molar production rate of all the ESR products is needed in order to calculate the partial pressure of hydrogen in the

catalytic zone (around the membrane). The calculated molar production rates of the ESR products (catalytic zone) are presented in Fig. 5.6. The dashed lines represent the 10% error (discrepancy between experiment and measurement). The x-axis (modeled) and y-axis (measured) are referred to the values calculated by the static model and obtained via experiments, respectively.
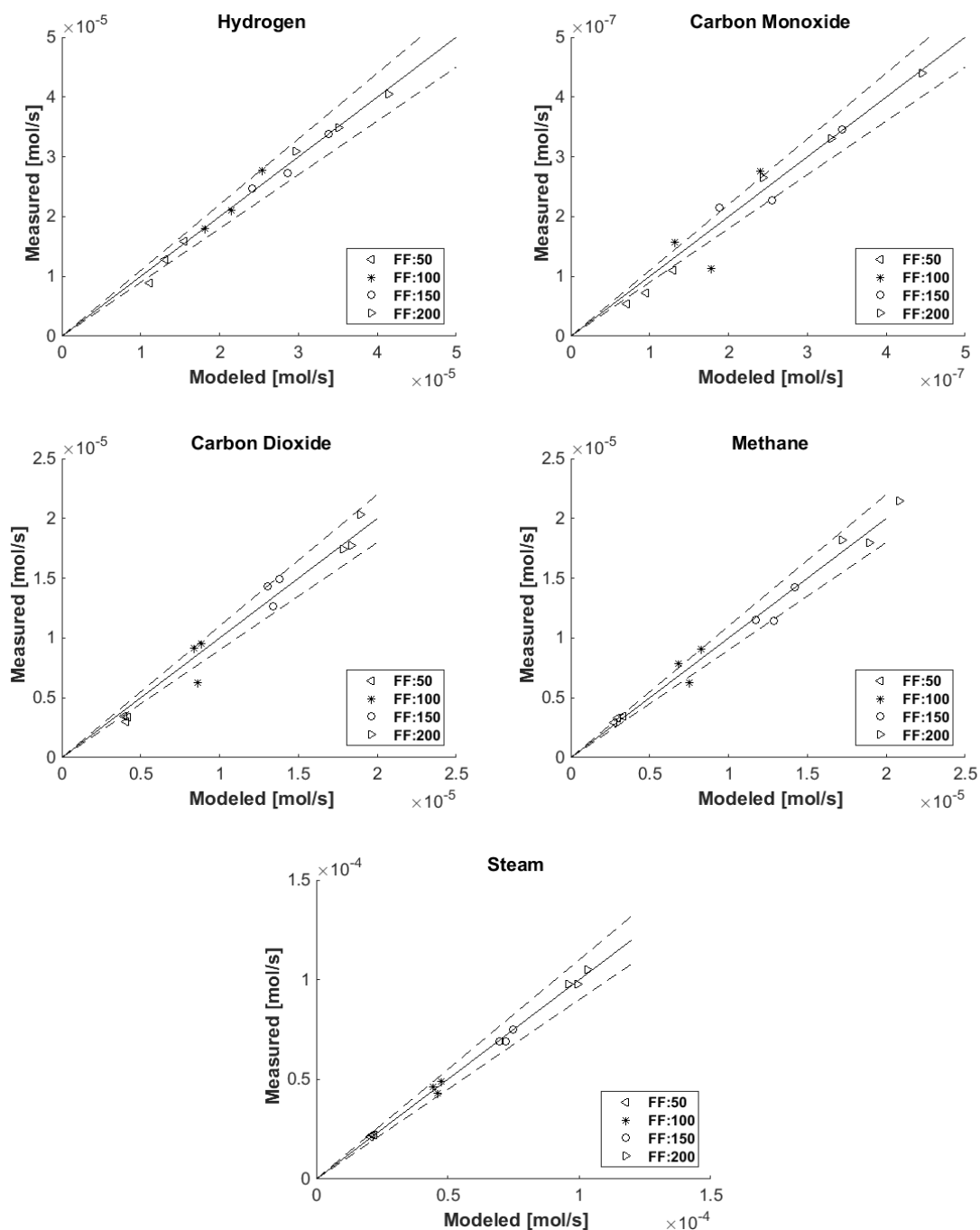
Fig. 5.6 Parity plots of the ESR products calculated by the static model (eq. 5.5).

The modeled values could fit the experimental results within the 10% error, especially in the case of production rate of hydrogen. The values of the fitting parameters (eq. 5.5) for all the gases are given in Table 5.5.

specie	α_{specie} [mol.m^{-3}]	β_{specie} [-]	γ_{specie} [J.mol^{-1}.Pa^{-1}]	ϵ_{specie} [J.mol^{-1}]	R^2
H_2	1.1	0.71	8.4×10^{-7}	-0.1	0.995
CO	75.5	0.9	-1.5×10^{-6}	-4.3	0.985
CO_2	133.9	1.1	-1.5×10^{-7}	1.2	0.991
CH_4	560.3	1.3	-4.8×10^{-7}	3.7	0.995
H_2O	226.1	1.1	-1.8×10^{-7}	2.7	0.999

Table 5.5 Fitting parameters of the steady state model for the ESR products production rate model (eq. 5.5)

According to eq. 5.5, it can be seen that the values of $\gamma \times P$ are very small compared to ϵ, except in the case of hydrogen. The most effective factor on the hydrogen permeation is the partial pressure of hydrogen in the reactor; hence, the value of $\gamma \times P$ is higher in this case. The same explanation can be given regarding the parameter β. In the case of hydrogen, the effect of pressure in the CMR configuration is dominant in comparison with the fuel flow rate, resulting in the smallest value of β in the case of hydrogen. Conversely, the value of β in the case of CH_4 is the highest among the gases because the only source of CH_4 is the ethanol decomposition reaction (eq. 2.1). At complete ethanol conversion, the higher the fuel flow rate is, the higher the production rate of CH_4 is. The value of β in the case of H_2O is nearly one, which is very relevant since the ESR reaction were performed at SC=3 where there is a large amount of excess water. It can be concluded that the molar flow rate of water in the retentate stream is proportional to the inlet molar flow rate of water in the fuel mixture (ethanol + water). At SC=3, a large portion of the inlet water (70-90%) leaves the reactor in the form of steam as unreacted water. The value of γ in the case of CO is one order of magnitude smaller than other gases, which is attributed to the very small amount of CO detected at the outlet of the reactor. The values of γ proves that at higher pressures, less byproducts (CO, CO_2, CH_4, and H_2O) and more hydrogen are generated, which is totally in agreement with the experimental results and the aim of the application of the CMR, where ESR reaction is promoted (the shift effect).

The results of the modeling of the molar flow rate of the ESR products by all the formulations presented in Table 5.1 and Table 5.2 (general models and specific models, respectively) are given in appendix B.

The result of the pre-exponential factor model (eq. 5.9) shows that the model fits very well to the calculated values except at P=6 bar, so that the coefficient of determination (R^2) increases from 0.68 to 0.91 when the measured value at 6 bar are not presented due to

membrane diffusion limitation at pressures lower than 6 bar. The modeling results (Q_0^{model}) are presented in Fig. 5.7a and b. The dashed lines show the 15% error range.
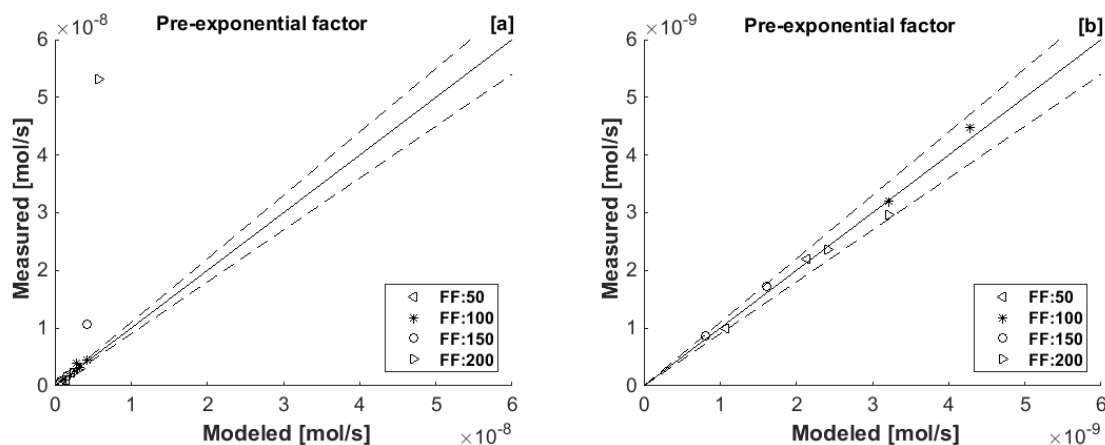
Fig. 5.7 Result of the pre-exponential factor model (eq. 5.9) when P=6 bar is included (a) and is not included (b)

The fitting parameters of the pre-exponential model (eq. 5.9) are given in Table 5.6.

parameter	k_1	k_2
value	0.602	-3.4823×10^{-6}
unit	$[mol.m^{-2}.Pa^{-0.5}]$	$[Pa^{-1}]$

Table 5.6 Fitting parameters of the pre-exponential factor model (eq. 5.9)

Regarding the value of k_2, the diverse effect of pressure is obvious (see eq. 5.9). This is attributed to the fact that at higher pressure, the concentration of hydrogen is higher around the membrane (permeation zone) leading to the lower concentration of the other gases, which directly means that the permeation behavior of the membrane is less affected. This is completely in agreement with the experimental results and the assumption of the negative effect of CO and H_2O on the permeation behavior of the Pd-Ag membrane.

Taking into account Fig. 5.7, the immediate effect of the consideration of the values at P=6 bar is the lower accuracy of the final Sieverts' law model in predicting the pure hydrogen permeation rate. The result of the Sieverts' law model (permeation zone) is shown in Fig. 5.8a and b. The partial pressure of hydrogen in the reactor (obtained based on the molar production rates of the ESR products calculated by the Arrhenius based static model) was used in the Sieverts' law to obtain the pure hydrogen permeation rate. The dashed lines represent 15% error range.
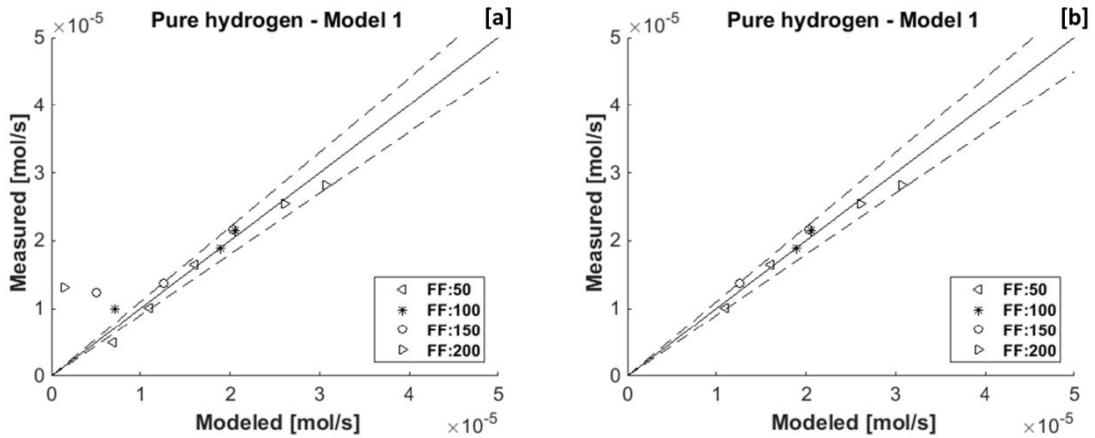
Fig. 5.8 Parity plots of the hydrogen permeation rate obtained by the Sieverts' law model
(model 1) when P=6 bar is included (a) and is not included (b)

If values of the pure hydrogen production rate at P=6 bar are excluded, the model is more precise. In this case the coefficient of determination (R^2) increases from 0.81 (Fig. 5.8a) to 0.86 (Fig. 5.8b). All measured and modeled point including ones at P=6 bar were used in the dynamic simulation of the CMR.

The results of the model 2 based on eq. 5.10 (black box model) are shown in Fig. 5.9. Hydrogen production rate in the CMR ($\dot{n}_{H2}$) calculated based on the Arrhenius based steady state model (eq. 5.5) was used as an input for the model 2.
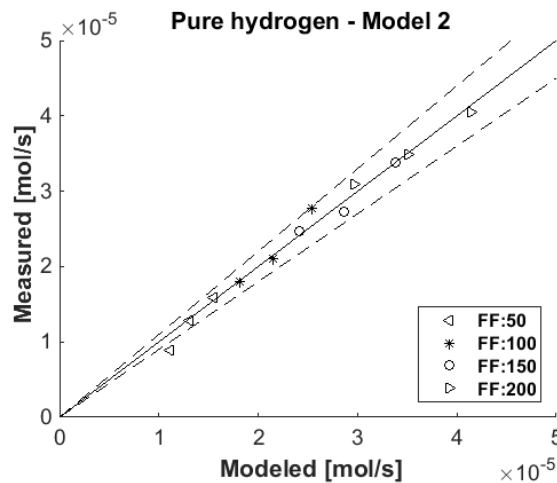
Fig. 5.9 Parity plots of the hydrogen permeation rate obtained by the black box model
(model 2)

The fitting parameters of the black box model (eq. 5.10) are given in Table 5.7.

Parameter	a	b	c	e
value	2.1×10^{-11}	0.7	1.5	3.1×10^{-6}
Unit	[Pa^{-1}]	[-]	[-]	[mol.s^{-1}]

Table 5.7 Fitting parameters of the black box model (eq. 5.10)

The fitting parameters of the model 2 (a, b, c, and e) do not possess a physical meaning, but the value of the parameter 'c' proves the noticeable effect of pressure on the hydrogen permeation rate. Besides, as the value of the parameter 'e' is very small, it is shown that at the pressure or fuel flow rate of zero, almost no hydrogen is generated.

5.3.2 Isothermal Dynamic simulation

- **Pressure change simulation**

Keeping in mind the configuration of the CMR, when the pressure of the reactor is set at a higher value, the outlet of the reactor is blocked, the flow rate of the retentate gas ($\dot{m}_r$) is zero (see eq. 5.10), so that the inlet fuel is added to the volume of the reactor to increase the pressure. On the contrary, when reactor pressure is set at a lower value, the pressure valve is opened so that gas is released and reactor pressure drops rapidly. The different behavior of the system during pressure increasing and decreasing steps is due to the different act of the pressure controlling system on the pressure valve (see Fig. 5.2). Therefore, the dynamics of the pressure control differs in different steps. The importance of such a performance lies in the dependency of pure hydrogen permeation rate through the membrane on the partial pressure of hydrogen in the reactor. The simulated pressure change behavior of the reformer system is shown in Fig. 5.10.
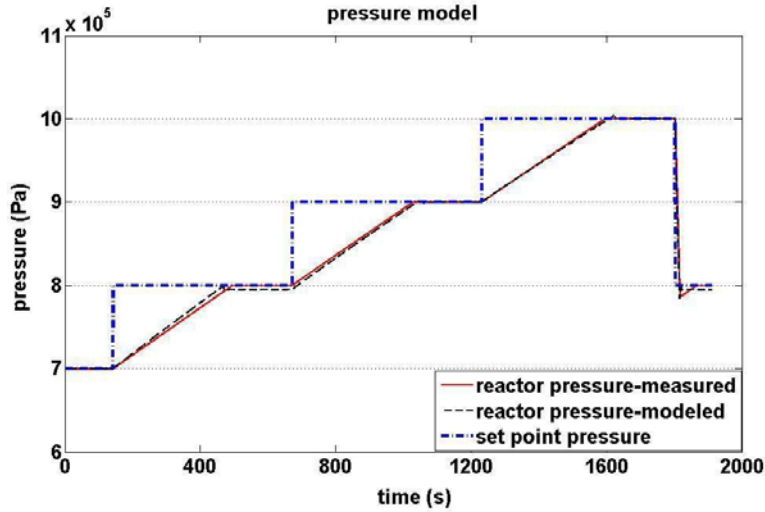
Fig. 5.10 Measured and simulated reactor pressures in the pressure change dynamic tests.
T=923 K, FF=200 µl/min.

It is clear that the results of simulation of reactor pressure by means of the ideal gas law fit the measurement very well.

As mentioned before, the hydrogen partial pressure difference at the retentate and permeate sides is the driving force for hydrogen permeation, which is stated by the Sieverts' law. Therefore, consideration of the Sieverts' law as the base of simulation of hydrogen permeation dynamic performance is essential. The simulated dynamic performance of the reforming system based on the Sieverts' law (model 1) in the case of pressure change dynamic tests is shown in Fig. 5.11.
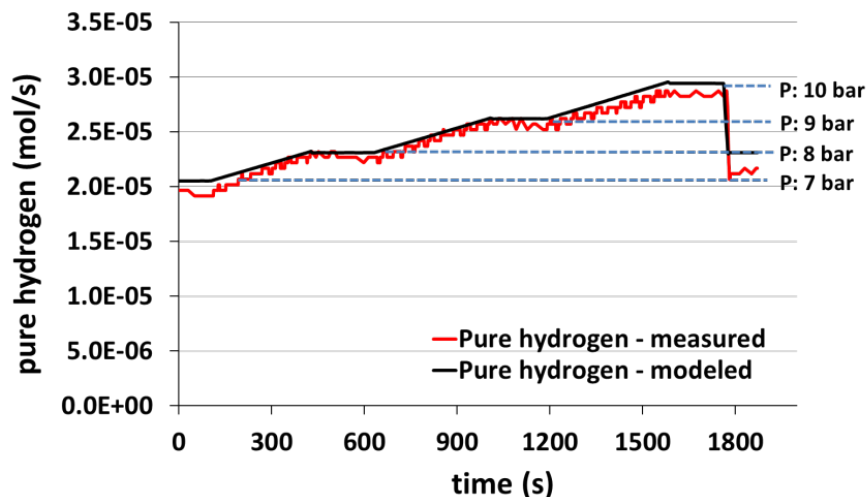
Fig. 5.11 Sieverts' law simulation (model 1) results of pure hydrogen production for pressure change dynamic tests. T=923 K, FF=200 µl/min.

The small fluctuations of the pure hydrogen measurement during the experiments are attributed to the small variations of the pressure inside the reactor, as the pressure valve acts on the outlet retentate stream. This fluctuation is ca. 0.11×10^{-5} mol/s of pure hydrogen. The simulation of the pressure change steps fitted the experimental observation very well, proving the successful modeling and application of the Sieverts' law.

The dynamic simulation based on the model 2 (black box model) is given in Fig. 5.12. As expected, at constant temperature and fuel flow rate, pure hydrogen production rate follows the variation of reactor pressure by time.
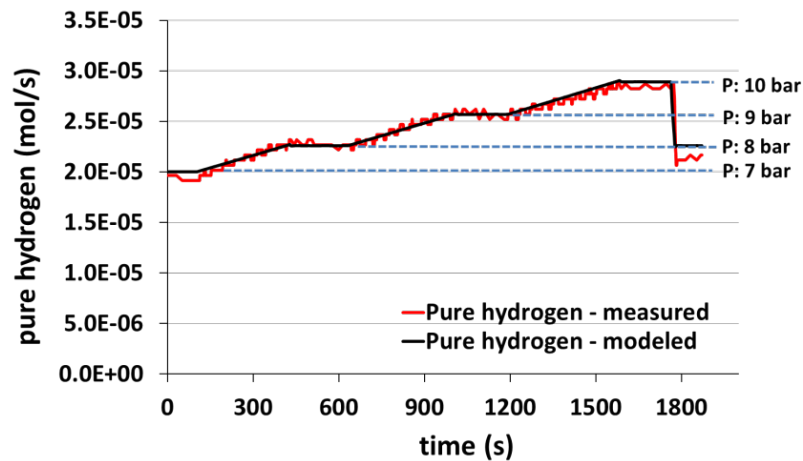
Fig. 5.12 Black box (model 2) simulation results for pressure change dynamic tests. T=923 K, FF=200 µl/min.

Similar to the Sieverts law model, the black box simulation results could predict the dynamics of the hydrogen permeation very well, proving that both models are reliable in simulation of the pure hydrogen production rate at unsteady state when the pressure set point of the CMR is changed.

- **Fuel flow rate change simulation**

In comparison with the pressure change models, it is more essential to develop a model on the fuel flow rate change. The importance of fuel flow rate change model lies in the fact that acting on fuel flow rate is much faster than acting on system pressure. The CMR time constant in the fuel flow rate change tests was 55 seconds. The simulated result of the model 1 is presented in Fig. 5.13.
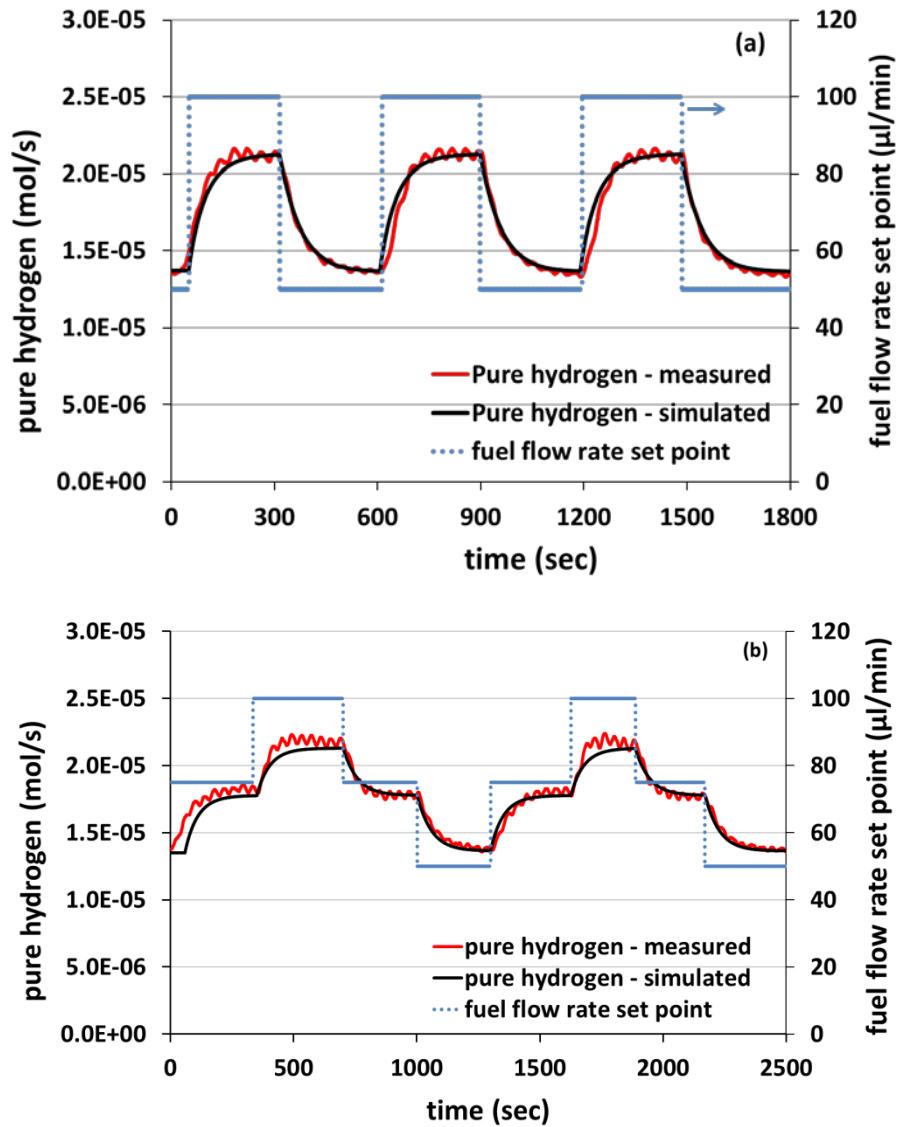
Fig. 5.13 Sieverts' law simulation (model 1) results of pure hydrogen production for fuel flow rate change dynamic tests. a) Steps of 50 μl/min, b) steps of 25 μl/min (P=10 bar)

The Sieverts' law simulation results in the case of the fuel flow rate change fitted very well to the experimental observation. This is an outstanding result since the accuracy of the prediction of the pure hydrogen dynamics together with fast response of the reforming system to the fuel flow rate adjustments can build up a robust essential step toward further control studies.

The simulation results of the model 2 are illustrated in Fig. 5.14. Measured values were obtained via dynamic experiments at constant pressure (10 bar).
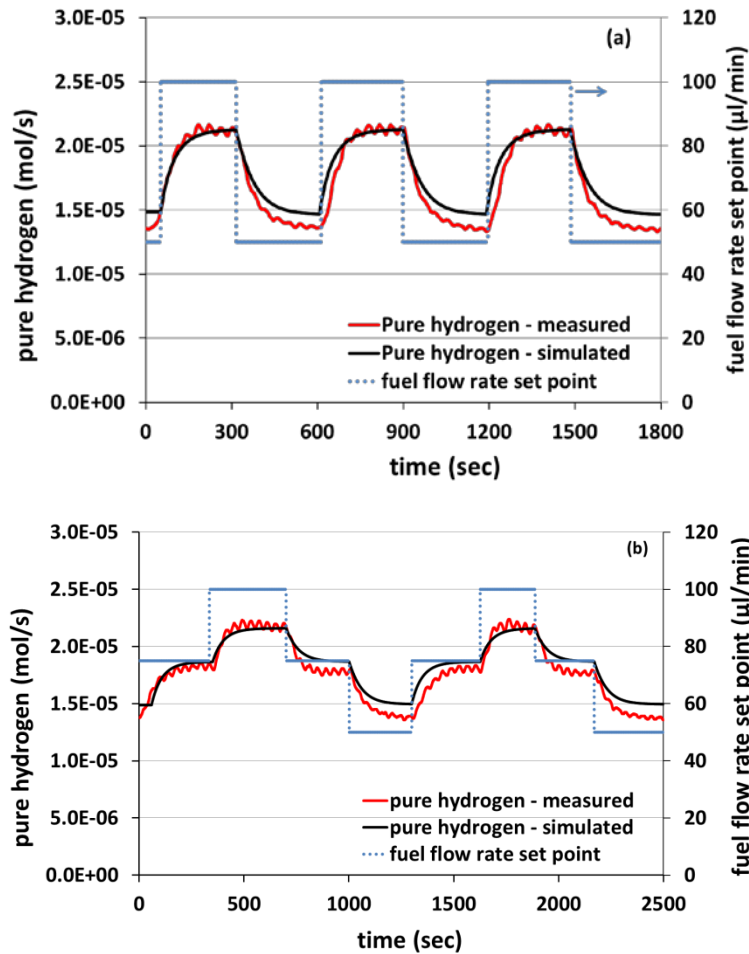
Fig. 5.14 Black box (model 2) simulation pure hydrogen production for fuel flow rate change dynamic tests. a) Steps of 50 μl/min, b) steps of 25 μl/min (P=10 bar)

At constant pressure, only hydrogen production rate inside the reactor was considered as the variable of the model 2. The model fitted the experimental results very well, capable of prediction of the pure hydrogen flow rate variation with good accuracy.

The isothermal dynamic simulation of pure hydrogen production via ESR in the CMR considering the fuel flow rate and pressure changes can play an essential role for a general model of the dynamic performance of the system when connecting to a fuel cell for its online feeding and control.

It was shown that the Sieverts' law based model is able to predict the permeation rate of hydrogen taking into account the molar production rate of the ESR products. In fact, the effect of the operating conditions can be interpreted into the variations in the molar flow rate (concentration of gases in the catalytic zone) by means of Sieverts' law. This is a clear advantage of the Sieverts law where it can be extended to the wider range of operating

133

conditions. The black box model is a simulation based on pure fittings, which may be totally dependent on certain operating conditions.

5.4 Conclusion

Ethanol steam reforming (ESR) over Pd-Rh/CeO$_2$ catalyst was performed in a CMR unit at 923 K, 6-10 bar, and fuel flow rates of 50 to 200 µl/min using a mixture of ethanol and distilled water with steam to carbon ratio of 3. A steady state model was proposed based on the Arrhenius law as a function of fuel flow rate and reactor pressure. The model was based on the experimental results and predicted correctly the performance of the ESR in terms of the molar production rate of ESR products, i.e. CO, CO$_2$, CH$_4$, H$_2$, and H$_2$O inside the reactor (catalytic zone). The pure hydrogen production rate (permeate zone) at steady state conditions was simulated by means of two steady state models, i.e. the Sieverts' law model named as model 1, and the black box model named as model 2. Finally, the dynamic simulation was performed under ideal gas law assumptions to simulate the permeation behavior of the membrane and the dynamics of the pure hydrogen production rate (permeation zone) in the case of the fuel flow rate or the operational pressure set point adjustment at isothermal conditions. The simulation results based on both model 1 and model 2 fitted the experimental observations. The effective critical factors such as hydrogen partial pressure in the CMR and the influence of the co-existence of the ESR products on the permeation behavior of the membrane were taken into account by the Sieverts' law model, presenting a robust simulation. Although the pressure change steps simulation results were more satisfactory, the simulation of the dynamics of the fuel flow rate change is more essential, as the system responds much faster to such an adjustment. The presented dynamic models resembled hydrogen flow rate adjustments needed to follow changes in the electric load of a fuel cell when fed online, which is an essential step to design, control, and optimize an ethanol to electricity system.

Chapter 6

General conclusion

On-site pure hydrogen production in a catalytic membrane reactor by ethanol steam reforming

In this work, a comprehensive investigation of production of fuel cell grade hydrogen (pure hydrogen) in a catalytic membrane reactor (CMR) via ethanol steam reforming (ESR) over a $Rh_{0.5}$-$Pd_{0.5}/CeO_2$ catalyst was given.

The highlights of the experimental investigation of the ESR in the CMR are summarized as:

- The ESR experiments at several operating conditions showed high selectivity of the catalyst towards H_2 (>50% volume) together with very low molar production rate of CO per mol of ethanol in the feed. Besides, complete ethanol conversion was reached at all the operating conditions.

- The shift effect resulted in significantly higher hydrogen production, thanks to the especial configuration of the CMR where the membrane was fully covered by the catalyst pellets. The equilibrium limitations were conquered at high pressure as a result of the shift effect, leading to a positive effect of pressure on the performance of the CMR despite unfavorable thermodynamic conditions at high pressure.

- The influence of species present in the CMR such as CO and CH_4 was shown based on the experimental results of the permeation tests in the atmosphere of pure hydrogen and ethanol steam reforming.

- A comparison between the CMR and the SMR (staged membrane reactor) clearly revealed the superior performance of the CMR. Thanks to the special configuration of the CMR and brilliant reactivity of the catalyst, pure hydrogen production rate and methane conversion were promoted at high pressure in the case of the CMR.

- 0.9 L_N pure hydrogen/ml EtOH at 12 bar and 923 K was obtained, equal to 3.2 mol of pure hydrogen per mol of inlet EtOH. A hydrogen yield of 0.55 was reached at 12 bar and 923 K, much higher than that of SMR, 0.2. Hydrogen recovery reached values up to 95% in the CMR, significantly higher than 70% in the case of the SMR.

The results of the thermodynamic analysis are as follow:

- Exergy analysis was introduced as a relevant tool to explain the effects of operating conditions and thermodynamic losses on both pure hydrogen production rate and total efficiency of the membrane reactor.

- A significant effect of pressure and temperature on the exergy efficiency was observed. Following the pure hydrogen production rate, the exergy efficiency increased with pressure because of the shift effect, where more methane was converted at higher pressure resulting in higher production rate of pure hydrogen.

138

- Exergy analysis showed that the highest exergy destruction occurred via the retentate gas stream and heat losses. The exergy content of the retentate gas especially at lower pressures could provide the reactor with a notable fraction of its required heat at steady state conditions. This would result in a notable increase of the exergy efficiency of the system.

- By using the retentate gas in an insulated reactor, the exergy efficiency was increased drastically and placed between 70-90%. This result was expected since, in one hand, exergy destruction decreased and, on the other hand, the energy requirement of the system was partially or totally met by utilization of the retentate gas. In the case of an insulated reactor, exergy efficiency up to around 50% was reached at 12 bar and 923 K. In the case of recovery of the retentate gas and insulation of the reactor, exergy efficiency placed between 70-90%.

- Based on the exergy evaluation, the best operating conditions were calculated at the highest pressure and temperature used in this work (923 K and 12 bar) and the lowest S/C ratio of 1.5, where carbon deposition is probable.

- Thermal efficiency of the CMR was between 60-90% for an insulated reactor system and decreased to around 40-60% when the heat loss was considered. The consideration of the thermal efficiency revealed that while thermal efficiency offers an ideal performance at high pressure and temperature, exergy efficiency discloses inevitable irreversibilities even in the case of an insulated reactor.

- In the case of the SMR, at least 80% of the inlet exergy was lost by heat losses and the retentate stream. The insulation of the SMR resulted in a significant increase of the thermal efficiency, but not exergy efficiency since a large amount of methane and unpermeated hydrogen left the reactor as unused exergy.

- In the case of the recovery of the retentate gas in an insulated reactor, the exergy efficiency of the SMR was slightly higher than the CMR, however, much higher pure hydrogen yield and production rate is obtained in the case of the CMR.

Finally, the outcomes of the dynamic simulation of the CMR are:

- A static model for the catalytic zone was derived from the Arrhenius law as a function of operating conditions based on the experimental results to simulate the total molar production rates of ESR products. The results of the model fitted the experimental value very well (coefficient of determination $R^2 = 0.993$).

- The permeation zone (membrane) was modeled based on the Sieverts' law as the physical definition of hydrogen permeation through the membrane via which the robustness of the simulation was proved ($R^2 = 0.86$). Besides, a black box model as a function of the fuel flow rate and the operating pressure was developed and successfully fitted to the experimental values ($R^2 = 0.91$).

- A dynamic model was proposed under ideal gas law assumptions to simulate the dynamics of pure hydrogen production rate in the case of the fuel flow rate or the operational pressure set point adjustments (transient state) at isothermal conditions. Both pressure and fuel flow rate change steps simulations fitted the experimental values very well, proving a successful essential step needed to simulate an "Ethanol to Electricity" system. The simulation of the dynamics of the fuel flow rate change was more essential, as the system responds much faster to such an adjustment.

- The results of the dynamic simulation based on the Sieverts' law proved the robustness of the simulation and reinforced and supported the aim of the simulation of the CMR. Several critical factors such as the partial pressure of hydrogen, the activation energy of the hydrogen permeation process, and most importantly, the effect of co-presence of the ESR products on the permeation activity of the membrane were taken into account by means of the Sieverts' law.

- **Future avenues**

A comprehensive experimental and thermodynamic study of pure hydrogen producing system was given in this PhD thesis. However, there are promising opportunities to continue the presented work and fulfil the application of the studied system.

Future works can be devoted to the study of different noble based catalysts in the CMR. The activity of different catalysts in terms of ethanol conversion, hydrogen selectivity, and hydrogen yield and recovery can be studied similar to what reported in this thesis, to compare different catalysts in the studied membrane reactor in wider ranges of the operating conditions.

Besides, the exergy evaluation data presented in this thesis can be used for the exergonomic evaluation of the reforming system, which is an essential and modern way to scale up. Additionally, life cycle assessment of such a reforming system, especially in connection to a fuel cell is a promising method to give a comprehensive idea on the environmental impact of the studied reforming system in this thesis. The mentioned methods (exergonomic and life cycle assessment) may add additional value to the introduction and commercialization of the reforming system.

Moreover, the advanced aspect of the control of the reforming system in connection with a real end user (for example a PEMFC) can be investigated and simulated.

References

[1]   Capros P, Vita A De, Tasios N, Al. E. EU Energy, Transport and GHG Emissions Trending to 2050-Rerefence Scenario 2013. Luxembourg: 2013.

[2]   López E, Divins NJ, Llorca J. Hydrogen production from ethanol over Pd–Rh/CeO2 with a metallic membrane reactor. Catalysis Today 2012;193:145–50.

[3]   Koch R, López E, Divins NJ, Allué M, Jossen A, Riera J, et al. Ethanol catalytic membrane reformer for direct PEM FC feeding. International Journal of Hydrogen Energy 2013;38:5605–15.

[4]   NASA polynomials. University of California, Berkeley n.d.

[5]   Intergovernmental Panel on Climate Change IPCC. Climate Change 2013; The Physical Science Basis, Working Group I Contribution to the Fifth Assessment Report of the Intergovernmental Panel on Climate Change. 2013.

[6]   Arrhenius S. On the Influence of Carbonic Acid in the Air upon the Temperature of the Ground. Journal of Science 1896;41:237–76.

[7]   Bernstein L. Climate Change 2007: An Assessment of the Intergovernmental Panel on Climate Change. 2007.

[8]   International Energy Outlook. vol. 0484. U.S. Department of Energy DOE; 2010.

[9]   Intergovernmental Panel on Climate Change. IPCC Fourth Assessment Report: Climate Change 2007 (AR4). Switzerland: 2007.

[10]   Swiss Cooperation Office Kosovo. Human Development Report 2007- Energy for Development. 2007.

[11]   Klugman J. Human Development Report 2010. New York: 2010.

[12]   Kapsalaki M, Leal V, Santamouris M. A methodology for economic efficient design of Net Zero Energy Buildings. Energy and Buildings 2012;55:765–78.

[13]   Union of the Electricity Industry – Eurelectric. Power Statistics & Trends 2013. 2013.

[14]   Marszal AJ, Heiselberg P, Bourrelle JS, Musall E, Voss K, Sartori I, et al. Zero Energy Building – A review of definitions and calculation methodologies. Energy and Buildings 2011;43:971–9.

[15]   Sartori I, Napolitano A, Voss K. Net zero energy buildings: A consistent definition framework. Energy and Buildings 2012;48:220–32.

[16]   U.S. Department of Energy DOE. Building Technologies Program;Planned Program Activities for 2008-2012. 2012.

[17]   Sharaf OZ, Orhan MF. An overview of fuel cell technology: Fundamentals and

applications. Renewable and Sustainable Energy Reviews 2014;32:810–53.

[18]   Freni S, Maggio G, Cavallaro S. Ethanol steam reforming in a molten carbonate fuel cell: a thermodynamic approach. Journal of Power Sources 1996;62:67–73.

[19]   Kamarudin MZF, Kamarudin SK, Masdar MS, Daud WRW. Review: Direct ethanol fuel cells. International Journal of Hydrogen Energy 2013;38:9438–53.

[20]   Abdullah S, Kamarudin SK, Hasran UA, Masdar MS, Daud WRW. Modeling and simulation of a direct ethanol fuel cell: An overview. Journal of Power Sources 2014;262:401–6.

[21]   Leone P, Lanzini A, Ortigoza-Villalba GA, Borchiellini R. Operation of a solid oxide fuel cell under direct internal reforming of liquid fuels. Chemical Engineering Journal 2012;191:349–55.

[22]   Llorca J, Cortés Corberán V., Divins J.N., Fraile R.O., Elena Taboada E. Hydrogen from bio-ethanol. In: Gandía LM, Arzamendi G D, PM E, editors. Renewable Hydrogen Technologies, Amsterdam: Elsevier; 2013.

[23]   Deluga GA, Salge JR, Schmidt LD, Verykios XE. Renewable hydrogen from ethanol by autothermal reforming. Science (New York, NY) 2004;303:993–7.

[24]   World Fuel Ethanol Production | RFA: Renewable Fuels Association 2013.

[25]   Markets C, Energy R, Eu T, Technology RES, Campaign M. " Creating Markets for Renewable Energy Technologies EU RES Technology Marketing Campaign " Bioethanol Production and Use. 2006.

[26]   Tosti S, Basile A, Bettinali L, Borgognoni F, Gallucci F, Rizzello C. Design and process study of Pd membrane reactors. International Journal of Hydrogen Energy 2008;33:5098–105.

[27]   Gallucci F, Basile A. Pd–Ag membrane reactor for steam reforming reactions: A comparison between different fuels. International Journal of Hydrogen Energy 2008;33:1671–87.

[28]   Contreras JL, Salmones J, Colín-Luna JA, Nuño L, Quintana B, Córdova I, et al. Catalysts for H2 production using the ethanol steam reforming (a review). International Journal of Hydrogen Energy 2014;39:18835–53.

[29]   Goltsov VA, Goltsova LF. Biosphere synergism and the humankind virtual path to the hydrogen civilization era. International Journal of Hydrogen Energy 2014;39:9931–42.

[30]   Verne J. Twenty thousand leagues under the sea. Paris: 1869.

[31]   Cipriani G, Di Dio V, Genduso F, La Cascia D, Liga R, Miceli R, et al. Perspective on hydrogen energy carrier and its automotive applications. International Journal of Hydrogen Energy 2014;39:8482–94.

[32]   Bleischwitz R, Bader N. Policies for the transition towards a hydrogen economy: the EU case. Energy Policy 2010;38:5388–98.

[33]   Commission E. Comunication from the commission to the European parliament, the council, the European economic and social committee and the committee of the region. 2011.

[34]   Luis M. Gandia, Gurutze Arzamendi PMD. Renewable Hydrogen Technologies. 1st ed. 2013.

[35]   Mcdowall, William ME. Forecasts , Scenarios , Visions , Bachcasts and Roadmaps to the Hydrogen Economy : A Review of the Hydrogen Futures Literature for UK-SHEC. 2004.

[36]   European Commission Directorate-General for Research. HYWAYS the European Hydrogen Roadmap. 2008.

[37]   Ros ME, Weeda M, Jeeninga H. Snapshots of hydrogen uptake in the future A comparison study. 2007.

[38]   IEA IEAO. Prospects for Hydrogen and Fuel Cells. France: 2005.

[39]   Turner J, Sverdrup G, Mann MK, Maness P-C, Kroposki B, Ghirardi M, et al. Renewable hydrogen production. International Journal of Energy Research 2008;32:379–407.

[40]   Domínguez M, Taboada E, Molins E, Llorca J. Ethanol steam reforming at very low temperature over cobalt talc in a membrane reactor. Catalysis Today 2012;193:101–6.

[41]   Divins NJ, López E, Rodríguez Á, Vega D, Llorca J. Bio-ethanol steam reforming and autothermal reforming in 3-μm channels coated with RhPd/CeO2 for hydrogen generation. Chemical Engineering and Processing: Process Intensification 2013;64:31–7.

[42]   Men Y, Kolb G, Zapf R, Hessel V, Löwe H. Ethanol Steam Reforming in a Microchannel Reactor. Process Safety and Environmental Protection 2007;85:413–8.

[43]   Vaidya PD, Rodrigues AE. Kinetics of Steam Reforming of Ethanol over a Ru / Al 2 O 3 Catalyst. Industrial & Engineering Chemistry Research 2006:6614–8.

[44]   Lu P-J, Chen T-S, Chern J-M. Reaction network and kinetic analysis of ethanol steam reforming over a Ru/Al2O3 catalyst. Catalysis Today 2011;174:17–24.

[45]   Palma V, Castaldo F, Ciambelli P, Iaquaniello G, Capitani G. On the activity of bimetallic catalysts for ethanol steam reforming. International Journal of Hydrogen Energy 2013;38:6633–45.

[46]   Ni M, Leung DYC, Leung MKH. A review on reforming bio-ethanol for hydrogen production. International Journal of Hydrogen Energy 2007;32:3238–47.

[47]   Lopez E, Gepert V, Gritsch A, Nieken U, Eigenberger G. Ethanol Steam Reforming Thermally Coupled with Fuel Combustion in a Parallel Plate Reactor. Industrial & Engineering Chemistry Research 2012;51:4143–51.

[48]   Haryanto A, Fernando S, Murali N, Adhikari S. Current status of hydrogen production techniques by steam reforming of ethanol: A review. Energy and Fuels 2005;19:2098–106.

[49]   Koh ACW, Leong WK, Chen L, Ang TP, Lin J, Johnson BFG, et al. Highly efficient ruthenium and ruthenium–platinum cluster-derived nanocatalysts for hydrogen production via ethanol steam reforming. Catalysis Communications 2008;9:170–5.

[50]   Andonova S, de Ávila CN, Arishtirova K, Bueno JMC, Damyanova S. Structure and redox properties of Co promoted Ni/Al2O3 catalysts for oxidative steam reforming of ethanol. Applied Catalysis B: Environmental 2011;105:346–60.

[51]   Shi Q, Peng Z, Chen W, Zhang N. La2O2CO3 supported Ni-Fe catalysts for hydrogen production from steam reforming of ethanol. Journal of Rare Earths 2011;29:861–5.

[52]   Scott M, Goeffroy M, Chiu W, Blackford M a., Idriss H. Hydrogen production from ethanol over Rh-Pd/CeO2 catalysts. Topics in Catalysis 2008;51:13–21.

[53]   Jun Su Lee, Dongjin Kim B-HC and MK. Hydrogen-rich gas production from ethanol steam- reforming reaction using NiZr-loaded MCM-48 catalysts at mild temperature. International Journal of Energy Research 2013;37:1896–907.

[54]   Batista MS, Santos RK., Assaf EM, Assaf JM, Ticianelli EA. High efficiency steam reforming of ethanol by cobalt-based catalysts. Journal of Power Sources 2004;134:27–32.

[55]   Lucredio AF, Bellido JDA, Zawadzki A, Assaf EM. Co catalysts supported on SiO2 and γ-Al2O3 applied to ethanol steam reforming: Effect of the solvent used in the catalyst preparation method. Fuel 2011;90:1424–30.

[56]   Llorca J, Homs N, Sales J, de la Piscina PR. Efficient Production of Hydrogen over Supported Cobalt Catalysts from Ethanol Steam Reforming. Journal of Catalysis 2002;209:306–17.

[57]   Llorca J, Dalmon J-A, Ramírez de la Piscina P, Homs N. In situ magnetic characterisation of supported cobalt catalysts under steam-reforming of ethanol. Applied Catalysis A: General 2003;243:261–9.

[58]   Llorca J, Casanovas A, Trifonov T, Rodriguez A, Alcubilla R. First use of macroporous silicon loaded with catalyst film for a chemical reaction: A microreformer for producing hydrogen from ethanol steam reforming. Journal of Catalysis 2008;255:228–33.

[59]   Soykal II, Bayram B, Sohn H, Gawade P, Miller JT, Ozkan US. Ethanol steam

reforming over Co/CeO2 catalysts: Investigation of the effect of ceria morphology. Applied Catalysis A: General 2012;449:47–58.

[60]   Bayram B, Soykal II, von Deak D, Miller JT, Ozkan US. Ethanol steam reforming over Co-based catalysts: Investigation of cobalt coordination environment under reaction conditions. Journal of Catalysis 2011;284:77–89.

[61]   Da Silva AM, De Souza KR, Mattos L V., Jacobs G, Davis BH, Noronha FB. The effect of support reducibility on the stability of Co/CeO2 for the oxidative steam reforming of ethanol. Catalysis Today 2011;164:234–9.

[62]   Lin SS-Y, Kim DH, Ha SY. Hydrogen Production from Ethanol Steam Reforming Over Supported Cobalt Catalysts. Catalysis Letters 2008;122:295–301.

[63]   Espinal R, Taboada E, Molins E, Chimentao RJ, Medina F, Llorca J. Cobalt hydrotalcite for the steam reforming of ethanol with scarce carbon production. RSC Advances 2012;2:2946.

[64]   Domínguez M, Taboada E, Molins E, Llorca J. Co-Fe-Si Aerogel Catalytic Honeycombs for Low Temperature Ethanol Steam Reforming. Catalysts 2012;2:386–99.

[65]   Espinal R, Taboada E, Molins E, Chimentao RJ, Medina F, Llorca J. Cobalt hydrotalcites as catalysts for bioethanol steam reforming. The promoting effect of potassium on catalyst activity and long-term stability. Applied Catalysis B: Environmental 2012;127:59–67.

[66]   Espinal R, A. Anzola, E. Adrover, E. Lopez, R. Chimentao, F. Medina, et al. Ethanol steam reforming in a catalitic membrane reactor loaded with a hydrotalcite-derived cobalt catalyst. 11th International Conference on catalysis in Membrane Reactors ICCMR11, 2013.

[67]   Murakami M, Matsuda T. Metal-catalysed cleavage of carbon-carbon bonds. Chemical Communications (Cambridge, England) 2011;47:1100–5.

[68]   Vinci A, Chiodo V, Papageridis K, Cavallaro S, Freni S, Tsiakaras P, et al. Ethanol Steam Reforming in a Two-Step Process . Short-Time Feasibility Tests. ENERGY & FUELS 2013:1570–5.

[69]   Zhang C, Yue H, Huang Z, Li S, Wu G, Gong J. Hydrogen Production via Steam Reforming of Ethanol on Phyllosilicate-Derived Ni/SiO 2 : Enhanced Metal − Support Interaction and Catalytic Stability. ACS Sustainable Chemistry and Engineering 2013:161–73.

[70]   Xu W, Liu Z, Johnston-peck AC, Senanayake SD, Zhou G, Stacchiola D, et al. Steam Reforming of Ethanol on Ni/CeO 2 : Reaction Pathway and Interaction between Ni and the CeO 2 Support. Catalysts 2013:975–84.

[71]   Cerritos C, Ramírez RF, Alvarado AFA, Rosales JMM, García V, Esquivel IRG. Steam Reforming of Ethanol over Ni/Al2O3-La2O3 Catalysts Synthesized by Sol-

Gel. I & EC Research 2011;50:2576–84.

[72]   Li S, Li M, Zhang C, Wang S, Ma X, Gong J. Steam reforming of ethanol over Ni/ZrO2 catalysts: Effect of support on product distribution. International Journal of Hydrogen Energy 2012;37:2940–9.

[73]   Laosiripojana N, Assabumrungrat S. Catalytic steam reforming of ethanol over high surface area CeO2: The role of CeO2 as an internal pre-reforming catalyst. Applied Catalysis B: Environmental 2006;66:29–39.

[74]   Chen SQ, Li YD, Liu Y, Bai X. Regenerable and durable catalyst for hydrogen production from ethanol steam reforming. International Journal of Hydrogen Energy 2011;36:5849–56.

[75]   Youn MH, Seo JG, Kim P, Kim JJ, Lee H-I, Song IK. Hydrogen production by auto-thermal reforming of ethanol over Ni/γ-Al2O3 catalysts: Effect of second metal addition. Journal of Power Sources 2006;162:1270–4.

[76]   Youn MH, Seo JG, Kim P, Song IK. Role and effect of molybdenum on the performance of Ni-Mo/γ-Al2O3 catalysts in the hydrogen production by auto-thermal reforming of ethanol. Journal of Molecular Catalysis A: Chemical 2007;261:276–81.

[77]   Vizcaino A, Arena P, Baronetti G, Carrero A, Calles J, Laborde M, et al. Ethanol steam reforming on Ni/Al2O3 catalysts: Effect of Mg addition. International Journal of Hydrogen Energy 2008;33:3489–92.

[78]   Özkan G, Gök S, Özkan G. Active carbon-supported Ni, Ni/Cu and Ni/Cu/Pd catalysed steam reforming of ethanol for the production of hydrogen. Chemical Engineering Journal 2011;171:1270–5.

[79]   Sanchezsanchez M, Navaro R, Fierro J. Ethanol steam reforming over Ni/La–Al2O3 catalysts: Influence of lanthanum loading. Catalysis Today 2007;129:336–45.

[80]   Vizcaino A, Arena P, Baronetti G, Carrero A, Calles J, Laborde M, et al. Ethanol steam reforming on Ni/Al2O3 catalysts: Effect of Mg addition. International Journal of Hydrogen Energy 2008;33:3489–92.

[81]   Hernández IP, Gochi-Ponce Y, Contreras Larios JL, Fernández AM. Steam reforming of ethanol over nickel-tungsten catalyst. International Journal of Hydrogen Energy 2010;35:12098–104.

[82]   Barroso MN, Gomez MF, Arrúa LA, Abello MC. Reactivity of aluminum spinels in the ethanol steam reforming reaction. Catalysis Letters 2006;109:13–9.

[83]   Galetti AE, Barroso MN, Gomez MF, Arrua L a., Monzón A, Abello MC. Promotion of Ni/MgAl2O4 catalysts with rare earths for the ethanol steam reforming reaction. Catalysis Letters 2012;142:1461–9.

[84]   Biswas P, Kunzru D. Steam reforming of ethanol on Ni-CeO2-ZrO2 catalysts:

Effect of doping with copper, cobalt and calcium. Catalysis Letters 2007;118:36–49.

[85]   Yang Y, Ma J, Wu F. Production of hydrogen by steam reforming of ethanol over a Ni/ZnO catalyst. International Journal of Hydrogen Energy 2006;31:877–82.

[86]   de Souza G, Ávila VC, Marcílio NR, Perez-Lopez OW. Synthesis Gas Production by Steam Reforming of Ethanol over M-Ni-Al Hydrotalcite-type Catalysts; M=Mg, Zn, Mo, Co. Procedia Engineering 2012;42:1805–15.

[87]   Idriss H, Scott M, Llorca J, Chan SC, Chiu W, Sheng P-Y, et al. A phenomenological study of the metal-oxide interface: the role of catalysis in hydrogen production from renewable resources. ChemSusChem 2008;1:905–10.

[88]   Dömök M, Oszkó a., Baán K, Sarusi I, Erdőhelyi a. Reforming of ethanol on Pt/Al2O3-ZrO2 catalyst. Applied Catalysis A: General 2010;383:33–42.

[89]   Ciambelli P, Palma V, Ruggiero A. Low temperature catalytic steam reforming of ethanol. 2. Preliminary kinetic investigation of Pt/CeO2 catalysts. Applied Catalysis B: Environmental 2010;96:190–7.

[90]   Palma V, Castaldo F, Ciambelli P, Iaquaniello G. CeO2-supported Pt/Ni catalyst for the renewable and clean H2 production via ethanol steam reforming. Applied Catalysis B: Environmental 2014;145:73–84.

[91]   Goula MA, Kontou SK, Tsiakaras PE. Hydrogen production by ethanol steam reforming over a commercial Pd/γ-Al2O3 catalyst. Applied Catalysis B: Environmental 2004;49:135–44.

[92]   Auprêtre F, Descorme C, Duprez D. Bio-ethanol catalytic steam reforming over supported metal catalysts. Catalysis Communications 2002;3:263–7.

[93]   Chen Meng Nan, Zhang Dong-Yun, Thompson Levi T, Ma Zi-Feng. Hydrogen Production from Steam Reforming of Ethanol over Pd Promoted ZnO/Al2 O3 Catalysts. Acta Phys -Chim Sin 2011;27:2185–90.

[94]   Ramos IAC, Montini T, Lorenzut B, Troiani H, Gennari FC, Graziani M, et al. Hydrogen production from ethanol steam reforming on M/CeO2/YSZ (M=Ru, Pd, Ag) nanocomposites. Catalysis Today 2012;180:96–104.

[95]   Qi Wang, Long Guo XBL. Steam Reforming of Model Compounds from Bio-Oil for Hydrogen Production over Pd/HZSM-5 Catalyst. In: Zili Liu FP and XL, editor. Advances in Chemical Engineering II, vol. 550-533, Advances in Chemical Engineering II; 2012, p. 558–62.

[96]   Frusteri F, Freni S, Spadaro L, Chiodo V, Bonura G, Donato S, et al. H2 production for MC fuel cell by steam reforming of ethanol over MgO supported Pd, Rh, Ni and Co catalysts. Catalysis Communications 2004;5:611–5.

[97]   Alonso CG, Furtado AC, Cantão MP, Santos OAA Dos, Fernandes-Machado NRC. Temperature Effect on Hydrogen Production from Reactions between Ethanol and

Steam in the Presence of Pd-Ru/Nb2O5-TiO2 Catalyst. International Journal of Chemical Reactor Engineering 2009;7:1542–6580.

[98]   Birot A, Epron F, Descorme C, Duprez D. Ethanol steam reforming over Rh/CexZr1−xO2 catalysts: Impact of the CO–CO2–CH4 interconversion reactions on the H2 production. Applied Catalysis B: Environmental 2008;79:17–25.

[99]   Roh HS, Wang Y, King DL, Platon A, Chin YH. Low temperature and H2 selective catalysts for ethanol steam reforming. Catalysis Letters 2006;108:15–9.

[100]   Karim AM, Su Y, Sun J, Yang C, Strohm JJ, King DL, et al. A comparative study between Co and Rh for steam reforming of ethanol. Applied Catalysis B: Environmental 2010;96:441–8.

[101]   Huang L, Choong C, Chen L, Wang Z, Zhong Z, Campos- Cuerva C JL. Monometallic Carbonyl-Derived CeO2-Supported Rh and Co Bicomponent Catalysts for CO-Free, High-Yield H2 Generation from Low-Temperature Ethanol Steam Reforming. CHEMCATCHEM CATALYSIS 2013;5:220–34.

[102]   Kawi X, Sibudjing W. Steam reforming of ethanol to H2 over Rh/Y2O3: crucial roles of Y2O3 oxidizing ability, space velocity, and H2/C. Energy & Environmental Science 2010;3:334–42.

[103]   Chen L, Choong CKS, Zhong Z, Huang L, Ang TP, Hong L, et al. Carbon monoxide-free hydrogen production via low-temperature steam reforming of ethanol over iron-promoted Rh catalyst. Journal of Catalysis 2010;276:197–200.

[104]   Le Valant A, Bion N, Can F, Duprez D, Epron F. Preparation and characterization of bimetallic Rh-Ni/Y2O3-Al2O3 for hydrogen production by raw bioethanol steam reforming: influence of the addition of nickel on the catalyst performances and stability. Applied Catalysis B: Environmental 2010;97:72–81.

[105]   da Silva AM, de Souza KR, Jacobs G, Graham UM, Davis BH, Mattos L V., et al. Steam and CO2 reforming of ethanol over Rh/CeO2 catalyst. Applied Catalysis B: Environmental 2011;102:94–109.

[106]   Peela NR, Mubayi A, Kunzru D. Steam reforming of ethanol over Rh/CeO2/Al2O3 catalysts in a microchannel reactor. Chemical Engineering Journal 2011;167:578–87.

[107]   Wanat EC, Venkataraman K, Schmidt LD. Steam reforming and water–gas shift of ethanol on Rh and Rh–Ce catalysts in a catalytic wall reactor. Applied Catalysis A: General 2004;276:155–62.

[108]   Moura JS, Souza MOG, Bellido JDA, Assaf EM, Opportus M, Reyes P, et al. Ethanol steam reforming over rhodium and cobalt-based catalysts: Effect of the support. International Journal of Hydrogen Energy 2012;37:3213–24.

[109]   Churakova EM, Badmaev SD, Snytnikov P V., Gubanov a. I, Filatov EY, Plyusnin PE, et al. Bimetallic Rh-Co/ZrO2 catalysts for ethanol steam reforming into hydrogen-containing gas. Kinetics and Catalysis 2010;51:893–7.

[110]   Gucciardi E, Chiodo V, Freni S, Cavallaro S, Galvagno a., Bart JCJ. Ethanol and dimethyl ether steam reforming on Rh/Al2O3 catalysts for high-temperature fuel-cell feeds. Reaction Kinetics, Mechanisms and Catalysis 2011;104:75–87.

[111]   Cobo M, Pieruccini D, Abello R, Ariza L, Córdoba LF, Conesa J a. Steam reforming of ethanol over bimetallic RhPt/La2O3: Long-term stability under favorable reaction conditions. International Journal of Hydrogen Energy 2013;38:5580–93.

[112]   Cavallaro S. Ethanol Steam Reforming on Rh/Al2O3 Catalysts. Energy & Fuels 2000;14:1195–9.

[113]   Breen J., Burch R, Coleman H. Metal-catalysed steam reforming of ethanol in the production of hydrogen for fuel cell applications. Applied Catalysis B: Environmental 2002;39:65–74.

[114]   Romero-Sarria F, Vargas JC, Roger A-C, Kiennemann A. Hydrogen production by steam reforming of ethanol. Catalysis Today 2008;133-135:149–53.

[115]   Liguras DK, Kondarides DI, Verykios XE. Production of hydrogen for fuel cells by steam reforming of ethanol over supported noble metal catalysts. Applied Catalysis B: Environmental 2003;43:345–54.

[116]   Sundararajan D, Azad A-M. Cooperative Synergy in Nanoscale Ceria-Based Systems. Science of Advanced Materials 2011;3:739–62.

[117]   Basile A. Hydrogen Production Using Pd-based Membrane Reactors for Fuel Cells. Topics in Catalysis 2008;51:107–22.

[118]   Mendes D, Tosti S, Borgognoni F, Mendes A, Madeira LM. Integrated analysis of a membrane-based process for hydrogen production from ethanol steam reforming. Catalysis Today 2010;156:107–17.

[119]   Montané D, Bolshak E, Abelló S. Thermodynamic analysis of fuel processors based on catalytic-wall reactors and membrane systems for ethanol steam reforming. Chemical Engineering Journal 2011;175:519–33.

[120]   Hedayati A, Le Corre O, Lacarrière B, Llorca J. Exergetic study of catalytic steam reforming of bio-ethanol over Pd–Rh/CeO2 with hydrogen purification in a membrane reactor. International Journal of Hydrogen Energy 2015;40:3574–81.

[121]   Ward TL, Dao T. Model of hydrogen permeation behavior in palladium membranes. Journal of Membrane Science 1999;153:211–31.

[122]   Koros WJ, Fleming GK. Membrane-based gas separation. Journal of Membrane Science 1993;83:1–80.

[123]   Al-Mufachi NA, Rees NV, Steinberger-Wilkens R. Hydrogen selective membranes: A review of palladium-based dense metal membranes. Renewable and Sustainable Energy Reviews 2015;47:540–51.

[124] Gao H, Lin YS, Li Y, Zhang B. Chemical Stability and Its Improvement of Palladium-Based Metallic Membranes. Industrial & Engineering Chemistry Research 2004;43:6920–30.

[125] Burkhanov GS, Gorina NB, Kolchugina NB, Roshan NR, Slovetsky DI, Chistov EM. Palladium-Based Alloy Membranes for Separation of High Purity Hydrogen from Hydrogen-Containing Gas Mixtures. Platinum Metals Review 2011;55:3–12.

[126] Uemiya S. Brief Review of Steam Reforming Using a Metal Membrane Reactor. Topics in Catalysis 2004;29:79–84.

[127] Tosti S, Bettinali L. Diffusion bonding of pd-ag rolled membranes. Journal of Materials Science 2004;39:3041–6.

[128] Tosti S, Basile A, Bettinali L, Borgognoni F, Chiaravalloti F, Gallucci F. Long-term tests of Pd–Ag thin wall permeator tube. Journal of Membrane Science 2006;284:393–7.

[129] Iulianelli A, Basile A. Hydrogen production from ethanol via inorganic membrane reactors technology: a review. Catalysis Science & Technology 2011;1:366.

[130] Gallucci F, Basile A, Tosti S, Iulianelli A, Drioli E. Methanol and ethanol steam reforming in membrane reactors: An experimental study. International Journal of Hydrogen Energy 2007;32:1201–10.

[131] Basile A, Gallucci F, Iulianelli A, Tosti S. CO-Free Hydrogen Production by Ethanol Steam Reforming in a Pd–Ag Membrane Reactor. Fuel Cells 2008;8:62–8.

[132] Basile, A.; Gallucci, F.; Iulianelli, A.; De Falco, M.; Liguori S. Hydrogen Production by Ethanol Steam Reforming: Experimental Study of a Pd-Ag Membrane Reactor and Traditional Reactor Behaviour. International Journal of Chemical Reactor Engineering 2008;6:1542–6580.

[133] Tosti S, Basile A, Borgognoni F, Capaldo V, Cordiner S, Di Cave S, et al. Low temperature ethanol steam reforming in a Pd-Ag membrane reactorPart 1: Ru-based catalyst. Journal of Membrane Science 2008;308:250–7.

[134] Tosti S, Basile A, Borgognoni F, Capaldo V, Cordiner S, Di Cave S, et al. Low-temperature ethanol steam reforming in a Pd–Ag membrane reactorPart 2. Pt-based and Ni-based catalysts and general comparison. Journal of Membrane Science 2008;308:258–63.

[135] Tosti S, Basile A, Borelli R, Borgognoni F, Castelli S, Fabbricino M, et al. Ethanol steam reforming kinetics of a Pd–Ag membrane reactor. International Journal of Hydrogen Energy 2009;34:4747–54.

[136] Tosti S, Fabbricino M, Moriani A, Agatiello G, Scudieri C, Borgognoni F, et al. Pressure effect in ethanol steam reforming via dense Pd-based membranes. Journal of Membrane Science 2011;377:65–74.

[137]   Iulianelli A, Longo T, Liguori S, Seelam PK, Keiski RL, Basile A. Oxidative steam reforming of ethanol over Ru–Al2O3 catalyst in a dense Pd–Ag membrane reactor to produce hydrogen for PEM fuel cells. International Journal of Hydrogen Energy 2009;34:8558–65.

[138]   Borgognoni F, Tosti S, Vadrucci M, Santucci A. Combined methane and ethanol reforming for pure hydrogen production through Pd-based membranes. International Journal of Hydrogen Energy 2013;38:1430–8.

[139]   Iulianelli A, Basile A. An experimental study on bio-ethanol steam reforming in a catalytic membrane reactor. Part I: Temperature and sweep-gas flow configuration effects. International Journal of Hydrogen Energy 2010;35:3170–7.

[140]   Iulianelli A, Liguori S, Longo T, Tosti S, Pinacci P, Basile A. An experimental study on bio-ethanol steam reforming in a catalytic membrane reactor. Part II: Reaction pressure, sweep factor and WHSV effects. International Journal of Hydrogen Energy 2010;35:3159–64.

[141]   Basile A, Pinacci P, Iulianelli A, Broglia M, Drago F, Liguori S, et al. Ethanol steam reforming reaction in a porous stainless steel supported palladium membrane reactor. International Journal of Hydrogen Energy 2011;36:2029–37.

[142]   Seelam PK, Liguori S, Iulianelli A, Pinacci P, Calabrò V, Huuhtanen M, et al. Hydrogen production from bio-ethanol steam reforming reaction in a Pd/PSS membrane reactor. Catalysis Today 2012;193:42–8.

[143]   Papadias DD, Lee SHD, Ferrandon M, Ahmed S. An analytical and experimental investigation of high-pressure catalytic steam reforming of ethanol in a hydrogen selective membrane reactor. International Journal of Hydrogen Energy 2010;35:2004–17.

[144]   Iulianelli A, Liguori S, Vita A, Italiano C, Fabiano C, Huang Y, et al. The oncoming energy vector: Hydrogen produced in Pd-composite membrane reactor via bioethanol reforming over Ni/CeO2 catalyst. Catalysis Today 2015;IN PRESS.

[145]   Janas D, Kreft SK, Koziol KKK. Steam reforming on reactive carbon nanotube membranes. Journal of Industrial and Engineering Chemistry 2015;25:222–8.

[146]   Murmura MA, Patrascu M, Annesini MC, Palma V, Ruocco C, Sheintuch M. Directing selectivity of ethanol steam reforming in membrane reactors. International Journal of Hydrogen Energy 2015;40:5837–48.

[147]   da Silva AM, Mattos L V., Múnera J, Lombardo E, Noronha FB, Cornaglia L. Study of the performance of Rh/La2O3–SiO2 and Rh/CeO2 catalysts for SR of ethanol in a conventional fixed-bed reactor and a membrane reactor. International Journal of Hydrogen Energy 2015;40:4154–66.

[148]   Yu C-Y, Lee D-W, Park S-J, Lee K-Y, Lee K-H. Ethanol steam reforming in a membrane reactor with Pt-impregnated Knudsen membranes. Applied Catalysis B: Environmental 2009;86:121–6.

[149]   Yu C-Y, Lee D-W, Park S-J, Lee K-Y, Lee K-H. Study on a catalytic membrane reactor for hydrogen production from ethanol steam reforming. International Journal of Hydrogen Energy 2009;34:2947–54.

[150]   Lim H, Gu Y, Oyama ST. Reaction of primary and secondary products in a membrane reactor: Studies of ethanol steam reforming with a silica–alumina composite membrane. Journal of Membrane Science 2010;351:149–59.

[151]   Lim H, Gu Y, Oyama ST. Studies of the effect of pressure and hydrogen permeance on the ethanol steam reforming reaction with palladium- and silica-based membranes. Journal of Membrane Science 2012;396:119–27.

[152]   Yun S, Lim H, Ted Oyama S. Experimental and kinetic studies of the ethanol steam reforming reaction equipped with ultrathin Pd and Pd–Cu membranes for improved conversion and hydrogen yield. Journal of Membrane Science 2012;409-410:222–31.

[153]   Zhu N, Dong X, Liu Z, Zhang G, Jin W, Xu N. Toward highly-effective and sustainable hydrogen production: bio-ethanol oxidative steam reforming coupled with water splitting in a thin tubular membrane reactor. Chemical Communications (Cambridge, England) 2012;48:7137–9.

[154]   Rahman MA, García-García FR, Li K. On-board H2 generation by a catalytic hollow fibre microreactor for portable device applications. Catalysis Communications 2011;16:128–32.

[155]   Rahman MA, García-García FR, Li K. Development of a catalytic hollow fibre membrane microreactor as a microreformer unit for automotive application. Journal of Membrane Science 2012;390-391:68–75.

[156]   Amandusson H, Ekedahl L-G, Dannetun H. The effect of CO and O2 on hydrogen permeation through a palladium membrane. Applied Surface Science 2000;153:259–67.

[157]   Catalano J, Giacinti Baschetti M, Sarti GC. Influence of the gas phase resistance on hydrogen flux through thin palladium–silver membranes. Journal of Membrane Science 2009;339:57–67.

[158]   Coroneo M, Montante G, Catalano J, Paglianti A. Modelling the effect of operating conditions on hydrodynamics and mass transfer in a Pd–Ag membrane module for H2 purification. Journal of Membrane Science 2009;343:34–41.

[159]   Gallucci F, Chiaravalloti F, Tosti S, Drioli E, Basile A. The effect of mixture gas on hydrogen permeation through a palladium membrane: Experimental study and theoretical approach. International Journal of Hydrogen Energy 2007;32:1837–45.

[160]   Israni SH, Harold MP. Methanol steam reforming in single-fiber packed bed Pd–Ag membrane reactor: Experiments and modeling. Journal of Membrane Science 2011;369:375–87.

[161]   Li A, Liang W, Hughes R. The effect of carbon monoxide and steam on the hydrogen permeability of a Pd/stainless steel membrane. Journal of Membrane Science 2000;165:135–41.

[162]   Nekhamkina O, Sheintuch M. Effective approximations for concentration-polarization in Pd-membrane separators. Chemical Engineering Journal 2015;260:835–45.

[163]   Peters T a., Stange M, Klette H, Bredesen R. High pressure performance of thin Pd-23%Ag/stainless steel composite membranes in water gas shift gas mixtures; influence of dilution, mass transfer and surface effects on the hydrogen flux. Journal of Membrane Science 2008;316:119–27.

[164]   Unemoto A, Kaimai A, Sato K, Otake T, Yashiro K, Mizusaki J, et al. The effect of co-existing gases from the process of steam reforming reaction on hydrogen permeability of palladium alloy membrane at high temperatures. International Journal of Hydrogen Energy 2007;32:2881–7.

[165]   Catalano J, Giacinti Baschetti M, Sarti GC. Hydrogen permeation in palladium-based membranes in the presence of carbon monoxide. Journal of Membrane Science 2010;362:221–33.

[166]   Barbieri G, Scura F, Lentini F, Deluca G, Drioli E. A novel model equation for the permeation of hydrogen in mixture with carbon monoxide through Pd–Ag membranes. Separation and Purification Technology 2008;61:217–24.

[167]   Mejdell AL, Chen D, Peters TA, Bredesen R, Venvik HJ. The effect of heat treatment in air on CO inhibition of a ~3μm Pd–Ag (23wt.%) membrane. Journal of Membrane Science 2010;350:371–7.

[168]   Sanz R, Calles JA, Alique D, Furones L. H2 production via water gas shift in a composite Pd membrane reactor prepared by the pore-plating method. International Journal of Hydrogen Energy 2014;39:4739–48.

[169]   Catalano J, Giacinti Baschetti M, Sarti GC. Influence of water vapor on hydrogen permeation through 2.5 μm Pd–Ag membranes. International Journal of Hydrogen Energy 2011;36:8658–73.

[170]   Barreiro MM, Maroño M, Sánchez JM. Hydrogen permeation through a Pd-based membrane and RWGS conversion in H2/CO2, H2/N2/CO2 and H2/H2O/CO2 mixtures. International Journal of Hydrogen Energy 2014;39:4710–6.

[171]   Gielens FC, Knibbeler RJJ, Duysinx PFJ, Tong HD, Vorstman MAG, Keurentjes JTF. Influence of steam and carbon dioxide on the hydrogen flux through thin Pd/Ag and Pd membranes. Journal of Membrane Science 2006;279:176–85.

[172]   Hou K, Hughes R. The effect of external mass transfer, competitive adsorption and coking on hydrogen permeation through thin Pd/Ag membranes. Journal of Membrane Science 2002;206:119–30.

[173]   Patrascu M, Sheintuch M. On-site pure hydrogen production by methane steam reforming in high flux membrane reactor: Experimental validation, model predictions and membrane inhibition. Chemical Engineering Journal 2015;262:862–74.

[174]   Cornaglia L, Múnera J, Lombardo E. Recent advances in catalysts, palladium alloys and high temperature WGS membrane reactors. International Journal of Hydrogen Energy 2015;40:3423–37.

[175]   Casanovas A, de Leitenburg C, Trovarelli A, Llorca J. Catalytic monoliths for ethanol steam reforming. Catalysis Today 2008;138:187–92.

[176]   Heck RM, Gulati S, Farrauto RJ. The application of monoliths for gas phase catalytic reactions. Chemical Engineering Journal 2001;82:149–56.

[177]   López E, Divins NJ, Anzola A, Schbib S, Borio D, Llorca J. Ethanol steam reforming for hydrogen generation over structured catalysts. International Journal of Hydrogen Energy 2013;38:4418–28.

[178]   Espinal R, Anzola A, Adrover E, Roig M, Chimentao R, Medina F, et al. Durable ethanol steam reforming in a catalytic membrane reactor at moderate temperature over cobalt hydrotalcite. International Journal of Hydrogen Energy 2014;39:10902–10.

[179] Reb Research & Consulting, accessed on 2015-09-23, http://www.rebresearch.com/ 2015.

[180]   Chen W-H, Hsu P-C, Lin B-J. Hydrogen permeation dynamics across a palladium membrane in a varying pressure environment. International Journal of Hydrogen Energy 2010;35:5410–8.

[181]   Rossi A, Lamonaca G, Santucci A, Tosti S. Validation of a dynamic model of hydrogen permeation through Pd-based membranes. International Journal of Greenhouse Gas Control 2011;5:521–30.

[182]   Chen W-H, Hsu P-C. Hydrogen permeation measurements of Pd and Pd–Cu membranes using dynamic pressure difference method. International Journal of Hydrogen Energy 2011;36:9355–66.

[183]   Adrian bejan, George Tsatsarnois MM. Thermal Design and optimization.pdf. New York, USA: John Wiley; 1996.

[184]   Sato N. Chemical Energy and Exergy. Amsterdam: Elsevier Science & Technology Books; 2004.

[185]   Khila Z, Hajjaji N, Pons M-N, Renaudin V, Houas A. A comparative study on energetic and exergetic assessment of hydrogen production from bioethanol via steam reforming, partial oxidation and auto-thermal reforming processes. Fuel Processing Technology 2013;112:19–27.

[186] Casas-Ledón Y, Arteaga-Perez LE, Morales-Perez MC, Peralta-Suárez LM. Thermodynamic Analysis of the Hydrogen Production from Ethanol: First and Second Laws Approaches. ISRN Thermodynamics 2012:1–8.

[187] Kalinci Y, Hepbasli A, Dincer I. Efficiency assessment of an integrated gasifier/boiler system for hydrogen production with different biomass types. International Journal of Hydrogen Energy 2010;35:4991–5000.

[188] Modarresi A, Wukovits W, Friedl A. Application of exergy balances for evaluation of process configurations for biological hydrogen production. Applied Thermal Engineering 2010;30:70–6.

[189] Simpson AP, Lutz A. Exergy analysis of hydrogen production via steam methane reforming. International Journal of Hydrogen Energy 2007;32:4811–20.

[190] Tippawan P, Arpornwichanop A. Energy and exergy analysis of an ethanol reforming process for solid oxide fuel cell applications. Bioresource Technology 2014;157:231–9.

[191] Cohce MK, Dincer I, Rosen M a. Energy and exergy analyses of a biomass-based hydrogen production system. Bioresource Technology 2011;102:8466–74.

[192] Hinderink AP, Kerkhof FPJM, Lie ABK, De Swaan Arons J, Van Der Kooi HJ. Exergy analysis with a flowsheeting simulator—I. Theory; calculating exergies of material streams. Chemical Engineering Science 1996;51:4693–700.

[193] Montané D, Bolshak E, Abelló S. Thermodynamic analysis of fuel processors based on catalytic-wall reactors and membrane systems for ethanol steam reforming. Chemical Engineering Journal 2011;175:519–33.

[194] Wu Y-J, Li P, Yu J-G, Cunha AF, Rodrigues AE. Sorption-enhanced steam reforming of ethanol on NiMgAl multifunctional materials: Experimental and numerical investigation. Chemical Engineering Journal 2013;231:36–48.

[195] He L, Manuel J, Parra S, Blekkan EA, Chen D. Towards efficient hydrogen production from glycerol by sorption enhanced steam reforming. Energy & Environmental Science 2010;3:253.

[196] Llorca J, Hedayati A. Alcohols and Bio-alcohols Steam and Autothermal Reforming in a Membrane Reactor. In: Angelo Basile, Dalena F, editors. Alcohols and Bioalcohols: Characteristics, Production and Uses, New York, USA: NOVA Publication; 2014, p. 181–204.

[197] Bej B, Pradhan NC, Neogi S. Production of hydrogen by steam reforming of ethanol over alumina supported nano-NiO/SiO2 catalyst. Catalysis Today 2014;237:80–8.

[198] Wang F, Cai W, Descorme C, Provendier H, Shen W, Mirodatos C, et al. From mechanistic to kinetic analyses of ethanol steam reforming over Ir/CeO2 catalyst. International Journal of Hydrogen Energy 2014;39:18005–15.

[199]   López E, Divins NJ, Anzola A, Schbib S, Borio D, Llorca J. Ethanol steam reforming for hydrogen generation over structured catalysts. International Journal of Hydrogen Energy 2013;38:4418–28.

[200]   Gallucci F, Defalco M, Tosti S, Marrelli L, Basile A. Co-current and counter-current configurations for ethanol steam reforming in a dense Pd–Ag membrane reactor. International Journal of Hydrogen Energy 2008;33:6165–71.

[201]   Hla SS, Morpeth LD, Dolan MD. Modelling and experimental studies of a water-gas shift catalytic membrane reactor. Chemical Engineering Journal 2015;276:289–302.

[202]   Basile A, Curcio S, Bagnato G, Liguori S, Jokar SM, Iulianelli A. Water gas shift reaction in membrane reactors: Theoretical investigation by artificial neural networks model and experimental validation. International Journal of Hydrogen Energy 2015;40:5897–906.

[203]   Sanz R, Calles JA, Alique D, Furones L, Ordóñez S, Marín P. Hydrogen production in a Pore-Plated Pd-membrane reactor: Experimental analysis and model validation for the Water Gas Shift reaction. International Journal of Hydrogen Energy 2015;40:3472–84.

[204]   Dong X, Wang H, Rui Z, Lin YS. Tubular dual-layer MFI zeolite membrane reactor for hydrogen production via the WGS reaction: Experimental and modeling studies. Chemical Engineering Journal 2015;268:219–29.

[205]   Chein RY, Chen YC, Chyou YP, Chung JN. Three-dimensional numerical modeling on high pressure membrane reactors for high temperature water-gas shift reaction. International Journal of Hydrogen Energy 2014;39:15517–29.

[206]   Di Marcoberardino G, Sosio F, Manzolini G, Campanari S. Fixed bed membrane reactor for hydrogen production from steam methane reforming: Experimental and modeling approach. International Journal of Hydrogen Energy 2015;40:7559–67.

[207]   Iulianelli A, Liguori S, Huang Y, Basile A. Model biogas steam reforming in a thin Pd-supported membrane reactor to generate clean hydrogen for fuel cells. Journal of Power Sources 2015;273:25–32.

[208]   Zhang C, Liu Z, Zhou W, Chan SH, Wang Y. Dynamic performance of a high-temperature PEM fuel cell – An experimental study. Energy 2015;90:1949–55.

[209]   García VM, López E, Serra M, Llorca J. Dynamic modeling of a three-stage low-temperature ethanol reformer for fuel cell application. Journal of Power Sources 2009;192:208–15.

[210]   García VM, López E, Serra M, Llorca J, Riera J. Dynamic modeling and controllability analysis of an ethanol reformer for fuel cell application. International Journal of Hydrogen Energy 2010;35:9768–75.

[211]   Funke M, Kühl H-D, Faulhaber S, Pawlik J. A dynamic model of the fuel processor

for a residential PEM fuel cell energy system. Chemical Engineering Science 2009;64:1860–7.

[212]   Jahn H-J, Schroer W. Dynamic simulation model of a steam reformer for a residential fuel cell power plant. Journal of Power Sources 2005;150:101–9.

[213]   Stamps AT, Gatzke EP. Dynamic modeling of a methanol reformer—PEMFC stack system for analysis and design. Journal of Power Sources 2006;161:356–70.

[214]   Kvamsdal HM, Svendsen HF, Olsvik O, Hertzberg T. Dynamic simulation and optimization of a catalytic steam reformer. Chemical Engineering Science 1999;54:2697–706.

[215]   Lin S, Chen Y, Yu C, Liu Y, Lee C. Dynamic modeling and control structure design of an experimental fuel processor. International Journal of Hydrogen Energy 2006;31:413–26.

[216]   Tsourapas V, Sun J, Nickens A. Modeling and dynamics of an autothermal JP5 fuel reformer for marine fuel cell applications. Energy 2008;33:300–10.

[217]   Jakobsen, A. H. Chemical Reactor Modeling: Multiphase Reactive Flows. 2nd ed. London: Springer; 2014.

[218]   Bell S. A Beginner's Guide to Uncertainty of Measurement 1999:33.

[219]   Evaluation of measurement data — Guide to the expression of uncertainty in measurement. JCGM publications; 2008.

Appendix A – Uncertainty Analysis

Reporting the measurement results is complete only when it is accompanied with uncertainty analysis. Because of inevitable errors during a measurement, a range of uncertainty is given to indicate a specific margin of doubt during which the measurement can be reliable. In fact, uncertainty of measurement states the doubt about the measurement results, and it differs from measurement error, which is the difference between the true value and the measured one.

In this work, uncertainty analysis is presented for experimental results and exergetic evaluation of the reforming system. Uncertainty of the measurement is rooted in the measuring instrument and the operator who is measuring a property. Accordingly, the uncertainty is calculated taking into account two sources of errors:

- Human error: the error in reading values during fuel blend preparation (water + ethanol) and measurement of several experimental properties and results through experiments in the laboratory
- Error in laboratory equipment: beakers, graduated cylinder, flask, and so on, used in the preparation of fuel mixtures, together with the mass flow meters, the pressure valves, and specially the Gas Chromatograph.

The human error is considered in two stages. Firstly, the preparation of the fuel mixture where specific volume of water had to be mixed with a specific volume of ethanol to obtain a specific S/C ratio. It is assumed that a maximum human error of $\pm$ 0.5 ml is inevitable when measuring the value of the volume of the liquids by means of a graduated cylinder. Secondly, since the waste gas flow rate (retentate) is measured by mean of a bubble meter and a stopwatch, a human error of ± 1 ml is considered in reading the volume of the gas, which has passed a certain volume of the bubble meter in a specific time.

The errors of laboratory measurement equipment are listed as:

- Selectivity of the gases measured by Gas Chromatograph (GC): $\pm 5\%$ absolute
- Mass flow meter of the pure hydrogen stream: ± 1.5 ml/min $= \pm 10^{-6}$ mole/s

When the measured value by an instrument lies in a certain and known domain ($\pm a$), the uncertainty of the measurement is calculated as [218,219]:

$$u(c) = \frac{a}{\sqrt{3}}$$
A1

Where u(c) is the standard uncertainty of the measured value. This is applicable in the case of the GC and mass flow meter of pure hydrogen.

In the case of the retentate flow rate measurement, for every experimental point (certain temperature, pressure, S/C ratio, and fuel flow rate), 5 measurements were carried out and the arithmetic mean value of the measurements was used for experimental evaluation purposes:

$$\bar{X}_i = \frac{1}{n}\sum_{j=1}^{n} X_j \qquad\qquad A2$$

$\bar{X}_i$ is the arithmetic mean of the 5 measurements (n=5) of X_j (retentate flow rate). Then, the variance of the probability distribution of X_j is:

$$S^2(X_i) = \frac{1}{n-1}\sum_{j=1}^{n}(X_j - \bar{X}_i)^2 \qquad\qquad A3$$

The variance of the mean is given as:

$$S^2(\bar{X}_i) = \frac{S^2(X_i)}{n} \qquad\qquad A4$$

Finally, the standard uncertainty is obtained:

$$u(X_i) = S(\bar{X}_i) \qquad\qquad A5$$

If an evaluation equation (y) is considered as a function of the independent measured factors:

$$Y = f(x_1, x_2, x_3, \ldots x_n) \qquad\qquad A6$$

The standard combined uncertainty ($u_c(y)$) is defined as:

$$u_c^2(y) = \sum_{i=1}^{n}\left(\frac{\partial f}{\partial x_i}\right)^2 u^2(x_i) \qquad\qquad A7$$

This method is used to calculate the uncertainty of several experimental and thermodynamic factors that are calculated by different formulations. The detailed analysis of the uncertainty analysis of the experimental and thermodynamic factors is given in the following sections.

A.1 The uncertainty of the experimental evaluation factors

$$Y_{H_2} = \frac{F_{H2.perm}}{6 \times F_{EtOH}} \qquad\qquad \text{Hydrogen yield} \qquad\qquad \text{A8}$$

$$R_{H_2} = \frac{F_{H2.perm}}{F_{H2.total}} \qquad\qquad \text{Hydrogen recovery} \qquad\qquad \text{A9}$$

$$\Theta_{H_2} = \frac{F_{H2.perm}}{F_{H2.in}} \qquad\qquad \text{Pure hydrogen efficiency} \qquad\qquad \text{A10}$$

'F' is the molar flow rate in mol/s. $F_{H2.total}$ represents the total hydrogen production rate via ESR in the CMR. Inlet hydrogen consists of the hydrogen content of the fuel mixture (water + ethanol). Therefore, the uncertainty of each equation is given:

A.1.1 Hydrogen yield

$$u^2(Y_{H_2}) = \left(\frac{\partial Y_{H2}}{\partial F_{H2.perm}}\right)^2 u^2(F_{H2.perm}) + \left(\frac{\partial Y_{H2}}{\partial F_{EtOH}}\right)^2 u^2(F_{EtOH}) \qquad\qquad \text{A11}$$

$$\frac{\partial Y_{H2}}{\partial F_{H2.perm}} = \frac{1}{6 \times F_{EtOH}} \qquad\qquad \text{A12}$$

$$\frac{\partial Y_{H2}}{\partial F_{EtOH}} = \frac{-F_{H2.perm}}{6 \times (F_{EtOH})^2} \qquad\qquad \text{A13}$$

The uncertainty of $F_{H2.pure}$ is the same as the uncertainty of the pure hydrogen mass flow measurement.

A.1.2 Hydrogen recovery

$$R_{H_2} = \frac{F_{H2.perm}}{F_{H2.total}} = \frac{F_{H2.perm}}{F_{H2.perm} + F_{H2.ret}} \qquad\qquad \text{A14}$$

$$\frac{\partial R_{H2}}{\partial F_{H2.perm}} = \frac{F_{H2.ret}}{(F_{H2.perm} + F_{H2.ret})^2} \qquad\qquad \text{A16}$$

$$\frac{\partial R_{H2}}{\partial F_{F_{H2.ret}}} = \frac{-F_{H2.perm}}{(F_{H2.perm} + F_{H2.ret})^2} \qquad\qquad \text{A17}$$

$$u^2(R_{H2}) = \left(\frac{\partial R_{H2}}{\partial F_{H2.perm}}\right)^2 u^2(F_{H2.perm}) + \left(\frac{\partial R_{H2}}{\partial F_{H2.ret}}\right)^2 u^2(F_{H2.ret}) \qquad\qquad \text{A18}$$

$F_{H2.ret}$ is the flow rate of unpermeated hydrogen which appears in the retentate stream. $u(F_{F_{H2.ret}})$ Itself is obtained separately through a similar method. The molar flow rate of CO_2, H_2, CH_4, and CO in the retentate stream is a function of the selectivity analysis done by the GC and the flow rate of the retentate gas measured by human by using a bubble meter. If the flow rate of the retentate is in ml/min and the selectivity of the retentate gas in percentage, then the molar flow rate of any gaseous product in mol/s is calculated as:

$$F_{\text{gas in ret}} = A \times F_{ret} \times S_{GC} \qquad \text{A19}$$

A is a constant value for each gas for the unit conversion, to obtain the flow rate of each gas in mol/s. $F_{\text{retentate}}$ represents the retentate flow rate (ml/min). S_{GC} is the selectivity of gas, in percent ($0 < S_{GC} < 100$). Knowing the uncertainty of the F_{ret} and S_{GC}:

$$u^2\left(F_{\text{gas in ret}}\right) = \left(\frac{\partial F_{\text{gas in ret}}}{\partial F_{ret}}\right)^2 u^2(F_{ret}) + \left(\frac{\partial F_{\text{gas in ret}}}{\partial S_{GC}}\right)^2 u^2(S_{GC}) \qquad \text{A20}$$

$$u^2\left(F_{\text{gas in ret}}\right) = A^2 S_{GC}{}^2 u^2(F_{ret}) + A^2 F_{ret}{}^2 u^2(S_{GC}) \qquad \text{A21}$$

A.1.3 Pure hydrogen efficiency

$$u^2\left(\Theta_{H_2}\right) = \left(\frac{\partial \theta}{\partial F_{H2.perm}}\right)^2 u^2\left(F_{H2.perm}\right) + \left(\frac{\partial \theta}{\partial F_{inlet\,H2}}\right)^2 u^2(F_{inlet\,H2}) \qquad \text{A22}$$

$$\frac{\partial \theta}{\partial F_{H2.perm}} = \frac{1}{F_{inlet\,H2}} \qquad \text{A23}$$

$$\frac{\partial \theta}{\partial F_{inlet\,H2}} = \frac{-F_{H2.perm}}{(F_{inlet\,H2})^2} \qquad \text{A24}$$

$$F_{inlet\,H2} = F_{H2O} + 3 \times F_{EtOH} \qquad \text{A25}$$

$$u^2(F_{inlet\,H2}) = u^2(F_{H2O}) + 9 \times u^2(F_{EtOH}) \qquad \text{A26}$$

'F' is the molar flow rate in mol/s.

A.1.4 The uncertainty of the fuel blend (S/C ratio) and molar fuel flow rate

The fuel is a mixture of distilled water and pure ethanol. It is assumed that water and ethanol are pure. A graduated cylinder is used for measurement of the required volume of each component for fuel preparation. The accuracy of the graduated cylinder is ±0.1 ml. A constant human error of ±0.5 ml is considered. Therefore, the total maximum error of ±0.6 ml is considered in the measurement of the required volume of water and ethanol. This is

equal to 0.033 and 0.010 mole of water (n_{H2O}) and ethanol (n_{EtOH}), respectively. The uncertainty of the S/C ratio is calculated as:

$$S/C = \frac{n_{H2O}}{2 \times n_{EtOH}}$$ A27

n represents the number of the moles:

$$u^2(S/C) = (\frac{\partial(S/C)}{\partial n_{H2O}})^2 u^2(n_{H2O}) + (\frac{\partial(S/C)}{\partial n_{EtOH}})^2 u^2(n_{EtOH})$$ A28

$$\frac{\partial(S/C)}{\partial n_{H2O}} = \frac{1}{2 \times n_{EtOH}}$$ A29

$$\frac{\partial(S/C)}{\partial n_{EtOH}} = \frac{-n_{H2O}}{2 \times n_{EtOH}^2}$$ A30

The experiments were performed at two fuel flow rates i.e. FF=50 μl/min (0.05 ml/min) and FF=100 μl/min (0.1 ml/min). The uncertainty of the molar flow rate of water and ethanol because of the errors in fuel preparation is calculated as:

$$u(n_{H2O})^{mixture} = \frac{0.033 \times FF}{V_{mixture}}$$ A31

$$u(n_{EtOH})^{mixture} = \frac{0.010 \times F_F}{V_{mixture}}$$ A32

$V_{mixture}$ is the volume of the mixture of the ethanol and water. At each S/C ratio, 100 ml ethanol is mixed with the relevant volume of water, which is 187, 123.6, and 100 ml of water to make a mixture with S/C ratio of 3, 2, and 1.6, respectively. Therefore, $V_{mixture}$ is equal to 287, 223.6, and 200 ml at S/C ratio of 3, 2, and 1.6, respectively.

The pump used in the experimental setup showed an error equal to 5% in the flow rate of the fuel, which means 2.5 and 5 μl/min at FF=50 and 100 μl/min, respectively. It is assumed that the error of the pump stays unchanged at higher pressures (maximum pressure of 12 bar was reached in this work).

Finally, the maximum possible uncertainty of the molar flow rate of ethanol and water was considered to be the sum of uncertainty of fuel blend preparation and the uncertainty of the pump ($u(n_{H2O})^{pump}$ and $u(n_{EtOH})^{pump}$):

$$u(n_{H2O}) = u(n_{H2O})^{mixture} + u(n_{H2O})^{pump}$$ A33

$$u(n_{EtOH}) = u(n_{EtOH})^{mixture} + u(n_{EtOH})^{pump}$$ A34

A.1.5 Steam in the reactor (unreacted water) $S_{reactor}$

Unreacted steam in the reactor was used in the estimation of the hydrogen fraction in the gases inside the reactor (around the membrane) to be used in the Sieverts' law equation. The unreacted steam in the reactor ($S_{reactor}$) is supposed to be difference between the inlet steam (S_{inlet}) and the amount of steam used in the reforming reactions (S_{used}):

$$S_{reactor} = S_{inlrt} - S_{used} \qquad \text{A35}$$

The uncertainty of the inlet flow rate of steam is the same as inlet water in the fuel:

$$u(S_{inlet}) = u(\dot{n}_{H2O}) \qquad \text{A36}$$

Steam is used in water gas shift reaction WGSR (S_{used}^{WGSR}) and methane steam reforming (S_{used}^{MSR}) reactions:

$$S_{used} = S_{used}^{WGSR} + S_{used}^{MSR} \qquad \text{A37}$$

According to the ESR reactions mechanism (eq. 2.2 and 2.3), total rate of steam consumption is equal to the rate of CO consumption plus twice of the rate of CH_4 consumption. For each mole of decomposed ethanol, one mole of methane and one mole of carbon monoxide are formed. Therefore:

$$S_{used}^{WGSR} = n_{reacted\ CO} = \dot{n}_{EtOH} - \dot{n}_{CO} \qquad \text{A38}$$

$$S_{used}^{MSR} = 2 \times n_{reacted\ CH4} = 2 \times (\dot{n}_{EtOH} - \dot{n}_{CH4}) \qquad \text{A39}$$

Accordingly:

$$S_{used} = 3 \times \dot{n}_{EtOH} - \dot{n}_{CO} - 2 \times \dot{n}_{CH4} \qquad \text{A40}$$

$$u(S_{used}) = 3 \times u(\dot{n}_{EtOH}) + u(\dot{n}_{CO}) + 2 \times u(\dot{n}_{CH4}) \qquad \text{A41}$$

Finally:

$$u(S_{reactor}) = u(S_{inlet}) + u(S_{used}) \qquad \text{A42}$$

A.2 Uncertainty analysis of the exergy evaluation

To introduce the formulation of uncertainty analysis of the exergetic evaluation, some exergy terms are recalled:

$$EX_{destruction} = EX_{in} - EX_{out} \qquad\qquad \text{A43}$$

$$EX_{unused} = EX_{destruction} - EX_{retentate} \qquad\qquad \text{A44}$$

$$\eta_{ex} = 1 - \frac{EX_{unused}}{EX_{in}} \qquad\qquad \text{A45}$$

A.2.1 Inlet exergy

$$EX_{W_{el}} = EX_{H_2O} + EX_{EtOH} + EX_{W_{el}} \qquad\qquad \text{A46}$$

W_{el} represents the electrical exergy rate, which is assumed equal to the exergy rate needed for the ESR plus the heat losses.

A.2.2 Uncertainty of the exergy rates of water (EX_{H_2O}) and ethanol (EX_{EtOH})

The exergy of every species consists of physical ($ex_{physical}$), chemical ($ex_{chemical}$), and mixing exergy (ex_{mixing}):

$$ex = ex_{physical} + ex_{chemical} + ex_{mixing} \qquad\qquad \text{A47}$$

Mixing exergy is very small in front of the chemical and physical exergy ($\frac{ex_{mixing}}{ex_{Ethanol}} < 0.005$), therefore, this term is neglected in uncertainty analysis calculations:

$$u(ex) = u\left(ex_{physical}\right) + u(ex_{chemical}) \qquad\qquad \text{A48}$$

Uncertainty of chemical exergy is easily calculated since the thermodynamic tables were used to obtain the standard chemical exergy of the species:

$$EX_{chemical} = ex_{chemical}^{standard} \times \dot{n}_i \qquad\qquad \text{A49}$$

$$u(EX_{chemical}) = ex_{chemical}^{standard} \times u(\dot{n}_i) \qquad\qquad \text{A50}$$

Physical exergy is obtained as a function of the specific enthalpy and entropy:

$$ex_{physical}^{molar} = h - h_0 - T_0(s - s_0) \qquad\qquad \text{A51}$$

h and s are the specific enthalpy and entropy at reaction conditions (T_r). h_0 and s_0 (specific enthalpy and entropy at reaction conditions) are considered fixed without error since the reference temperature is assumed to be 298 K. NASA polynomials are used to calculate the specific enthalpy and entropy:

$$\frac{h}{RT} = a_1 + a_2 \frac{T}{2} + a_3 \frac{T^2}{3} + a_4 \frac{T^3}{4} + a_5 \frac{T^4}{5} + \frac{a_6}{T} \qquad \text{A52}$$

$$\frac{S}{R} = a_1 Ln(T) + a_2 T + a_3 \frac{T^2}{2} + a_4 \frac{T^3}{3} + a_5 \frac{T^4}{4} + a_7 \qquad \text{A53}$$

Then:

$$\frac{\partial h}{\partial T} = R \times (a_1 + a_2 T + a_3 T^2 + a_4 T^3 + a_5 T^4) \qquad \text{A54}$$

$$\frac{\partial S}{\partial T} = R \times (\frac{a_1}{T} + a_2 + a_3 T + a_4 T^2 + a_5 T^3) \qquad \text{A55}$$

$$u(h) = \frac{\partial h}{\partial T} \times u(T_r) \qquad \text{A56}$$

$$u(S) = \frac{\partial S}{\partial T} \times u(T_r) \qquad \text{A57}$$

$$u^2(ex_{physical}^{molar}) = u^2(h) + T_0^2 \times u^2(s) \qquad \text{A58}$$

$$EX_{physical} = ex_{physical}^{molar} \times \dot{n}_i \qquad \text{A59}$$

$$u^2(EX_{physical}) = (\frac{\partial EX_{physical}}{\partial ex_{physical}^{molar}})^2 \times u^2(ex_{physical}^{molar}) + (\frac{\partial EX_{physical}}{\partial \dot{n}_i})^2 \times u^2(\dot{n}_i) \qquad \text{A60}$$

$$= \dot{n}_i^2 \times u^2(ex_{physical}^{molar}) + ex_{physical}^{molar}{}^2 \times u^2(\dot{n}_i) \qquad \text{A61}$$

This formulation is also true for the physical and chemical exergy content of the components of the retentate gas. For ethanol and water, the physical exergy is assumed zero, since they enter the system at reference conditions.

A.2.3 EX_{Wel}

Uncertainty of electrical energy consumption (in the form of exergy) consists of three terms, i.e. the required exergy for fuel evaporation and heat up to required temperature (T_r), required heat for the ESR reactions, and heat losses.

$$EX_{W_{el}} = EX_{Q_{evaporation}} + EX_{Q_{reaction}} + EX_{Q_{loss}} \qquad \text{A62}$$

$$u(EX_{W_{el}}) = u\left(EX_{Q_{evaporation}}\right) + u(EX_{Q_{reaction}}) + u(EX_{Q_{loss}}) \qquad \text{A63}$$

A.2.4 Uncertainty of $EX_{Q_{reaction}}$

The reaction promotion of WGS and MSR are measured by means of the consumption rate (reaction) of CO and CH_4, respectively. Therefore, the required heat for ESR is obtained based on the promotion of WGS and MSR reactions.

$$EX_{Q_{reaction}} = \Delta H^{WGS} \times \dot{n}_{CO}^{reacted} + \Delta H^{MSR} \times \dot{n}_{CH4}^{reacted} \qquad \text{A64}$$

ΔH represents the enthalpy change of the reaction.

$$u\left(EX_{Q_{reaction}}\right) = \Delta H^{WGS} \times u\left(\dot{n}_{CO}^{reacted}\right) + \Delta H^{MSR} \times u\left(\dot{n}_{CH4}^{reacted}\right) \qquad \text{A65}$$

$$u\left(\dot{n}_{CO}^{reacted}\right) = u(\dot{n}_{EtOH}) + u(\dot{n}_{CO}) \qquad \text{A66}$$

$$u\left(\dot{n}_{CH4}^{reacted}\right) = u(\dot{n}_{EtOH}) + u(\dot{n}_{CH4}) \qquad \text{A67}$$

A.2.5 Uncertainty of $EX_{Q_{evaporation}}$

$Q_{evaporation}$ stands for the required exergy needed for the evaporation of the water ($\Delta H_{evaporation}^{H2O}$) and ethanol ($\Delta H_{evaporation}^{EtOH}$) and to heat the vapors up to the reaction temperature (T_r).

$$EX_{Q_{evaporation}} = \Delta H_{evaporation}^{EtOH} \times \dot{n}_{EtOH} + \Delta H_{evaporation}^{H2O} \times \dot{n}_{H2O} \qquad \text{A68}$$

$$u\left(EX_{Q_{evaporation}}\right) = \Delta H_{evaporation}^{EtOH} \times u(\dot{n}_{EtOH}) + \Delta H_{evaporation}^{H2O} \times u(\dot{n}_{H2O}) \qquad \text{A69}$$

A.2.6 Uncertainty of $EX_{Q_{loss}}$

The reactor vessel is a stainless still cylinder via which the heat is transferred (lost) to the reference environment.

$$EX_{Q_{loss}} = \frac{2\pi LK(T_r - T_{wall})}{Ln\left(\frac{r_0}{r_i}\right)} \qquad \text{A70}$$

'L' is the length of the tube (reactor) and 'K' stands for the thermal conductivity of the insulation, which is glass wool. T_{wall} and T_r represent the reactor vessel wall temperature and the reaction (reactor) temperature, respectively.

$$u\left(EX_{Q_{loss}}\right) = \frac{2\pi LK}{Ln\left(\frac{r_0}{r_i}\right)} \times (u(T_r) + u(T_{wall})) \qquad \text{A71}$$

A.2.7 Uncertainty in temperature reading:

The reactor (reaction) temperature is measured by means of a K-type thermocouple. The same method was used to measure the wall temperature. The temperature measurement equipment has the following errors:

- Thermometer: 0.3% reading+1°C digit
- K-type thermocouple: 0.75% of the read value
  (Reference: the data base/data sheet of the product)

Based on the mentioned error, uncertainty of T_{wall} and T_r and two different temperatures operated in this work (873 and 923 K) is calculated:

- $u(T_{wall})$

  T_{wall} (at $T_r = 873$ K) $= 378\ K$, thermometer error: $\pm 0.32\ K$, u(thermometer)$= \frac{0.32}{\sqrt{3}} = 0.2\ K$

  T_{wall} ($at\ T_r = 873$ K) $= 378\ K$, K-type error: $\pm 0.8\ K$, u(K-type)$= \frac{0.8}{\sqrt{3}} = 0.5\ K$

  T_{wall} (at $T_r = 923$ K) $= 393\ K$, thermometer error: $\pm 0.36\ K$, u(thermometer)$= \frac{0.36}{\sqrt{3}} = 0.21\ K$

  T_{wall} ($at\ T_r = 923$ K) $= 393\ K$, K-type error: $\pm 0.9\ K$, u(K-type)$= \frac{0.9}{\sqrt{3}} = 0.52\ K$

  $u(T_{wall}) = 0.7\ K\ at\ 873\ K\ and\ 0.73K\ at\ 923\ K$

- $u(T_r)$

  $T_r = 873$ K, thermometer error: $\pm 1.8\ K$, u(thermometer)$= \frac{1.8}{\sqrt{3}} = 1$ K

  $T_r = 873$ K, K-type error: $\pm 4.5\ K$, u(K-type)$= \frac{4.5}{\sqrt{3}} = 2.6$ K

  $T_r = 923$ K, thermometer error: $\pm 2\ K$, u(thermometer)$= \frac{2}{\sqrt{3}} = 1.2\ K$

  $T_r = 923$ K, K-type error: $\pm 4.9\ K$, u(K-type)$= \frac{4.9}{\sqrt{3}} = 2.8$ K

  $u(T_r) = 3.6\ K\ at\ 873\ K\ and\ 4\ K\ at\ 923\ K$

$$u(EX_{in}) = u(EX_{EtOH}) + u(EX_{H2O}) + u(EX_{Wel})$$

A.2.8 Outlet exergy

The outlet exergy rate consists of the exergy rate of the retentate gas and the exergy rate of the pure hydrogen stream permeating through the membrane:

$$EX_{out} = EX_{retentate} + EX_{H2\ pure} \qquad\qquad A72$$

$$u(EX_{out}) = u(EX_{retentate}) + u(EX_{H2.perm}) \qquad\qquad A73$$

The exergy rate of the retentate gas is composed of the exergy rate of each component (i), which exists in the stream, i.e. H_2, CO, CO_2, CH_4, plus condensing water:

$$EX_{retentate} = \sum_i \dot{n}_i(ex_{physical_i} + ex_{chemical_i}) \qquad\qquad A74$$

$$u(EX_{retentate}) = \sum_i u(EX_i) \qquad\qquad A75$$

$$EX_{H2\ pure} = \dot{n}_{H2.perm}(ex_{physical_{H2.perm}} + ex_{chemical_{H2.perm}}) \qquad\qquad A76$$

And finally:

$$u(EX_{detruction}) = u(EX_{in}) + u(EX_{out}) \qquad\qquad A77$$

$$u(EX_{unused}) = u(EX_{detruction}) + u(EX_{retentate}) \qquad\qquad A78$$

A.2.9 Uncertainty of exergy efficiency:

$$\eta_{ex} = 1 - \frac{EX_{unused}}{EX_{in}} \qquad\qquad A79$$

$$u^2(\eta_{ex}) = \left(\frac{\partial \eta_{ex}}{\partial ex_{unused}}\right)^2 u^2(ex_{unused}) + \left(\frac{\partial \eta_{ex}}{\partial ex_{in}}\right)^2 u^2(ex_{in}) \qquad\qquad A80$$

$$u^2(\eta_{ex}) = \left(\frac{1}{ex_{in}}\right)^2 \times u^2(ex_{unused}) + \left(\frac{ex_{unused}}{ex_{in}^2}\right)^2 \times u^2(ex_{in}) \qquad\qquad A81$$

A.3 The results of the uncertainty analysis of the experimental evaluation factors

The uncertainty of the pure hydrogen mass flow meter is 5.77×10^{-7} mol/s or 0.87 ml/min, regardless of the operating conditions.

T [K]	FF [µl/min]	S/C
923	50	1.6

Parameter	S/C [-]	F_{EtOH} [mol/s]	F_{H2O} [mol/s]	GC [%]
Value	1.6	7.08E-06	2.31E-05	5
Uncertainty (u)	0.014	7.10E-07	2.80E-06	2.9

	Molar flow rate of the species present in the retentate stream (mol/s)					Uncertainty (mol/s)				
P [bar]	CO_2	H_2	CH_4	CO	H_2O	CO_2	H_2	CH_4	CO	H_2O
4	3.63E-06	4.01E-06	7.21E-06	2.49E-07	1.65E-05	4.52E-07	4.52E-07	4.56E-07	4.51E-07	5.85E-06
6	3.88E-06	3.94E-06	6.72E-06	3.22E-07	1.56E-05	4.11E-07	4.11E-07	4.12E-07	4.10E-07	5.76E-06
8	3.61E-06	1.99E-06	5.03E-06	3.16E-07	1.22E-05	3.17E-07	3.16E-07	3.19E-07	3.16E-07	5.57E-06
10	2.55E-06	1.79E-06	4.20E-06	3.11E-07	1.06E-05	2.40E-07	2.38E-07	2.47E-07	2.36E-07	5.43E-06
12	2.00E-06	1.51E-06	3.30E-06	2.95E-07	8.77E-06	1.40E-07	1.38E-07	1.45E-07	1.36E-07	5.23E-06

P [bar]	Y_{H2}	$u(Y_{H2})$	R_{H2}	$u(R_{H2})$	θ_{H2}	$u(\theta_{H2})$	$F_{H2.perm}$ (mol/s)	$u(F_{H2.perm})$
4	0.07	0.015	0.43	0.055	0.03	0.014	2.98E-06	5.77E-07
6	0.20	0.024	0.68	0.027	0.11	0.020	8.40E-06	5.77E-07
8	0.29	0.032	0.86	0.020	0.19	0.026	1.24E-05	5.77E-07
10	0.38	0.040	0.90	0.012	0.25	0.032	1.61E-05	5.77E-07
12	0.46	0.048	0.93	0.006	0.31	0.037	1.95E-05	5.77E-07

T [K]	FF [µl/min]	S/C
923	100	1.6

Parameter	S/C [-]	F_{EtOH} [mol/s]	F_{H2O} [mol/s]	GC [%]
Value	1.6	1.42E-05	4.62E-05	5
Uncertainty (u)	0.014	7.10E-07	2.80E-06	2.9

	Molar flow rate of the species present in the retentate stream (mol/s)					Uncertainty (mol/s)				
P [bar]	CO_2	H_2	CH_4	CO	H_2O	CO_2	H_2	CH_4	CO	H_2O
4	8.29E-06	9.52E-06	1.67E-05	4.43E-07	3.77E-05	1.05E-06	1.05E-06	1.07E-06	1.04E-06	7.06E-06
6	7.51E-06	7.95E-06	1.39E-05	5.71E-07	3.22E-05	9.73E-07	9.73E-07	9.79E-07	9.72E-07	6.89E-06
8	9.27E-06	4.84E-06	1.36E-05	4.36E-07	3.14E-05	8.24E-07	8.23E-07	8.28E-07	8.22E-07	6.59E-06
10	8.38E-06	3.15E-06	1.05E-05	3.73E-07	2.51E-05	6.72E-07	6.67E-07	6.76E-07	6.67E-07	6.29E-06
12	6.30E-06	2.54E-06	9.09E-06	3.21E-07	2.23E-05	5.52E-07	5.48E-07	5.58E-07	5.47E-07	6.05E-06

P [bar]	Y_{H2}	$u(Y_{H2})$	R_{H2}	$u(R_{H2})$	θ_{H2}	$u(\theta_{H2})$	$F_{H2.perm}$ (mol/s)	$u(F_{H2.perm})$
4	0.04	0.007	0.27	0.039	0.03	0.007	3.54E-06	5.77E-07
6	0.15	0.010	0.61	0.031	0.11	0.009	1.25E-05	5.77E-07
8	0.22	0.013	0.79	0.028	0.19	0.010	1.84E-05	5.77E-07
10	0.28	0.016	0.88	0.022	0.25	0.013	2.39E-05	5.77E-07
12	0.35	0.019	0.92	0.016	0.31	0.015	3.00E-05	5.77E-07

T [K]	FF [µl/min]	S/C
923	50	2

Parameter	S/C [-]	F_{EtOH} [mol/s]	F_{H2O} [mol/s]	GC [%]
Value	2	6.33E-06	2.56E-05	5
Uncertainty (u)	0.015	3.55E-07	1.40E-06	2.9

Molar flow rate of the species present in the retentate stream (mol/s)					Uncertainty (mol/s)				
P [bar]	CO_2	H_2	CH_4	CO	H_2O	CO_2	H_2	CH_4	CO	H_2O
4	3.88E-06	4.70E-06	6.64E-06	1.29E-07	2.00E-05	4.47E-07	4.47E-07	4.50E-07	4.45E-07	3.37E-06
6	3.06E-06	3.32E-06	5.33E-06	8.95E-08	1.73E-05	3.46E-07	3.48E-07	3.66E-07	3.36E-07	3.20E-06
8	3.75E-06	2.68E-06	4.69E-06	1.06E-07	1.61E-05	3.27E-07	3.24E-07	3.31E-07	3.21E-07	3.13E-06
10	3.07E-06	1.95E-06	3.57E-06	8.17E-08	1.38E-05	2.52E-07	2.50E-07	2.54E-07	2.49E-07	2.97E-06
12	3.06E-06	1.70E-06	3.34E-06	7.29E-08	1.33E-05	2.52E-07	2.42E-07	2.55E-07	2.37E-07	2.98E-06

P [bar]	Y_{H2}	$u(Y_{H2})$	R_{H2}	$u(R_{H2})$	θ_{H2}	$u(\theta_{H2})$	$F_{H2.perm}$ (mol/s)	$u(F_{H2.perm})$
4	0.05	0.015	0.31	0.062	0.05	0.013	2.08E-06	5.77E-07
6	0.18	0.018	0.67	0.030	0.15	0.014	6.72E-06	5.77E-07
8	0.29	0.022	0.81	0.021	0.25	0.016	1.11E-05	5.77E-07
10	0.39	0.027	0.88	0.014	0.33	0.018	1.48E-05	5.77E-07
12	0.47	0.030	0.91	0.012	0.40	0.020	1.78E-05	5.77E-07

T [K]	FF [µl/min]	S/C
923	100	2

Parameter	S/C [-]	F_{EtOH} [mol/s]	F_{H2O} [mol/s]	GC [%]
Value	2	1.27E-05	5.11E-05	5
Uncertainty (u)	0.015	7.10E-07	2.80E-06	2.9

Molar flow rate of the species present in the retentate stream (mol/s)					Uncertainty (mol/s)				
P [bar]	CO_2	H_2	CH_4	CO	H_2O	CO_2	H_2	CH_4	CO	H_2O
4	7.70E-06	9.04E-06	1.34E-05	2.38E-07	4.02E-05	5.22E-07	5.22E-07	5.24E-07	5.22E-07	5.98E-06
6	7.58E-06	6.98E-06	1.21E-05	1.91E-07	3.74E-05	5.91E-07	5.91E-07	5.94E-07	5.90E-07	6.12E-06
8	8.36E-06	5.32E-06	1.02E-05	2.14E-07	3.37E-05	6.39E-07	6.38E-07	6.41E-07	6.37E-07	6.22E-06
10	8.56E-06	4.31E-06	9.01E-06	1.97E-07	3.13E-05	7.11E-07	7.10E-07	7.13E-07	7.10E-07	6.36E-06
12	9.34E-06	4.38E-06	9.69E-06	2.10E-07	3.27E-05	6.37E-07	6.33E-07	6.38E-07	6.33E-07	6.21E-06

P [bar]	Y_{H2}	$u(Y_{H2})$	R_{H2}	$u(R_{H2})$	θ_{H2}	$u(\theta_{H2})$	$F_{H2.perm}$ (mol/s)	$u(F_{H2.perm})$
4	0.04	0.008	0.23	0.039	0.03	0.007	2.69E-06	5.77E-07
6	0.13	0.011	0.59	0.025	0.11	0.008	1.01E-05	5.77E-07
8	0.23	0.015	0.76	0.023	0.19	0.010	1.71E-05	5.77E-07
10	0.30	0.018	0.84	0.022	0.25	0.012	2.25E-05	5.77E-07
12	0.36	0.022	0.86	0.017	0.31	0.014	2.76E-05	5.77E-07

T [K]	FF [µl/min]	S/C
923	50	3

Parameter	S/C [-]	F_{EtOH} [mol/s]	F_{H2O} [mol/s]	GC [%]
Value	3	4.93E-06	3.01E-05	5
Uncertainty (u)	0.02	2.77E-07	1.60E-06	2.9

	Molar flow rate of the species present in the retentate stream (mol/s)					Uncertainty (mol/s)				
P [bar]	CO_2	H_2	CH_4	CO	H_2O	CO_2	H_2	CH_4	CO	H_2O
4	4.96E-06	6.10E-06	5.58E-06	2.05E-07	2.46E-05	5.16E-07	5.40E-07	5.29E-07	4.66E-07	3.49E-06
6	3.37E-06	3.96E-06	3.46E-06	1.10E-07	3.03E-05	3.19E-07	3.25E-07	3.20E-07	3.02E-07	3.07E-06
8	2.98E-06	2.76E-06	3.32E-06	7.18E-08	3.10E-05	2.68E-07	2.68E-07	2.69E-07	2.67E-07	2.97E-06
10	3.47E-06	2.19E-06	2.90E-06	5.46E-08	2.98E-05	2.55E-07	2.50E-07	2.53E-07	2.46E-07	2.94E-06
12	1.81E-06	1.81E-06	3.07E-06	3.06E-08	3.36E-05	2.14E-07	2.14E-07	2.24E-07	2.08E-07	2.88E-06

P [bar]	Y_{H2}	$u(Y_{H2})$	R_{H2}	$u(R_{H2})$	θ_{H2}	$u(\theta_{H2})$	$F_{H2.perm}$ (mol/s)	$u(F_{H2.perm})$
4	0.02	0.020	0.07	0.082	0.01	0.013	4.70E-07	5.77E-07
6	0.17	0.022	0.56	0.035	0.11	0.014	4.97E-06	5.77E-07
8	0.34	0.027	0.79	0.019	0.23	0.016	1.01E-05	5.77E-07
10	0.46	0.032	0.86	0.014	0.31	0.018	1.37E-05	5.77E-07
12	0.53	0.036	0.90	0.011	0.35	0.019	1.58E-05	5.77E-07

T [K]	FF [μl/min]	S/C
923	100	3

Parameter	S/C [-]	F_{EtOH} [mol/s]	F_{H2O} [mol/s]	GC [%]
Value	3	9.87E-06	6.03E-05	5
Uncertainty (u)	0.02	5.53E-07	3.21E-06	2.9

Molar flow rate of the species present in the retentate stream (mol/s)					Uncertainty (mol/s)				
P [bar]	CO_2	H_2	CH_4	CO	H_2O	CO_2	H_2	CH_4	CO	H_2O
4	1.01E-05	1.06E-05	1.16E-05	3.34E-07	4.88E-05	1.94E-06	2.03E-06	2.19E-06	7.51E-07	9.25E-06
6	9.50E-06	8.07E-06	9.08E-06	2.76E-07	5.18E-05	7.47E-07	7.40E-07	7.46E-07	7.23E-07	6.36E-06
8	6.26E-06	4.60E-06	6.28E-06	1.13E-07	6.21E-05	4.97E-07	4.86E-07	4.98E-07	4.74E-07	5.86E-06
10	9.17E-06	6.04E-06	7.86E-06	1.57E-07	5.28E-05	6.48E-07	6.43E-07	6.47E-07	6.39E-07	6.16E-06
12	5.18E-06	4.96E-06	8.47E-06	8.64E-08	6.18E-05	5.91E-07	5.90E-07	6.12E-07	5.78E-07	6.09E-06

P [bar]	Y_{H2}	$u(Y_{H2})$	R_{H2}	$u(R_{H2})$	θ_{H2}	$u(\theta_{H2})$	$F_{H2.perm}$ (mol/s)	$u(F_{H2.perm})$
4	0.01	0.010	0.07	0.049	0.01	0.006	8.07E-07	5.77E-07
6	0.17	0.014	0.55	0.027	0.11	0.008	9.88E-06	5.77E-07
8	0.28	0.018	0.78	0.019	0.18	0.010	1.65E-05	5.77E-07
10	0.37	0.023	0.78	0.019	0.24	0.012	2.16E-05	5.77E-07
12	0.43	0.026	0.84	0.017	0.28	0.013	2.52E-05	5.77E-07

T [K]	FF [µl/min]	S/C
873	50	1.6

Parameter	S/C [-]	F_{EtOH} [mol/s]	F_{H2O} [mol/s]	GC [%]
Value	1.6	7.08E-06	2.31E-05	5
Uncertainty (u)	0.014	7.10E-07	2.80E-06	2.9

	Molar flow rate of the species present in the retentate stream (mol/s)					Uncertainty (mol/s)				
P [bar]	CO_2	H_2	CH_4	CO	H_2O	CO_2	H_2	CH_4	CO	H_2O
4	4.20E-06	3.53E-06	8.61E-06	2.21E-07	1.93E-05	5.40E-07	5.40E-07	5.42E-07	5.39E-07	6.02E-06
6	3.44E-06	2.97E-06	7.49E-06	2.42E-07	1.71E-05	4.03E-07	4.03E-07	4.09E-07	4.02E-07	5.75E-06
8	3.22E-06	2.35E-06	6.58E-06	2.12E-07	1.53E-05	3.47E-07	3.47E-07	3.50E-07	3.46E-07	5.63E-06
10	3.05E-06	1.40E-06	5.34E-06	1.37E-07	1.27E-05	2.93E-07	2.93E-07	2.95E-07	2.93E-07	5.52E-06
12	2.60E-06	1.03E-06	4.47E-06	1.30E-07	1.09E-05	2.48E-07	2.47E-07	2.50E-07	2.47E-07	5.43E-06

P [bar]	Y_{H2}	$u(Y_{H2})$	R_{H2}	$u(R_{H2})$	θ_{H2}	$u(\theta_{H2})$	$F_{H2.perm}$ (mol/s)	$u(F_{H2.perm})$
4	0.02	0.014	0.16	0.117	0.03	0.013	6.69E-07	5.77E-07
6	0.09	0.016	0.56	0.050	0.11	0.015	3.78E-06	5.77E-07
8	0.13	0.019	0.71	0.037	0.19	0.016	5.65E-06	5.77E-07
10	0.22	0.026	0.87	0.025	0.25	0.021	9.20E-06	5.77E-07
12	0.28	0.031	0.92	0.018	0.31	0.025	1.19E-05	5.77E-07

T [K]	FF [µl/min]	S/C
873	100	1.6

Parameter	S/C [-]	F_{EtOH} [mol/s]	F_{H2O} [mol/s]	GC [%]
Value	1.6	1.42E-05	4.62E-05	5
Uncertainty (u)	0.014	7.10E-07	2.80E-06	2.9

	Molar flow rate of the species present in the retentate stream (mol/s)					Uncertainty (mol/s)				
P [bar]	CO_2	H_2	CH_4	CO	H_2O	CO_2	H_2	CH_4	CO	H_2O
4	8.85E-06	7.22E-06	1.87E-05	2.70E-07	4.14E-05	1.07E-06	1.07E-06	1.07E-06	1.07E-06	7.08E-06
6	8.65E-06	6.07E-06	1.80E-05	4.63E-07	4.03E-05	9.47E-07	9.46E-07	9.53E-07	9.46E-07	6.84E-06
8	8.70E-06	4.99E-06	1.71E-05	4.37E-07	3.83E-05	8.87E-07	8.85E-07	8.94E-07	8.85E-07	6.72E-06
10	7.39E-06	3.85E-06	1.47E-05	1.78E-07	3.33E-05	7.62E-07	7.61E-07	7.66E-07	7.61E-07	6.47E-06
12	6.80E-06	3.13E-06	1.36E-05	1.60E-07	3.12E-05	6.93E-07	6.93E-07	6.97E-07	6.93E-07	6.33E-06

P [bar]	Y_{H2}	$u(Y_{H2})$	R_{H2}	$u(R_{H2})$	θ_{H2}	$u(\theta_{H2})$	$F_{H2.perm}$ (mol/s)	$u(F_{H2.perm})$
4	0.01	0.007	0.08	0.068	0.03	0.007	6.50E-07	5.77E-07
6	0.05	0.007	0.43	0.049	0.11	0.007	4.51E-06	5.77E-07
8	0.08	0.008	0.57	0.048	0.19	0.007	6.65E-06	5.77E-07
10	0.14	0.010	0.75	0.038	0.25	0.008	1.16E-05	5.77E-07
12	0.18	0.011	0.83	0.032	0.31	0.009	1.49E-05	5.77E-07

T [K]	FF [μl/min]	S/C
873	50	2

Parameter	S/C [-]	F_{EtOH} [mol/s]	F_{H2O} [mol/s]	GC [%]
Value	2	6.33E-06	2.56E-05	5
Uncertainty (u)	0.015	3.55E-07	1.40E-06	2.9

	Molar flow rate of the species present in the retentate stream (mol/s)					Uncertainty (mol/s)				
P [bar]	CO_2	H_2	CH_4	CO	H_2O	CO_2	H_2	CH_4	CO	H_2O
4	3.90E-06	3.96E-06	8.05E-06	8.80E-08	2.27E-05	9.77E-07	9.77E-07	9.82E-07	9.76E-07	1.96E-06
6	3.84E-06	3.23E-06	8.27E-06	6.13E-08	2.32E-05	1.02E-06	1.02E-06	1.03E-06	1.02E-06	2.05E-06
8	3.30E-06	2.69E-06	7.41E-06	4.92E-08	2.14E-05	1.17E-06	1.17E-06	1.18E-06	1.17E-06	2.35E-06
10	2.64E-06	2.03E-06	6.05E-06	3.64E-08	1.87E-05	1.53E-06	1.52E-06	1.68E-06	1.50E-06	3.18E-06
12	2.03E-06	1.43E-06	4.71E-06	2.78E-08	1.60E-05	1.98E-06	1.97E-06	2.06E-06	1.96E-06	4.02E-06

P [bar]	Y_{H2}	$u(Y_{H2})$	R_{H2}	$u(R_{H2})$	θ_{H2}	$u(\theta_{H2})$	$F_{H2.perm}$ (mol/s)	$u(F_{H2.perm})$
4	0.02	0.015	0.18	0.104	0.02	0.013	8.74E-07	5.77E-07
6	0.06	0.016	0.41	0.099	0.05	0.013	2.22E-06	5.77E-07
8	0.09	0.016	0.56	0.116	0.08	0.013	3.36E-06	5.77E-07
10	0.16	0.018	0.75	0.142	0.14	0.014	6.05E-06	5.77E-07
12	0.23	0.020	0.86	0.167	0.20	0.015	8.74E-06	5.77E-07

T [K]	FF [µl/min]	S/C
873	100	2

Parameter	S/C [-]	F_{EtOH} [mol/s]	F_{H2O} [mol/s]	GC [%]
Value	2	1.27E-05	5.11E-05	5
Uncertainty (u)	0.015	7.10E-07	2.80E-06	2.9

	Molar flow rate of the species present in the retentate stream (mol/s)					Uncertainty (mol/s)				
P [bar]	CO_2	H_2	CH_4	CO	H_2O	CO_2	H_2	CH_4	CO	H_2O
4	8.31E-06	8.19E-06	1.72E-05	1.80E-07	4.77E-05	4.73E-07	4.73E-07	4.75E-07	4.73E-07	9.48E-07
6	7.92E-06	6.72E-06	1.71E-05	1.32E-07	4.75E-05	4.94E-07	4.94E-07	4.98E-07	4.93E-07	9.91E-07
8	7.47E-06	5.58E-06	1.60E-05	1.15E-07	4.53E-05	5.45E-07	5.43E-07	5.60E-07	5.41E-07	1.10E-06
10	7.08E-06	4.83E-06	1.50E-05	9.75E-08	4.32E-05	5.88E-07	5.87E-07	5.91E-07	5.87E-07	1.18E-06
12	6.62E-06	3.86E-06	1.33E-05	8.46E-08	3.97E-05	6.75E-07	6.73E-07	6.85E-07	6.72E-07	1.36E-06

P [bar]	Y_{H2}	$u(Y_{H2})$	R_{H2}	$u(R_{H2})$	θ_{H2}	$u(\theta_{H2})$	$F_{H2.perm}$ (mol/s)	$u(F_{H2.perm})$
4	0.01	0.008	0.10	0.058	0.01	0.006	8.74E-07	5.77E-07
6	0.04	0.008	0.29	0.046	0.03	0.007	2.69E-06	5.77E-07
8	0.06	0.008	0.44	0.040	0.05	0.007	4.37E-06	5.77E-07
10	0.10	0.009	0.62	0.034	0.09	0.007	7.73E-06	5.77E-07
12	0.16	0.012	0.76	0.033	0.14	0.008	1.21E-05	5.77E-07

T [K]	FF [µl/min]	S/C
873	50	3

Parameter	S/C [-]	F_{EtOH} [mol/s]	F_{H2O} [mol/s]	GC [%]
Value	3	4.93E-06	3.01E-05	5
Uncertainty (u)	0.02	2.77E-07	1.60E-06	2.9

	Molar flow rate of the species present in the retentate stream (mol/s)					Uncertainty (mol/s)				
P [bar]	CO_2	H_2	CH_4	CO	H_2O	CO_2	H_2	CH_4	CO	H_2O
4	3.34E-06	4.13E-06	6.24E-06	5.32E-08	2.79E-05	5.79E-07	5.81E-07	5.88E-07	5.76E-07	3.61E-06
6	2.95E-06	3.36E-06	5.60E-06	4.27E-08	2.66E-05	1.75E-06	1.96E-06	3.15E-06	6.56E-07	8.73E-06
8	2.77E-06	2.89E-06	5.10E-06	3.89E-08	2.56E-05	7.42E-07	7.44E-07	7.93E-07	7.20E-07	4.02E-06
10	2.13E-06	2.27E-06	3.90E-06	3.09E-08	2.32E-05	9.49E-07	9.49E-07	9.61E-07	9.45E-07	4.36E-06
12	1.77E-06	1.58E-06	3.09E-06	2.52E-08	2.15E-05	1.30E-06	1.28E-06	1.43E-06	1.23E-06	5.30E-06

P [bar]	Y_{H2}	$u(Y_{H2})$	R_{H2}	$u(R_{H2})$	θ_{H2}	$u(\theta_{H2})$	$F_{H2.perm}$ (mol/s)	$u(F_{H2.perm})$
4	0.01	0.019	0.05	0.127	0.00	0.013	2.02E-07	5.77E-07
6	0.03	0.020	0.21	0.144	0.02	0.013	8.74E-07	5.77E-07
8	0.04	0.020	0.37	0.113	0.04	0.013	1.21E-06	5.77E-07
10	0.13	0.021	0.62	0.105	0.08	0.013	3.76E-06	5.77E-07
12	0.20	0.022	0.79	0.138	0.13	0.014	5.78E-06	5.77E-07

T [K]	FF [μl/min]	S/C
873	100	3

Parameter	S/C [-]	F_{EtOH} [mol/s]	F_{H2O} [mol/s]	GC [%]
Value	3	9.87E-06	6.03E-05	5
Uncertainty (u)	0.02	5.54E-07	3.22E-06	2.9

	Molar flow rate of the species present in the retentate stream (mol/s)					Uncertainty (mol/s)				
P [bar]	CO_2	H_2	CH_4	CO	H_2O	CO_2	H_2	CH_4	CO	H_2O
4	6.66E-06	8.30E-06	1.24E-05	1.12E-07	5.57E-05	2.88E-07	2.88E-07	2.89E-07	2.88E-07	5.45E-06
6	6.35E-06	7.13E-06	1.21E-05	9.38E-08	5.50E-05	3.14E-07	3.15E-07	3.26E-07	3.09E-07	5.52E-06
8	6.13E-06	5.96E-06	1.13E-05	8.21E-08	5.34E-05	3.36E-07	3.35E-07	3.47E-07	3.31E-07	5.56E-06
10	5.98E-06	5.15E-06	1.05E-05	7.13E-08	5.16E-05	3.69E-07	3.69E-07	3.76E-07	3.66E-07	5.62E-06
12	5.67E-06	4.27E-06	9.18E-06	7.04E-08	4.91E-05	4.27E-07	4.20E-07	4.53E-07	4.11E-07	5.77E-06

P [bar]	Y_{H2}	$u(Y_{H2})$	R_{H2}	$u(R_{H2})$	θ_{H2}	$u(\theta_{H2})$	$F_{H2.perm}$ (mol/s)	$u(F_{H2.perm})$
4	0.00	0.010	0.02	0.066	0.00	0.006	2.02E-07	5.77E-07
6	0.02	0.010	0.14	0.060	0.01	0.006	1.14E-06	5.77E-07
8	0.04	0.010	0.28	0.051	0.03	0.007	2.35E-06	5.77E-07
10	0.09	0.011	0.50	0.033	0.06	0.007	5.11E-06	5.77E-07
12	0.15	0.013	0.68	0.026	0.10	0.008	9.07E-06	5.77E-07

A.4 The results of the uncertainty analysis of the exergy analysis

All exergy factors are given in Watt [W].

T [K]	FF [µl/min]	S/C
973	50	1.6

Parameter	$EX_{H2.perm}$ [W]	EX_{fuel} [W]	T_r [K]	T_w [K]
Value	Given in next table	9.6	923	393
Uncertainty (u)	0.14	0.6	4	0.73

P [bar]	EX_{Wel}	EX_{in}	$EX_{retentate}$	EX_{out}	$EX_{destruction}$	EX_{unused}	$EX_{H2.perm}$	η_{ex} [%]	η_{ex} [%]
4	12.1	21.7	7.5	8.3	12.4	20.0	0.7	3	7
6	12.2	21.8	7.1	9.2	11.6	18.7	2.1	10	19
8	12.5	22.1	5.1	8.2	12.9	18.0	3.0	14	28
10	12.6	22.2	4.3	8.3	12.9	17.2	3.9	19	35
12	12.7	22.3	3.4	8.2	13.1	16.6	4.8	22	42

P [bar]	$u(EX_{Wel})$	$u(Ex_{in})$	$u(EX_{retentate})$	$u(EX_{out})$	$u(EX_{destruction})$	$u(EX_{unused})$	$u(\eta_{ex})$	
							Non-Insulate reactor	Insulate reactor
4	0.53	1.13	0.71	0.86	1.98	2.70	0.15	0.015
6	0.52	1.12	0.65	0.79	1.91	2.57	0.14	0.014
8	0.51	1.10	0.52	0.66	1.76	2.28	0.12	0.012
10	0.50	1.09	0.41	0.55	1.64	2.05	0.11	0.011
12	0.48	1.08	0.26	0.40	1.48	1.74	0.10	0.009

All exergy factors are given in Watt [W].

T [K]	FF [µl/min]	S/C
973	100	1.6

Parameter	$EX_{H2.perm}$ [W]	EX_{fuel} [W]	T_r [K]	T_w [K]
Value	Given in next table	19.2	923	393
Uncertainty (u)	0.14	1.09	4	0.73

P [bar]	EX_{Wel}	EX_{in}	$EX_{retentate}$	EX_{out}	$EX_{destruction}$	EX_{unused}	$EX_{H2.perm}$	η_{ex} [%]	η_{ex} [%]
4	12.8	32.0	17.5	18.3	12.7	30.1	0.9	3	4
6	13.3	32.5	14.6	17.7	13.8	28.4	3.1	10	14
8	13.3	32.5	13.6	18.1	13.4	27.0	4.5	14	21
10	13.8	33.0	10.4	16.3	15.7	26.2	5.9	18	27
12	14.1	33.3	9.0	16.3	15.9	24.9	7.4	23	33

P [bar]	$u(EX_{Wel})$	$u(Ex_{in})$	$u(EX_{retentate})$	$u(EX_{out})$	$u(EX_{destruction})$	$u(EX_{unused})$	$u(\eta_{ex})$	
							Non-Insulate reactor	Insulate reactor
4	0.75	1.84	1.63	1.78	3.62	5.25	0.28	0.029
6	0.74	1.83	1.52	1.66	3.49	5.01	0.27	0.027
8	0.72	1.81	1.30	1.44	3.25	4.54	0.24	0.024
10	0.69	1.78	1.08	1.22	3.00	4.07	0.21	0.021
12	0.67	1.76	0.90	1.05	2.81	3.71	0.20	0.019

All exergy factors are given in Watt [W].

T [K]	FF [µl/min]	S/C
973	50	2

Parameter	$EX_{H2.perm}$ [W]	EX_{fuel} [W]	T_r [K]	T_w [K]
Value	Given in next table	8.6	923	393
Uncertainty (u)	0.14	0.49	4	0.73

P [bar]	EX_{Wel}	EX_{in}	$EX_{retentate}$	EX_{out}	$EX_{destruction}$	EX_{unused}	$EX_{H2.perm}$	η_{ex} [%]	η_{ex} [%]
4	12.1	20.6	7.2	7.8	11.9	19.1	0.5	3	5
6	12.3	20.9	5.7	7.4	12.5	18.2	1.6	8	17
8	12.4	21.0	5.0	7.8	12.2	17.3	2.7	14	27
10	12.6	21.1	3.8	7.5	12.7	16.5	3.6	18	36
12	12.6	21.2	3.6	7.9	12.2	15.8	4.4	22	43

P [bar]	$u(EX_{Wel})$	$u(Ex_{in})$	$u(EX_{retentate})$	$u(EX_{out})$	$u(EX_{destruction})$	$u(EX_{unused})$	$u(\eta_{ex})$	
							Non-Insulate reactor	Insulate reactor
4	0.51	1.00	0.70	0.84	1.84	2.55	0.14	0.014
6	0.49	0.99	0.57	0.71	1.70	2.26	0.12	0.012
8	0.49	0.98	0.53	0.67	1.65	2.18	0.12	0.012
10	0.48	0.97	0.42	0.56	1.53	1.94	0.10	0.010
12	0.48	0.97	0.41	0.55	1.52	1.94	0.10	0.010

All exergy factors are given in Watt [W].

T [K]	FF [μl/min]	S/C
973	100	2

Parameter	EX$_{H2.perm}$ [W]	EX$_{fuel}$ [W]	T$_r$ [K]	T$_w$ [K]
Value	Given in next table	17.2	923	393
Uncertainty (u)	0.14	0.99	4	0.73

P [bar]	EX$_{Wel}$	EX$_{in}$	EX$_{retentate}$	EX$_{out}$	EX$_{destruction}$	EX$_{unused}$	EX$_{H2.perm}$	η$_{ex}$ [%]	η$_{ex}$ [%]
4	13.1	30.3	14.6	15.2	14.1	28.6	0.7	2	3
6	13.3	30.5	12.8	15.3	14.2	27.0	2.5	8	13
8	13.6	30.8	10.8	15.0	14.8	25.6	4.2	14	21
10	13.8	31.0	9.5	15.0	15.0	24.5	5.5	18	28
12	13.7	30.9	10.2	16.9	13.0	23.1	6.7	23	34

P [bar]	u(EX$_{Wel}$)	u(Ex$_{in}$)	u(EX$_{retentate}$)	u(EX$_{out}$)	u(EX$_{destruction}$)	u(EX$_{unused}$)	u(η$_{ex}$)	
							Non-Insulate reactor	Insulate reactor
4	0.65	1.64	0.86	1.00	2.64	3.50	0.20	0.020
6	0.66	1.65	0.96	1.10	2.75	3.72	0.20	0.020
8	0.67	1.66	1.03	1.17	2.83	3.86	0.21	0.021
10	0.68	1.67	1.13	1.27	2.95	4.08	0.21	0.021
12	0.67	1.66	1.02	1.17	2.83	3.85	0.20	0.020

All exergy factors are given in Watt [W].

T [K]	FF [µl/min]	S/C
973	50	3

Parameter	$EX_{H2.perm}$ [W]	EX_{fuel} [W]	T_r [K]	T_w [K]
Value	Given in next table	6.7	923	393
Uncertainty (u)	0.14	0.39	4	0.73

P [bar]	EX_{Wel}	EX_{in}	$EX_{retentate}$	EX_{out}	$EX_{destruction}$	EX_{unused}	$EX_{H2.perm}$	η_{ex} [%]	η_{ex} [%]
4	12.0	18.7	6.8	6.9	10.7	17.6	0.1	1	1
6	12.3	19.0	4.6	5.8	12.3	16.8	1.2	7	15
8	12.4	19.1	4.2	6.6	11.4	15.6	2.5	14	31
10	12.4	19.1	3.7	7.0	11.1	14.8	3.4	19	41
12	12.4	19.1	3.7	7.6	10.5	14.2	3.9	21	48

P [bar]	$u(EX_{Wel})$	$u(Ex_{in})$	$u(EX_{retentate})$	$u(EX_{out})$	$u(EX_{destruction})$	$u(EX_{unused})$	$u(\eta_{ex})$	
							Non-Insulate reactor	Insulate reactor
4	0.50	0.89	0.80	0.94	1.84	2.64	0.14	0.015
6	0.47	0.86	0.51	0.65	1.51	2.02	0.11	0.011
8	0.46	0.85	0.44	0.58	1.43	1.87	0.10	0.010
10	0.46	0.85	0.41	0.56	1.40	1.82	0.10	0.010
12	0.45	0.84	0.37	0.51	1.35	1.72	0.09	0.009

All exergy factors are given in Watt [W].

T [K]	FF [µl/min]	S/C
973	100	3

Parameter	$EX_{H2.perm}$ [W]	EX_{fuel} [W]	T_r [K]	T_w [K]
Value	Given in next table	13.4	923	393
Uncertainty (u)	0.14	0.78	4	0.73

P [bar]	EX_{Wel}	EX_{in}	$EX_{retentate}$	EX_{out}	$EX_{destruction}$	EX_{unused}	$EX_{H2.perm}$	η_{ex} [%]	η_{ex} [%]
4	12.9	26.3	13.6	13.8	11.5	25.1	0.2	1	1
6	13.3	26.7	10.9	13.3	12.4	23.3	2.4	9	15
8	13.8	27.2	7.8	11.8	14.3	22.1	4.0	15	25
10	13.5	26.9	9.4	14.7	11.2	20.6	5.3	20	33
12	13.4	26.8	9.7	15.8	10.0	19.6	6.2	24	39

P [bar]	$u(EX_{Wel})$	$u(Ex_{in})$	$u(EX_{retentate})$	$u(EX_{out})$	$u(EX_{destruction})$	$u(EX_{unused})$	$u(\eta_{ex})$	
							Non-Insulate reactor	Insulate reactor
4	0.89	1.67	2.82	2.96	4.63	7.45	0.39	0.040
6	0.65	1.43	1.17	1.32	2.75	3.92	0.21	0.021
8	0.61	1.39	0.81	0.95	2.35	3.16	0.17	0.017
10	0.64	1.42	1.03	1.18	2.59	3.63	0.19	0.019
12	0.63	1.41	0.97	1.11	2.53	3.50	0.18	0.018

All exergy factors are given in Watt [W].

T [K]	FF [μl/min]	S/C
873	50	1.6

Parameter	$EX_{H2.perm}$ [W]	EX_{fuel} [W]	T_r [K]	T_w [K]
Value	Given in next table	9.6	873	378
Uncertainty (u)	0.14	0.6	3.6	0.7

P [bar]	EX_{Wel}	EX_{in}	$EX_{retentate}$	EX_{out}	$EX_{destruction}$	EX_{unused}	$EX_{H2.perm}$	η_{ex} [%]	η_{ex} [%]
4	11.8	21.4	8.6	8.8	11.6	20.2	0.2	1	2
6	12.0	21.6	7.5	8.4	12.2	19.6	0.9	4	9
8	12.1	21.7	6.5	7.9	12.8	19.3	1.4	7	13
10	12.3	21.9	5.2	7.4	13.5	18.7	2.2	11	21
12	12.4	22.0	4.3	7.2	13.8	18.1	2.9	14	26

P [bar]	$u(EX_{Wel})$	$u(Ex_{in})$	$u(EX_{retentate})$	$u(EX_{out})$	$u(EX_{destruction})$	$u(EX_{unused})$	$u(\eta_{ex})$	
							Non-Insulate reactor	Insulate reactor
4	0.52	1.11	0.84	0.98	2.10	2.94	0.16	0.017
6	0.49	1.09	0.64	0.79	1.88	2.52	0.14	0.014
8	0.48	1.08	0.56	0.70	1.78	2.35	0.13	0.013
10	0.48	1.07	0.48	0.62	1.70	2.18	0.12	0.011
12	0.47	1.07	0.42	0.56	1.62	2.04	0.11	0.011

All exergy factors are given in Watt [W].

T [K]	FF [µl/min]	S/C
873	100	1.6

Parameter	$EX_{H2.perm}$ [W]	EX_{fuel} [W]	T_r [K]	T_w [K]
Value	Given in next table	19.2	873	378
Uncertainty (u)	0.14	1.09	3.6	0.7

P [bar]	EX_{Wel}	EX_{in}	$EX_{retentate}$	EX_{out}	$EX_{destruction}$	EX_{unused}	$EX_{H2.perm}$	η_{ex} [%]	η_{ex} [%]
4	12.3	31.5	18.5	18.7	11.8	30.3	0.2	1	1
6	12.4	31.6	17.7	18.8	11.8	29.5	1.1	4	5
8	12.6	31.8	16.6	18.2	12.6	29.1	1.6	5	8
10	13.0	32.1	14.1	16.9	14.2	28.3	2.8	9	13
12	13.1	32.3	13.0	16.6	14.7	27.7	3.6	12	17

P [bar]	$u(EX_{Wel})$	$u(Ex_{in})$	$u(EX_{retentate})$	$u(EX_{out})$	$u(EX_{destruction})$	$u(EX_{unused})$	$u(\eta_{ex})$	
							Non-Insulate reactor	Insulate reactor
4	0.73	1.82	1.65	1.79	3.61	5.27	0.28	0.029
6	0.71	1.80	1.48	1.62	3.42	4.90	0.26	0.026
8	0.70	1.79	1.39	1.53	3.32	4.72	0.25	0.025
10	0.68	1.77	1.21	1.35	3.12	4.33	0.23	0.022
12	0.67	1.76	1.11	1.25	3.01	4.12	0.22	0.021

All exergy factors are given in Watt [W].

T [K]	FF [μl/min]	S/C
873	50	2

Parameter	$EX_{H2.perm}$ [W]	EX_{fuel} [W]	T_r [K]	T_w [K]
Value	Given in next table	8.6	873	378
Uncertainty (u)	0.14	0.49	3.6	0.7

P [bar]	EX_{Wel}	EX_{in}	$EX_{retentate}$	EX_{out}	$EX_{destruction}$	EX_{unused}	$EX_{H2.perm}$	η_{ex} [%]	η_{ex} [%]
4	11.7	20.3	8.2	8.5	10.9	19.1	0.2	1	2
6	11.7	20.3	8.3	8.8	10.5	18.7	0.5	3	6
8	11.8	20.4	7.4	8.2	11.2	18.6	0.8	4	9
10	12.1	20.6	6.0	7.5	12.2	18.2	1.5	8	15
12	12.3	20.9	4.7	6.8	13.1	17.7	2.1	11	22

P [bar]	$u(EX_{Wel})$	$u(Ex_{in})$	$u(EX_{retentate})$	$u(EX_{out})$	$u(EX_{destruction})$	$u(EX_{unused})$	$u(\eta_{ex})$	
							Non-Insulate reactor	Insulate reactor
4	0.57	1.06	1.46	1.60	2.66	4.12	0.22	0.022
6	0.57	1.07	1.53	1.67	2.74	4.26	0.22	0.022
8	0.60	1.09	1.74	1.89	2.98	4.72	0.24	0.024
10	0.68	1.18	2.37	2.51	3.69	6.06	0.30	0.030
12	0.74	1.24	2.96	3.10	4.34	7.31	0.37	0.036

All exergy factors are given in Watt [W].

T [K]	FF [µl/min]	S/C
873	100	2

Parameter	$EX_{H2.perm}$ [W]	EX_{fuel} [W]	T_r [K]	T_w [K]
Value	Given in next table	17.2	873	378
Uncertainty (u)	0.14	0.99	3.6	0.7

P [bar]	EX_{Wel}	EX_{in}	$EX_{retentate}$	EX_{out}	$EX_{destruction}$	EX_{unused}	$EX_{H2.perm}$	η_{ex} [%]	η_{ex} [%]
4	12.3	29.5	17.5	17.7	10.7	28.2	0.2	1	1
6	12.3	29.5	17.1	17.7	10.7	27.8	0.7	2	4
8	12.5	29.6	15.9	16.9	11.7	27.6	1.1	4	6
10	12.6	29.8	14.7	16.6	12.2	26.9	1.9	7	10
12	12.9	30.1	13.0	15.9	13.2	26.1	2.9	10	15

P [bar]	$u(EX_{Wel})$	$u(Ex_{in})$	$u(EX_{retentate})$	$u(EX_{out})$	$u(EX_{destruction})$	$u(EX_{unused})$	$u(\eta_{ex})$	
							Non-Insulate reactor	Insulate reactor
4	0.61	1.61	0.78	0.92	2.52	3.30	0.19	0.019
6	0.62	1.61	0.81	0.95	2.56	3.37	0.19	0.019
8	0.63	1.62	0.89	1.03	2.65	3.54	0.19	0.019
10	0.63	1.62	0.94	1.09	2.71	3.65	0.19	0.019
12	0.65	1.64	1.08	1.22	2.86	3.93	0.20	0.020

All exergy factors are given in Watt [W].

T [K]	FF [μl/min]	S/C
873	50	3

Parameter	$EX_{H2.perm}$ [W]	EX_{fuel} [W]	T_r [K]	T_w [K]
Value	Given in next table	6.7	873	378
Uncertainty (u)	0.14	0.39	3.6	0.7

P [bar]	EX_{Wel}	EX_{in}	$EX_{retentate}$	EX_{out}	$EX_{destruction}$	EX_{unused}	$EX_{H2.perm}$	η_{ex} [%]	η_{ex} [%]
4	11.8	18.5	6.8	6.9	10.6	17.4	0.0	0	1
6	11.9	18.6	6.1	6.3	11.3	17.4	0.2	1	3
8	12.0	18.7	5.5	5.8	11.9	17.4	0.3	2	4
10	12.2	18.9	4.3	5.2	12.7	16.9	0.9	5	12
12	12.3	19.0	3.4	4.8	13.2	16.6	1.4	8	18

P [bar]	$u(EX_{Wel})$	$u(Ex_{in})$	$u(EX_{retentate})$	$u(EX_{out})$	$u(EX_{destruction})$	$u(EX_{unused})$	$u(\eta_{ex})$	
							Non-Insulate reactor	Insulate reactor
4	0.49	0.88	0.89	1.03	1.91	2.79	0.15	0.015
6	0.91	1.30	3.55	3.69	4.99	8.53	0.43	0.044
8	0.52	0.91	1.16	1.30	2.21	3.36	0.17	0.017
10	0.55	0.94	1.42	1.56	2.50	3.93	0.20	0.020
12	0.62	1.01	2.01	2.15	3.17	5.18	0.26	0.025

All exergy factors are given in Watt [W].

T [K]	FF [μl/min]	S/C
873	100	3

Parameter	$EX_{H2.perm}$ [W]	EX_{fuel} [W]	T_r [K]	T_w [K]
Value	Given in next table	13.4	873	378
Uncertainty (u)	0.14	0.78	3.6	0.7

P [bar]	EX_{Wel}	EX_{in}	$EX_{retentate}$	EX_{out}	$EX_{destruction}$	EX_{unused}	$EX_{H2.perm}$	η_{ex} [%]	η_{ex} [%]
4	12.6	26.0	13.6	13.7	11.3	24.9	0.0	0	0
6	12.6	26.0	13.1	13.3	11.7	24.7	0.3	1	2
8	12.8	26.2	12.1	12.6	12.5	24.6	0.6	2	4
10	12.9	26.3	11.1	12.4	12.9	24.1	1.2	5	8
12	13.1	26.5	9.8	12.0	13.5	23.3	2.2	9	14

P [bar]	$u(EX_{Wel})$	$u(Ex_{in})$	$u(EX_{retentate})$	$u(EX_{out})$	$u(EX_{destruction})$	$u(EX_{unused})$	$u(\eta_{ex})$	
							Non-Insulate reactor	Insulate reactor
4	0.55	1.33	0.51	0.65	1.98	2.49	0.14	0.015
6	0.56	1.34	0.56	0.70	2.04	2.59	0.14	0.015
8	0.56	1.34	0.59	0.73	2.07	2.66	0.15	0.015
10	0.56	1.35	0.63	0.77	2.12	2.75	0.15	0.014
12	0.58	1.36	0.73	0.87	2.23	2.95	0.16	0.015

Appendix B – general and specific models

The results of the static models given in chapter 4 are presented here in two sections, i.e. the general models (B.1) and specific models (B.2).

The fitting parameters of the models together with the coefficient of determination (R^2) of the species (H_2, CO, CO_2, CH_4, and H_2O) are given in the tables. The average coefficient of determination of the modeling (R^2_{mean}) is the arithmetic mean of the R^2 values of the five species:

$$R^2_{mean} = \frac{R^2_{H2} + R^2_{CO} + R^2_{CO2} + R^2_{CH4} + R^2_{H2O}}{5} \qquad \text{B.1}$$

B.1 General Models

Model	$\dot{n}_{specie}$	R^2_{mean}
1	$\alpha \times F \times P \times \exp(\dfrac{\omega \times SC + \lambda}{RT})$	0.6895
2	$\alpha \times F \times P^\beta \times \exp(\dfrac{\omega \times SC + \lambda}{RT})$	0.9523
3	$\alpha \times F \times SC^\theta \times \exp(\dfrac{\gamma \times P + \lambda}{RT})$	0.9571
4	$\alpha \times F \times P \times SC \times \exp(\dfrac{\gamma \times P + \omega \times SC + \lambda}{RT})$	0.9485
5	$\alpha \times F \times P^\beta \times \exp(\dfrac{\gamma \times SC^\lambda}{RT})$	0.6996
6	$\alpha \times F \times P^\beta \times \exp(\dfrac{\gamma \times SC^\lambda}{RT})$	0.9550
7	$\alpha \times F \times P \times \exp(\dfrac{\gamma \times SC^\lambda + \varepsilon}{RT})$	0.6940
8	$\alpha \times F \times P^\beta \times \exp(\dfrac{\gamma \times SC^\lambda + \varepsilon}{RT})$	0.9668

Model 1: $\dot{n}_{specie} = \alpha \times F \times P \times exp(\frac{\omega \times SC + \lambda}{RT})$
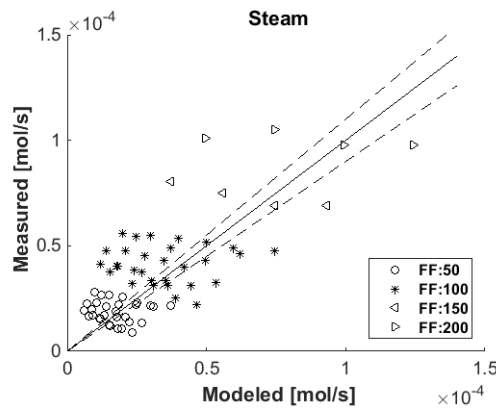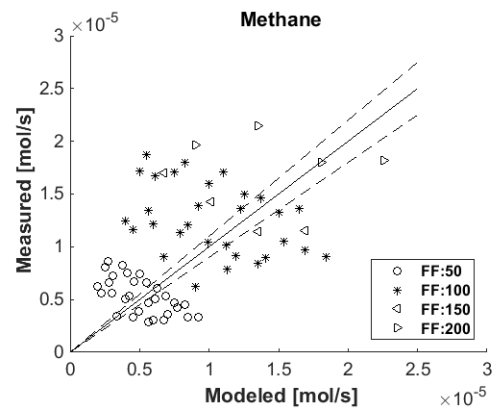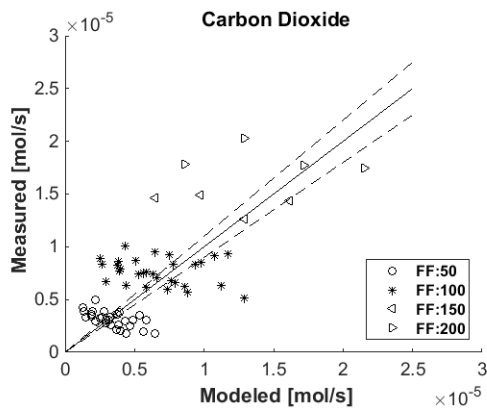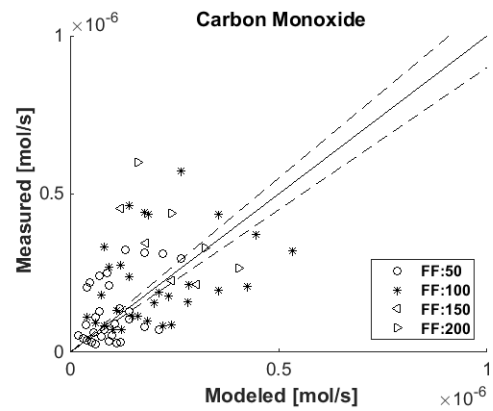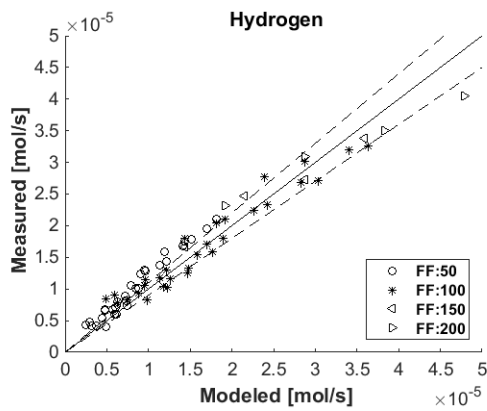
specie	α [mol/m^3.Pa]	ω [J/mol]	λ [J/mol]	R^2
H_2	26.3	-1.3×10^3	-8.5×10^4	0.9790
CO	0.3	-4.3×10^3	-7.8×10^4	0.4593
CO_2	8.4×10^{-2}	7.5×10^2	-5.3×10^4	0.7225
CH_4	1×10^{-3}	-1.6×10^3	-1.2×10^4	0.5130
H_2O	3×10^{-2}	2.6×10^3	-3.8×10^4	0.7737

The values of ω in the case of CO_2 and are positive, proving that at higher S/C ratio, more CO_2 is formed, and naturally, there is excess water fed into and leaving the reactor. The smallest value of ω belongs to CO that has the lowest selectivity among the ESR products. Very high values of λ can be ascribed to the significant effect of the temperature on the ESR reaction promotion and hydrogen permeation rate.
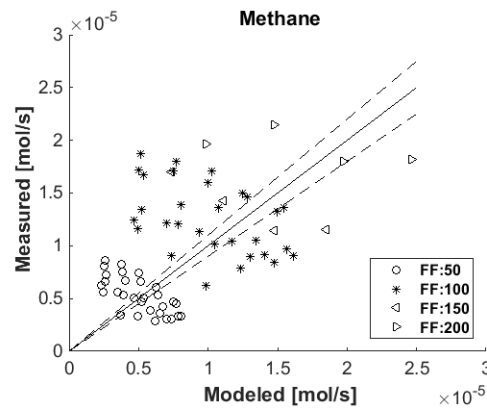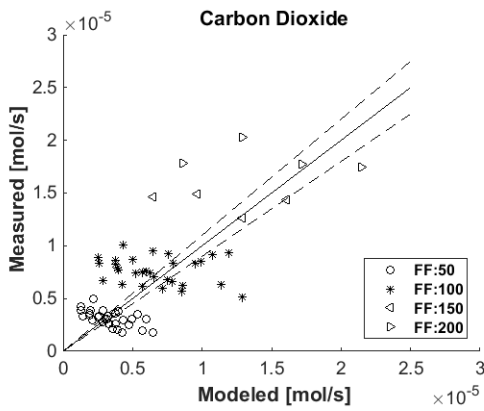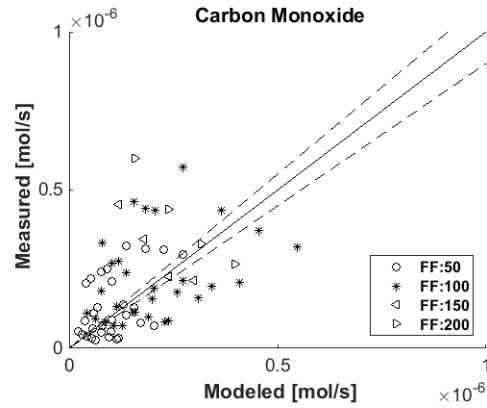
Model 2: $\dot{n}_{specie} = \alpha \times F \times P^{\beta} \times exp(\frac{\omega \times SC + \lambda}{RT})$
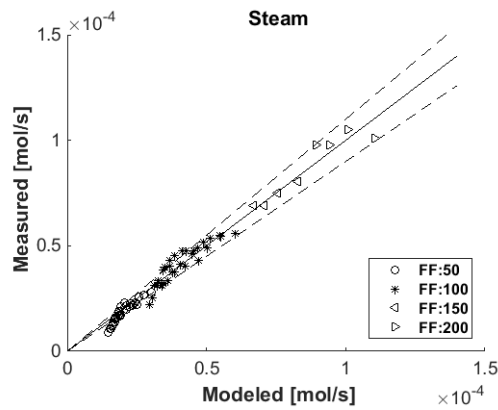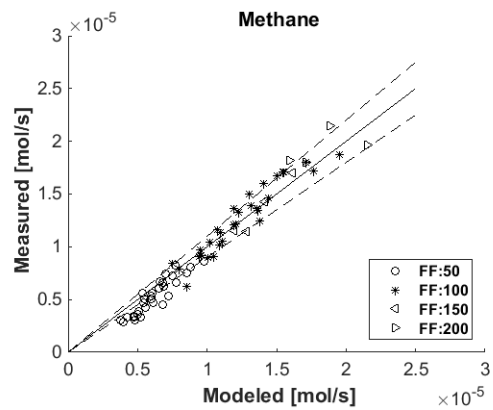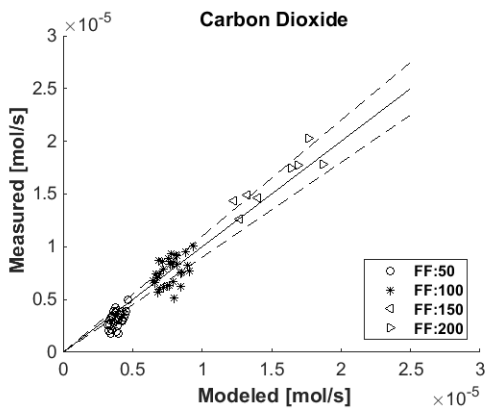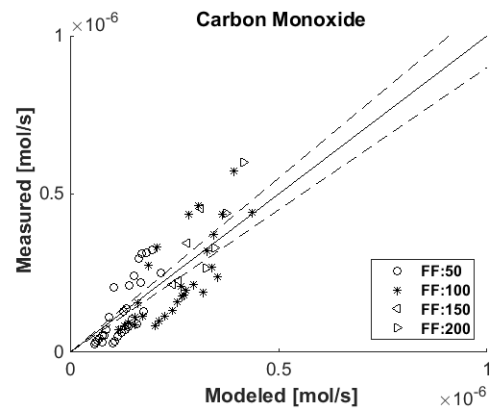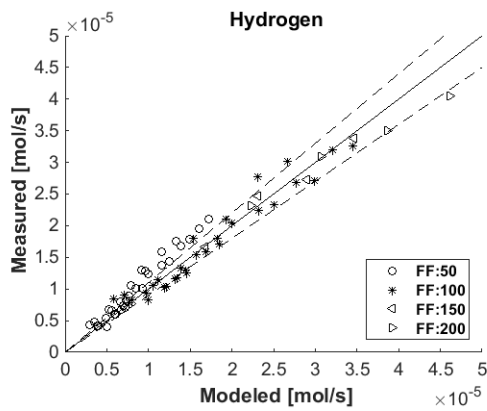
specie	α [mol/m^3.Pa]	β [-]	ω [J/mol]	λ [J/mol]	R^2
H_2	3.7×10^2	0.8	-1.4×10^3	-8.4×10^4	0.9786
CO	9.9×10^3	-0.3	-4×10^3	-2.7×10^4	0.8362
CO_2	1×10^4	-0.1	2.4×10^2	-2.2×10^4	0.9728
CH_4	1.1×10^2	-0.3	-1.8×10^3	3.8×10^4	0.9814
H_2O	2.4×10^3	-0.2	2.1×10^3	5.7×10^3	0.9926

The value of β is positive only in the case of hydrogen, which proves that the production rate of hydrogen in the CMR is directly proportional to the operating pressure. The values of ω in the case of CO_2 and H_2O are positive, proving that at higher S/C ratio, more CO_2 is formed, and naturally, there is excess water fed into and leaving the reactor. The smallest value of ω belongs to CO that has the lowest selectivity among the ESR products. Very high values of λ can be ascribed to the significant effect of the temperature on the ESR reaction promotion and hydrogen permeation rate.

Model 3: $\dot{n}_{specie} = \alpha \times F \times SC^{\theta} \times \exp(\frac{\gamma \times P + \lambda}{RT})$
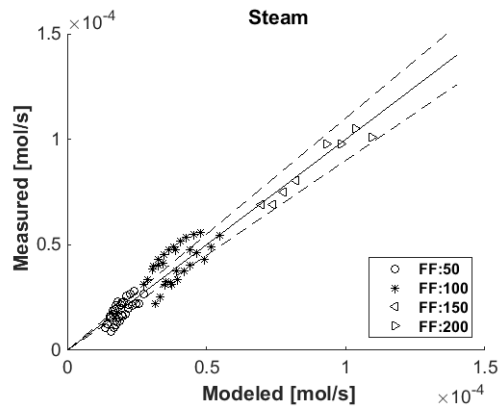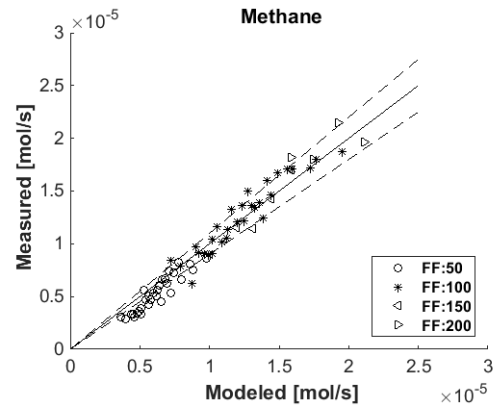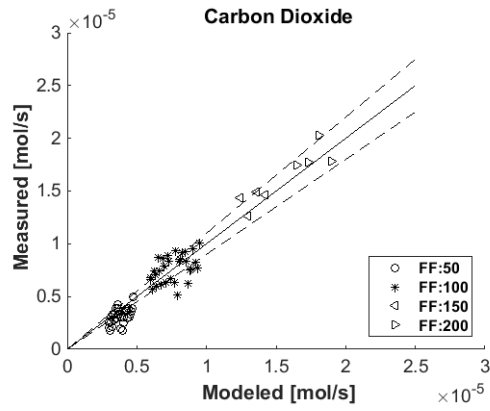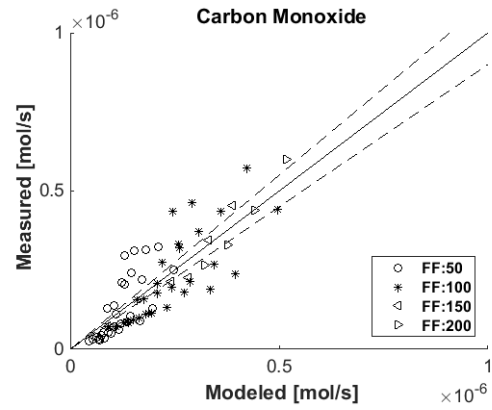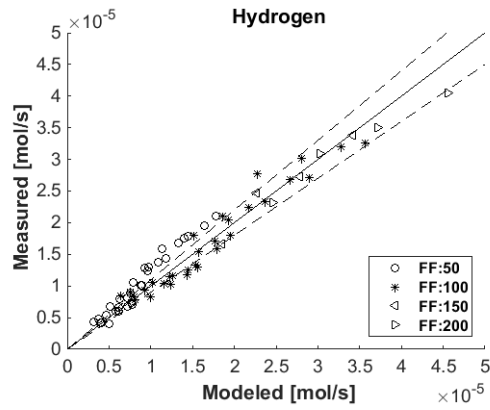
specie	α [mol/m^3]	θ [-]	γ [J/mol.Pa]	λ [J/mol]	R^2
H_2	1.6×10^7	-0.4	7.9×10^{-3}	-9×10^4	0.9787
CO	4.7×10^3	-1	-6.1×10^{-3}	-4.6×10^4	0.8567
CO_2	6.7×10^3	3.9×10^{-3}	-1.7×10^{-3}	-3.2×10^4	0.9740
CH_4	1.8	-0.5	-3.6×10^{-3}	3.7×10^4	0.9822
H_2O	3×10^3	0.5	-2.1×10^{-3}	-1.7×10^4	0.9937

Considering θ, the negative values in the case of H_2, CO, and CH_4 proves that the production rates of these species are conversely proportional to S/C ratio, which is in agreement with the experimental results. The high positive value in the case of H_2O represents the effect of excess water at higher S/C ratios. The value of γ in the case of H2 is positive and higher since the most effective factor on the hydrogen production (and permeation) is the operating pressure (and the partial pressure of hydrogen in the reactor). Very high values of λ can be ascribed to the significant effect of the temperature on the ESR reaction promotion and hydrogen permeation rate.

Model 4: $\dot{n}_{specie} = \alpha \times F \times P \times SC \times \exp(\frac{\gamma \times P + \omega \times SC + \lambda}{RT})$
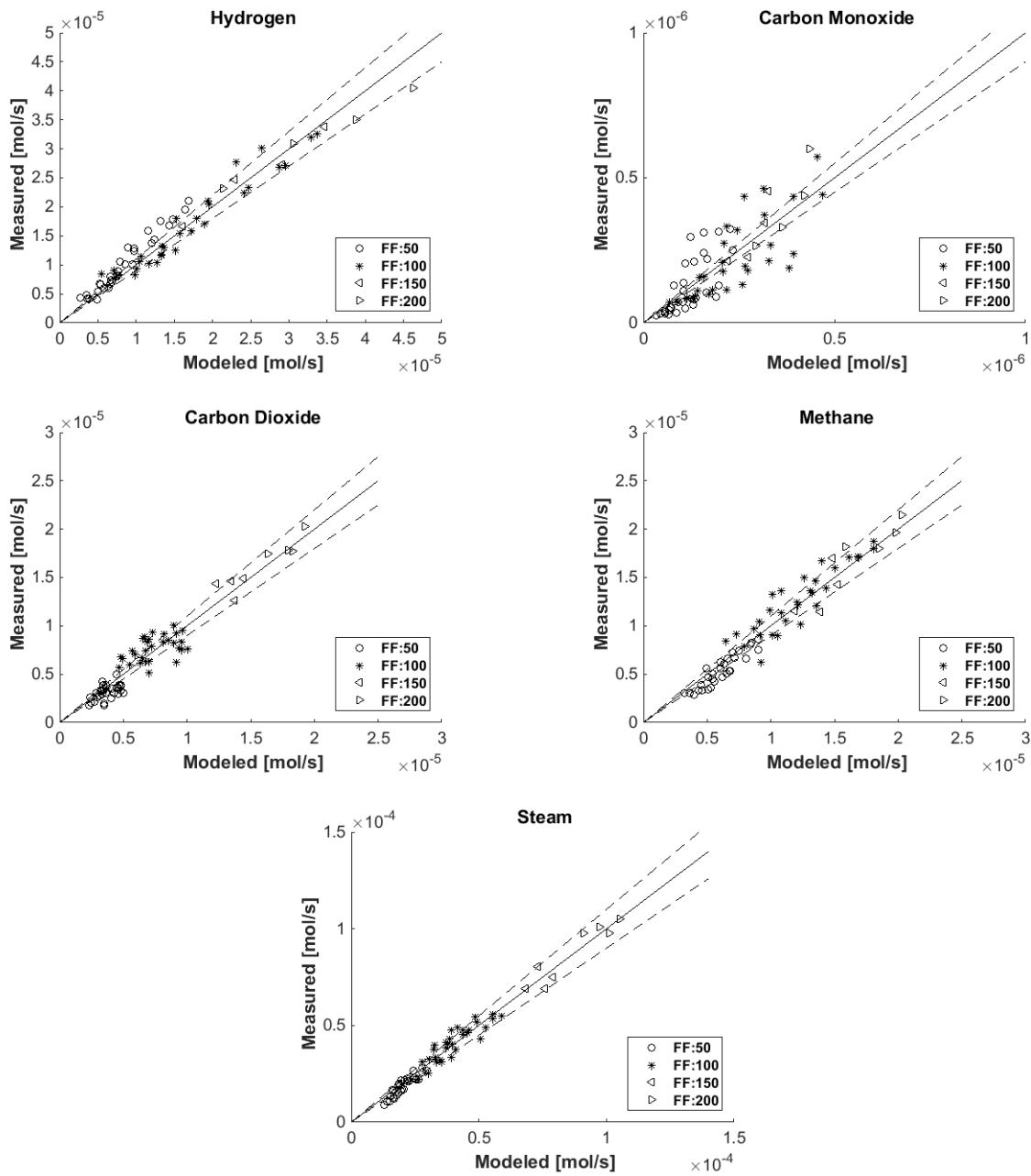
Specie	α [mol/m^3.Pa]	γ [J/mol.Pa]	ω [J/mol]	λ J/mol	R^2
H_2	10.6	-4.8×10^3	-1.9×10^{-3}	-7.5×10^4	0.9778
CO	2.9×10^{-3}	-7.7×10^3	-1.7×10^{-2}	-2.7×10^4	0.8250
CO_2	2.5×10^{-2}	-3.4×10^3	-1.3×10^{-2}	-2.9×10^4	0.9745
CH_4	2.5×10^{-6}	-5.3×10^3	-1.5×10^{-2}	4.9×10^4	0.9753
H_2O	4×10^{-5}	-1.2×10^3	-1.3×10^{-2}	2.6×10^4	0.9897

In this model, the combination of the effects of the pressure and S/C ratio can be seen. The values of $\gamma \times P$ are very large (40000<P<120000 Pa) compared to the values of ω (1.6<SC<3), which is attributed to the dominant effect of pressure on the production rate of species. The values of λ place in a wild range similar to the values of α, which can be due to the combined effects of the operating conditions considered in this formulation. As seen, in the case of CH_4 and H_2O, λ is very large and positive, while the values of α are some orders of magnitude smaller in comparison with the other three species.

**Model 5:** $\dot{n}_{specie} = \alpha \times F \times P \times exp(\frac{\gamma \times SC^{\lambda}}{RT})$

Hydrogen

Carbon Monoxide

Carbon Dioxide

Methane

Steam
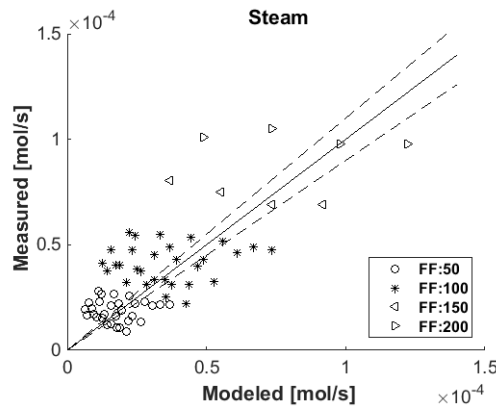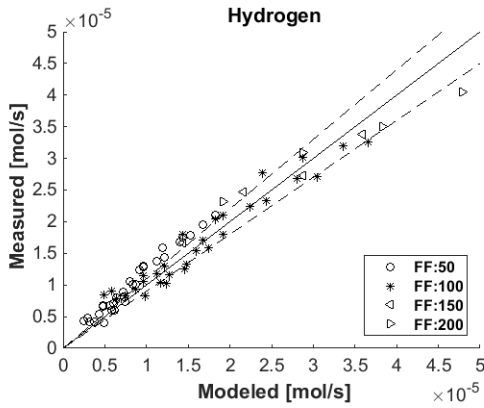
specie	α [mol/m³.Pa]	γ [J/mol]	λ [-]	R²
H_2	25.6	-8.5×10^4	3.3×10^{-2}	0.9791
CO	0.1	-7.1×10^4	0.1	0.4763
CO_2	0.1	-5.6×10^4	-2×10^{-2}	0.7273
CH_4	3×10^{-4}	-5.6×10^3	0.2	0.4971
H_2O	3.1×10^{-3}	-2×10^4	-0.5	0.8181

The value of α is very large in the case of H2, which can be attributed to the effect of pressure (in the pre-exponential term) on the production rate of hydrogen. The values of SC^λ are negligible ($\lambda < 1$) compared to γ, which can be interpreted as the minor effect of S/C ratio in comparison with temperature.

Model 6: $\dot{n}_{specie}= \alpha \times F \times P^{\beta} \times exp(\frac{\gamma \times SC^{\lambda}}{RT})$
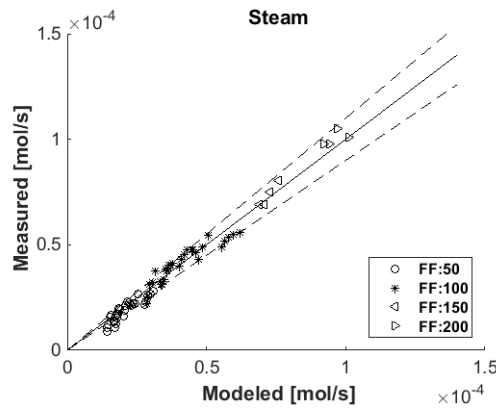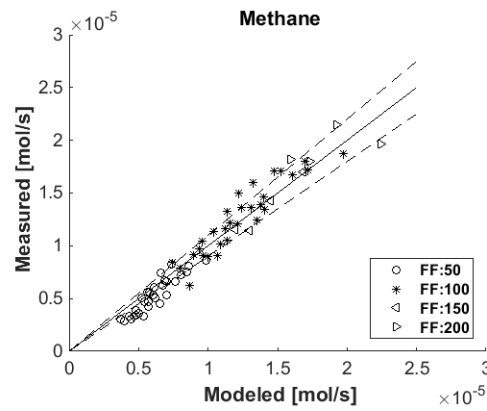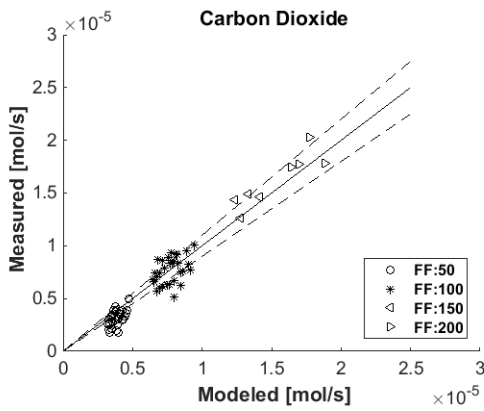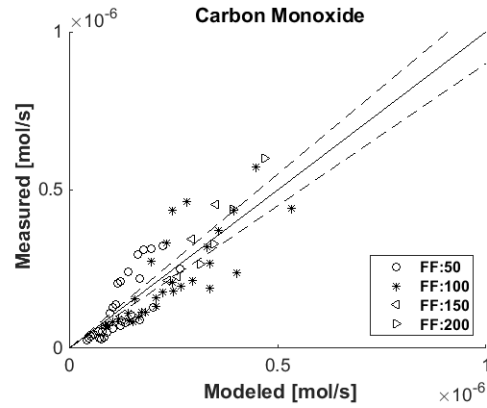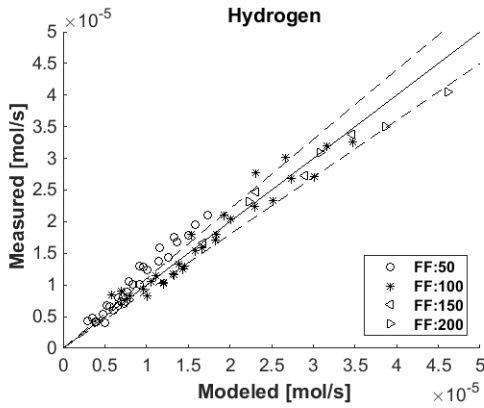
specie	α [mol/m³.Pa]	β [-]	γ [J/mol]	λ [-]	R²
H_2	3.6×10^2	0.8	-8.4×10^4	4×10^{-2}	0.9786
CO	4.8×10^6	-0.4	-5.7×10^4	0.2	0.8505
CO_2	1.2×10^4	-0.1	-2.3×10^4	-2×10^{-2}	0.9728
CH_4	5.6×10^2	-0.4	2.9×10^4	0.2	0.9801
H_2O	50	-0.1	2.1×10^4	0.2	0.9929

The value of β is positive and larger in the case of hydrogen, which proves that the production rate of hydrogen in the CMR is directly proportional to the operating pressure. The values of SC^{λ} are negligible ($\lambda<1$) compared to γ, which can be interpreted as the minor effect of S/C ratio in comparison with temperature.

Model 7: $\dot{n}_{specie} = \alpha \times F \times P \times \exp(\frac{\gamma \times SC^\lambda + \varepsilon}{RT})$
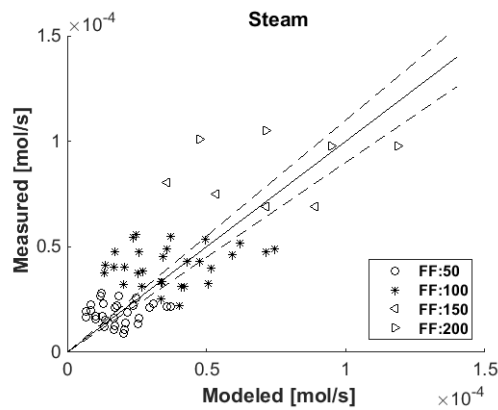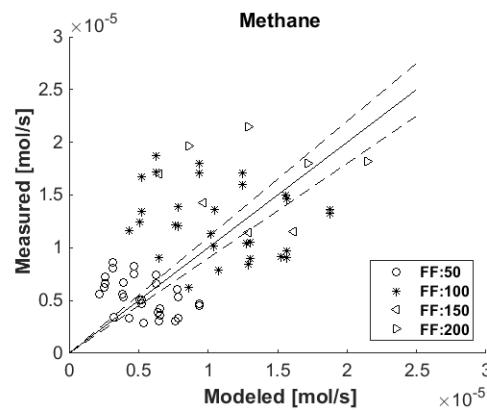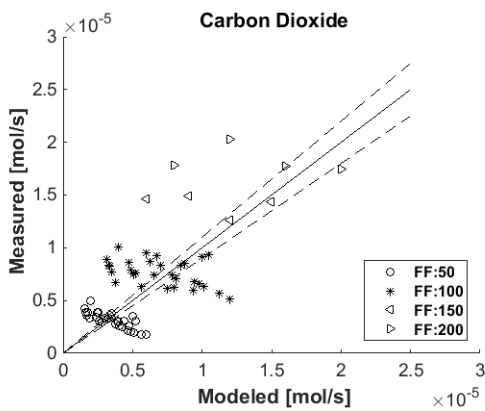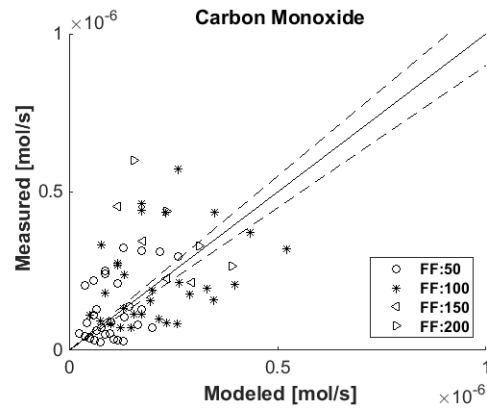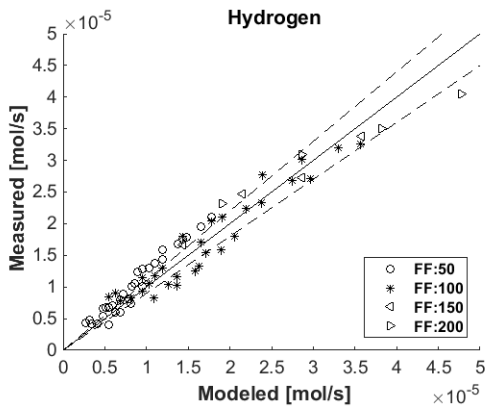
specie	α [mol/m^3.Pa]	γ [J/mol]	λ [-]	ε [J/mol]
H_2	4.4	-4.1×10^7	6.3×10^{-5}	4.1×10^7
CO	5.5×10^{-3}	-4.9×10^4	0.2	-9.6×10^2
CO_2	3×10^{-4}	1.4×10^2	2.2	1×10^4
CH_4	5.5×10^{-6}	2.6×10^{-3}	12	2.4×10^4
H_2O	2.7×10^{-4}	-1.8×10^4	-0.6	1.6×10^4

In the case of H_2, the value of λ is very small, but on the other hand the value of α is much higher compared to other ESR product. Considering the formulation of this model, the difference between the values of λ and α is interpreted as the significant effect of pressure on the hydrogen production rate and the minor effect of S/C ratio. Besides, the very large value of ε in the case of hydrogen, represents the effect of temperature.

Model 8: $\dot{n}_{specie} = \alpha \times F \times P^{\beta} \times exp(\frac{\gamma \times SC^{\lambda} + \varepsilon}{RT})$
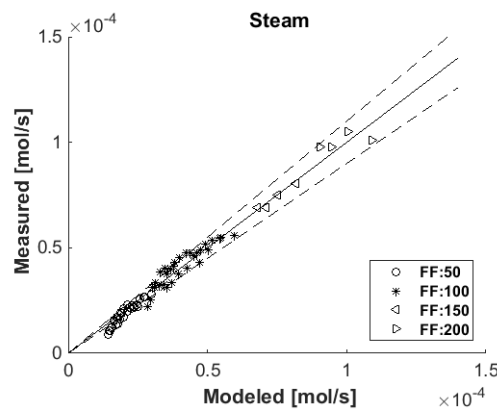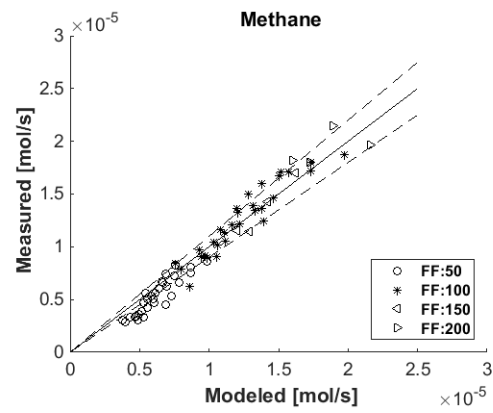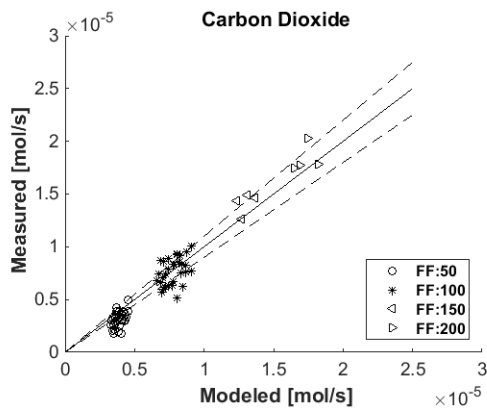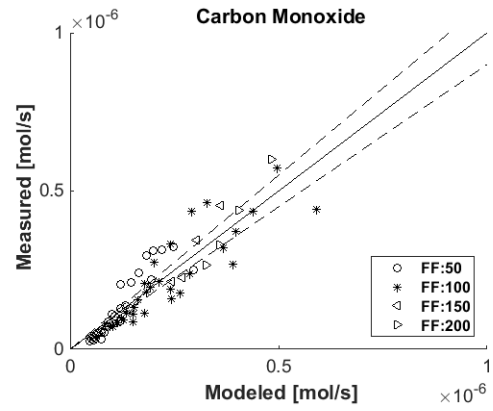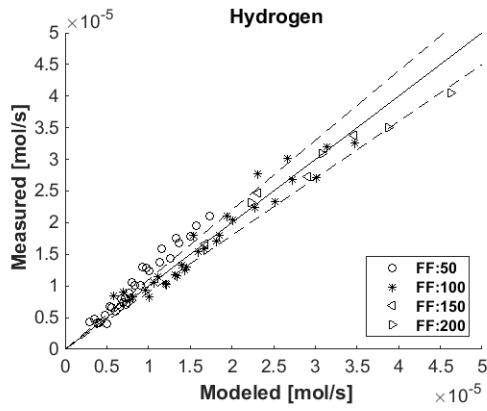
specie	α [mol/m³.Pa]	β [-]	γ [J/mol]	λ [-]	ε [J/mol]	R^2
H_2	3.3×10^2	0.8	1.1×10^4	-0.4	9.3×10^4	0.9787
CO	2.7×10^2	0.2	1.9×10^4	-2.1	1.8×10^4	0.9091
CO_2	5.5×10^3	0.1	3.4×10^4	-9.8	2×10^4	0.9729
CH_4	89	0.3	1.8×10^4	-0.3	2×10^4	0.9802
H_2O	1.5×10^3	0.2	1.1×10^4	1.1	1.5×10^4	0.9932

The value of β is larger in the case of hydrogen, which proves that the production rate of hydrogen in the CMR is directly proportional to the operating pressure. Very large values of γ specially compared to λ can be explained by the significant effect of temperature in comparison with the S/C ratio. The value of λ is near 1 in the case of H_2O since the amount of eater is proportional to the S/C ratio. Very high values of ε can be ascribed to the significant effect of the temperature on the ESR reaction promotion and hydrogen permeation rate.

B.2 Specific Models

The specific models were developed at T=923 K.

| Model	$\dot{n}_{specie}$	R^2_{mean}
1	$\alpha \times F \times P \times \exp(\dfrac{\omega \times SC}{RT})$	0.7076
2	$\alpha \times F \times P^\beta \times \exp(\dfrac{\omega \times SC}{RT})$	0.9469
3	$\alpha \times F \times SC^\theta \times \exp(\dfrac{\gamma \times P}{RT})$	0.9542
4	$\alpha \times F \times SC^\theta \times \exp(\dfrac{\gamma \times P^\omega}{RT})$	0.9542
5	$\alpha \times F^\beta \times SC^\theta \times \exp(\dfrac{\gamma \times P^\omega + \varepsilon}{RT})$	0.9574

Model 1: $\dot{n}_{specie} = \alpha \times F \times P \times \exp(\frac{\omega \times SC}{RT})$
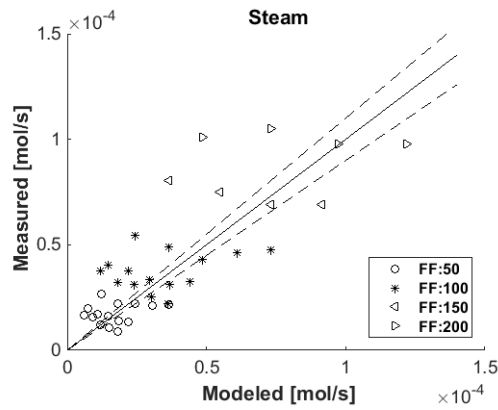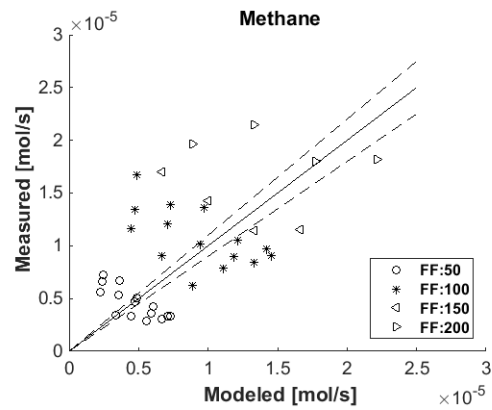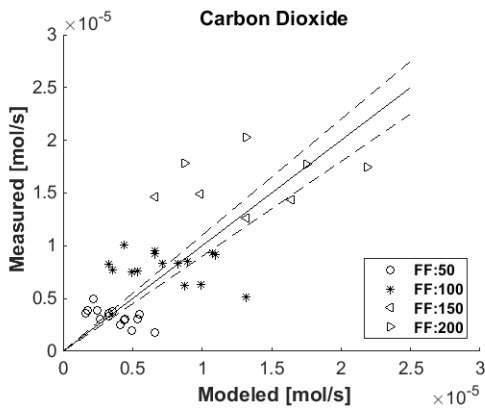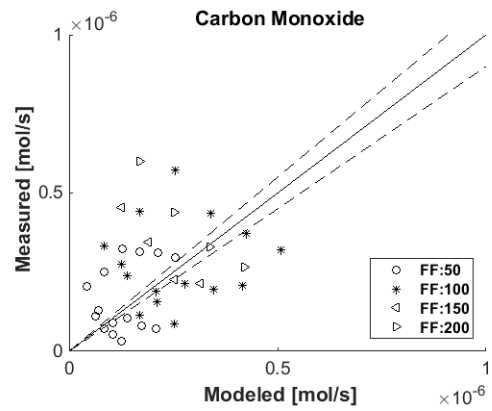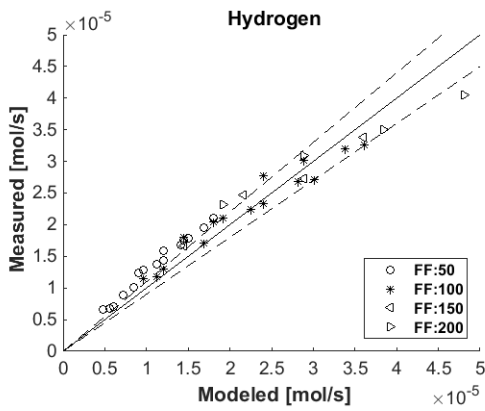
Specie	α [mol/m^3.Pa]	ω [J/mol]	R^2
H_2	3.9×10^{-4}	-1.2×10^3	0.9817
CO	9.5×10^{-6}	-3.8×10^3	0.3664
CO_2	6×10^{-5}	1.5×10^3	0.7652
CH_4	1.3×10^{-4}	-4.9×10^2	0.5891
H_2O	1.3×10^{-4}	3.9×10^3	0.8354

H_2O has the highest value of ω that is attributed to the effect of S/C ratio on the production rate of H_2O. The amount of excess water increased with S/C ratio. Comparatively, the value of ω in the case of hydrogen presents the minor effect of S/C ratio on the production rate of H_2. The positive values of ω in the case of CO_2 and H_2O can be attributed to the fact that the ESR reaction is promoted better at higher S/C ratio, probably due to the availability of excess water. The highest value of α belongs to H_2, proving the effect of pressure on the hydrogen production rate.

Model 2: $\dot{n}_{specie} = \alpha \times F \times P^{\beta} \times \exp(\frac{\omega \times SC}{RT})$
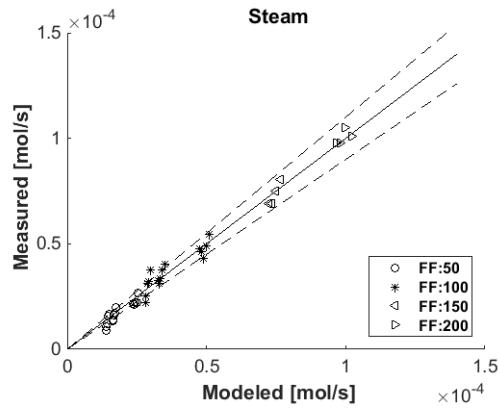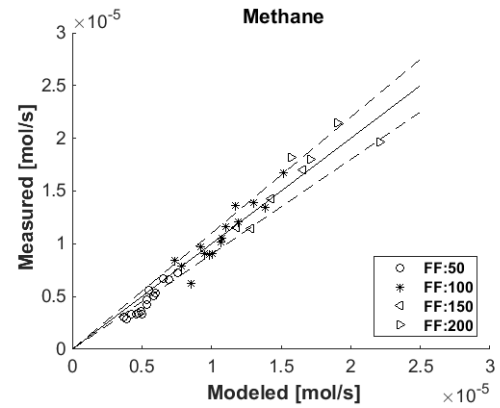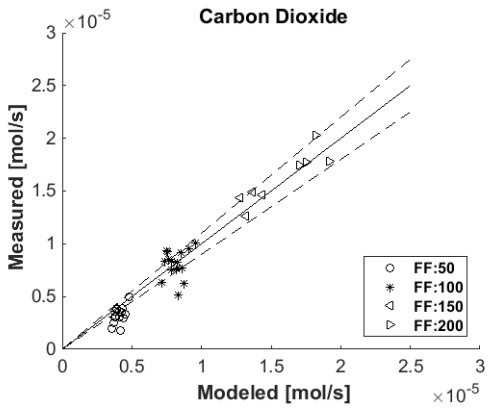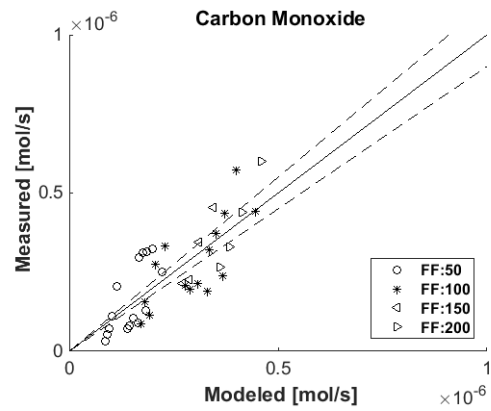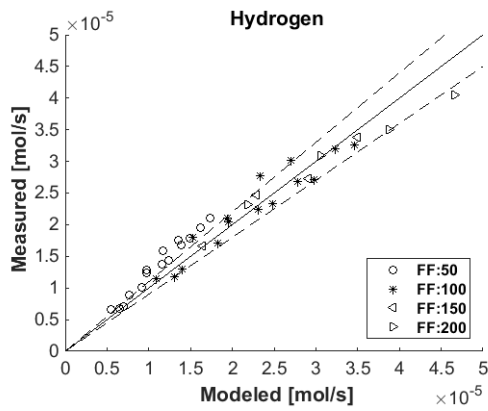
Specie	α [mol/m^3.Pa]	β [-]	ω [J/mol]	R^2
H$_2$	4.5×10^{-3}	0.8	-1.3×10^3	0.9773
CO	2.7×10^2	-0.3	-3.6×10^3	0.8051
CO$_2$	3.6×10^2	-0.1	8.3×10^2	0.9767
CH$_4$	2.7×10^4	-0.4	-1.7×10^3	0.9809
H$_2$O	3.6×10^2	-6.2×10^{-2}	2.9×10^3	0.9944

The value of β is larger in the case of hydrogen, which proves that the production rate of hydrogen in the CMR is directly proportional to the operating pressure. The positive values of ω in the case of CO_2 and H_2O can be attributed to the fact that the ESR reaction is promoted better at higher S/C ratio, probably due to the availability of excess water.

Model 3: $\dot{n}_{specie} = \alpha \times F \times SC^{\theta} \times \exp(\frac{\gamma \times P}{RT})$
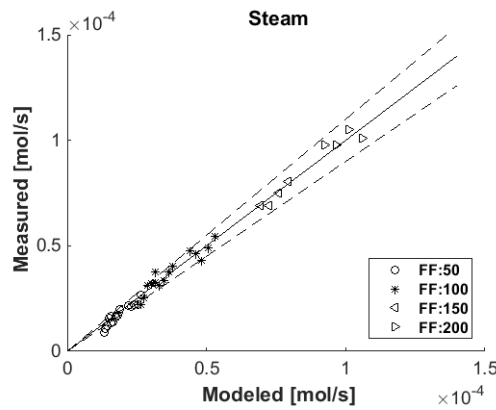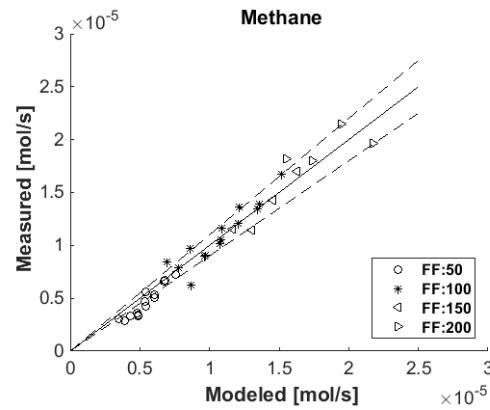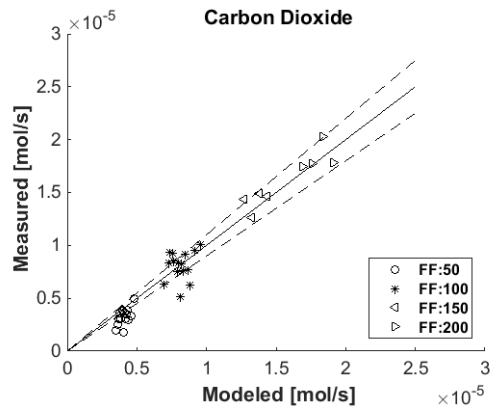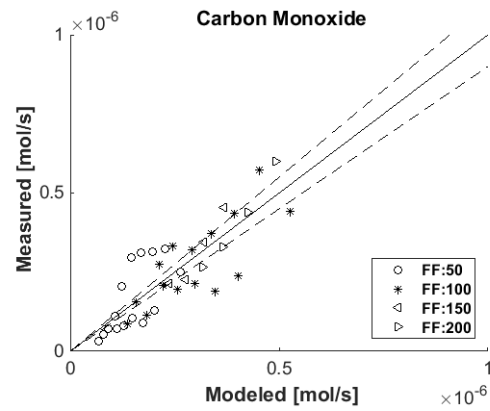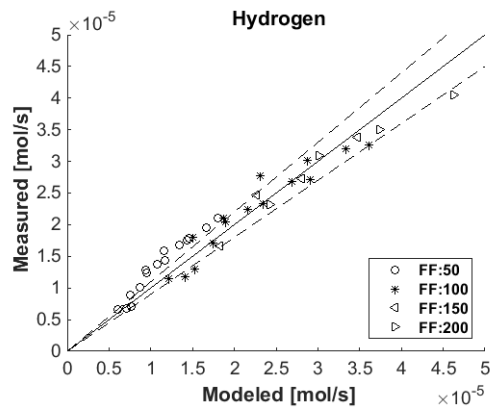
Specie	α [mol/m^3]	θ [-]	γ [J/mol.Pa]	R^2
H_2	1.2×10^2	-0.4	8.3×10^{-3}	0.9755
CO	12.5	-1.2	-5.6×10^{-3}	0.8398
CO_2	80	0.2	-1.6×10^{-3}	0.9776
CH_4	2.4×10^2	-0.5	-4.3×10^{-3}	0.9823
H_2O	2.4×10^2	0.8	-1.7×10^{-3}	0.9958

The positive and larger value of γ in the case of hydrogen proves that the production rate of hydrogen in the CMR is directly proportional to the operating pressure. The positive values of θ in the case of CO_2 and H_2O can be attributed to the fact that the ESR reaction is promoted better at higher S/C ratio, probably due to the availability of excess water.
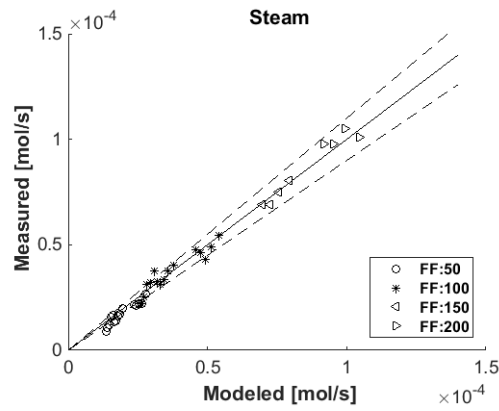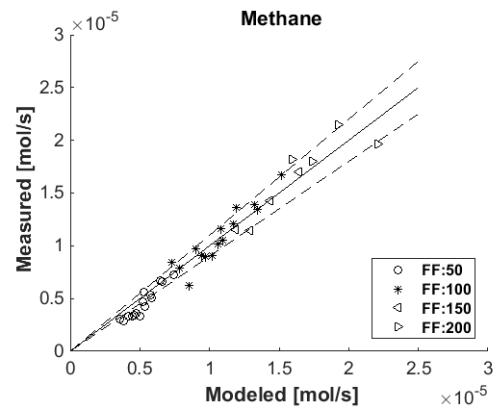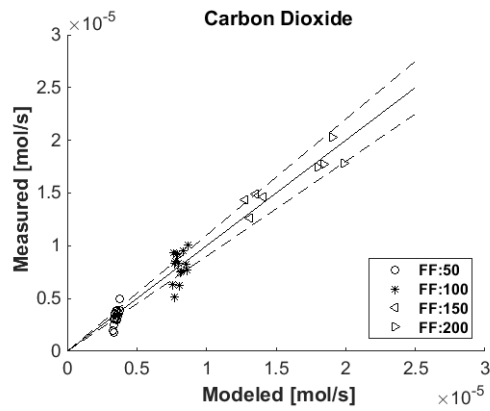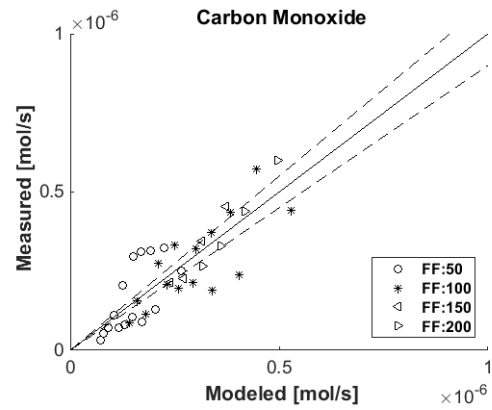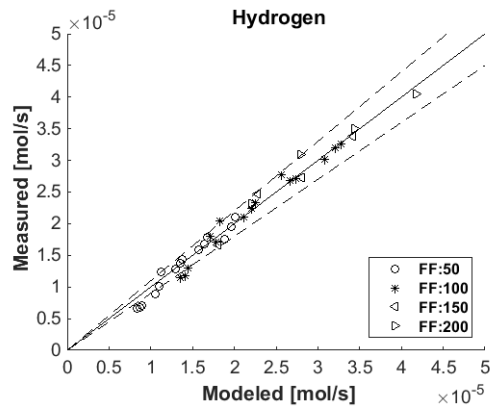
Model 4: $\dot{n}_{specie} = \alpha \times F \times SC^{\theta} \times \exp\left(\frac{\gamma \times P^{\omega}}{RT}\right)$
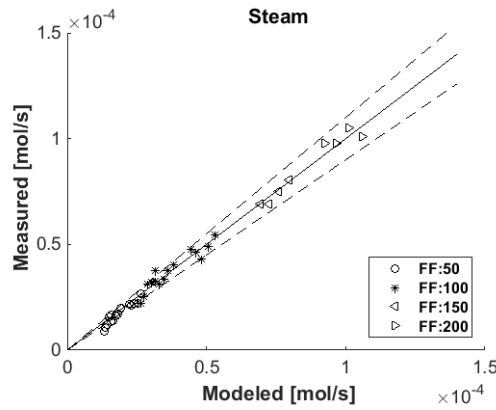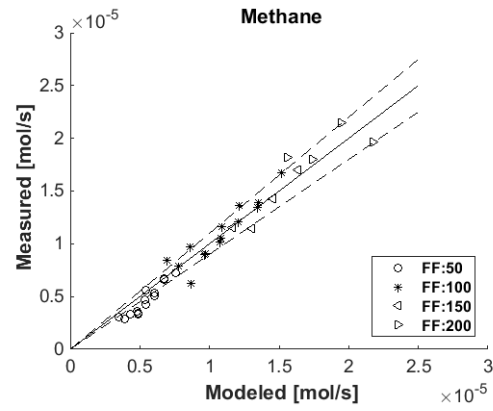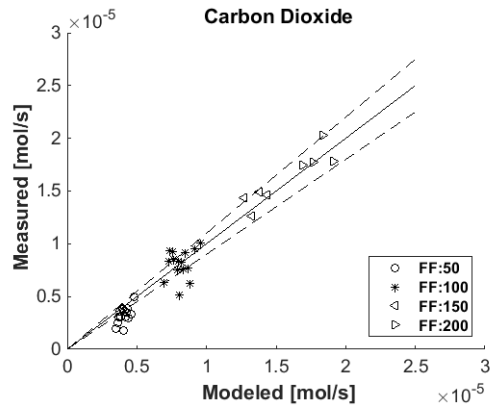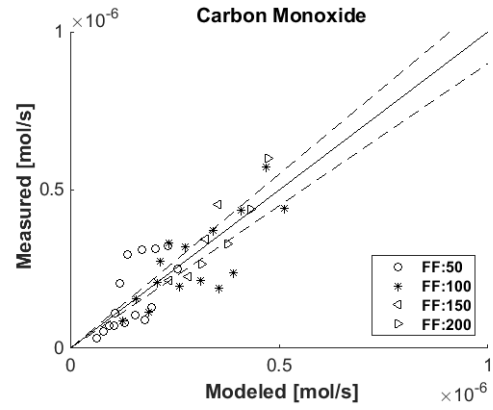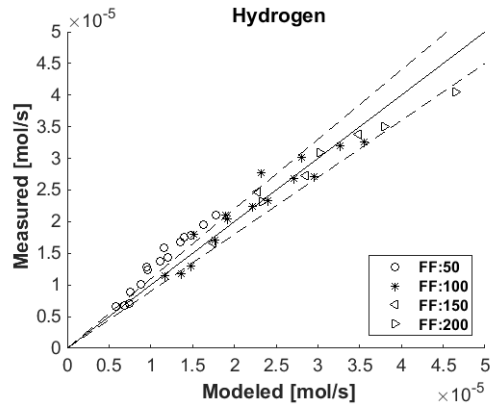
Specie	α [mol/m^3]	θ [-]	γ [J/mol.Pa]	ω [-]	R^2
H$_2$	66.9	-0.4	3.9	0.6	0.9771
CO	9.8	-1.2	-5.9×10^{-10}	2.1	0.8379
CO$_2$	78	0.2	-1.7×10^{-4}	1.2	0.9778
CH$_4$	2.5×10^2	-0.5	-6.2×10^{-3}	0.9	0.9823
H$_2$O	2.4×10^2	0.8	-2.3×10^{-3}	0.8	0.9958

The positive values of θ in the case of CO_2 and H_2O can be attributed to the fact that the ESR reaction is promoted better at higher S/C ratio, probably due to the availability of excess water. The positive and larger value of γ in the case of hydrogen proves that the production rate of hydrogen in the CMR is directly proportional to the operating pressure. Although the value of ω is higher in the case of CO, the value of γ is several orders of magnitude smaller than other species.

Model 5: $\dot{n}_{specie} = \alpha \times F^{\beta} \times SC^{\theta} \times exp(\frac{\gamma \times P^{\omega} + \varepsilon}{RT})$

Specie	α [mol/m³]	β [-]	θ [-]	γ [J/mol.Pa]	ω [-]	ε [J/mol]	R²
H_2	0.6	0.7	-0.1	0.8	0.7	0.7	0.9908
CO	16.8	1	-1.2	-7	0.5	-15.5	0.8392
CO_2	1.2×10^2	1.2	3.2×10^{-2}	-4×10^3	7.5×10^{-2}	3.2×10^4	0.9794
CH_4	2.2×10^3	1	-0.5	-8.7×10^2	0.2	-2.8×10^3	0.9824
H_2O	1.1×10^2	0.9	0.9	-0.4	0.6	-1.3×10^2	0.9951

The positive values of θ in the case of CO_2 and H_2O can be attributed to the fact that the ESR reaction is promoted better at higher S/C ratio, probably due to the availability of excess water. The positive and larger value of γ in the case of hydrogen proves that the production rate of hydrogen in the CMR is directly proportional to the operating pressure. the same explanation can be given in the case of ω. Considering the value of $\alpha \times F^\beta$, the lower value is obtained in the case of H_2, which can be attributed to the significant effect of pressure, which appears in the exponential term.